FUranic TUnable REsins for Sustainable materials

Pierre Dellière

UNIVERSITÉ CÔTE D'AZUR | ÉCOLE DOCTORALE SCIENCES FONDAMENTALE ET APPLIQUÉES

Résines furaniques modulables et durables

Pierre Dellière

Institut de chimie de Nice

Présentée en vue de l'obtention du grade de docteur en Chimie **d'**Université Côte d'Azur

Dirigée par : Dr. Nathanaël Guigo
Soutenue le : 17/11/2023

Devant le jury, composé de :
Rapporteurs
Mohamed Naceur Belgacem, Professeur, Ecole Internationale du papier, de la communication imprimée et des biomatériau - INP Grenoble
Minna Hakkarainen, Professeure, KTH Royal Institute of Technology
Examinateurs
Marco Sangermano, Professeur, Politecnico di Torino
François Jerôme, Directeur de recherche CNRS, Institut de chimie des milieux et matériaux de Poitier- IC2MP, Université de Poitier
Directeur de thèse
Nathanaël Guigo, Maître de conférences, Université Côte d'Azur

anr

Résumé

Cette thèse de doctorat s'est déroulée dans le cadre du projet ANR FUTURES (Furanic TUnable REsins for Sustainable materials, i.e., Résines furaniques modulables et durables). L'alcool polyfurfurylique (PFA) est un polymère thermodurcissable biosourcé qui possède d'excellentes propriétés chimiques et thermiques malgré un comportement cassant. L'objectif de ce projet est d'ouvrir la voie à de nouvelles applications pour le PFA en exploitant les réactions secondaires qui ont lieu lors de la polymérisation. Cela permettra d'apporter de nouvelles fonctionnalités au matériau réticulé et de jouer sur la fragilité du matériau. Les groupements C=O résultants de l'ouverture du cycle furanique lors de la polymérisation du PFA ont été quantifiés par potentiométrie et RMN quantitative. Les facteurs influençant le taux de carbonyles dans le polymère ont été évalués et la présence additionnelle d'eau au cours de la polymérisation s'est révélé être un facteur capital. L'environnement chimique des carbonyles a été apprécié par l'utilisation de RMN bidimensionnelle et un nouveau phénomène de réticulation de surface a été identifié et expliqué. L'impact de cette réticulation de surface sur les propriétés finales du matériau a été également mis en avant. Enfin, la présence de C=O résultant de l'ouverture de cycle a été exploitée pour fonctionnaliser le polymère post-réticulation. En utilisant des amines flexibles, le matériau passe progressivement d'un comportement cassant à un comportement plus ductile, permettant ainsi d'entrevoir de nouvelles applications. Les facteurs gouvernant les propriétés des matériaux fonctionnalisés par les amines ont également été étudiés.

Mots clefs : thermodurcissables biosourcés, degradation, bioraffinerie, propriétés thermo-mécaniques, analyse structurale, polymères furaniques

Abstract

This doctoral project was conducted within the ANR FUTURES (FUranic TUnable REsins for Sustainable materials) project. Poly(furfuryl alcohol) is a bio-based thermoset with excellent chemical and thermal properties. Yet, it may mechanically behave in a brittle manner. The aim of the project was to pave the way for new applications of poly(furfuryl alcohol) by exploiting side reactions occurring during polymerization. This leads to additional functionalities that could be exploited to, among others, reduce the brittleness of the material. First, the reactive carbonyl resulting from the furan ring opening side reaction were quantified by potentiometry and quantitative NMR. The key factors that were influencing the carbonyl content were assessed and water proved to be the main one. The chemical nature of the carbonyls was thoroughly investigated by 2D NMR and a new surface crosslinking phenomenon was identified and explained. The impact of this surface crosslinking on the materials' properties was evaluated. Finally, the presence of carbonyls due to the ring-opening side reaction was exploited to functionalize the polymer. The use of large flexible amines allowed to shift the materials properties from brittle to ductile therefore paving to way to new applications for poly(furfuryl alcohol). Finally, factors governing the properties of the amine-functionalized materials were studied.

Keywords: Biobased thermoset, degradation, biorefinery, thermo-mechanical properties, structural analysis, furanic polymers.

Résumé détaillé

Cette thèse de doctorat s'est déroulée dans le cadre du projet ANR FUTURES (Furanic TUnable REsins for Sustainable materials, i.e., Résines furaniques modulables et durables). L'alcool polyfurfurylique (PFA) est un polymère thermodurcissable biosourcé qui possède d'excellentes propriétés chimiques et thermiques malgré un comportement cassant. L'objectif de ce projet est d'ouvrir la voie à de nouvelles applications pour l'alcool polyfurfurylique en exploitant les réactions secondaires qui ont lieu lors de la polymérisation. Cela permettra d'apporter de nouvelles fonctionnalités au matériau réticulé et de jouer sur la fragilité du matériau.

Pour appréhender l'importance de ces ouvertures de cycle furanique pendant la polymérisation du FA, deux méthodes de quantification, par RMN du ^{19}F et par ont été adaptées. En fonction de la méthode utilisée, il est possible d'obtenir des informations sur l'accessibilité chimique des groupements C=O au sein du PFA. D'autre part, le taux de carbonyles a été mesuré tout au long de la polymérisation. Également, deux types de résine PFA ont été préparés. Celle intitulée « PFA° » a été préparée uniquement en présence d'alcool furfurylique (FA) et d'un catalyseur. La résine intitulée « PFA+ » a été préparée dans un mélange 50/50 FA/eau. L'addition d'eau dès le début de la polymérisation permet d'augmenter significativement le taux de carbonyle. En effet, à des taux de conversion élevés, le PFA° possède environ 2,2 $mmol.g^{-1}$ de carbonyle contre 3.7 $mmol.g^{-1}$ pour le PFA+, soit environ 1,7 fois plus. Une étude sur les leviers disponibles pour agir sur le taux de carbonyle a également été conduite (variation du catalyseur, solvent, température). Celle-ci a montré que l'eau est le facteur principal qui affecte le taux de C=O. D'autre part, celui-ci est limité à environ 3.7 $mmol.g^{-1}$ pour des résines solubles.

Dans un deuxième temps, l'environnement chimique des carbonyles au sein de PFA° et PFA+ a été étudié par RMN bidimentionelle. Cette étude a permis de mettre en valeur les multiples environnements chimiques des composés carbonylés résultants de l'ouverture du cycle furane. Cette étude a mis également en lumière la propension toute particulière qu'on les cycles furaniques en bout de chaine à s'ouvrir. En effet, les furanes terminaux au sein du PFA peuvent être soit sous forme de furanes méthylés soit mono substitués.

Dans le premier cas, les furanes méthylés sont susceptibles de se transformer en lactones pour les systèmes PFA°. Pour les systèmes PFA+, les furanes méthylés s'hydrolysent en unités levuliniques. Enfin, les furanes monosubtitués sont sensibles à l'oxydation. Leur oxydation par l'air engendre des groupements aldéhydes. Ceux-ci ont été quantifiés et peuvent représenter jusqu'à 20 % du total des carbonyles.

Il a été souligné que l'ouverture des furanes terminaux en aldéhydes conjugués par voie oxydative participe à un phénomène de réticulation de surface. En effet, ces aldéhydes conjugués sont susceptibles de réagir par cycloaddition Diel-Alder avec des furanes non conjugués. Cela se traduit par la formation d'une croute dure et riche en C=O en surface des résines PFAs. L'impact de cette croute a été étudié d'un point de vue macroscopique sur des échantillons de PFA oxydés et non-oxydés. Les effets sur les propriétés en traction et sur les propriétés thermomécaniques restent limités. L'épaisseur de la croute a été estimé à environ 20 µm. Enfin, les cyclo-adduits sont susceptibles de s'aromatiser lorsque le matériau est exposé à des températures supérieures à 150 °C.

La dernière partie de ce manuscrit est consacrée à la fonctionnalisation des C=O du PFA par des amines primaires. Dans un premier temps, une preuve de concept a été réalisée en utilisant la Priamine 1071, une amine flexible et biosourcée. Concrètement, en faisant varier le taux de Priamine, il est possible faire varier la température de transition vitreuse (T_g) du matériau entre 20 °C et 60 °C. Par conséquent, il est possible de multiplier par sept l'élongation à la rupture du matériau, tout en divisant par cent son module d'Young avec en optimum ténacité pour un rapport molaire NH_2/C=O autour de 0.25.

Cette preuve de concept a été suivie d'une série d'étude plus approfondies autour des différents facteurs gouvernant les propriétés des matériaux PFA/Amine. La structure de l'amine, à savoir rigide ou flexible, permet de faire varier la T_g entre - 44 °C et 145 °C, soit une plage d'environ 200 °C.

L'environnement des matériaux (atmosphère inerte ou oxydante) pendant la post-cuisson s'est révélé capital dans le cas des systèmes PFA/Amine flexible. Alors que peu de variations sont observées lorsque le PFA est seul, dans certains cas une atmosphère oxydante peut faire passer la T_g du matériau au-dessus de la température ambiante via la formation d'une croute. Dans ces cas, les propriétés en traction peuvent être modifiées d'un ou plusieurs ordres de grandeur. Enfin, le PFA a été fonctionnalisé à différents stades de sa polymérisation, i.e. de 30 % à 95 % de conversion. Dans tous les cas, il est possible de fabriquer des matériaux PFA/Amine. En revanche, pour la préparation de systèmes rigides il est préférable d'utiliser des PFA polymérisés à 90 % ou plus pour éviter les problématiques liées à la nature basique des amines sur les dernières étapes de polymérisation.

Table of contents

Index of abbreviations

α	Conversion degree
ϕNHNH$_2$.HCl	Phenylhydrazine hydrochloride
ϕCF$_3$NHNH$_2$	4-(trifluoromethyl)phenylhydrazine
AC	Autoclave
CMR	Carcinogenic, mutagenic, reprotoxic
CPMAS	Cross-Polarization Magic-Angle-Spinning NMR
DEPT	Distortionless Enhancement by Polarization Transfer
DGEBA	Diglycidylether of bisphenol A
DMA	Dynamic mechanical analysis
DMSO	dimethylsulfoxyde
DOS	Degree of open structure
DSC	Differential scanning calorymetry
E'	Elastic modulus
E	Young's modulus
E_α	Activation energy
ECHA	European Chemical Agency
EtOAc	Ethyl acetate
EtOH	Ethanol
FA	Furfuryl alcohol
FTIR	Fourier-transformed infra-red
HMBC	Heteronuclear Multiple Bond Coherence
HPDEC	High-power decoupling with magic angle spinning
HSQC	Heteronuclear single quantum coherence spectroscopy
IPA	Isopropyl alcohol
MA	Maleic anhydride
MALDI ToF	Matrix Assisted Laser Desorption Ionization - Time of Flight
MMT	Montmorillonite
NH$_2$OH.HCL	Hydroxylamine hydrochloride
NMR	Nuclear magnetic resonance
OOT	Oxidation onset temperature
PFA	Poly(furfuryl alcohol)
RBF	Round bottom flask
REACH	Registration Evaluation and Authorization of CHemicals
ssNMR	Solid state nuclear magnetic resonance
Tan δ	Damping Factor

TfOH	Triflic acid
T_g	Glass transition temperature
TGA	Thermogravimetric analysis
UV	Ultraviolet
VOC	Volatile organic compounds

Introduction

Biomass and fossilized biomass (i.e. petroleum oil) represent the two sources of organic carbon available on earth. Refining and transforming crude oil allowed the development of modern life. In the course of the 20th century, oil was employed at a constantly increasing rate , mostly to produce commodity chemicals, materials and to propel vehicles. However, our consumption of petroleum exceeds by far its natural formation. In addition, the uses of petroleum are associated with the release of massive amounts of greenhouses gases (GHGs) in the atmosphere. Ultimately, the GHGs are disturbing earth balance. International groups such as the Intergovernmental Panel on Climate Change (IPCC) are urging humanity to take actions to drastically reduce GHGs emissions. In addition, the fossilization process required to produce petroleum occurs in a geological timescale. To tackle these issues, biorefinery processes emerged in the past decade to generate chemical building blocks, biofuels and polymers from terrestrial plants and in particular lignocellulosic biomass. On a more European level, biorefineries could allow a partial independence from the massive use of petroleum derivatives.

As regards to the climate and oil-depletion concerns, the issues relative to human health and environmental pollution lead to new regulations. In 2006 the REACH legislation was ratified (Registration, Evaluation, Authorization and restriction of Chemicals). Nowadays, all chemicals manufactured and/or imported in Europe for volumes superior to one ton per years need to be registered to the ECHA (European CHemical Agency). The health and environmental risks of the registered chemicals may lead to high restrictions. The monomers required for the production of thermosetting resins fall under the REACH legislation. Indeed, these resins are widely employed in structural applications (furniture, transportation industry, …). Phenols, melamine, urea and formaldehyde are among the most commonly employed raw materials for thermosetting resins. Yet some of these compounds may be harmful to humans. For instance, the emission of the carcinogenic formaldehyde from furniture will be severely limited by 2026. [1] Similarly, melamine is on the list of the substances of very high concern (SVHC). Phenols are also concerning compounds.

Yet, phenol, melamine, and formaldehyde are all commonly employed in the manufacture of thermosetting resins for structural purposes. Their excellent properties take roots in the rigidity of their molecular structure, especially the aromatic ones. Few sustainable alternatives are available. Lignins, polyphenols and tannins from woody biomass are promising alternatives. In addition, furanic molecules, such as furfuryl alcohol are also in the spotlight.

Furfuryl alcohol (FA) is one of the only compounds only manufactured from biomass in high volumes. It is produced from agricultural wastes, mainly sugarcane bagasse. FA can polymerize into poly(furfuryl alcohol) (PFA), a thermoset with properties somewhat similar to phenol, formaldehyde and melamine resins. Furfuryl alcohol is labeled both toxic and CMR. Nonetheless, FA can be oligomerized and the residual FA removed. This allows the production of low VOC resins. In addition, FA is exclusively produced from biomass, more specifically from agricultural wastes. Hence, PFA could be a sustainable alternative to the aforementioned resins.

In the line of furanic compounds, industrial humins are produced as a side product of sugar conversion into furanic building blocks. One promising route of valorization is the use of humins as thermosetting resins. Humins are structurally close to PFA, i.e. a tight network of furanic units. As a consequence, they share the same features, i.e., thermostability, difficult processing and brittleness. This PhD manuscript focus on the possibilities available to tune the properties and therefore provide new potential applications for both humins and PFA.

The chemistry of furanic thermoset networks (e.g. PFA, humins) is complex. This is especially true for the humins as the biorefinery feedstock affects their structure. Hence, PFA will be employed as a model. Its chemistry is also complex and comprises many features. The chemistry of PFA mainly revolves around the self-polycondensation of furfuryl unit crosslinked together via Diels-Alder cycloaddition. Yet, a number of other reactions occur during the polymerization (ring opening, conjugaison, formation of methyl and esters, …). One of them is the ring-opening side reaction which leads to carbonyls.

The ring-opening reaction is a feature stemming from the unique reactivity of furanic macromolecule. Yet, the ring-opening side reactions were often neglected and disregarded. Therefore, a gap of knowledge is present in this area.

The aim of this PhD manuscript is to take advantage of the carbonyls generated within the furanic network using PFA as a model in the scope of the project ANR JCJC FUTURES (FUranic TUnable REsins for Sustainable materials).

Objectives of the thesis

Exploiting the carbonyls formed within PFA and humins requires key knowledge on their occurrence. How many carbonyls are present and when do they form? Can the carbonyls be accurately and reproductively quantified? What are the leverages available to promote the furan ring-opening? In addition, precise knowledge on the chemical environment of the carbonyls is required to fully exploit their reactivity. Once the answers to these questions are established, the carbonyls present in PFA could be prone to chemical derivatization. To do so, this manuscript aims to pave the way to the functionalization of carbonyls, mainly using their reactivity with amines. Once the feasibility of the functionalization of PFA's carbonyls will be proved, the properties of the resulting materials will be assessed. In other words, is it possible to achieve new amine functionalized PFA materials? Could their brittleness be mitigated? What is the array of properties achievable through amine-functionalization? Are they recyclable? Can the thermal stability of PFA be maintained?

The scheme on the next page summarizes the major objectives of the FUTUREs project.

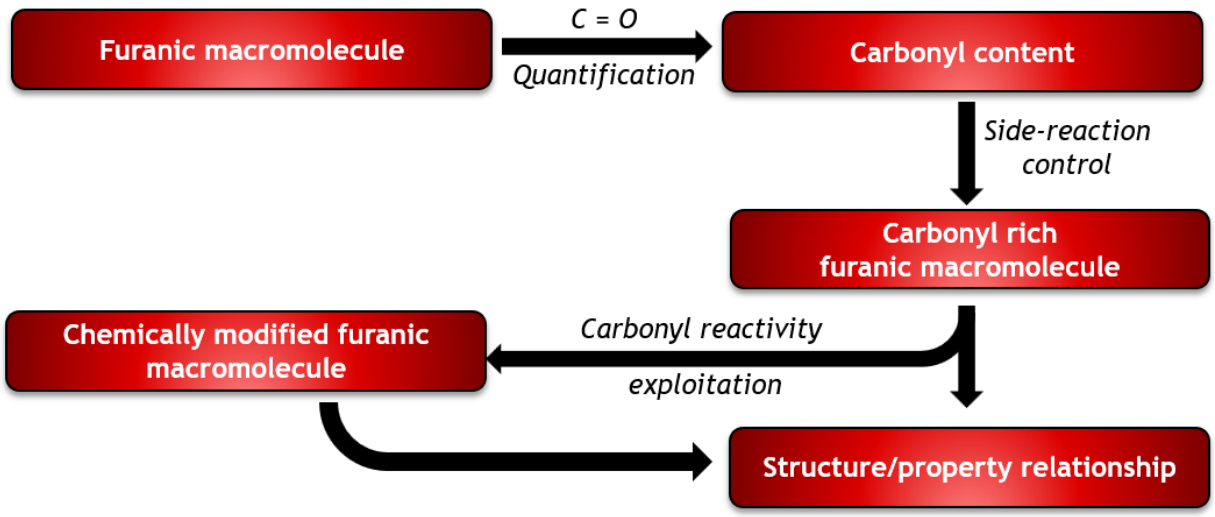

Outlines

Chapter 1 briefly contextualizes the current approaches to produce chemicals and materials from renewable resources. In this chapter, a specific state of the art on poly(furfuryl alcohol) applications, FA's polymerization mechanism and PFA's chemical structure and general features will be also reported.

In chapter 2, methods for quantifying the carbonyl content in PFA systems are developed. The carbonyls are quantified during the polymerization to establish their formation schedule. In addition, the leverages available to influence and optimize the carbonyl content of PFAs are explored.

Chapter 3 deals with the chemical environment of the carbonyls within PFA. Spectrometric investigations are employed to locate the carbonyls in PFAs' structures. The sensitivity of some furans towards oxidation is also highlighted and a new oxidation-induced surface crosslinking pathways is proposed.

Chapter 4 focuses on the structural evolution of PFAs upon heating under inert and oxidative atmospheres. It aims at bridging the gap of knowledge regarding the structure of PFA between its polymerization and its graphitization. The effect of oxidation-induced surface crosslinking on the materials' properties is assessed.

Chapter 5 explores the possibilities of functionalization offered by the carbonyls within PFA. This chapter exploits the reactivity of carbonyls with primary amines. After a proof of concept, the influence of several factors is determined. Namely, the amines structures, the post-curing environment, the advancement of PFA's polymerization and the influence of bases on furfuryl alcohol's acid-catalyzed polymerization.

Chapter 1. State of the art

1.1 2nd generation biomass: from wastes to value added products

1.1.1 Petroleum-based products at the crossroad of ubiquity and concern

Since the late 1800s there has been a significant improvement in the life expectancy and overall quality of life for people worldwide. The industrial revolution allowed this change through a facilitation food production to sustain a growing population, the development of drugs to improve health, and modern comfort. In all these examples, the petroleum products played a crucial role either in the form of feedstock for the syntheses of fertilizers and drugs, in the form of fuels to motorize agriculture and transport goods, in the form of polymers to produce vehicles, machines and everyday household appliances.

However, in the past decades, concerns on the negative impacts of the petroleum industry rose dramatically. One ecological concern is the widespread burning of petroleum products in motorized vehicles or in heat and electricity generation (Table 1.1-1). [2] Consequently, carbon dioxide, methane and other greenhouse gases are massively liberated and are increasingly disturbing the climate balance.

Table 1.1-1. Oil demand by sector, built on 2021 data from the organization of the petroleum exporting countries [2]

Sector	Share of crude oil demand (%)
Transportation	**56.2**
Petrochemicals	**14.2**
Other industries	**13.2**
Residential, commercial, agricultural	**11.4**
Electricity generation	**5.1**

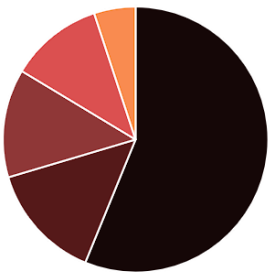

In addition to ecological concerns, petroleum oil is a non-renewable resource which will only deplete in the future. Currently, about 14 % of the crude oil is used by the petrochemical industry. These 14 % play a major role in our lives, in the forms of fertilizers, drugs, specialty chemicals and mostly plastics. Hence, new feedstocks and new value chains are required to reduce ou dependence on petroleum. Table 1.1-2 provides an overview of the uses of plastics by sectors, all directly impacting us daily. Synthetic polymers are ubiquitous, they are found in the packaging used to increase food's lifespan, in our furniture either as a load-bearing elements or as glues, in paints, electric and electronic equipment biomedical implants and goods, textiles, vehicles and even in the coating of the cover of this manuscript. Mankind could decide to ban all these items to annihilate petroleum-induced issues. Yet, very few people would be willing to do so. Hence, new feedstocks and new value chains are required to reduce our dependance on petroleum.

Table 1.1-2. Shares of plastics production by Sectors, built on data from 2015. [3]

Sector	Share of plastics production (%)
Packaging	35.9
Construction	16.0
Textiles	14.5
Others	11.5
Consumer products	10.3
Transportation	6.6
Electrical, electronic	4.4
Industrial machinery	0.7

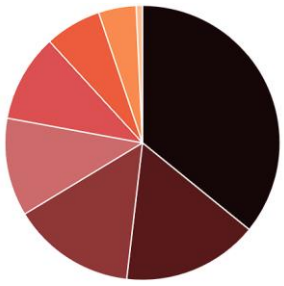

In addition to the depletion of fossil resources and in a more local context, European countries are highly dependent on both petroleum and petroleum exporting countries. Indeed, as detailed in Table 1.1-3, the crude oil production of Europe account for about 5 % of the world's production.

Table 1.1-3. World crude oil production by region, build on 2010 data from the US Energy Information Administration. [4]

Area	% oil of production
Middle East	30.7
Former Soviet Union	17.0
North America	14.6
Africa	13.5
Asia	9.8
Central & South America	8.7
Europe	5.1
Oceania	0.7

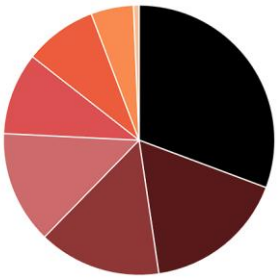

Yet, Europe is far from covering its needs by local production only. As a matter of facts, in 2021, Europe imported about 7.6 million of petroleum barrel per day which translates to about 1 000 000 tons per day. [5] Therefore, increasing the share of renewable and locally available resources is essential to ensure Europe's security and independence in the face of future geopolitical perturbations and ultimately the depletion of fossil resources. In the following sections, the possibilities offered by living biomass, i.e. "carbons above the ground" to produce renewable chemicals and materials are overviewed.

1.1.2 Current and future opportunities for renewable feedstocks

Renewable resources can be classed in several manners. One approach is to consider land use and edibility of the biomass. The biofuel industry commonly agrees on four generation of biomass, although one could extent this vision to all chemicals. They are illustrated in Figure 1.1-1.

The first generation corresponds to the use of edible biomass, such as starch (found in corn, wheat, …), to produce chemicals primarily through fermentation processes. It is the most developed generation with well-established industries such as Roquette Frères, NatureWorks or Total Corbion. For example, ethanol can be made in that manner to substitute or complement fuels. As well, polymers such as poly(lactic acid) and bio-based poly(ethylene) may also be manufactured

from edible biomass. Although the chemicals from edible biomass are renewable, their production enters in competition with the production of food and impact its price. Furthermore, the reduction of GHGs may not be guaranteed when chemicals are sourced from renewable feedstocks. This is especially true in the case of not yet optimized production processes. [6] [7]

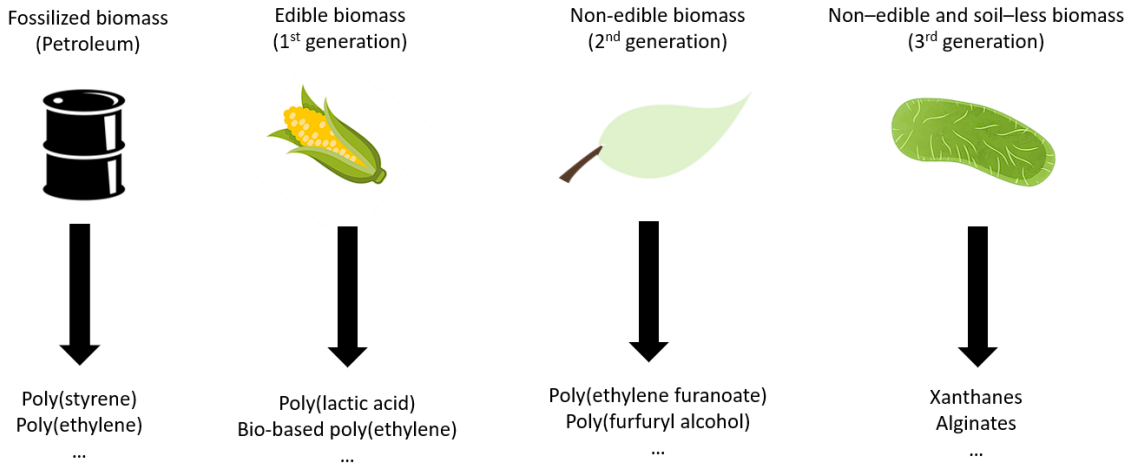

Figure 1.1-1. Available and developing routes for the production of chemicals

The second generation encompasses resources obtained from non-edible biomass. Typical examples include wastes from crop production such as sugarcane or corn bagasse. Some chemicals such as furfural are produced by this route since decades. Yet, the production of other building blocks is still largely at laboratory or pilot scale. The furanic molecules emerging from the second-generation biomass often require a reduction reaction to be used as fuels. [8] The products and value chains from this generation will be further detailed in section 1.2.

The third generation involves the non-edible and soil-less biomass. This route tames microorganisms such as algae and bacteria to produce chemicals. In most cases, the production of chemicals by this route is at a laboratory or pilot scale. Nonetheless, some polymers like xanthans, alginates and poly(hydroxy alkanoates) are produced for the food, pharmaceutical and cosmetic industries. [9]

The third generation is highly promising as the yield of chemicals per m^2 is higher than the other routes. [6] A fourth generation is emerging and utilizes genetic modifications to tailor the outputs of the third-generation biomass.

Another classifying method for renewable feedstocks is their fractionation in the key intermediates obtained from biorefineries. The International Energy Agency reported a series of major platform molecules. It should be noted that these intermediates are rarely single molecules but rather complex mixtures. Among the platforms, one can find pyrolysis oils, CO_2, synthetic gases, bio-oils, organic solutions, lignins and sugars. [10] To stay in the scope of this manuscript only the sugar and lignin platforms are discussed in the followings.

1.1.3 Lignocellulosic biomass

Before delving into the outputs of the sugar and the lignin value chain, a brief contextualization of their origin is helpful. The sugars and lignins come from the lignocellulosic biomass which constitute the major portion of the terrestrial plant kingdom. The macro-organization of plants is both complex and varying between species, thus it is not discussed here. However, some key physico-chemical features are given.

First, the lignocellulosic biomass is composed mainly of three main macromolecules: cellulose, hemicellulose and lignin. Cellulose is organized in microfibrils and gives the mechanical strength of plants. Lignins is the matrix embedding the cellulose fibrils. It brings hydrophobicity and further enhances the plants' structural integrity. [11] Finally, the hemicelluloses act as a compatibilizer between cellulose and lignin. They are chemically linked to lignin chains and interact trough hydrogen bonds with the celluloses. [12] A simplistic illustration of this organization is provided in Figure 1.1-2. The interplay between the components of lignocellulosic biomass are source challenges for biorefinery as these physical interactions and chemical bonds need to be broken to produce platform chemicals. Furthermore, side-products are often generated during the treatment of the lignocellulosic biomass. This decreases the yields and it introduces a need to valorize the side-products.

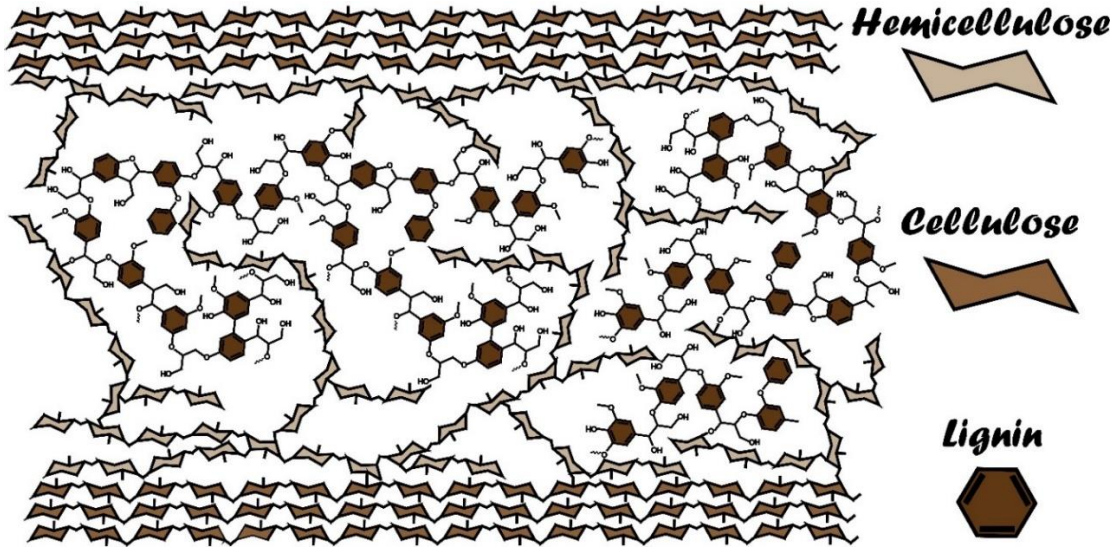

Figure 1.1-2. Illustration of the organization of celluloses, hemicellulose and lignins in lignocellulosic biomass. Drawing inspired by a previous illustration from Koddenberg et al. [13]

In terms of composition, significant variations are found between the plants as detailed in Table 1.1-4. Hence, biorefineries need to adapt their processes to accommodate the specificities of each feedstock. The feedstock composition is dependent both on the plant species and its growth conditions. The structures and applications of the three main macromolecules of lignocellulosic biomass are briefly reviewed in the following sections.

Table 1.1-4. Examples of lignocellulosic biomass composition

	Cellulose (%)	Hemicellulose (%)	Lignin (%)	Reference
Hardwood[i]	40 – 55	24 - 40	15-25	[13, 14, 15, 16, 17]
Softwood	40 - 50	25 - 35	25-35	[13, 14, 16, 17]
Agricultural residues[ii]	25-45	12-36	6-25	[17]
Grasses	25-40	35-50	10-30	[17]

[i] Hardwoods typically have broad leaves and are denser and darker and grow slower than softwoods. Hardwoods include species such as oak, elm, birch. Softwoods are conifers such as pine, fir, spruce, …

[ii] Values for: wheet straw, rice straw/husk, barley straw, oat straw, corn cob/stalks, sugarcane bagasse

1.1.3.1 Cellulose

Cellulose is the most abundant natural polymer. The structure of cellulose consists in a linear arrangement of D-glucose units. The most common structure is the α-1,4 cellulose, depicted in Scheme 1.1-1. [11]

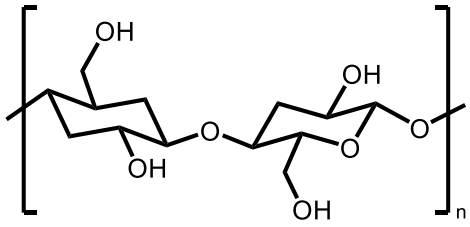

Scheme 1.1-1. Chemical structure of cellulose (type α-1,4)

Applications of cellulose developed through the ages, exploiting the properties of cellulose at different scales as illustrated by Scheme 1.1-2. The development of cellulose-based products began with use of fibers for textiles, followed by the rise of the paper industry. Then, the scope of cellulose uses expanded through the exploitation of its chemical reactivity. [18] The chemical derivatization of cellulose began with its nitration to nitrocellulose in the 1850s. Nitrocellulose was used as an explosive at that time and later found coating applications in the automotive and wood industries. [19] Once discovered possible, the chemical modifications of cellulose led to many cellulose-derived polymers still used nowadays. While the list is long, relevant examples include cellulose acetates mainly employed as membranes and filters [20] and carboxymethyl celluloses as rheology modifiers in food, paints, as well as uses in drug delivery systems. [21] Other examples of cellulose derivatives include cellulose sulfates, nitrates and ethyl/methyl cellulose and so forth [22] The uses of nano/micro fibrillated celluloses also gained interest in the past years. However, their production still faces challenges to reduce to production costs, energy consumption and routes to mitigate the hydrophilicity of the fibers. [23]

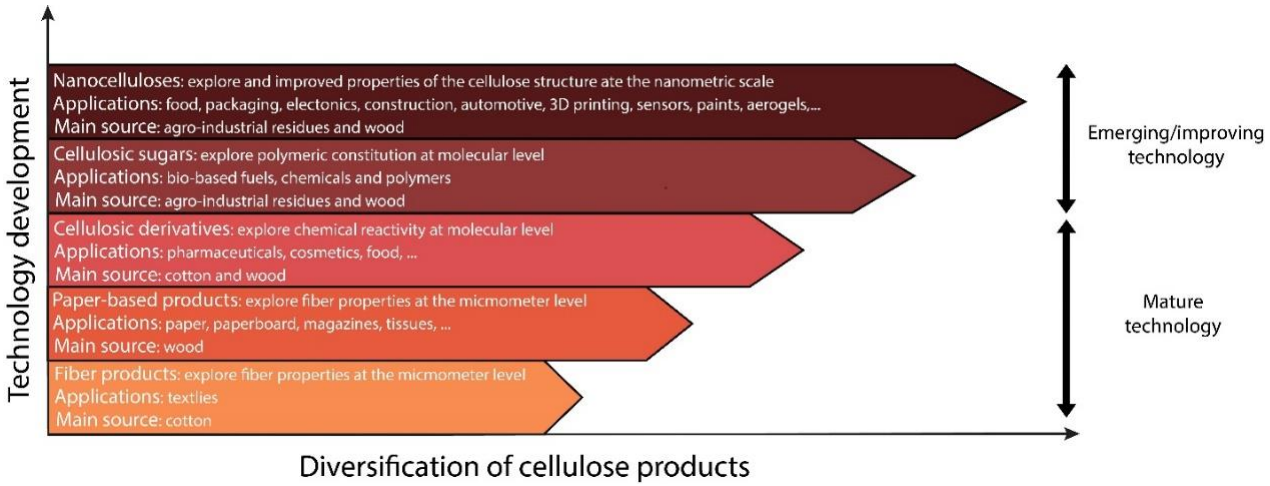

Scheme 1.1-2. Cellulose based products technologies development, adapted from Arantes et al. [18]

In contemporary times, research shifted towards increasingly complex applications such as cellulose nanocomposites [24,25], humidity sensors [26] or additive manufacturing. [27] Another important field is the decomposition of cellulose to ethanol for biofuels to reduce petroleum consumption and mitigate greenhouse gases emissions. [28,10] At last, cellulose can be used as a feedstock for the renewable production of platform chemicals. [10,29]

1.1.3.2 Lignin

The term "lignin" is a generic term to describe the products from the condensation of phenolic compounds called "monolignols". The most common ones are depicted in Scheme 1.1-3.

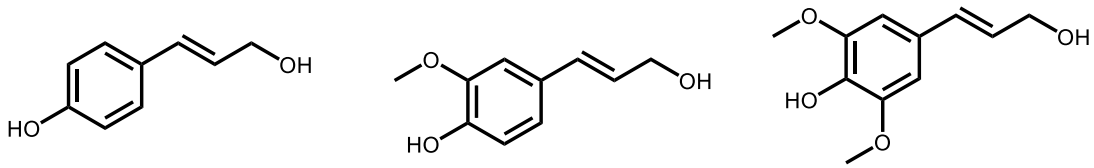

p-Coumaryl alcohol *Coniferyl alcohol* *Synapyl alcohol*

Scheme 1.1-3. Most common lignin precursors

Lignin is the most naturally abundant aromatic polymer on earth. [14,11] The chemical structure of lignin is both complex and highly dependent on the botanical origin. [30] An example of structure is provided in Scheme 1.1-4 although it is not representative of all the lignins, the main functional groups and linkages are depicted. The technical lignins are a sub-group of the lignins. Technical lignins are mainly generated as byproducts of the paper industry and the production of cellulosic ethanol. [10, 31, 32] In terms of uses, more than 95 % of the technical lignins are burned for energy recovery purposes. [10, 32] However, technical lignin derivatives called "lignosulfonates" are an established product in the construction market, especially as concrete admixtures. [31,32]

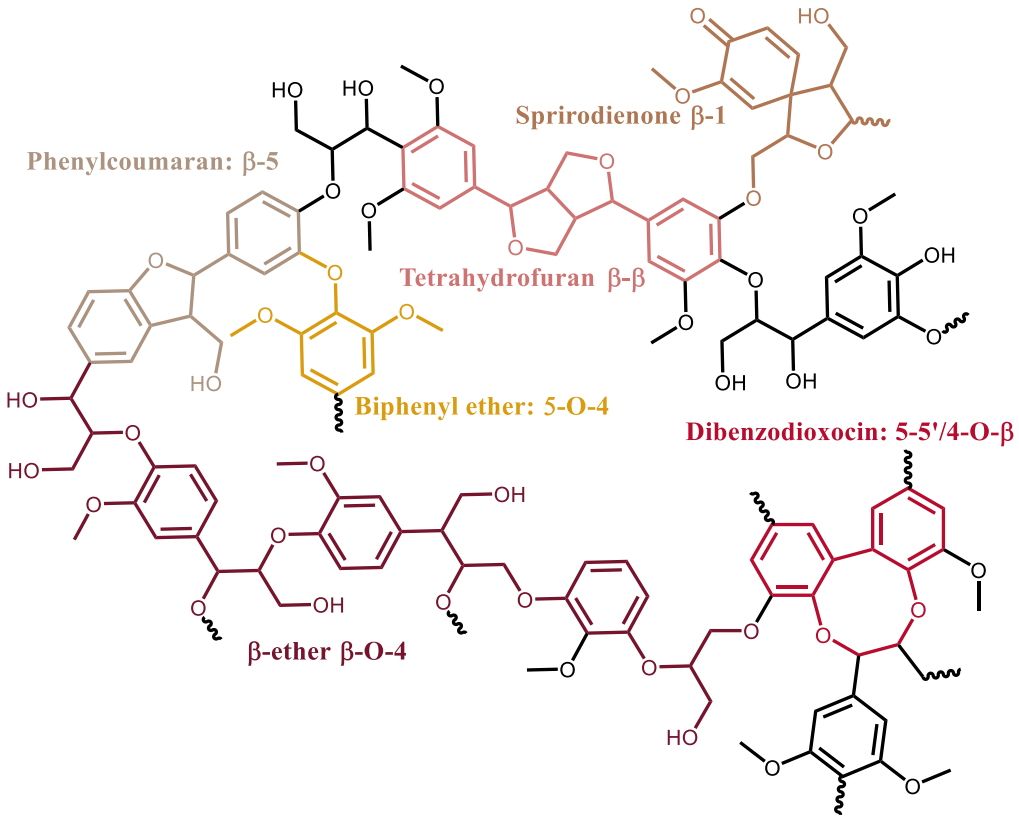

Scheme 1.1-4. Example of lignin structure with some linkages, based on Ralph et al. [30]

Considerable resources are dedicated to the valorization of lignins. Ongoing research examples include the use of technical lignins in composites, in lead acid batteries, as dust suppressant, metal adsorbents, flocculants, or additives in polymers. [31, 33] Yet, the main field of research is the depolymerization of lignins. [14, 34] Depolymerizing technical lignins yields a variety of aromatic compounds which allow an increase in reactivity. The resulting monomers may be repolymerized to biobased polymers with properties competitive with conventional ones. [35, 36] Lastly, the removal of functional groups allows access to aromatics such as benzenes, naphthenes and other hydrocarbons. [34]

1.1.3.3 Hemicellulose

"Hemicellulose" is a general term originally proposed to refer to the extractable substances of plant cell walls under basic conditions. Nowadays, it is used to designate the non-cellulose polysaccharides parts of the plant's cell walls. The hemicelluloses are a mixture of six and five carbon saccharides and are typically connected with cellulose and lignin. The hemicelluloses can be divided in four main groups: the xyloglucans, xylans, mannans and β-glucans. Scheme 1.1-5 gives a general structure with the various linkage found in xylans, including the ferulic acid which serves as a covalent bridge to connect with lignin. [11, 14]

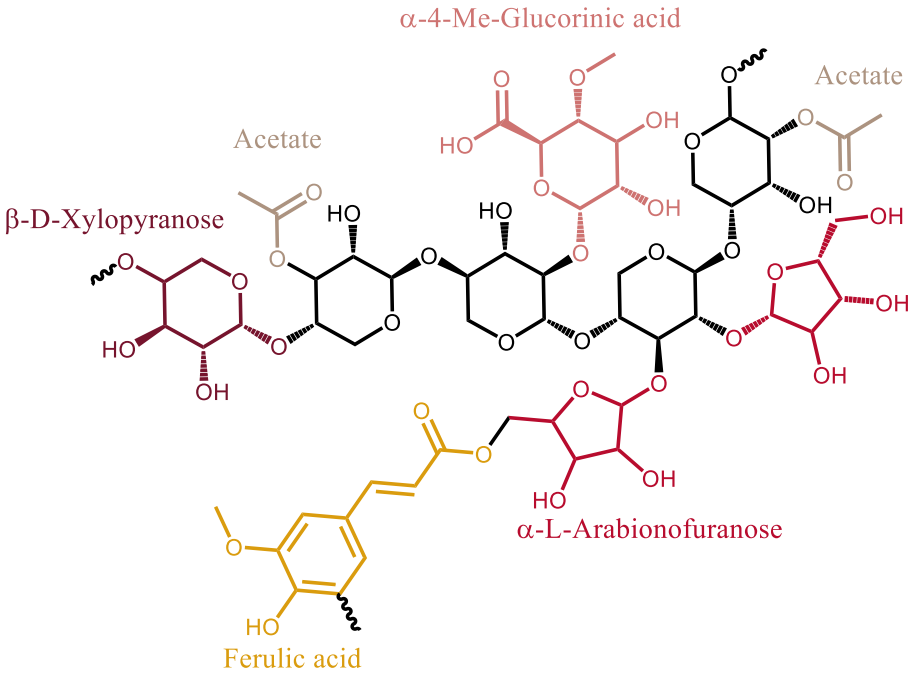

Scheme 1.1-5. General structures of the various linkages found in a variety of xylan isolated from plant cell walls. This structure was adapted from Wertz et al. [11]

The direct applications of hemicelluloses are currently limited by the high-cost associated with their extraction and purification. [37, 12] Ongoing research aims to use native or derivatized hemicelluloses in packaging, cosmetics, food additives, biochar and drug delivery. [38, 39, 37, 12] Finally, as in the case of cellulose and lignins, hemicelluloses are investigated as a renewable feedstock for the production of fuels and platform chemicals. [10, 29, 37]

1.1.3.4 Concluding remarks on the lignocellulosic biomass

Among the options available to substitute fossil feedstock for renewable ones, the lignocellulosic biomass offers an array of opportunities and challenges. The major challenges include the selectivity of chemical reactions, the need for depolymerization and reduction of both polysaccharides and technical lignins. In the followings, some of these aspects will be discussed through the specific examples of furanic building blocks obtained from polysaccharides.

1.2 Furan Value Chain

Furanic compounds can be obtained from the lignocellulosic biomass via two routes. First, the hexose route is briefly reviewed followed by the pentose one.

1.2.1 Production and uses of furanic compounds from hexoses

One of the main furanic compound derived from hexoses is 5-hydroxymethylfurfural (HMF). HMF can be obtained from a triple dehydration of hexoses, as shown in Scheme 1.2-1. HMF is composed of three functional groups, an aldehyde, an alcohol and a furan heterocycle.

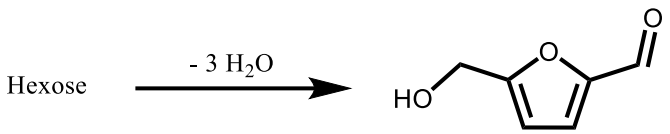

Scheme 1.2-1. Dehydration of hexoses to HMF.

In 2023, the market of HMF is still small with between 10 to 100 tons manufactured and/or imported in Europe each year. [40] Yet the high functionality of HMF allows a wide range of derivatives and promising applications. [41] Laboratory scale examples include the mild oxidation of HMF to furan-2,5-dicarbaldehyde. This dialdehyde was polymerized with amines to produce polymers with physical and chemical reprocessability. [42] HMF may also partially substitute formaldehyde in urea/formaldehyde resins. In addition, HMF and derivatives may be incorporated in other polymeric networks such as, poly(urethanes) or poly(acrylates). [43]

A more mature application of HMF derivatives is the production of poly(ethylene furanoate) (PEF). PEF is advertised by the Avantium company as a replacement for poly(ethylene terephthalate), one of the most produced polymers (Mtons per year). In comparison with PET, PEF has the advantages of higher barrier properties, i.e., longer storage capability of food and beverages, higher T_g and elastics modulus. Moreover, PEF is compatible with the current shaping processes of PET. [44, 45, 46]

Additionally, PEF is compatible with the current recycling streams of PET.[47] Nowadays, the production of PEF is at the pilot scale. The process uses the methoxylated version of HMF (5-(methoxymethyl)-2-furaldehyde) which is oxidized to 2,5-furandicarboxylic acid (2,5-FDCA). 5-(methoxymethyl)-2-furaldehyde is employed instead of HMF for stability purposes. More specifically, the ethers of HMF form much faster than HMF decomposes under the acid conditions required for its formation. In addition, ethers of HMF are much less susceptible to ring-opening reactions and condensation into humins. [48] 2,5-FDCA is then copolymerized with ethylene glycol to reach PEF. The route to PEF is illustrated in Scheme 1.2-2.

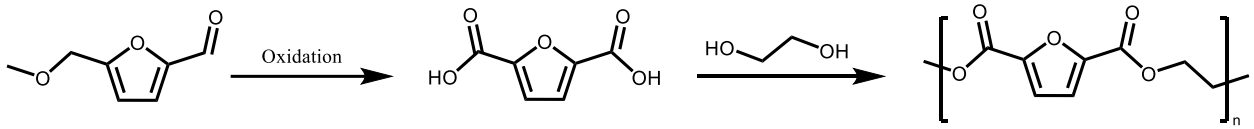

5-(methoxymethyl)-2-furaldehyde *2,5-furandicarboxylic acid* *poly(ethylene furanoate)*

Scheme 1.2-2. Synthesis route of PEF from 5-(methoxymethyl)-2-furaldehyde.

Furan compounds are sensitive to ring opening reactions. Hydrolysis of HMF, yields levulinic acid (LA) and formic acid. If HMF is open in alcoholic solvent or if an ether form of HMF is used, alkyl levulinates are obtained. On one hand, methyl levulinate is a co-product of the sugar conversion to 2,5-FDCA in the Avantium process. [47] On the other hand, levulinic acid is produced by the petrochemical industry in relatively small volumes and from furfural in even smaller volumes. The yearly volumes of LA manufactured and/or imported in Europe are between 100 to 1000 tons. [49]

Nowadays, LA has a few applications in the pharmaceutic, cosmetic and food industries. [50] Yet, more than a decade ago, LA was identified as one of the most promising platform chemicals and its potential still holds true today. [10, 51, 52] Indeed, the carboxylic acid and ketone functionality of LA enables a wide range a derivatization and some of them are depicted in Scheme 1.2-3. LA can be transformed into specialty chemicals such as halogenated or amino compounds, acrylates, ketals, alcohols, carboxylic acids and so forth.

The highest potential of the levulinate derivatives resides in their performance as fuel additives. Indeed, the C1 to C4 esters of LA were labeled “sustainable fuel additives”. They generally increase fuel properties such as the cold flow, spark property, flash point, stability and so forth. [53]

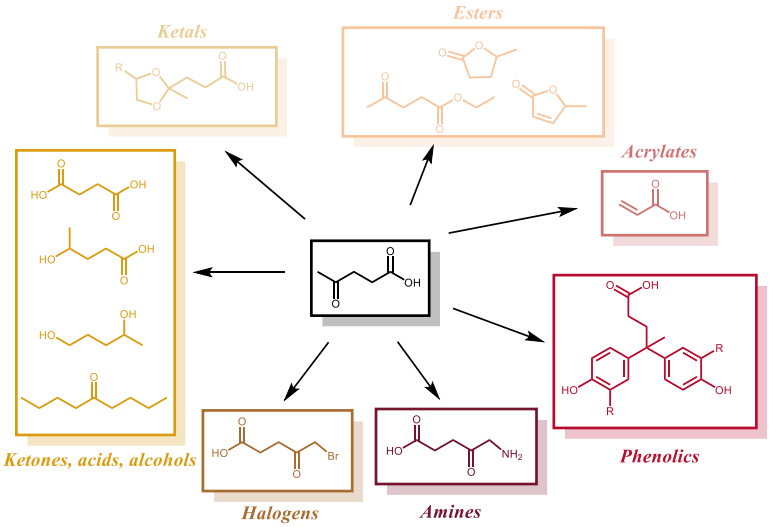

Scheme 1.2-3. Examples of levulinic acid and levulinate derivatives. [50, 54]

1.2.2 Production and uses of furanic compounds from pentoses

The five carbon saccharides within hemicellulose can be exploited for the production of furanic compounds. The biggest markets for the furan from hemicellulose are the furfural and furfuryl alcohol markets.

1.2.2.1 Furfural

Furfural or 2-furaldehyde (CAS 98-01-1) is among the few organic compound which are only produced from renewable feedstocks. The manufacture of furfural through the biomass route is often reported as more economically competitive than the petroleum route although it is not specified how much. [7, 55, 56, 57]

Chemically, furfural is composed of a furan heterocycle moiety and an aldehyde group, as shown in Scheme 1.2-4. It is a good example of a naturally occurring compound which can be harmful to humans.

Furfural is found at low concentrations in coffee, tea, cocoa and some fruits. [55] In addition, furfural participate in the smell of old books. [58] However, furfural is labeled as a toxic and CMR (carcinogenic, mutagenic and/or reprotoxic) substance. It's sister molecule, furfuryl alcohol suffers of the same safety issues. Hence, these compounds need to be handled carefully. Fortunately, such safety issues can be circumvented in the case of polymerized FA, as discussed later in section 1.3.1.

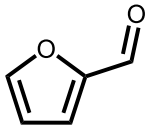

Scheme 1.2-4. Chemical structure of Furfural.

Starting from the beginning, furfural was discovered in the 19th century. The large-scale production of furfural began in the early 1920s with the Quarker oats company. At the time, the goal was to valorize cereal side-products, *i.e.*, oat hulls. [55, 56] Nowadays, it is estimated that 200 000 to 360 000 tons/year of furfural are produced worldwide, mainly from corn cobs and sugarcane bagasse in China, Dominican republic and South Africa. [7, 10, 56] According to the ECHA, furfural is registered for manufacture and/or import volumes between to 10 000 and 100 000 tons each year in the European economic area. [59] The production of furfural usually follows the steps depicted in Scheme 1.2-5.

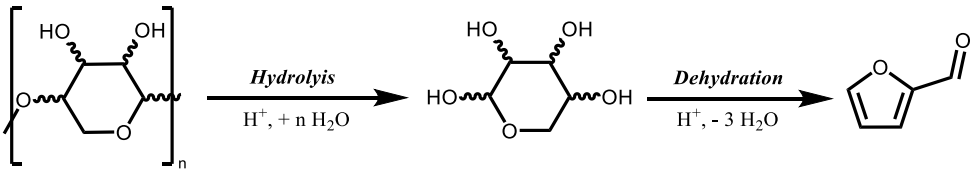

Scheme 1.2-5. Illustration of the two-step production process of furfural.

First, the hemicellulose in the biomass is hydrolyzed to pentoses. The second step consists in the dehydration of monomeric sugars to furfural. These steps are usually carried out with non-oxidant mineral acids and at temperatures between 150 – 190 °C. [55, 56, 60] Usually, furfural is continuously evacuated by steam distillation to limit the formation of side-products. [56]

In terms of yields, the literature reports that around 45-50 %w of the pentoses are converted to furfural for most processes [55, 60]. The main feedstocks, i.e., corncobs and sugarcane bagasse, comprise up to 30 %w of pentosans. Consequently, the yield of furfural is below 20 %w, with respect to the dry biomass. More recently, the Biofine process tackled the yield issue by developing units capable of coproducing furfural, formic acid and levulinic acid. This aims at increasing economic and ecological viability. [32, 61] According to Hoydonck et al. and Zeitsch et al., the major factor limiting the yield of furfural is the product from the acetalization of furfural, depicted in Scheme 1.2-6.[55, 57] The acetals, saccharides and other side-products may condensate to give furan bearing macromolecules called humins, an infamous biorefinery side-product. [7, 32] More details about humins are provided in section 1.2.4.

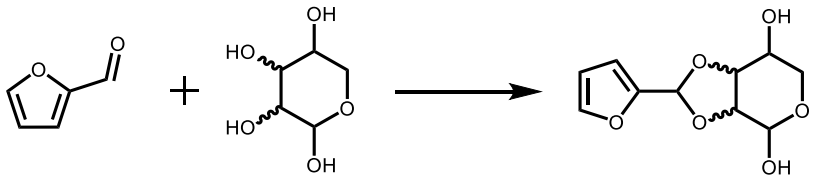

Scheme 1.2-6. Acetalization of furfural, adapted from. [55, 57]

Current research on the production of furfural is focused on the improvement of the furfural yield, diminution of steam requirements and uses of less corrosive catalysts. [60] In addition, water/organic solvents biphasic systems are studied to separate furfural from the water and thus limit furfural's degradation and condensation reactions, i.e., humins. [7, 62, 63] Other works focus on increasing the selectivity either during the dissolution of the hemicellulose or the dehydration of the pentoses or both. [64]

Here, the goal is to preserve the cellulose and lignin so they can be used for other purposes. In this line, the coproduction of furfural with ethanol and lignin was techno-economically assessed. [65] Zhang et al. extensively reviewed articles investigating the production of furfural with innovative solvent systems and catalysts. [66] Another relevant field of research regarding the production of furfural is the mitigation of furfural pollution in waste water. [67]

Regarding its applications, furfural can either be employed directly or converted in other chemicals. An overview of the applications of furfural is available in Figure 1.2-1.

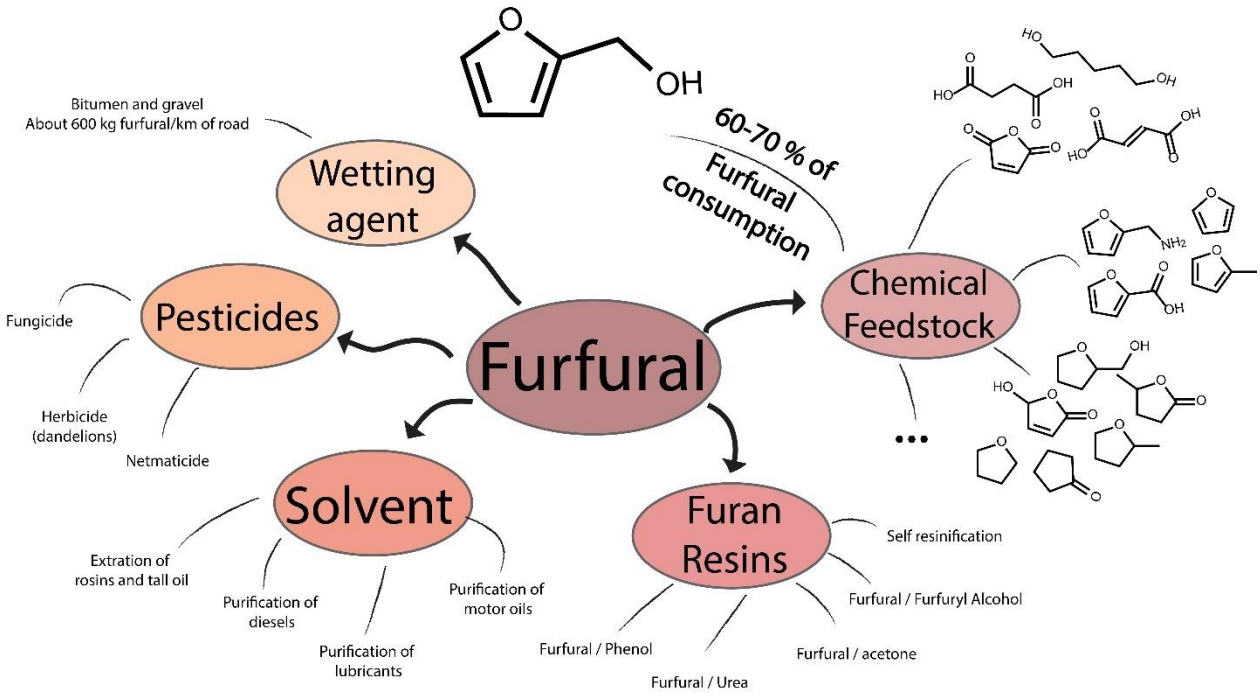

Figure 1.2-1. Applications of furfural. Scheme built on references. [7, 55, 57]

The direct applications of furfural are mainly as a solvent. Here, the ability of furfural to interact strongly with C=C bonds and weakly with alkyl compounds is exploited. Examples include the extraction of aromatic compounds in hydrocarbon systems such as lubricants, dyes, diesel, and so forth. In these cases, furfural is used for its high affinity with aromatic compounds and thus to remove them from the product. Another use of furfural as an extraction agent is to recover unsaturated molecules from vegetable oils or tall oil, a residue of the paper industry. [55, 57]

Furfural can be found in pesticides (fungicides, herbicides, nematicides). In addition, furfural may be used as a wetting agent in bitumen systems. In this case, furfural increases the binding strength between the bitumen and the gravel agent which induces a better cohesion and thus the road's lifespan. For this process about 600 kg of furfural are required by kilometers of road. [57]

Furfural can enter in the composition of furan resins. It may be alone or compounded with other molecules such as FA, urea, acetone, phenols and so forth. [7] On its own, furfural can polymerize overtime or when exposed to acids or bases. Gandini et al. reported the series of reactions in Scheme 1.2-7 as the major ones occurring during the resinification of furfural. [68]

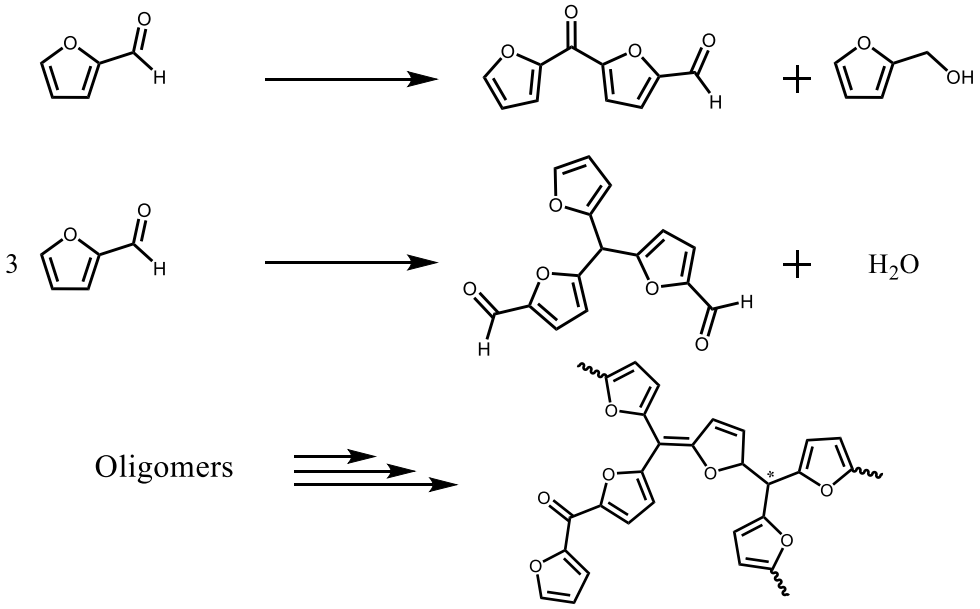

Scheme 1.2-7. Resinification of furfural, adapted from Gandini et al. [68]

Finally, furfural was highlighted as one of the most promising platform chemicals. [51] Thanks to its aldehyde group and aromatic reactivity, furfural can give birth to more than eighty molecules, some of them are depicted in Figure 1.2-1. [69] Nowadays, the majority of furfural is reduced to furfuryl alcohol. The synthesis and uses of FA are detailed in the next section of this chapter.

1.2.2.2 Furfuryl Alcohol

Furfuryl alcohol (FA) (CAS 98-00-0) is a colorless to pale yellow liquid. The chemical structure of FA is depicted in Scheme 1.2-8. .

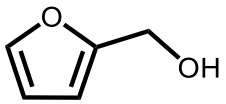

Scheme 1.2-8. Chemical structure of furfuryl alcohol.

Industrially, FA is produced through the hydrogenation furfural, mainly in vapor phase using copper-chromium catalysts with a selectivity superior to 99 % and yields above 95 %. The reaction is depicted in Scheme 1.2-9. [55] The production of FA represents 60 to 70 % of the worlds' consumption of furfural. [7, 10] In terms of volumes, between 10 000 and 100 000 tons of FA are manufactured and/or imported in Europe each year. [70]

The hydrogenation of furfural to FA is a well-established process. However, research is still conducted on this synthesis, especially to replace the chromium catalyst for less polluting ones. [71] Additionally, researchers are also looking for ways to produce FA directly from sugars in one-pot systems or using alternative solvents such as deep-eutectic solvents. [72, 73]

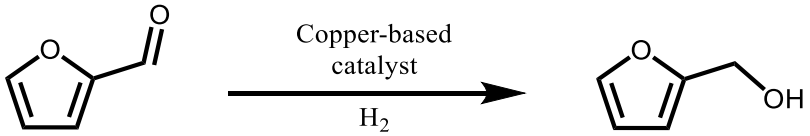

Scheme 1.2-9. Industrial synthesis of FA from furfural.

In terms of applications, the major use of FA is the manufacture of poly(furfuryl alcohol) and more generally furan resins. This subject is thoroughly detailed in section 1.3.1. FA also finds other uses as a solvent. It can be a reactive solvent in phenolic resins, a viscosity reducer for epoxy resins and a component of paint strippers. [55] The use of FA as an anti-freeze agent was also reported in the 1970s. [74] Furthermore, FA can enter in the composition of hypergolic mixtures. They were used to propel early French and American rockets. [57] Although FA-propelled rockets are more than sixty years old, research is still conducted nowadays to valorize its fuel wastes. [75] The fact that FA is able to form hypergolic mixture further supports the need for careful handling. This is especially true when exposing FA to strong acids and/or oxidizers.

Furfuryl alcohol can serve as a building block. Indeed, some compound such as tetrahydrofuran and an anti-ulcer drug (ranitidine) can be manufactured from FA. However, a promising use of FA as building block is the manufacture of levulinic acid. As detailed in section 1.2.1 LA is a promising platform molecule. It can be manufactured from HMF and also from FA. The mechanism of FA's opening to LA was investigated by Gonzales et al. and their suggested mechanism is available in Scheme 1.2-10. [76] The manufacture of levulinate esters can also be performed using alcohols to yield alkyl levulinates. [77] In all cases, humins are produced and their structures might be close to PFA's.

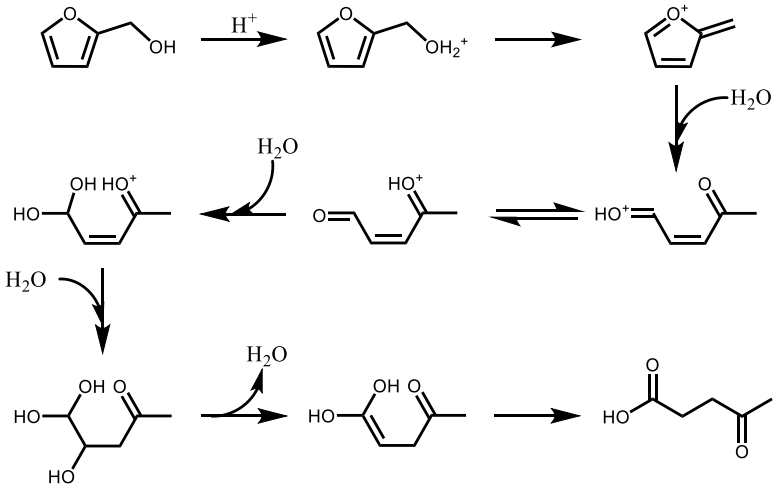

Scheme 1.2-10. Proposed mechanism for the ring opening of FA to LA in aqueous media. [76]

1.2.3 Routes from furan to molecules

To summarize, the lignocellulosic biomass is composed of lignin, cellulose and hemicellulose. The lignocellulosic biomass is a renewable source of aromatic compounds as well as sugars containing five or six carbons. These later can be into furanic compounds. Furanic compounds have a developing potential as chemical feedstock and already developed applications such as thermosetting resins. Figure 1.2-2 gives an overview of the value chain of furans, starting from lignocellulosic biomass.

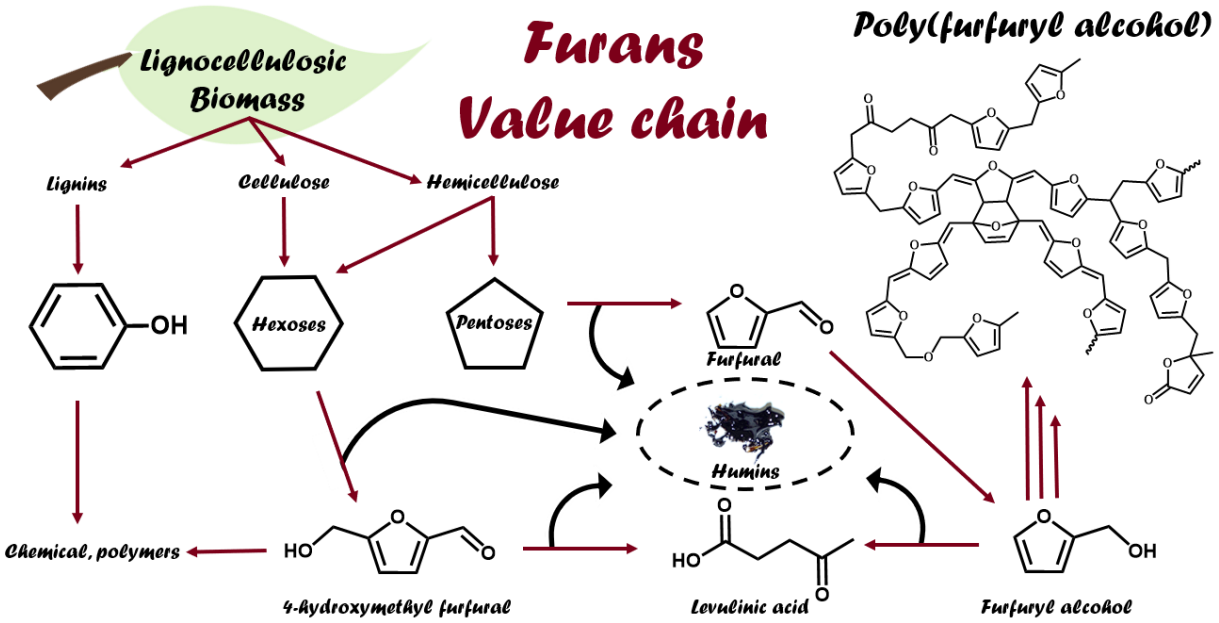

Figure 1.2-2. Simplified overview of the furan value chain.

In Figure 1.2-2, the routes to obtain previously mentioned molecules (furfural, FA, LA and HMF) are displayed. Additionally, the dark stain in the middle is genuinely unavoidable side product: the humins.

1.2.4 Humins as side products from the conversion of sugars into furans

The term « humins » can have several meanings. It can refer to the part of soil organic matter that remains insoluble in alkaline solutions. [78] In the context of this manuscript, the term "humins" is used to describe the variety of biorefinery side products from the treatment of lignocellulosic biomass. [41]

Humins can be formed through the condensation of sugars with dehydrated sugars, i.e., furans, in acid conditions. They are typically obtained in biorefinery processes aiming at the production of furanic molecules. The humins can also be the result of processes using furanic molecules as feedstock. Indeed, in acidic conditions furan-on-furan condensation reaction can occur. For example, humins are formed during the production of levulinic derivatives from furfuryl alcohol.

The structure of humins was extensively studied in the past decade, although a comprehensive understanding is beyond the scope of this section. [79, 80, 81, 82] Yet, it is worth mentioning that the structure of humins is variable depending on the chemical processes and feedstocks. Generally, the chemical structure of humins consists in furanic moities, conjugated and aliphatic moieties functionalized with ketones, aldehydes, alcohol and carboxylic acid. As examples, the proposed structure for xylose derived and glucose derived humins are displayed in Scheme 1.2-11.

Nowadays, humins are a constraint on the growth of economically viable biorefineries due to several unwanted effects. Firstly, the formation of humins reduce the yield of targeted products (LA, furans, …). Secondly, humins deposits can deactivate heterogeneous catalysts. Finally, humins complicate reactor design as they can cause plugging and fouling on the reactor walls. The deposits interfere with heat transfer and increase the maintenance of the reactors. [41] To address these issues, companies are looking for ways to decrease the yield of humins and/or altering their physical state. For example, Avantium uses alcoholic solvents in their process to obtain highly viscous humins instead of solid ones. [32, 47]

As humins are currently unavoidable, the humins are valorized trough heat generation or composting.[41, 47] Regarding the composting, an ecotoxicological study was performed on Avantium's humins and showed no immediate concern. [83]

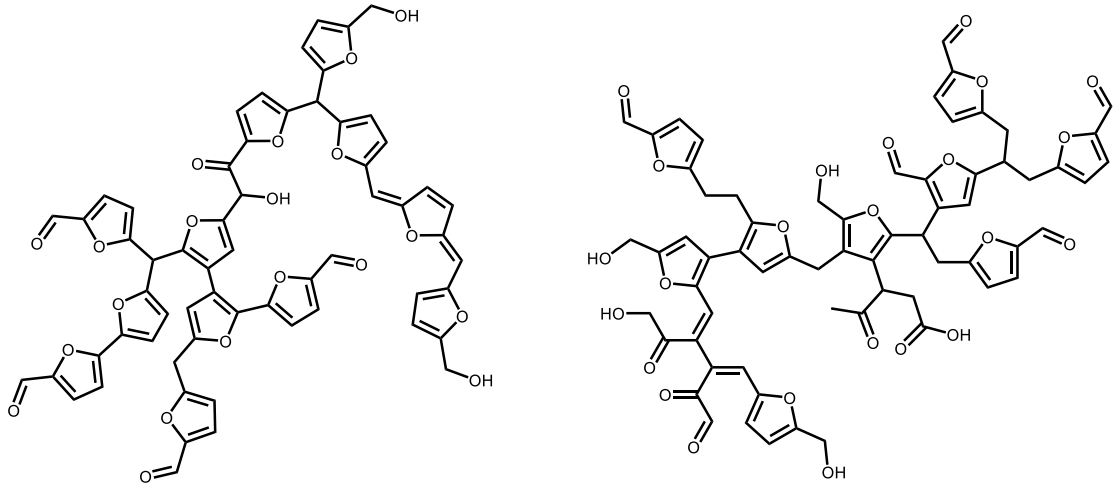

Xylose derived humins *Glucose derived humins*

Scheme 1.2-11. Proposed structure for xylose and glucose derived humins. [80]

Numerous studies focused on the valorization of humins. Examples include the use of humins as feedstock to produce formic and acetic acid by oxidation of humins. [84] The liquefaction of humins to produce biofuel additives or chemical feedstock was also foreseen. [85] The field of carbonaceous compounds also investigated the humins as precursor to microporous materials such as sorbents for wastewater or catalyst support, [86, 87] carbonaceous foams [88] or electrodes for supercapacitors. [89] In the material field, it was demonstrated that once thermally activated, humins behave as a thermosetting resin. [90] In addition, humins were studied in copolymerization with epoxies [91, 92], with FA in jute composite [93] with FA in cellulose composites [94], as wood reinforcing agent [95] or bitumen additives. [96]

The ANR JCJC FUTURES projects aims to pave to way for new means of valorization of humins. The ultimate goal of the project is to use the chemistry of the carbonyls in furanic macromolecules to provide new properties and therefore new applications. However, as the chemical structure of humins is highly dependent on the feedstock, poly(furfuryl alcohol) is used as a model. Indeed, PFA can be made with reproductible structure and in soluble and insoluble forms depending on the conversion degree of FA. These features will allow the development of robust C=O quantification protocols, furan ring-opening procedures and finally methods for preparing derivatized materials.

1.3 Poly (furfuryl alcohol)

Poly(furfuryl alcohol) being at the center of this manuscript, this section is dedicated to this polymer. First, both mature and developing applications of PFA are reviewed in section 1.3.1. As for section 1.3.2, it deals with the understanding of FA's polymerization from 1940s to nowadays.

1.3.1 Properties and applications of PFA

The polymerization of FA is detailed later in section 1.3.2. Briefly, PFA is composed of repeating furfuryl units densely crosslinked together by Diels-Alder cycloadduct. As the furan ring is sensitive to ring opening, some of the furans open into diketones. In terms of properties, PFA has attractive thermal and chemical resistance, which makes it suitable for various applications.

The main application of PFA and FA-based furan resins[i] in general is the manufacture of foundry molds. The fabrication of foundry molds typically involves 0.8 to 2 % of binder, the rest being aggregates. [97] The formulation of the furan resins may comprise FA alone, i.e., leading to PFA, or in combination with molecules such as formaldehyde, furfural, urea, phenol or resorcinol. The production of foundry molds and cores can be performed following several processes using numerous formulations. The conditions are dependent on the size of the molds, production volume, mechanical strength and type of metal or alloy desired. [98, 99] The pictures in Figure 1.3-1 illustrate the furan resin sand casting process.

Despite being a mature technology for more than half a century of existence, the furan resin-based casting molds remain an active field of research both in industry and academia. According to the European patent office, 35 patents were filled with the keywords "foundry" and "furan resin" in 2022, in China. [100] Examples of patents include 3D printing formulation and processes [101, 102], innovative formulation comprising furfuryl alcohol [103, 104], casting mold regeneration [105], innovations regarding the manufacturing process of casting molds [106, 107] and so forth.

[i] The terms "furan resins" englobe PFA and the mixture of FA and furfural with a multitude of compounds

In academia, research is oriented towards the improvement of the casting process, use of new additives and improvement of safety. Some examples include instruments capable of measuring the mechanical properties of molds at high temperatures [108], improvement of the casting quality [109], comprehension of gas permeability within the molds [110], uses of additives such as artificial sand [111] or saw dust [112], influence of resin formulations on casting quality [113] and the molds' mechanical properties [114], effect of reclaimed sand (i.e. recycled sand) [115], assessment of the release of aromatic compounds during the casting of metals [116] and the list goes on. In addition, 3D printing technologies using sand and furan resins are also investigated. [117, 118]

(A) (B)

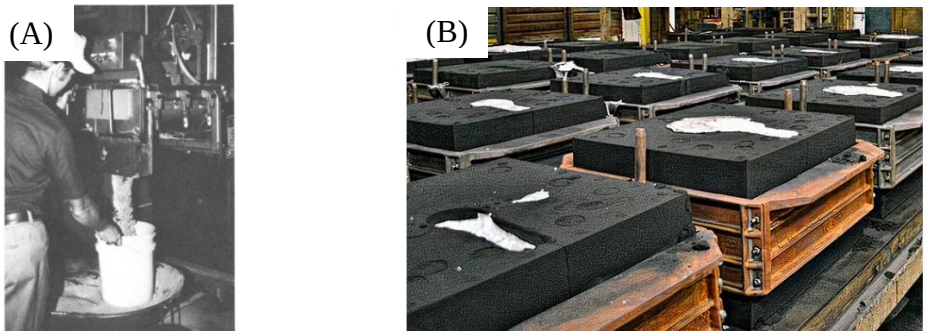

Figure 1.3-1. Pictures of a continuous foundry mixer taken before 1979 (A) [97] and furan resins casting molds nowadays (B).[119]

In the line of sand binders, furan resins have commercial applications as polymer concretes since the 1940s. Polymers concretes based on furan resins are used to manufacture setting beds capable of withstanding highly corrosive and hot environment. The formulations of mortars typically comprise about 30 % of resin while in the grouts it may go by up to 46 %. The rest of the formulation is usually silica aggregates or carbon flour. The furan-based polymer concretes are typically used as a setting bed for bricks including fire clay brick and carbon brick. While the fire clay brick are more resilient to thermal shock and physical impact, the carbon bricks are capable of resisting to hydrofluoric acid. More generally, the furan-based flooring systems can be employed in conditions where the floors are exposed to highly acidic or alkaline conditions, for example industries where harsh sanitizers are required. These systems are however not tolerant to oxidizers. [74, 97, 99]

Figure 1.3-2 showcases the fabrication and final results of furan-based flooring before 1979 and nowadays.

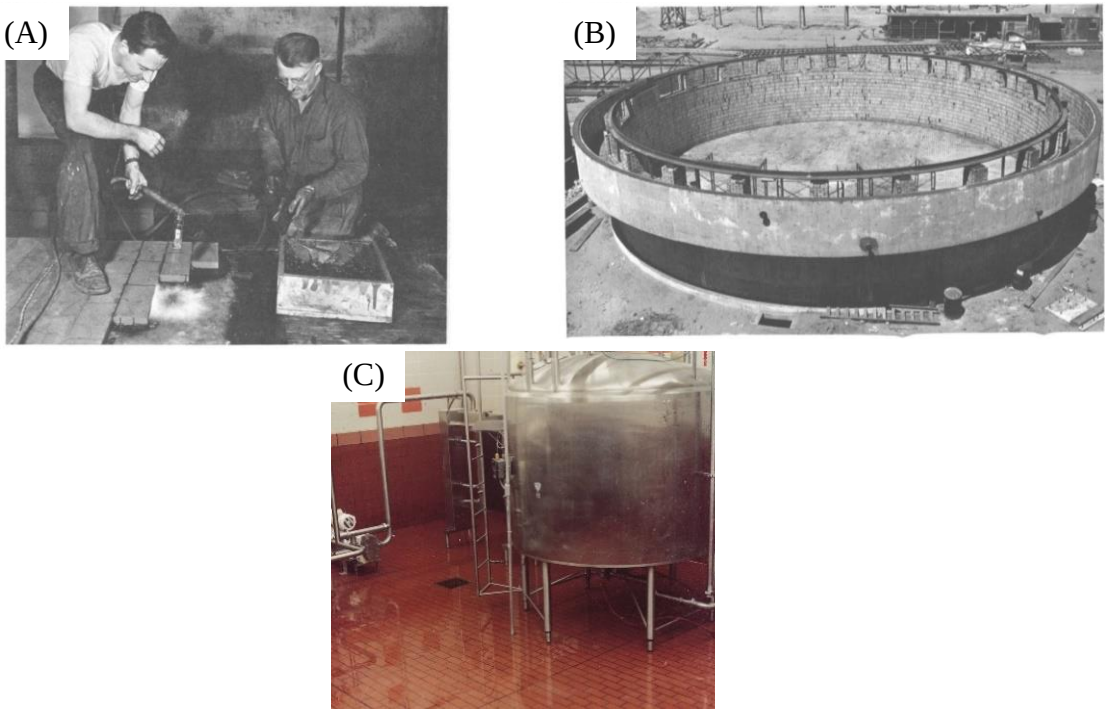

Figure 1.3-2. Pictures of the fabrication (A) and a final brick lining (B) taken before 1979. [97] (C) shows a floor furan-based grout from the ATLAS minerals & chemicals company, 2022[120]

In the past twenty years, researchers explored the properties and applications of furan-based polymer concretes. This includes investigations on of the mechanical properties and effect of the aggregate type and size on the resulting concrete. [121, 122, 123] In addition, investigation of furan resins to consolidate sand in oil wells [124, 125], soil stabilizers for road and helipads [126] were conducted together with the formulation of "all weather" repair resins for concretes and asphalt structures. [127] The reinforcement of oil wells with thermoset such as PFA seems to be a relatively active field as patents affiliated to sand consolidation are still issued nowadays. [128] Furan based resins were also reported as bitumen rheology modifiers [129], to increase the heat resistance of bitumen [130] and the resistance of asphalt to rutting. [131]

A growing application of furan resins, more specifically PFA is the reinforcement of softwood through a process called furfurylation. Pictures of furfurylated wood from the Kebony company are available in Figure 1.3-3. A patent from 2004 depicts an example of furfurylation process. The process involves the penetration of a solution of FA and maleic anhydride (MA), as acidic initiator, into wood pieces followed by an oven curing. [132] The furfurylation allows softwoods to increase their properties towards the ones of hardwoods. The furfurylation enhances softwoods in terms of dimensional stability, hardness, resistance to fungal attacks and resistance to marine environments. [133, 134, 135] As a consequence, research focusing on the interactions of FA/PFA and wood components were conducted [136, 137] Additionally, studies are still performed to improve the processability and properties of furfurylated woods. [138, 139] The full extent of the current knowledge on furfurylated wood falls out of the scope of this section and the bibliography is far from being exhaustive here.

Figure 1.3-3. Pictures of a terrace made of furfurylated wood (Kebony) in Porto-Vecchio (A) [140] and comparison between untreated softwood (light) and a furfurylated one (dark) (B). [141]

As for most thermosets, PFA is also employed in the composite industry. PFA has applications in fiber-glass composites were resistance to acids or halogenated solvents is required. Uses in pipes, tanks and scrubbers were reported. Figure 1.3-4A depicts an example of scrubber made from PFA and glass fibers.

Such containers may withstand continuous use at temperatures up to 120 °C in the presence of halogenated solvents or concentrated HCL. [74, 97, 99] More recently, PFA-fiberglass composites were used in prototypes of vehicle panels with the aim of replacing fossil-based epoxies or phenolics. A picture of one of the prototypes is available in Figure 1.3-4A. [142] Nowadays, patents related to PFA composites are still filled. For instance, the manufacture of paddle gates from PFA reinforced with glass or carbon fibers was patented worldwide in 2023. [143] In 2022, the manufacture of wear components such as doctor blades from PFA and fibers was patented in the US. [144] Four years earlier the company Saint-Gobain filled three patents relative the composition of glues comprising PFA and the process to manufacture insulation products from fiber based PFA composites. [145, 146, 147]

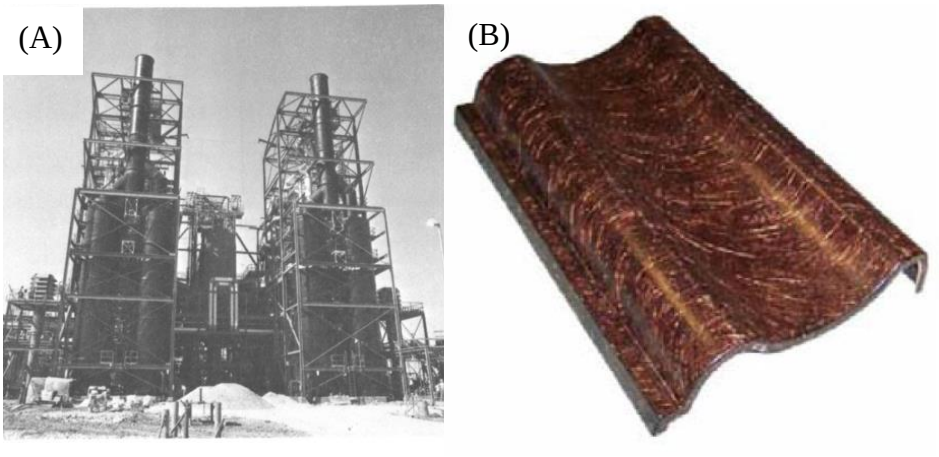

Figure 1.3-4. Scrubber made from PFA and glass fibers, picture taken before 1979 (A) [97] and prototype of exterior vehicle panel made from PFA and glass fibers (B).[142]

Since they first found commercial applications, PFA and glass fiber composites were studied over the years investigate parameters influencing their processability and general properties. [148, 149, 150] Still nowadays the properties of such materials keep being investigated [151] together with the kinetic of polymerization using modern tools. [152] However, the goal now progressively shifts from the production of high-performance materials towards the replacement of fossil-based counterpart or to mitigate toxicity of monomers.

Indeed, although FA is both toxic and CMR, it can be pre-polymerized and the FA can be distilled. The Belgian company TransFurans Chemicals has a portfolio of PFA resins with low volatile organic compounds for the aerospace, rail, automotive, furniture, insulation and foundry no-bake resins. [153]

In addition to PFA and glass fiber composites, a significant amount of research was conducted on PFA reinforced with other fibers. An article from 2020 investigated the fatigue behavior of PFA reinforced with carbon fiber under tensile solicitation. [154] In the line of inorganic fibers, research was conducted on basalt fibers impregnated with PFA alone and in combination with the diglycidyl ether of bisphenol A (DGEBA). The authors studied the mechanical and anticorrosive properties along with the processability of such composites. [155] Later, the performance of similar composites was characterized and the researchers proposed that a ring-opening reaction of PFA catalyzed the curing of the epoxy. [156] Other authors looked at the influence of microwaves on the curing of composites made of PFA and basalt fibers and suggested an improvement of the mechanical properties in comparison with classical thermal curing. [157] Finally, flame-retarded PFA reinforced basalt prepregs were prepared and characterized by Elejoste et al. [158]

With the increasing interest for more sustainable materials, a significant number of PFA reinforced with natural fibers composites were studied. For instance, semi-synthetic fibers (Rayon) were impregnated with PFA and characterized by Malaba et al. [159] The carbon storage capacity and mechanical properties of hemp reinforced PFA were investigated as well.[160, 148] Kenaf fibers composites were also studied by Deka et al. [161] In addition, systems comprising PFA and flax fibers were thoroughly investigated. The studies include the effect of aligned and/or random fibers on the properties and processability of PFA and flax composites. [142, 148, 162, 163] Among the other articles, composites made of PFA and flax fibers were combined with cellulose acetate butyrate and characterized by Toriz et al.[164] Finally, Motaung et al. proposed an alkali treatment of flax fibers which improved the flexural properties and the *Tg* of their PFA composite. [165]

Continuing on PFA combined with natural fillers, PFA and cork composites were characterized and suggested as a mean of valorization of cork powder residues from the cork stoppers industry. [166]. Furthermore, PFA and isolated soda lignin systems were proposed as a mean to valorize this side product from the paper industry. For instance, plasticized lignin was blended with PFA and their potential compatibility was suggested using Fox's equation. [167] Later, the flexural and impact behavior of PFA reinforced lignin with up to 20 % of lignin were studied. [168] Additionally, a mixture of lignin, FA, glyoxal and DGEBA was proposed for adhesive applications [169] together with oxidized lignin in combination with PFA for plywood glues. [170]

In the field of adhesives, FA was suggested several times as a co-reactant for adhesive purposes. Examples include the bonding of particleboards with FA/tannins/lignosulfonate mixtures [171, 172] and FA/urea/formaldehyde mixtures. [173] A furan resin/urea/formaldehyde mixture was also proposed as a plywood adhesive. [174] In the line of plywood adhesives, FA/tannins systems were proposed with tannins alone [175] and tannins in combination with silk. [176] Furthermore, FA/aldehydes systems (formaldehyde, glutaraldehyde, glyoxal) [177] and combinations of FA/Furfural/DGEBA/starch were also explored as plywood adhesives. [178] Overall, in adhesive systems, introducing FA or PFA in the formulations often aims at either reducing the amount of formaldehyde or replacing phenolic compounds.

Over the years, a wide array of PFA nanocomposites were prepared and characterized. First, the polymerization kinetics of FA catalyzed by montmorillonite clays was investigated [179, 180] along with the mechanical and thermal properties of the resulting nanocomposites. [181, 182, 183] Other publications using inorganic non-carbonaceous fillers are mostly focused on PFA reinforced with silica. In some cases, the thermal degradation pathways and fire resistance where at the center of the articles. [184, 185] Additionally, Bosq et al. reported the functionalization of silica nanoparticles with furanic moieties to increase the matrix-filler compatibility. Their functionalization strategy is illustrated in Scheme 1.3-1. [186] Furthermore, hollow microspheres of silica within a PFA matrix were suggested for applications requiring thermal insulation and fire resistance. [187]

Much earlier, in the 1990s, Spange et al. produced a series of publications involving the polymerization of FA with silica microparticles and the potential interaction between PFA and silica. [188, 189, 190]

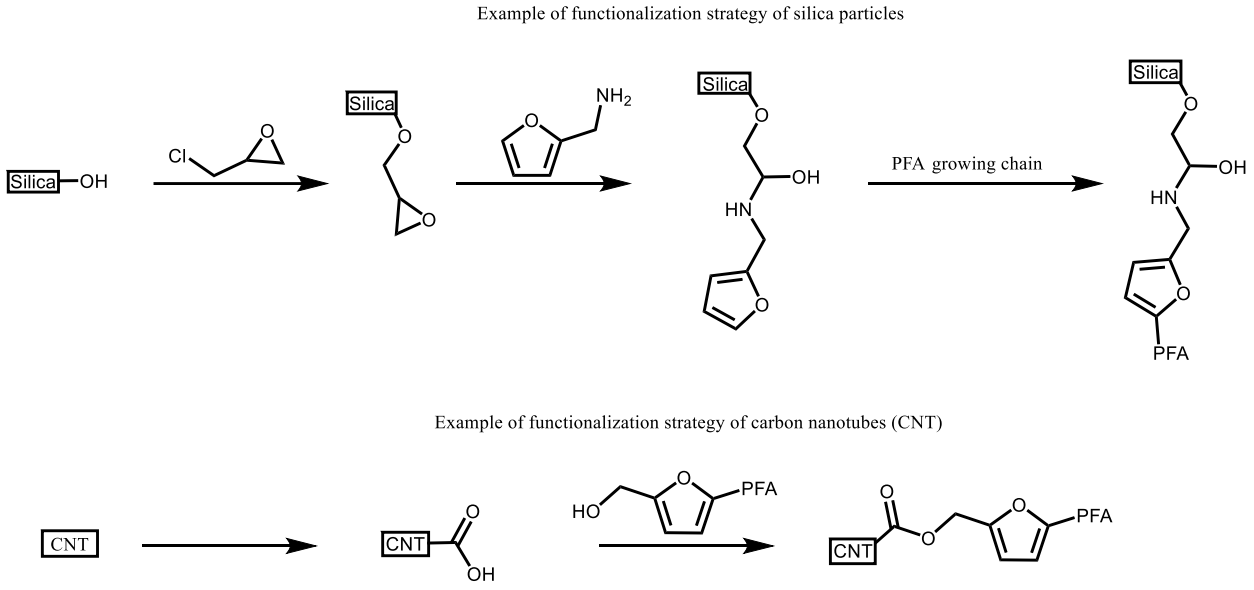

Scheme 1.3-1. Example of surface functionalization strategies proposed for silica particles (top) [186] and carbon nanotube (bottom) [192, 198].

A significant part of the nanocomposites reinforcing a PFA matrix involve carbonaceous nanoparticles. First, the works involving monodimentional fillers. For instance, phenylsulfonate functionalized single-walled carbon nanotubes [191] and COOH functionalized ones [192] were mixed with PFA. Ionic and esters bonds were proposed as the interface between the fillers and the matrix. The tribological properties of PFA filled with multiwalled carbon nanotubes functionalized with various chemicals were studied by Men et al.[193, 194] Neat carbon nanotubes blended with a FA/phenol/formaldehyde mix were subjected to thermal degradation studies without improvement in comparison with the corresponding FA/phenol/formaldehyde mix. [195] Finally, Montana et al. investigated the mechanical and electrical conductivity of PFA reinforced with multiwalled carbon nanotubes. [196]

Regarding bidimensional carbonaceous materials, a PFA and graphene oxide nanocomposite was tested as a glucose sensor. [197] Other authors investigated the thermal and mechanical properties of similar composites and suggested ester bond linking the COOH of the graphene oxide with OH groups of PFA. [198] Additionally, graphite nanosheets were blended with PFA, with the aim of introducing some electrical conductivity in the material. The electrical conductivity was increased from $\approx 10^{-10}$ $S.m^{-1}$ for PFA to 10^{-8} $S.m^{-1}$ for a PFA loaded with 2 %w of graphite nanosheets, i.e. below the limit between insulators and semiconductors. [199] Zhu et al. studied the tribological behavior of PFA – graphite composites [200] and Montana et al. their mechanical properties and electromagnetic interference shielding effectiveness. [196] Finally, a tridimensional carbonaceous nanoform (carbon black) was blended with PFA and the flexural properties [201] as well as tensile and electromagnetic properties were assessed. [196]

Concluding with PFA nanocomposites, several forms of nanocellulose were mixed with PFA. Pranger et al. investigated the tensile and thermal properties of PFA and cellulose whiskers. They highlighted improvement of the onset degradation temperature both under air and N_2 atmosphere in comparison with a PFA initiated by aluminum oxide. In addition, Pranger et al. observed a qualitatively higher amount of ring opening by FTIR for their PFA and cellulose whisker nanocomposite. [182, 183] Motaung et al. performed a similar study using cellulose whiskers more or less hydrolyzed. According to the authors, the starting degradation temperatures under N_2 increased with the more the whiskers were hydrolyzed. When loading PFA with whiskers the elastic moduli of the materials increase in the rubbery state. However, no significant variation of T_g was observed. [202] Ahmad et al. also studied PFA reinforced with cellulose whiskers, this time the whiskers were obtained by a freeze-drying process. [203] In the previously mentioned studies, the proportion of cellulose was below 5 %w. Lems et al. used a different approach consisting in reinforcing cellulose microfibril with up to 50 % of PFA. Their composites are illustrated in Figure 1.3-5. [204] Finally, PFA oligomers and cellulose powder were compounded as a 3D printing ink. The formulation and the process were patented in 2021. [205, 206]

Figure 1.3-5. Cellulose and cellulose reinforced PFA foams of Lems et al. [204]

In the field of foams, some publications involve PFA. One could note the articles on polymers from high internal phase emulsions (polyHIPES) where the emulsion structure is "frozen" to give rise to foams. In this scope, PFA was used as a coating in an already existing poly(styrene-codivinylbenzene) system. [207] Another foam based on a PFA and tannins system was developed by Szczurek et al. for thermal insulation purposes. [208] Outsides the emulsion-based foams, PFA and a foam accelerator were mixed and the resulting material was tested as a temperature-tolerant foam for spilled-oil recovery. [209] Also aiming at oil recovery applications, Feng et al. coated melamine sponges with PFA to increase the hydrophobicity of the sponge and therefore its oil adsorption capacity. [210] Other foams include thermally resistant PFA and montmorillonite aerogels [211], carbonaceous foams from copolymerized FA and epoxidized linseed oil [212] and carbonized copper filled PFA foams with electrical and thermal conductivity. [213] FA also entered in the formulation of self-blowing closed-cell foams together with laboratory humins, tannins and a foaming agent. [214] In this line, the manufacture of closed-cell tannin foams with PFA as a component was patented in 2012. [215] Finally, Acosta et al. grafted PFA to wood floor to decrease the water uptake of poly(urethane) foams loaded with wood flour. [216] Figure 1.3-6 illustrates examples of the previously mentioned foams.

(A) (B)

Figure 1.3-6. Example of a PFA-tannin foam (A) [208] and a cross section of a PFA foam for oil recovery (B) [209]

As a mean to access materials with new and/or modulable properties, FA was co-polymerized or blended with numerous monomers and polymers. To most common studies are the combination of FA or PFA oligomers with epoxies. Zohuriaan-Mehr et al. extensively studied these systems. Their work includes the kinetics of polymerization [217, 218] and properties of PFA with DGEBA [219], Novolac [220] and aromatic tetrafunctional epoxies. [221] Additionally, they polymerized furfurylated DGEBA oligomers with PFA oligomers using a bismaleimide based crosslinker for Diels-Alder based dynamic networks. [222] Interestingly, when the authors used primary amines hardeners, they observed the diminution of PFA's carbonyl band. They attributed this to the formation of a pyrrole cycle, as depicted in Scheme 1.3-2.

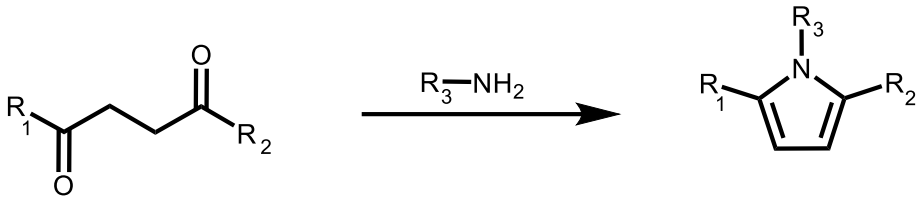

Scheme 1.3-2. Formation of a pyrrole cycle from 2,5-diketones and a primary amine by the Paal-Knorr reaction.

Other researchers studied the copolymerization of PFA and epoxies using epoxidized soybean [223] and linseed [224] oils to introduce flexibility in the materials. In the line of vegetable oils, tung oil was co-polymerized with FA [225] and then the copolymer was reinforced with cellulose nanofibers. [226] PFA was also blended and copolymerized with a protein model compound [227], natural phenolics monomers [228], tannins [171, 172, 175, 176, 208] and starch-epoxy systems.[229] Blends of PFA and polyesters were also studied, namely poly(caprolactone)[230], poly(lactic acid) [231] and unsaturated polyester resins. [232] Ruelens et al. studied the copolymerization of FA with α,α-dimethyl furfuryl alcohol as a mean to increase the toughness of PFA. [233] Other copolymerization studies include PFA oligomers with bismaleimide [234], DGEBA and poly(propylene carbonate) [235] and a complex system comprising silicones, phenolics and PFA oligomers. [236] A system comprising PFA and a silicone-based polymer was assessed as coating for anticorrosion purpose. [237] Similar blends were also tested as superhydrophobic surfaces. [238] In this line, systems comprising PFA with fluorinated acrylics [239], poly(tetrafluoroethylene) [240], stearic copper [241] and potassium stearate [242] were also investigated for superhydrophobic surfaces. Either by using fluorinated moieties or molecules bearing long alkyl chains, the authors of these four studies highlighted the possibility of integrating PFA in superhydrophobic systems, i.e. surfaces had contact angles > 150 ° with water. Some of the surfaces are illustrated in Figure 1.3-7.

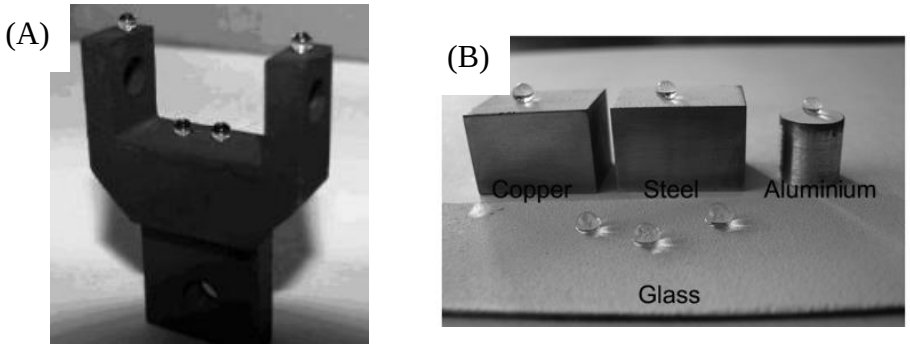

Figure 1.3-7. Example of PFA-based superhydrophobic surfaces, (A) [240] PFA - PTFE system and (B) PFA-potassium stearate system. [242]

As a mean of water desalinization purpose [243] and air enrichment of O_2 [244] PFA was impregnated on poly(sulfone) membranes. Following a similar principle, Nafion® membranes were impregnated with PFA as a mean to improve the membranes' ionic conductivity. [245] Moreover, gas separation membranes made from carbonized PFA were already studied in the late 1990s [246] and still are nowadays. [247]

As a matter of fact, PFA is recognized since at least the 1970s for its performance as a carbon precursor. Industrially, solutions of FA are impregnated on carbon scaffolds, polymerized and then carbonized under inter atmosphere. This densifying process densifies the material and the voids are removed. The impregnation may be repeated one or more time. As a consequence, products such as large carbon electrodes, heat exchanger tubing and anti-corrosion bearing for vacuum pumps can be manufactured. [74 97, 57] Both phenolic and furan resins can be used to impregnate and to densify carbon scaffolds. An example of impregnated graphite with a phenolic resin is available in Figure 1.3-8.

Figure 1.3-8. Heat exchanger made of impregnated graphite from the CGThermal company.[248]

The full extent of the knowledge on the carbonaceous materials prepared from PFA is beyond the scope of this manuscript. However, examples can still be given. The carbonized PFA as a mean to manufacture molecular sieves is known since more than twenty years. [249]

Yet, in 2023, researchers are still looking for ways to tune the size, adsorption capacity and selectivity of these materials. [250, 251] Interestingly, Machowski et al. decorated mesoporous silica with carbonized PFA and attributed an enhanced adsorption capacity of ketone bearing compounds to the ring-opening side-reaction.[252] The field of energy storage also studied carbonized PFA in the making of supercapacitors [253], “ultrafast” capacitors [254], solid oxide fuel cells [255], anodes for lithium batteries [256] and so forth. One could also note the assessment of carbonized PFA as a catalyst support for the oxidation of VOCs [257] as well as the compounding of PFA with cellulose and carbon nanotubes for carbonizable electrically conductive ink for 3D printing. [258] Finally, carbonized PFA was already used to produce carbonaceous materials with controlled structure in the 1970s. [259] Nowadays, “nanocasting” processes are being developed. They involve the deposition of PFA on silica templates followed by carbonization of PFA and removal of the silica by hydrofluoric acid. Here, the aim is the producion of carbon replicas of native silica structures. [260]

Oddly, articles are also dealing with photopolymerization and FA. As a matter of fact, some compound called photo-acids can decompose upon exposure to light and release acids capable of initiating the polymerization of FA. More oddly, when using such initiation “wrinkled” materials can be achieved. An example wrinkled PFA is provided in Figure 1.3-9. A few publications are dedicated to the understanding and control of the morphology of the wrinkles as they may give better results than lithography if large areas are targeted. [261, 262] In the late 1990s a series of publications investigated the use of PFA with acrylic molecules to produce negative photoresists. [263] Other procedures where PFA prepolymers were spin-coated on silicon wafer or solvent casted on glass plates prior to an exposure to UV-light were investigated. A photopolymerization pathway for the curing of PFA prepolymers prepared with trifluoroacetic acid was suggested. [264, 265,] Nonetheless, it is not clear if the film produced in these papers is the consequence of photopolymerization or the combination of the heat from the UV lights and left-over acids.

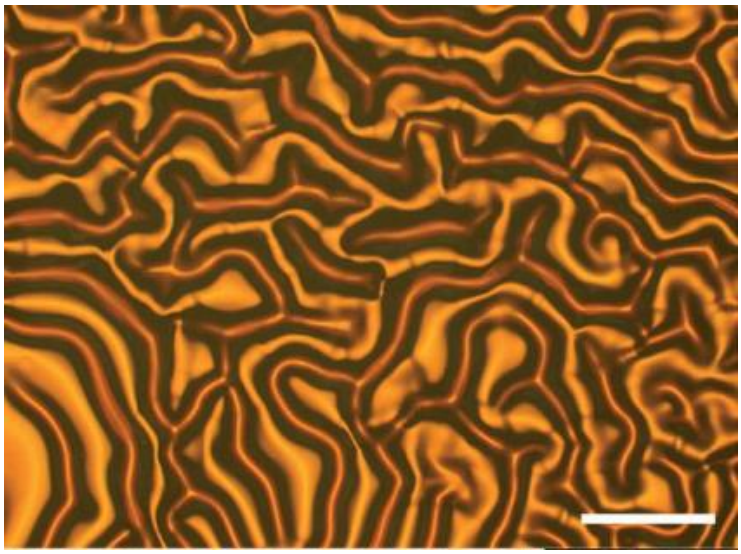

Figure 1.3-9. Wrinkles obtained after photoinitiation of PFA, the white bar has a length of 1 mm. [261]

Most of the applications and potential applications of PFA mentioned earlier aimed at the manufacture of materials. Nonetheless, PFA oligomers can be fuel precursors. Indeed, small oligomers (C5-C25) from FA's polycondensation can be hydrogenated to produce renewable fuels. Examples of studies in this field include the investigation of the thermodynamics and reaction pathways of the oligomerization of FA [266] or the kinetic of polymerization [267]. In addition, Chan et al. reported a purification method by liquid-liquid extraction of FA's oligomers. [268] Finally, Chappaz et al. issued a patent relative to the synthesis of alkyl levulinates from condensation products of FA. [269]

To conclude, PFA is mostly used in composite applications were thermal and chemical stability are required. Nowadays, the use of PFA is often branded as an eco-friendly material thanks to its renewable sourcing and possibility to be used as a low VOCs prepolymer. Finally, the applications of furan resins, including PFA, reviewed in this chapter are summarized in Figure 1.3-10.

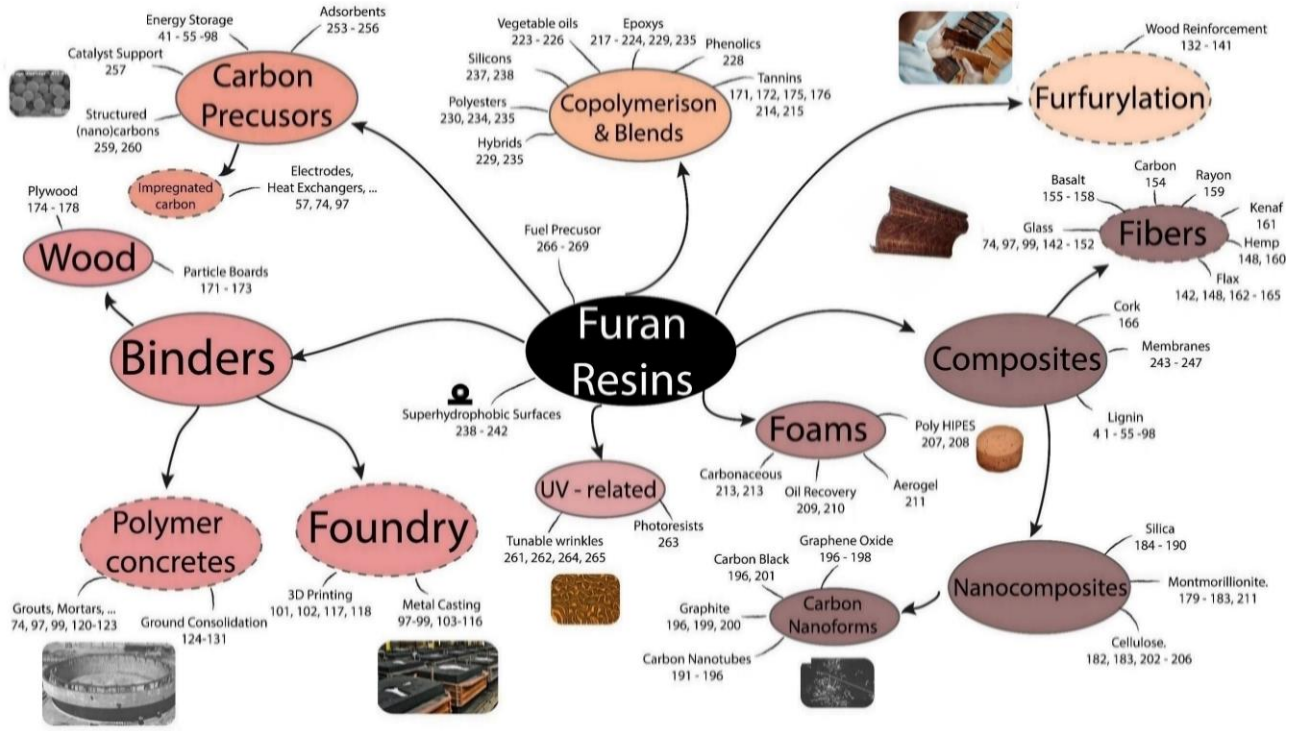

Figure 1.3-10: Overview of the applications of furan resins. The dashed lines correspond to industrially developed fields. The numbers correspond to the references.

1.3.2 Polymerization of furfuryl alcohol, a tribute to complexity

The polymerization of FA in acidic medium is complex and debated since the 1940s. Nowadays, there is a consensus on the major structural features and crosslinking mechanism. Yet, the proportions of each repeating units are still debated and were never quantified. The following sections are dedicated to the known features of PFA.

1.3.2.1 The polymerization of FA: structural features the polymerization

The understanding of the polymerization mechanisms of FA began in the 1940s around the same time as the Quaker Oats process was launched. In their article, Dunlop and Peters, employees of Quaker Oats, studied the "insoluble form of furfuryl alcohol". They observed a release of water upon heating FA. From this and in combination with elemental analysis and chemical function tests they deduced the formation of oligomers according to Scheme 1.3-3. [270] This linear structure is still widely accepted nowadays with a number of repeating units reaching from four and ten. [271]

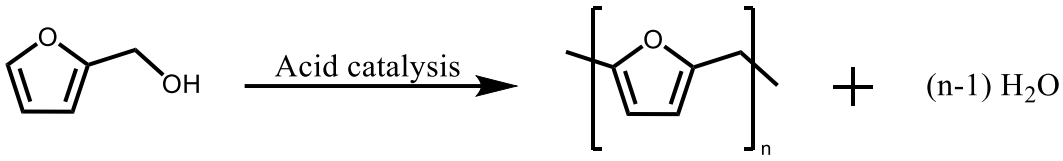

Scheme 1.3-3. Linear oligomerization of FA under acidic conditions.

In the 1960s, on the basis of a FTIR study, Conley and Metil added 1,4-dicarbonyls to the linear structure of PFA as the resultant of hydrolytic ring opening. [272] In the early 1970s, Werwerka et al. identified a lactone as a product from FA's polymerization using gas chromatography. [273] Around the same time, Barr and Wallon distilled PFA oligomers and analyzed the fraction by ^{1}H NMR. They found the presence of the linear arrangements of furfuryl units together with ether-linked furfuryl units and methyl-terminated oligomers. [274] Their findings were later confirmed by ^{13}C NMR. [275]

The structures mentioned above are depicted in Scheme 1.3-4. Although it is not very clear when it was first showed, the ether-linked furans were suggested to undergo dehydration reaction by freeing formaldehyde, as depicted in Scheme 1.3-5.

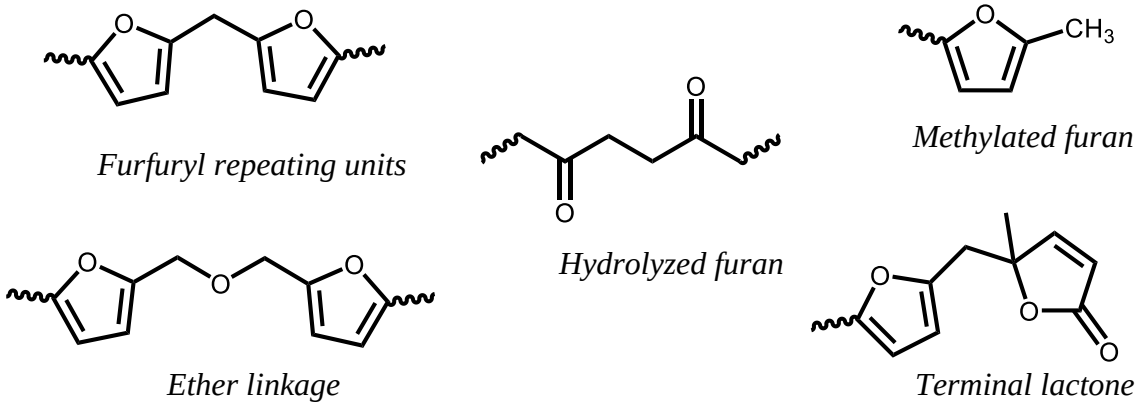

Scheme 1.3-4. Identified moieties found in PFA oligomers before 1980.

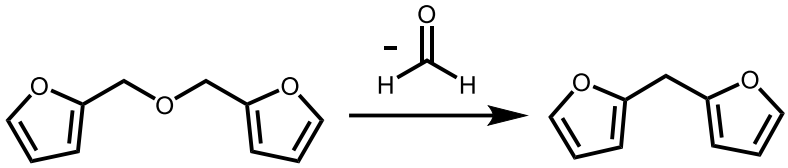

Scheme 1.3-5. Liberation of formaldehyde from ether linkages.

However, two major features of PFA were still not understood at the time. First, while FA is colorless, PFA oligomers range from yellow to dark red and the final material is black, as showcased in Figure 1.3-11.[i] However, none of the molecules in Scheme 1.3-4 display signs of colored organic molecules, such as high conjugation. Moreover, oligomers of PFA with between four to ten units are soluble and were isolated several times. Yet, the polymers would undergo a rapid crosslinking after a certain threshold. This left researchers with only hypotheses on the crosslinking mechanisms of PFA.

[i] Somethimes, a dark green color can be observed at the very beginning of the polymerization

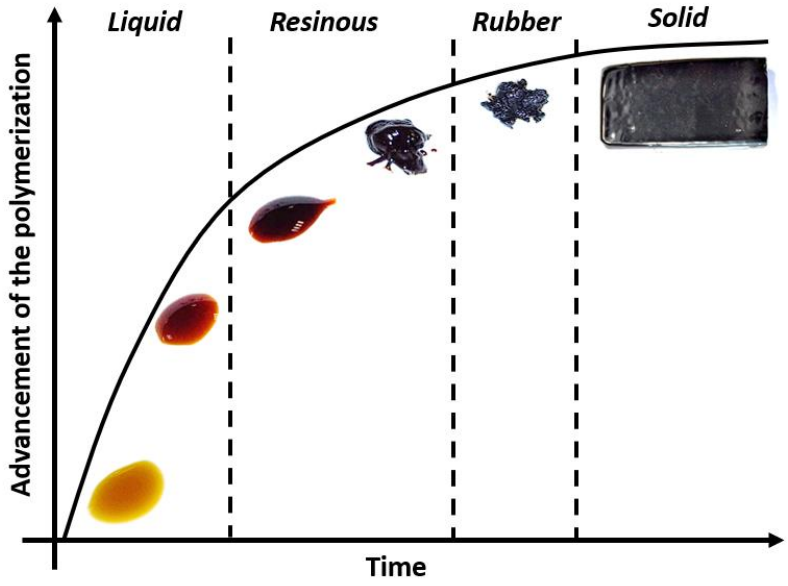

Figure 1.3-11. Illustration of the aspect of PFA over the course of its polymerization.

In 1982, Buchwalter et al. studied the polymerization of furfuryl acetate. [276] They used furfuryl acetate as a model of FA's polymerization. The absence of OH group in furfuryl acetate prevents the etherification reactions and thus the potential elimination of formaldehyde. Moreover, only acetic acid is formed during condensation, thus preventing the hydrolysis of the furan ring. Coupling NMR, UV/vis spectroscopy, a trityl cation and inspiration from an earlier paper of Gandini et al. on alkenyl furans. [277] Buchwalter et al. showed the formation of conjugated 2,5-dihydrofurans in Scheme 1.3-6. It occurred through a hydride ion abstraction process. The attributed the origin of the color of their poly(furfuryl acetate) to the highly conjugated species and suggested a similar process in PFA.

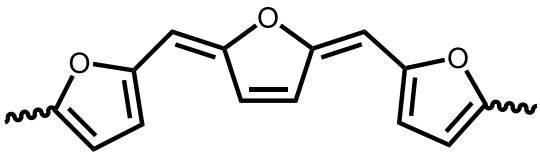

Scheme 1.3-6. Structure of conjugated 2,5-dihydrofurans with furan.

Regarding the crosslinking mechanism of PFA, various links were proposed. This includes the structures of Scheme 1.3-7. Methylene linkages were believed to form either by condensation of CH_2-OH on the CH_2 bridging furans or from a crosslinking involving formaldehyde. [278, 279, 280] However, in 1996 Choura et al. rejected these hypotheses through an extensive use of model compounds and confirmed the existence of conjugated moieties as proposed by Buchwalter et al. [281]

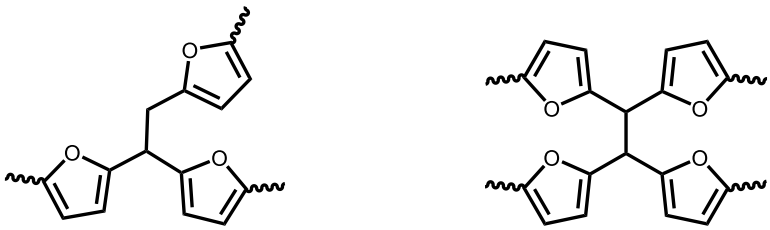

(A) (B)

Scheme 1.3-7. Methylene linkages proposed by Chuang et al. Structure (A): condensation of CH_2-OH. Structure (B): formaldehyde-induced crosslinking. [278, 279]

The article from Choura et al. [281] focused on the elucidation of the mechanisms of FA's polymerization. To do so, they used more than twenty model compounds to selectively simulate parts of FA's polymerization. They coupled this with NMR, FTIR, UV spectroscopy and molar mass determination technics. The authors confirmed the occurrence of conjugated species in PFA systems and proposed the mechanism in Scheme 1.3-8. They suggested that once a sufficient number of furfuryl units are linked together, the hydride abstraction process occurs. In concomitance, the furfuryl carbonium ions in the medium catch the leaving hydride to from terminal methyl groups. [281] The presence of the methyl groups on the ^{1}H NMR spectra served as indirect proof of the proposed mechanism. Indeed, the ^{1}H signals of the 2,5-dihydrofurans are believed to superimpose with the furan's signals.

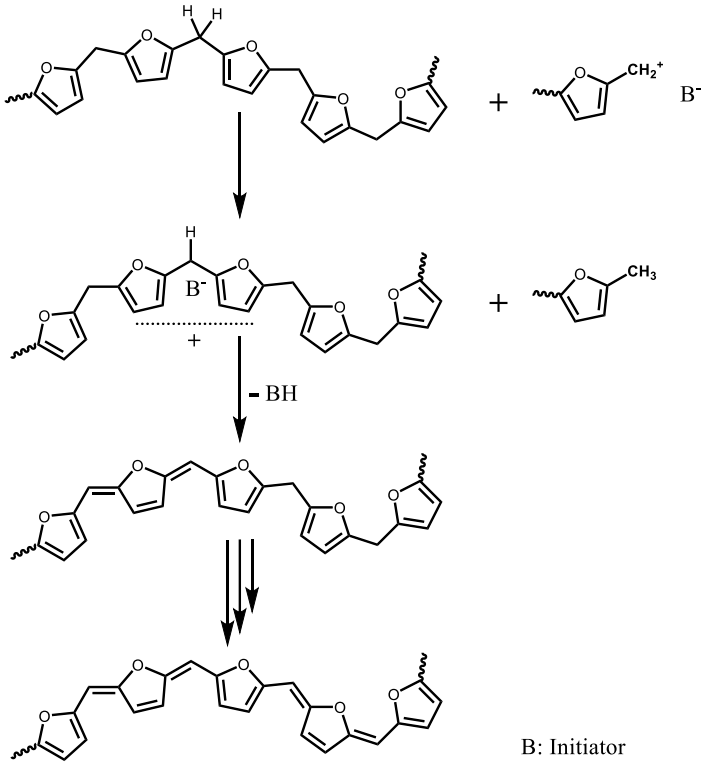

Scheme 1.3-8. Formation of conjugated moieties in PFA oligomers. [281]

Furthermore, the authors concluded that the crosslinking reactions in PFA involve the conjugated 2,5-dihydrofurans. They suggested a crosslinking pathway through the Diels-Alder 2,4 cycloaddition depicted in Scheme 1.3-9. Although no direct evidence of the reaction was given in this paper, one could look at papers providing ^{13}C NMR of cured PFA. In several of them, both old and recent, a broad ^{13}C NMR signal can be observed between 120 and 135 ppm and interpreted as non-conjugated the C=C in the Diels-Alder cycloadduct. [278, 282, 283, 284]

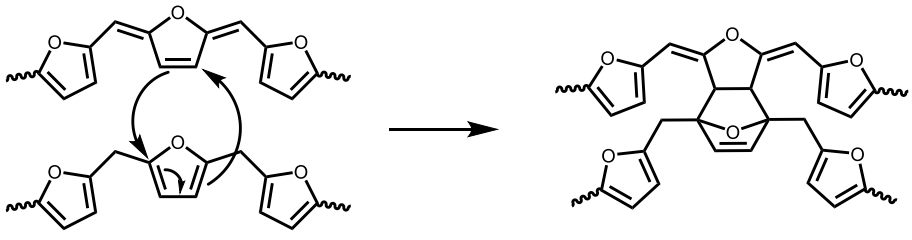

Scheme 1.3-9. Proposed crosslinking pathway in PFA: Diels-Alder cycloaddition.

Finally, the authors suggested the possibility of crosslinking through the condensation of primary OH on the conjugated sequences as depicted on the right of Scheme 1.3-10. [281] In the following years, structural studies were conducted to highlight such pathways. [285, 286] Principe et al. highlighted the presence of alkyl CH moieties by DEPT ^{13}C NMR in PFA. [285]

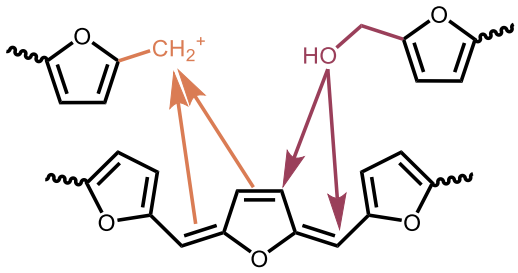

Scheme 1.3-10. Proposed crosslinking pathway in PFA: electrophilic substitution (left, orange) or condensation reaction (right, dark mauve).

In the 2000s, investigations on the mechanisms ruling FA's polymerization were still conducted thanks to the evolution of theoretical analysis. For instance, Montero et al., used theoretical modeling to simulate the crosslinking in PFA. [287] The calculations approved the feasibility of the Diels-Alder reaction although it is mitigated by steric hindrance. In addition, the electrophilic attacks were also feasible according to the authors. They also detailed one of the mechanisms as reported in Scheme 1.3-11. Interestingly, the resulting structures may present features proposed by Chuang et al. in Scheme 1.3-7, although the means to reach it are different. [279] In the line with the theoretical simulations, Bertarione et al. combined FTIR, Raman and UV-vis spectroscopy with simulations to study the formation of PFA oligomers in zeolite cavities.[288] In addition, Kim et al. studied the polymerization of FA with a thermodynamical approach coupled with Raman spectroscopy. [289] This first paper was followed by two other investigations on the effect of the solvent during FA's polymerization and the influence of the catalyst type on the structure of PFA's oligomers. [290, 291] Simulations were also employed by Barsberg et al. to predict and assign Raman and/or FTIR bands of furfuryl alcohol [292], PFA [293] and a lignin/PFA hybrid. [294] The latter one being a consequence of the blossoming of the furfurylation.

Indeed, understanding the interactions between PFA and wood is of great help to understand and improve the properties of furfurylated wood. Similar works were also performed using bidimensional NMR technics. [137, 295]

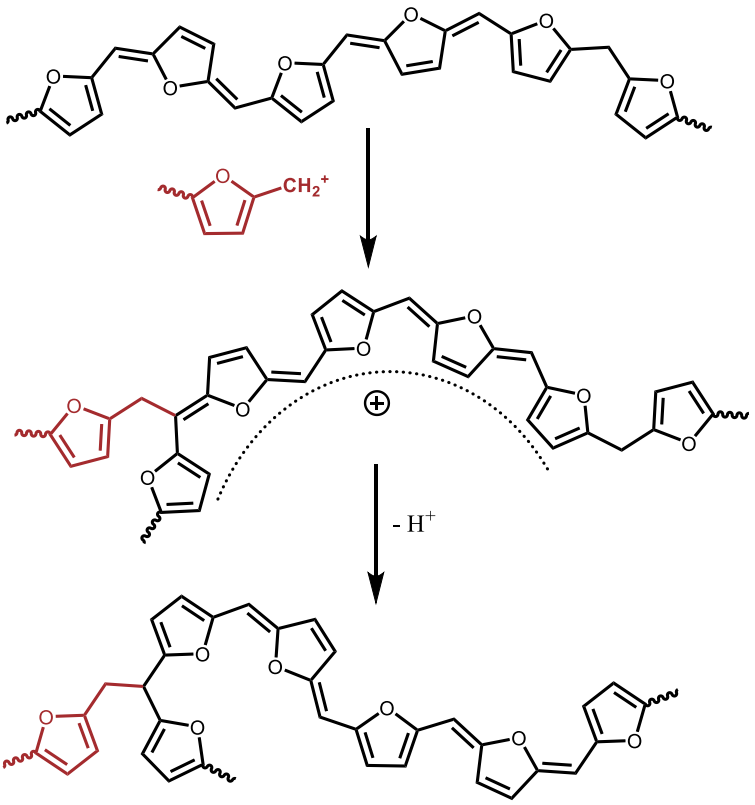

Scheme 1.3-11. Proposed crosslinking pathway in PFA: electrophilic attack. [287]

Finally, a series of tables is proposed as a conclusion of this section. They sum up the main spectrometric assignments of PFA across the years. Table 1.3-1 reports the main ^{1}H NMR peaks, Table 1.3-2 the main ^{13}C NMR peaks and Table 1.3-3 the main FTIR bands found in PFA systems.

Table 1.3-1. Main ^{1}H NMR peaks of PFA.

Chemical shift (ppm)	Attribution	Reference
1.8 – 2.2	Fu-CH_3	[275, 281]
3.5 – 4	Fu-CH_2-Fu	[275, 281, 285, 286]
4.2 – 4.5	Fu-CH_2-OH	[274, 281]
5.7 – 6.4	H3 and H4 of furans	[274, 275, 281, 285, 286]
7 – 7.2	H_5 monosubstituted furan	[274, 275, 281, 286, 285]

Table 1.3-2. Main ^{13}C NMR peaks of PFA.

Chemical shift (ppm)	Attribution	Reference
13	Methyl	[275, 283, 284]
25-30	Furan-CH_2	[275, 280 , 284, 285, 286]
30-50	CH_2-C=O, CH-CH_2, Quaternary C in Diels-Alder adduct, CH	[275, 283, 284, 285, 286]
55 - 65	Residual CH_2-OH, residual ether bridge	[275, 280, 282]
110	C_3 and C_4 Furan	[275, 280, 282, 283, 284, 285, 286]
120-130	C=C in Diels Alder Adducts	[283]
140	C5 monosubstituted furan	[275, 280, 282, 283, 284, 286]
150	C1-C5 disubstituted furan	[275, 280, 282, 283, 284, 285, 286]
170	Esters, Levulinic Acid	[283, 284, 285]
200 - 210	C=O	[283, 284]

Table 1.3-3. Main FTIR bands of PFA.

Wavenumber (cm^{-1})	Attribution	Reference
600 – 920	Several bands Furan	[291 292]
1000- 1020	Mixed Furan (C-O / C-H)	[280, 293]
1500-1510	C=C furan monosubstituted	[286, 289, 296]
1565	C=C 2,5-disubstituted furan	[291, 293, 296]
1710	C=O, C=C in Diels-Alder adduct	[271, 280, 283, 286, 291, 293, 296]
1740	Esters	[271, 283]
2930	Aliphatics	[280 286, 292]
3000-3150	Furan C-H	[291 292]
3200-3700	OH stretch	[281, 291, 292]

1.3.2.2 The polymerization of FA: other features

Apart from the mechanisms producing PFA's macromolecules, further features of the polymerization of FA were investigated over the years. The kinetic of FA's polymerization was studied at least since the 1970s. [297, 298] More than forty years later, the kinetics of FA's polymerization are still investigated either to understand the effect of different catalysts, [180, 299, 300] to understand the solvent effects [301], to assess the pot-life of oligomers [302, 303], to control the polymerization for the production of diesel precursors [267], to better apprehend the furfurylation process [304] or to characterize the reactivity of PFA with other compounds such as 2-furylethanol [305] or DGEBA [217, 218]. Most of the kinetic studies involve DSC or rheology, however one could note the work of Vargas et al. who investigated the kinetics of FA's polymerization using ^{1}H NMR, more specifically the relaxation time of the molecules. [306] In addition, a chemorheological study on PFA was performed to assess and it was suggested that the final crosslinking step of PFA is a diffusion-controlled process. [307] Using similar tools, other authors reported the dependence of the viscosity of PFA resins on the temperature. [308]

An important feature of the polymerization of FA is its high exothermicity. As a matter of fact, the polymerization of FA with concentrated strong mineral acids was more than once reported as potentially explosive. [74, 127, 182] The heat of polymerization can be easily visualized using a thermal camera. Figure 1.3-12 showcases the heat produced when about 2 mL or FA mixed with 0.5 mL of 50 %v H_2SO_4. Under these conditions, in about 10 seconds the outsides of the test tube reached nearly 100 °C. More quantitatively, the total heat release of FA's polymerization using mild catalysts is comprised between 400 and 700 $J.g^{-1}$ depending on the conditions. [180] Such high values of enthalpy make DSC a technic of choice when studying the polymerization of FA. DSC can be used to determinate the conversion degree of a given resin using Equation 1.3-1.

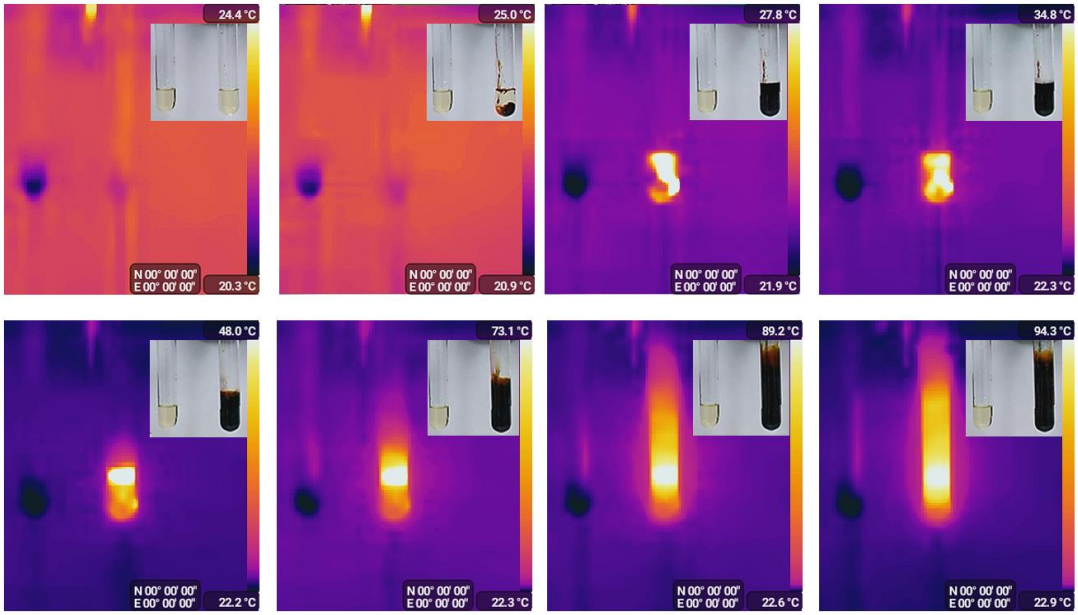

Figure 1.3-12. Visible and thermal vision of the polymerization of FA over the course of 10 s. Polymerization of 2 mL of FA with 0.5 mL of 50%v H_2SO_4. The pictures were taken one to two seconds apart and the emissivity was set to 0.95.

$$Conversion\ degree\ (\alpha) = \frac{Total\ heat\ release - Residual\ heat\ release}{Total\ heat\ release}$$ Equation 1.3-1

The conventional methods to prepare PFA are either at ambient temperature with strong mineral acids or with mild acids and conventional heating in an oil bath or an oven. Some articles focused on the effect of other processes. The polymerization of FA under UV light was already reported in section 1.3.1. Other examples of unconventional initiation include the effect of microwaves versus conventional heating on FA [309] and on basalt composites [157]. In addition, different studies on the polymerization of FA assisted by ultrasounds were conducted by Hoshi et al. [310, 311, 312] Overall, the microwaves and ultrasounds had little to no effects on the polymerization of FA, compared to conventional heating. One could also note the communication of Souza et al. on the polymerization of FA with gaseous HCL inside capillaries. [313] Swasti et al. investigated to polymerization of FA during the roasting of coffee with LC-MS and even suggested that the formed PFA oligomers may contribute to the brown color of roasted coffee. [314]

Finally, it should be mentioned that shaping a PFA material is not an easy task. This challenge is the result of the polycondensation reactions, i.e., the release of a substantial amount of water. Indeed, as detailed in Table 1.3-4, 100 g of FA yield about 80 g of PFA and 20 g of water. If no precautions are taken, the samples end-up in foamy structures which are usually unwanted. This may be counter acted by the use of slow curing, i.e. over tens of hours, with gradually increased temperature. [192, 231] Another possibility is the compression molding of gelated samples in a heated press. The use of gelated samples ensures that most of the polycondensation already occurred and thus, low amounts of water is formed during the shaping process. [283] While this method is much faster and allows thicker samples, careful control of the PFA's conversion degree prior to molding and the pressure during the molding process are required. If the pressure if too low during the compression molding, non-cohesive samples are obtained. If too much pressure is applied, PFA may squeeze out of the mold. In the case of composites, the bubble issue is still present although mitigated by the ability of some fillers to trap the water. Finally, when mechanical tests are performed, one should be careful in its interpretations as the ultimate properties might be lowered by the presence of these bubbles.

Table 1.3-4. Estimation of the production of water during FA's polymerization.

	FA	**Furfuryl unit**	**Water**
Chemical formula	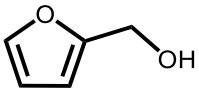	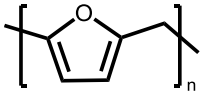	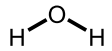
Moles	1 mol	1 mol	1 mol
Molecular weight	98 g.mol^{-1}	80 g.mol^{-1}	18 g.mol^{-1}
Mass	98 g	80 g	18 g

To sum-up, the polymerization of FA features numerous potential pathways and the final structure of PFA is dependent on the processing conditions. Overall, more than fifty articles and reviews were dedicated to the polymerization FA. Yet, the ring-opening reaction occurring during FA's polymerization is gaining interest in the past years. The following section particularly emphasizes the current knowledge on this reaction occurring during FA's polymerization that was generally categorized as a "side-reaction".

1.3.3 The furan ring-opening: a side reaction?

Based on the mechanisms reviewed in section 1.3.2, the structure in Scheme 1.3-12 regroups the various linkages found in PFA before 2010. Among the many moieties in this general structure, one can find the result of the hydrolysis of a furan. The ketonic moieties are often mentioned as "side products" or the result of "minor reactions" in the literature. [281] Yet, in the recent years, some articles reported the furan ring-opening as a significative reaction.

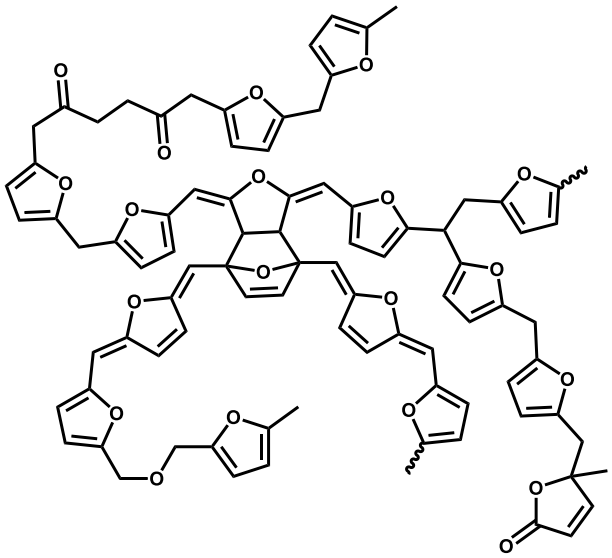

Scheme 1.3-12. Example of PFA structure, based on research earlier than 2010.

Falco et al. suggested that the polymerization of FA in polar protic solvents promoted the ring-opening reactions. They studied PFAs prepared in neat conditions, in water and in isopropanol with spectroscopic technics coupled with thermomechanical characterizations. The researchers found a qualitatively higher proportion of ketonic moieties in their aqueous system. In terms of thermomechanical properties, they found their aqueous systems to result in a lower T_g and lower crosslink density. The authors proposed the structures in Scheme 1.3-13 as terminal open units as well as the open structure initially proposed by Conley and Metil in Scheme 1.3-4. Such structures are only suggestions as the chemical environment of the C=O bonds was not studied in this article. [283]

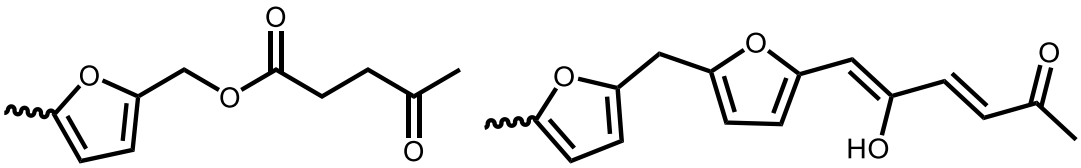

Scheme 1.3-13. Open furanic structures proposed by Falco et al. [283]

In addition to the work of Falco et al., Tondi et al. performed two studies focusing on the carbonyl structures within PFA. Using spectroscopic technics and computations, they proposed the Diels-Alder reaction in Scheme 1.3-14 as a crosslinking mechanism. [284, 296] This proposition in based on the existence of conjugated 1,4-diketones. To the best of our knowledge, this type of open furan in PFA was first drawn by Kim et al. in 2011 on the basis on thermodynamical calculations. [289] In addition, Tondi et al. suggested the presence of furfural and levulinate esters as terminal units. [296]

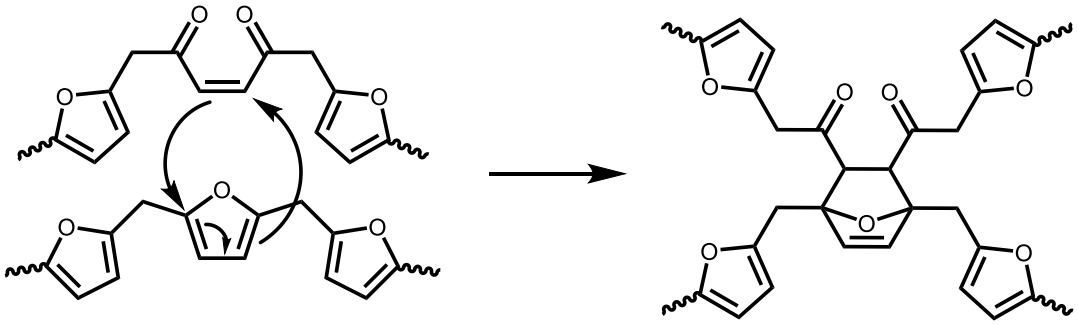

Scheme 1.3-14. Diels-Alder reaction based on open furan proposed by Tondi et al. [284]

The suggestion of conjugated diketones in PFA is coherent as the furan ring can open under oxidative conditions, especially if light is involved. [315, 316] The routes of furan ring opening are depicted in Scheme 1.3-15. However, the oxidation route requires an oxidizer which may not be present in all PFAs.

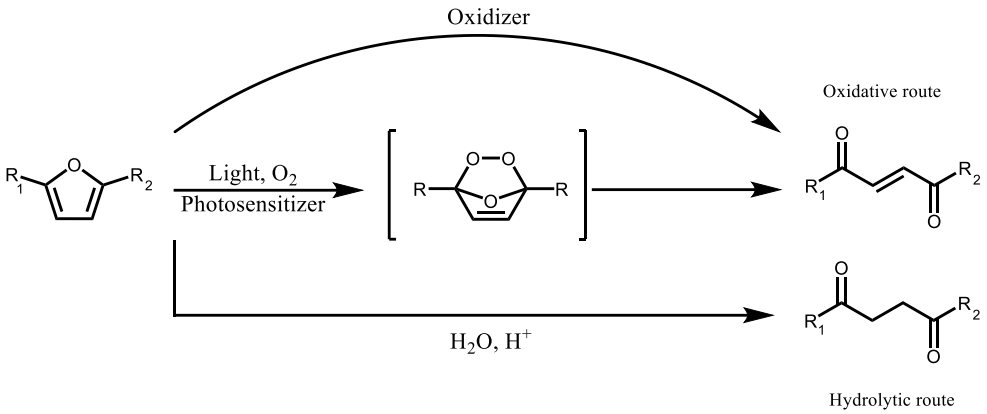

Scheme 1.3-15. Routes to open furan rings

Despite these observations, very few studies focused on the ring opening reactions occurring during the formation of PFA. This contrast with other biomass derived macromolecules whose carbonyl content has been extensively studied especially based on the oximation method of 1935. [317] For instance, the carbonyls of bio-oils and lignins were quantified by oximation [318, 319] and were confronted to further non-wet carbonyl quantification techniques using UV spectroscopy, gas chromatography [320, 321] and ^{13}C NMR [322]. Finally, large arrays of hydrazine-based derivatization methods followed by ^{19}F NMR quantification were dedicated to the carbonyl classification and quantification in bio-oils, lignins and humins. [323, 324, 325, 326]

Among all the studies mentioned in this chapter, the quantification of carbonyls in contained in PFA – due in particular to the ring opening - was never performed. Furthermore, means to control the ring-opening reaction were not investigated. Finally, the reaction between C=O and amines were suggested to occur in PFA/Epoxy/Amine systems. [218] Yet, the derivatization of the C=O as a source of tunability in furanic resin has never been a focus of research. In the following chapters, the quantification and control of C=O over the course of FA's polymerization is performed. The nature and chemical environment of PFA's carbonyls is also discussed. Finally, the final chapter is dedicated to the chemical functionalization of the C=O in PFA to tune its properties.

CHAPTER 2
Quantification and control of the furan ring opening side reaction in PFA

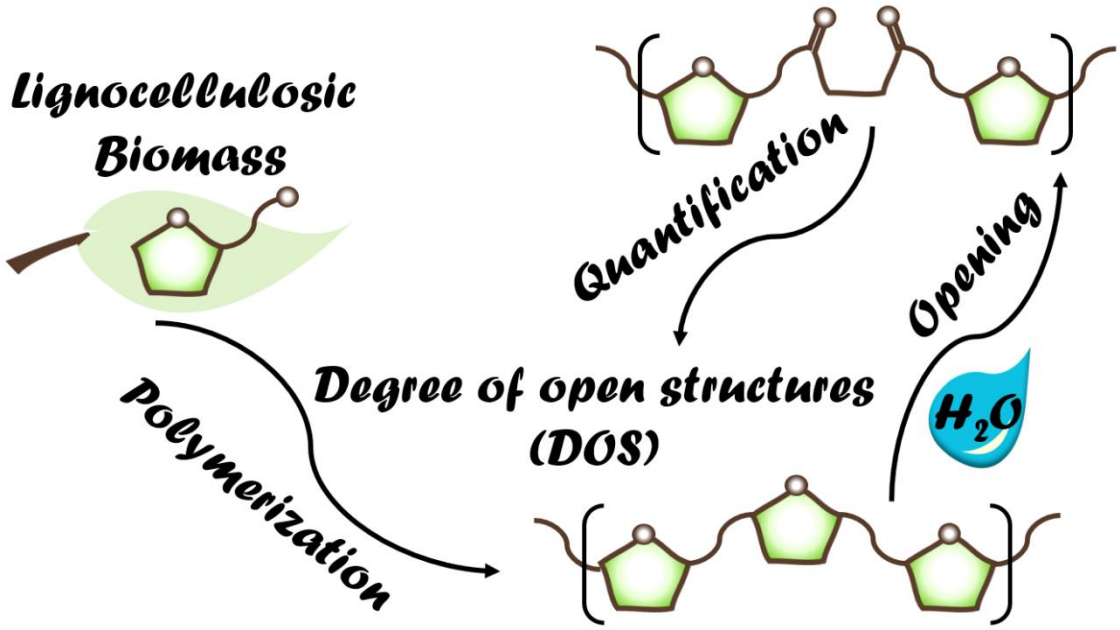

Based on:

Delliere, P.; Guigo, N. Monitoring the Degree of Carbonyl-Based Open Structure in a Furanic Macromolecular System. *Macromolecules* **2022**, *55* (4), 1196–1204. https://doi.org/10.1021/acs.macromol.1c02098.

and

Delliere, P.; Quinquet, L.; Guigo, N. Conditions to Control Furan Ring Opening during Furfuryl Alcohol Polymerization. *Molecules* **2022**, *27* (10), 3212. https://doi.org/10.3390/molecules27103212.

In the previous chapter the state of the art on PFA was detailed. Although numerous studies were dedicated to PFA, very few of them had the ring-opening side reaction as their focus. This chapter aims at breaking through the knowledge of the ring-opening side reaction in PFA. The following questions will be addressed. How can one quantify carbonyls in PFA? How many carbonyls are present in PFA systems? When does the side-reaction occur? How can one optimize the carbonyl content of PFAs?

Section 2.1 regroups the experimental details of this chapter.

Section 2.2 deals with the development of C=O quantification methods adapted to furanic macromolecules. In addition, the rate of formation of carbonyls in two kinds of PFA is also assessed. Furthermore, lab-scale humins are prepared and their C=O content quantified.

Section 2.3 deals with the synthesis of laboratory-scale humins and their characterization, more specifically their carbonyl content.

Section 2.4 is dedicated to the probing of the leverages available to control the carbonyl content of PFAs such as the type of catalyst and amount of water.

Finally, section 2.5 gives insight on the chemical nature of carbonyls within PFAs.

2.1 Experimental section

Materials:

Furfuryl Alcohol (96 %), 4-(trifluoromethyl)phenylhydrazine (96 %), oxalic acid (99 %), triethanolamine (99 %), 1,4-bis(trifluoromethyl)benzene (98 %), maleic anhydride (99 %), hydroxylamine hydrochloride (99 %), bromoacetaldehyde dimethyl acetal (97 %), boron trifluoride-methanol solution (14 %), trifluoromethanesulfonic acid (98 %), aluminium chloride ($AlCl_3$, 99%), bismuth(III) trifluoromethanesulfonate (99 %), triarylsulfonium hexafluoroantimonate salts (50 % in propylene carbonate), hydrogen peroxide solution (H_2O_2, 30 %w/v), ethyl lactate (98 %), 2,5-hexanedione (98 %), isopropanol (98 %), citric acid (99.5 %), acetic acid (99.5 %), MMT K10 (Montmorillonite K10), hydrochloric acid (37 %), dimethyl sulfoxyde (DMSO, 98 %) were purchased from Sigma-Aldrich. Chromium(III)acetylacetonate (97 %), amberlyst 15(H) and phenylhydrazine hydrochloride (99 %) were purchased from Alfa Aesar. The *d6*-DMSO was acquired from Eurisotop. Ethanol (96 %v) was purchased from VWR. Ethyl acetate (EtOAc, 99 %), Iodine (99 %) and formic acid (97 %) were purchased from carlo erba. Organically modified montmorillonite (Org-MMT) with octadecyl ammonium cations, was supplied from Nordmann, Rassmann GmbH (Nanomer I30E). Aluminoxid 90 neutral was acquired by Carl Roth.
Water was distilled with a SI analytics distillation unit (conductivity ≈1 µS/cm).

All chemicals were used as received, excepted FA which was used as received (i.e. commercial grade FA). Or was fractionally distilled two times at atmospheric pressure (distilled FA). The purity of distilled FA was investigated by DSC and found to be better than 98%.

Preparation of PFA resins:

For section 2.2, two kinds of PFA resins, namely PFA° and PFA+, were prepared. PFA° or PFA 100/0 refer to a PFA prepared in neat conditions and with 2 %w of MA. PFA+ or PFA 50/50 was prepared in 50 % aqueous solution from the beginning of polymerization and 2 %w of MA. It may be noted that FA and MA both have a molecular weight of 98.1 $g.mol^{-1}$. Thus, in a solution of FA, 2 %w of MA = 2 %mol of FA. In all cases, the percentage of catalyst is calculated on the amount of FA.

Typical syntheses of PFA were performed as follow: First, a room temperature mixing was conducted to ensure complete homogenization of components in 150 mL glass round bottom flask equipped with water condenser before initiating the polymerization. In this chapter, the batches of polymers were about 20-40 g, based on the initial amount of FA. Heating was controlled with regulated oil bath. The solutions were then gradually heated. In most cases, the temperature was set to 80-85 °C for 1 h, then the condenser was removed, and the temperature gradually increased up to 120 °C over the course of 1 to 5 h, depending on the conversion degree desired. In Section 2.4, many PFAs were prepared and analyzed. Their conditions of preparation are reported in Table 2.7-1 and Table 2.7-2. Samples were collected at different moments in the process, and stored at 4 °C. The sampling process is illustrated in Scheme 2.1-1.

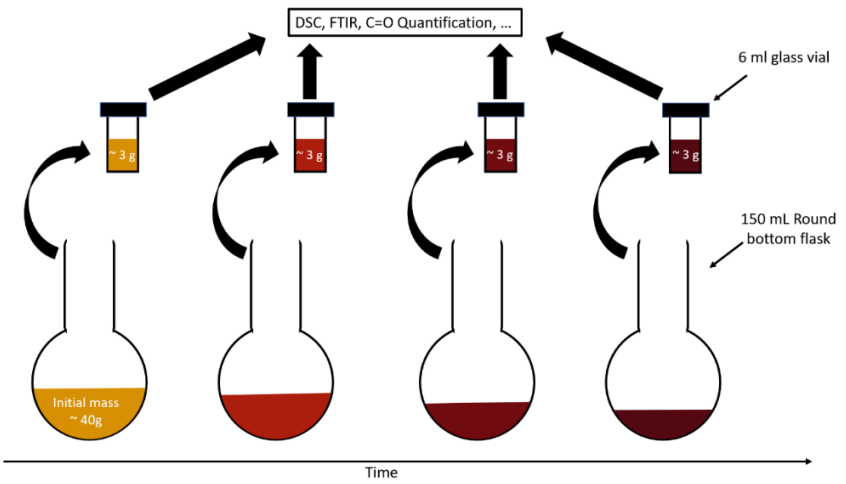

Scheme 2.1-1. Sampling process.

Carbonyl quantification by wet methods:

Based on previous work of Faix et al. and Black et al. [318, 319] three protocols were developed to quantify carbonyl groups and acid groups in PFA. Protocols are illustrated in Scheme 2.1-2.

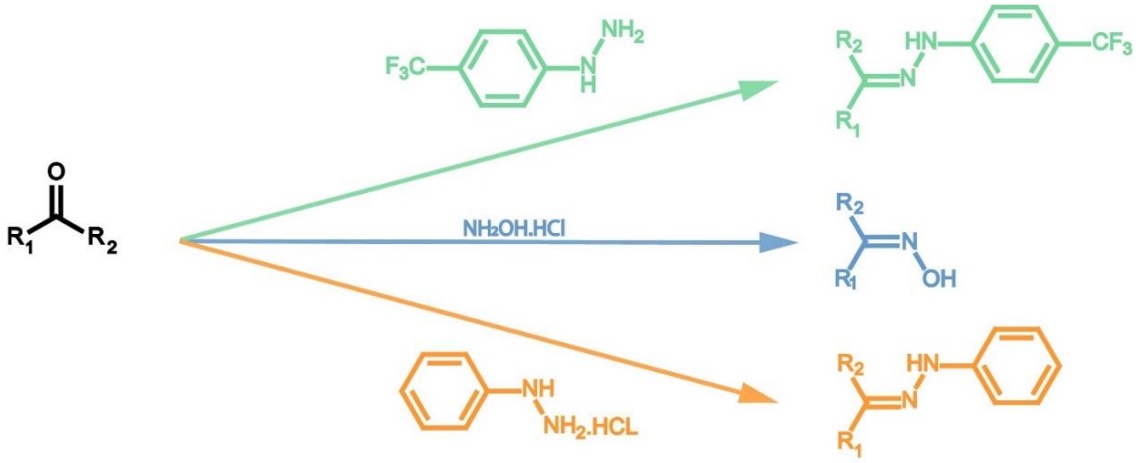

Scheme 2.1-2. Reaction schemes used for carbonyl quantifications methods.

In 13 mL glass vials, 90-150 mg of PFA were accurately weighted and 2 mL of DMSO were added. Mixtures were heated at 80 °C for 5 mins then shaken until complete dissolution of PFA. To the cooled-down DMSO - PFA solution, 2 mL of 0.44 N hydroxylamine hydrochloride ($NH_2OH.HCL$) solution in 80 %v EtOH were introduced followed by 2 mL of 0.52 N triethanolamine solution in 96 %v EtOH.

This protocol was replicated with phenylhydrazine hydrochloride ($\Phi NHNH_2.HCl$) as a replacement of $NH_2OH.HCL$. Only difference was the need to preheat $\Phi NHNH_2.HCl$ solution at 80 °C for solubility purposes.

Acids quantifications were conducted as follows. To the DMSO - PFA solution 2 mL of 80 %v EtOH were added followed by 2 mL of 0.52 N triethanolamine solution in 96 %v EtOH. Samples were triplicated and controls prepared every time.

In each case, vials were placed in an oven at 80 °C for 24 h before titration by 0.08 N HCL. Samples were allowed to cool down to room temperature before titration. HCl concentration was determined with dry Na_2CO_3. Carbonyl contents were calculated using Equation 2.1-1. V and V_0 are the endpoints of samples and blanks, respectively. Endpoint were determined using inflexion point ($3.5 < pH < 4.0$). m_{PFA} is the mass of PFA. The DOS obtained from this method is called $DOS_{Titri.}$

$$C = O\ content = \frac{(V_0 - V)}{m_{PFA}} * [HCl] \quad \text{Equation 2.1-1}$$

To calculate degree of open structures within the resins, Equation 2.2-1was re-adapted in Equation 2.1-2 taking into account the C=O content.

$$Degree\ of\ open\ structures\ (DOS) = \frac{1}{2}.1000.COcontent.M_{(furfuryl\ unit)} \quad \text{Equation 2.1-2}$$

As the oximation kinetics of carbonyls within PFA was unknown, experiments were carried out to determine the optimal duration of oximation. Figure 2.1-1 shows the calculated DOS_{Titri} against oximation time of PFA°. DOS_{Titri} increases until 20 h of oximation where a plateau if reached. This was also observed with PFA+. Therefore, an oximation time of 24 h was chosen to avoid underestimation of carbonyl content. Moreover, residues from the titrimetry were analyzed with FTIR (spectra in Figure 2.1-2) to ensure consumption of the carbonyls.

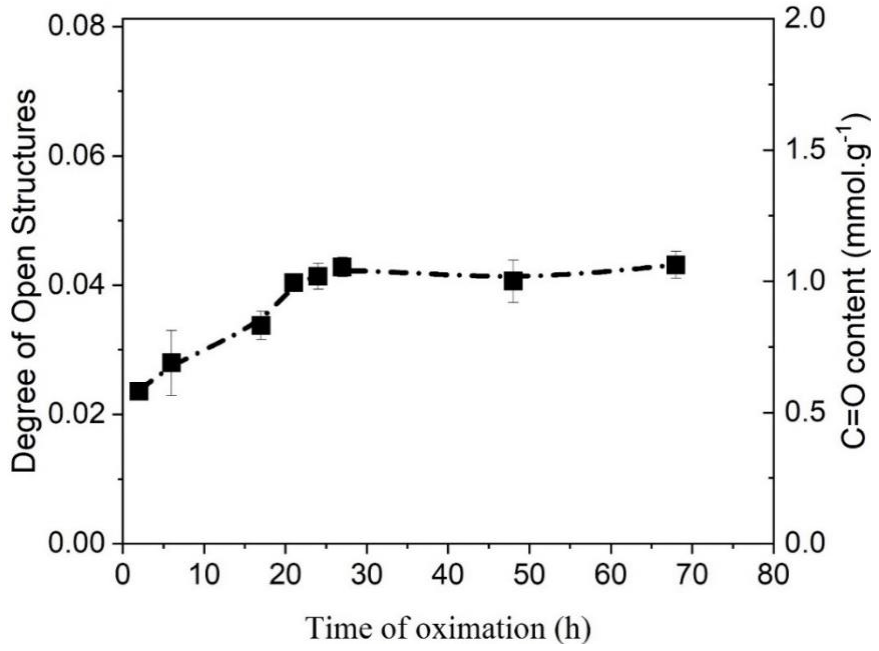

Figure 2.1-1. DOS_{Titri} of a PFA° as function of oximation time. Line is meant to guide the eyes.

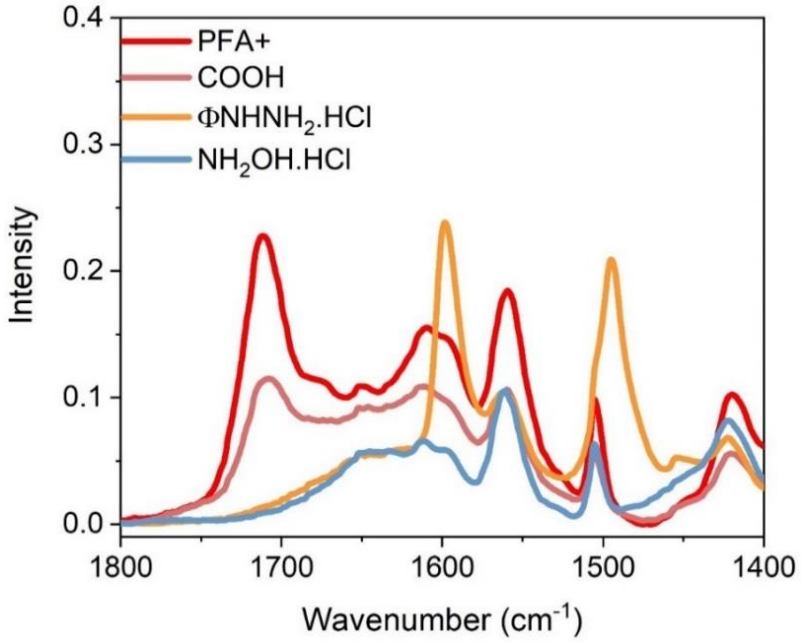

Figure 2.1-2. FTIR spectra of a PFA+ before and after titration with different derivatizing agents.

Carbonyl quantification by ^{19}F NMR:

Based on previous work of Constant et al. [326], the following protocol was adopted, it is illustrated in Scheme 2.1-2. In 1.5 mL vial, 70 - 130 mg of PFA were introduced, followed by about 140 mg of 4-(trifluoromethyl)- phenylhydrazine and ($CF_3\Phi NHNH_2$), 20 mg of 1,4-bis(trifluoromethyl)benzene internal standard. Then, 400 µL of d_6-DMSO were added before being shaken for ≈ 10 mins followed by 5 s centrifugation. Contents of vials were transferred to NMR tubes before being heated at 40 °C for 24 h. Just before analysis, 100 µL of 28 $mg.mL^{-1}$ relaxing agent - chromium acetyl acetonate- in d_6-DMSO were added and homogenized.

As highlighted by Constant et al., [326] commercial $CF_3\Phi NHNH_2$ contains about 3 % of an impurity which overlaps with hydrazones. Using a reference containing $CF_3\Phi NHNH_2$ and the internal standard, the impurity amount was determined for every batch and used as a correction factor. Carbonyl contents were calculated using Equation 2.1-3. A_C and A_{IS} respectively stand for hydrazones and internal standard areas. A 0.5 factor is used as the internal standard bears two CF_3 groups. M_{IS} and m_{IS} are the molar mass and mass of internal standard. A_{H° and m_{H° are the area of the impurity and the mass of $CF_3\Phi NHNH_2$ in the reference. The mass of hydrazine in the sample is m_H and m_{PFA} the mass of PFA. Then, Equation 2.1-2 and Equation 2.1-3 are used to calculated DOS_{NMR}.

$$C = O\ content\ _{NMR} = \frac{\left[A_c - \left(\frac{A_{H^\circ} * m_H}{m_{H^\circ}}\right)\right] * m_{IS}}{A_{IS} * 0.5 * m_{PFA} * M_{IS}} * 10^3 \quad \text{Equation 2.1-3}$$

Liquid state Nuclear Magnetic Resonance (NMR):

NMR spectra were recorded on a Bruker AVANCE III (400 MHz). Spectra were processed with MestReNova software.^{19}F NMR Spectra were carried out using standard fluorine 90° pulse program, a relaxation delay of 3 s and 256 scans acquired between -35 and -85 ppm. ^{19}F spectra chemical shifts are given in reference to internal standard at -62.15 ppm. The parameters were selected on the basis of the work of Constant et al. [326] Phase correction and a Breinstein polynomial (order 3) baseline correction were applied.

The ^{13}C NMR spectra were recorded with a 2 s relaxation delay and 6000 scans between -27.4 and 266.3 ppm. A high number of scans were used to ensure good signal/noise ratio in the carbonyl area.

Solid state Nuclear Magnetic Resonance (NMR):

The Solid-state ^{13}C spectra were obtained on a Bruker AVANCE III (400 MHz) NMR spectrometer using a double channel Bruker probe. About 100 mg of sample was placed in zirconium dioxide rotor of 4 mm outer diameter and spun at a Magic Angle Spinning rate of 10 kHz. The ^{13}C CPMAS technique was applied with a ramped ^{1}H-pulse starting at 100% power and decreasing to 50 % during the contact time (2 ms) to circumvent Hartmann−Hahn mismatches. For ^{13}C Single Pulse Experiment with ^{1}H Decoupling (HPDEC), the acquisition parameters were 3.4 µs 45° pulse, 10 s recycle delay and 5 K scans. [327] Spectra were processed with MestReNova software, phase correction and a Breinstein polynomial (order 3) baseline correction were applied. The ^{13}C chemical shifts were referenced to tetramethyl silane and calibrated with glycine carbonyl signal, set at 176.0 ppm.

Differential Scanning Calorimetry (DSC):

DSC were performed on DSC1 from Mettler Toledo in high-pressure gold-plated steel crucibles (30 µL) from 0 to 300 °C at 2 °C.min^{-1}. STARe software was used for evaluating the DSC data. DSC was calibrated with zinc and indium standards. The conversion degree - α - was calculated according to previous work (Equation 2.1-4)[180, 301, 307]

$$\alpha = \frac{\Delta H_{Max} - \Delta H_{residual}}{\Delta H_{Max}} \quad \text{Equation 2.1-4}$$

α values are given ± 0.02. ΔH_{Max} represents the maximum heat of polymerization related to pure FA and $\Delta H_{residual}$ the heat of reaction of the sample taken after a certain time/temperature of polymerization in the flask ΔH_{Max} was averaged out of 10 attempts, i.e. about 610 J.g^{-1}. An example of the exploitation method employed for DSC curves is given in Figure 2.1-3.

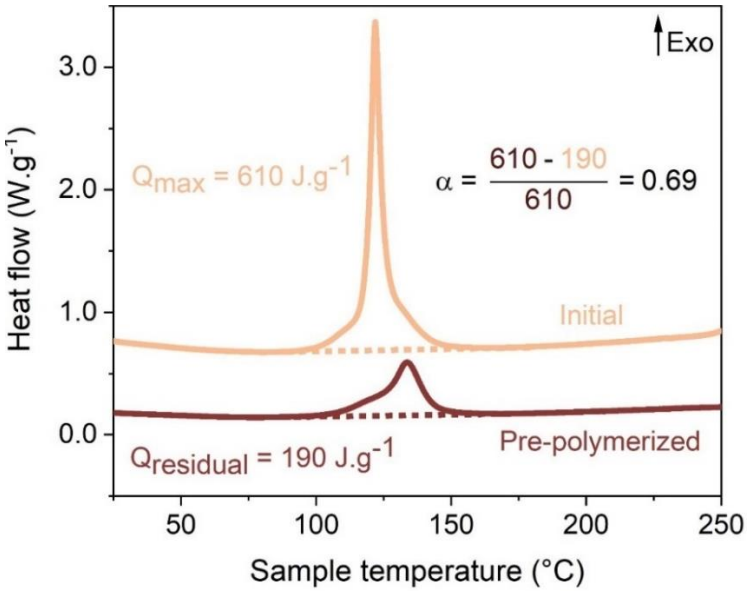

Figure 2.1-3. Example of an exploitation of a thermogram of PFA and α calculus. DSC scan at 2 °C.min^{-1} from 20 to 300 °C.

Fourier-Transform Insfrared Spectroscopy (FTIR):

A Thermoscientific Nicolet IS 20 equipped with an ATR device (Pike technologies gladiator -3 mm diamond crystal diameter-) was used. Spectra were recorded from 400 to 4 000 cm^{-1} with accumulation of 64 scans and a resolution of 4 cm^{-1} with spectrum of air as background. OMNIC and Origin softwares was used for data analysis.

Throughout the polymerization of FA, a very intense band is observed around 1010 cm^{-1}. It is mainly attributed to FA's furan ring C-O stretching at 1012 cm^{-1} which overlaps with 2,5-disubstituted ring C-H in plane wagging at 1018 cm^{-1} (among others), leading to a progressive shift.[293, 294] Overall, the band at ≈ 1000 cm^{-1} is intense and stable enough to be used for normalization. Normalization is mandatory here as it reduces the influence of sample – diamond interface which affects peaks intensities. Especially as PFA samples present progressive modification of their physical states from liquid, viscous and rubbery resins. Figure 2.1-4 gives a visual aspect of PFA resins collected during the polymerization. The FTIR C=O area was set to (1650 – 1870 cm^{-1}), to englobe all kinds of carbonyls. [328]

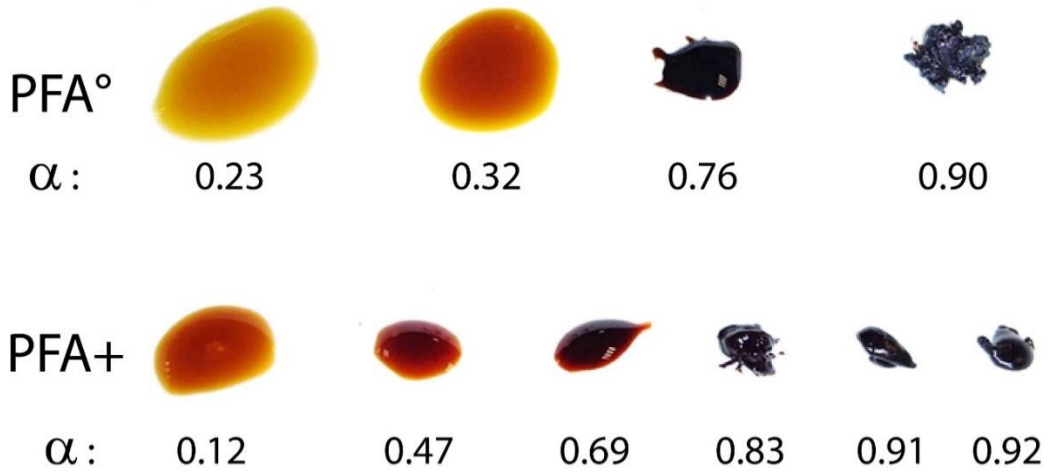

Figure 2.1-4. Visual appearance of PFA° and PFA+ with the conversion.

Lab scale humins

Lab-scale humins were prepared using process similar to van Zandvoort et al. [80, 329] Fructose (1 M in distilled water) was used as a sugar source and H_2SO_4 was employed for acidification. Humins were either prepared in a Teflon lined autoclave (AC, Figure 2.1-5) or in a round bottom flask (RBF). Table 2.1-1 reports the conditions of preparation of the lab scales humins and their yield. The crude humins were washed with distilled water, dried at 50 °C, ground, washed with distilled water and dried again. Figure 2.1-5 depicts the typical aspect of lab-scale humins. The yield of humins was calculated using the masses of washed and dried humins. The C=O content was determined by titrimetry only. Three kinds of humins were prepared, in a attempt to have more or less condensed humins. In Table 2.1-1 “Hu1” correspond to the most condensed humins, i.e the harshest conditions, Hu3 is the least consented humins and Hu2 is an intermediary.

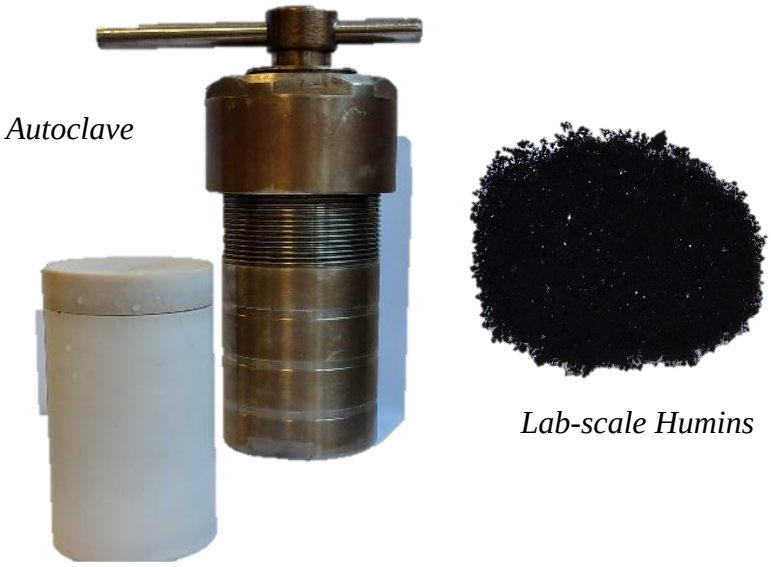

Figure 2.1-5. Pictures of the autoclave (left) and humins (right).

Table 2.1-1. Conditions of the preparation of humins and yields

Sample	Reactor type	Temperature (°C)	Time (h)	$[H_2SO_4]$ ($mol.L^{-1}$)	Yield of Humins
Hu1	AC	180	24 h	0.1 M	22.8 ± 1.3
Hu2	AC	180	24 h	0.01 M	30.2 ± 2.1
Hu3	RBF	Reflux	6 h	0.1 M	15.5 ± 4.0

**AC: Autoclave, RBF: Round Bottom Flask*

2.2 Development of quantification

This section deals with the development of C=O quantification methods adapted to furanic thermosets, i.e PFA and humins.

Two categories of PFA resins were synthetized. In the first type of resin, FA was polymerized in presence of an acidic initiator – maleic anhydride (MA) – without addition of any protic polar solvent to limit as much as possible the furan ring opening (PFA°). On the contrary, the second type of resin was prepared in 50 % aqueous solution (PFA+) to favor the ring opening reaction without compromising the polymerization reaction. For the first time, the carbonyl content was quantified with accurate methodologies (i.e. NMR quantification or titration) and not only quantitatively assessed. Interestingly the evolution of carbonyl content and consequently the C=O content was investigated with the course of polymerization. Different resins were prepared at different time/temperature of polymerization and the conversion degree of polymerization of each resin was precisely assessed from DSC and FTIR data.

Carbonyls in PFA were determined and quantified via two strategies which take advantage of the high reactivity of carbonyls towards hydrazine and hydroxylamines compounds to respectively form hydrazones and oximes. The first method was based on the oximation reaction of carbonyls with hydroxylamine hydrochloride followed by potentiometric titration. A preliminary investigation was necessary to understand the role played by the oximation time, and presence of acids. The second methodology involved a ^{19}F NMR quantification employing a fluorinated phenyl hydrazine. Finally, ^{13}C quantitative solid-state NMR was carried out to corroborate with the other methods.

2.2.1 Validation of the quantification methods

The main objective of this section is to breakthrough knowledge on the carbonyl formation in PFA resins through the comparison of the oximation with the ^{19}NMR quantification.

First, PFA+ samples were collected during the polymerization (from undistilled FA) to understand the process of carbonyls formation. A progressive darkening associated with cross-linking development is observed and it is correlated with a progressive increase of the viscosity (Figure 2.1-4). For each sample, the conversion degree of FA (α) was determined and employed to monitor the evolution of polymerization independently of time or temperature conditions. However, the complex polymerization process of FA involves several reactions. Therefore, highly exothermic reactions can mask nearly athermic ones. This effect is especially significant for solid state reactions. [301]

To circumvent this, the polymerization was also monitored using FTIR. This spectroscopic technique is complementary to DSC as it will be more sensitive to structural changes when athermic reactions in the solid state are becoming predominant. End of polymerization stages will be barely distinguishable with DSC while FTIR bands can vary strongly. This is the case for C=O stretching which can be seen from 1650 to 1870 cm^{-1} in FTIR spectra.[330]. As demonstrated by Faix et. al, the normalized FTIR C=O area is linear with the C=O content of lignins, provided the absence of species such as ketals and esters. [319] The same rationale was employed herein. Figure 2.2-1 shows the FTIR spectrum of undistilled FA (α = 0) and the spectral evolution with the conversion of FA. The formation of PFA network is clearly seen in the progressive increase of the peak at 1560 cm^{-1} that corresponds to the C=C stretching of 2,5-disubstituted furan rings. In the meantime, a broad peak between 1650 cm^{-1} and 1800 cm^{-1} is developing with conversion. This region corresponds to the C=O stretching of carbonyls. The appearance of this peak can be also noticed at early stage (α = 0.12). Such evolution is the direct consequence of the progressive carbonyl formation in the system. Therefore, the area of this peak can be taken to monitor the formation of carbonyls during FA polymerization.

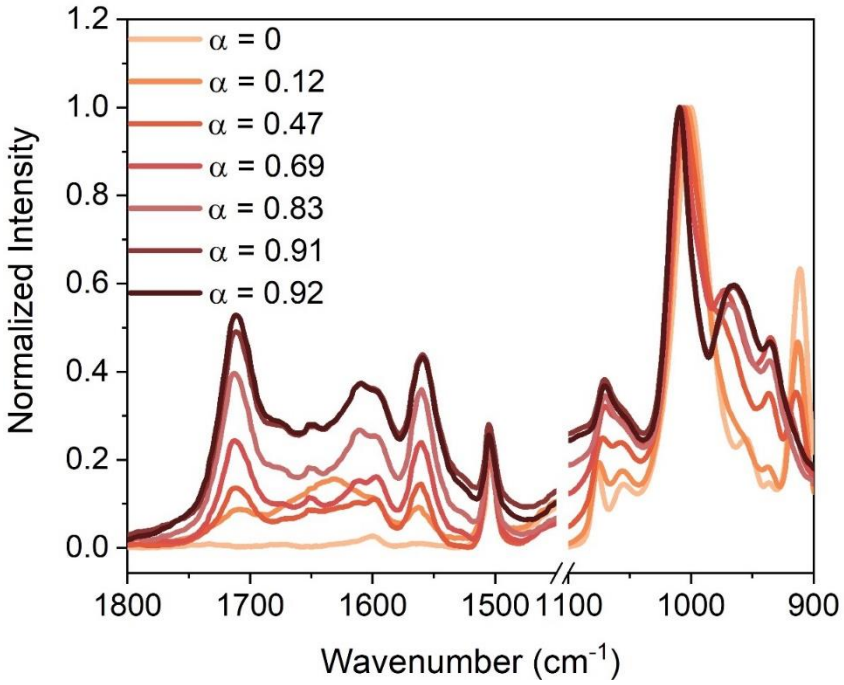

Figure 2.2-1. Normalized FTIR spectra of PFA+ (starting from undistilled FA) as function of conversion. α = 0 corresponds to the initial spectrum of undistilled FA.

PFA+ samples were subjected to three C=O quantification methods. In addition, carboxylic acids such as levulinic acid can be formed during the polymerization process, thus the COOH content was determined in PFA+. Initial carbonyl content was also determined on neat FA which contains some traces of furfural impurities.

The COOH content and C=O content by titration (employing two different derivatizing agents) and C=O content from ^{19}F NMR quantification is shown in Figure 2.2-2 as a function of the progress of carbonyl development during FA polymerization along with the conversion degree.

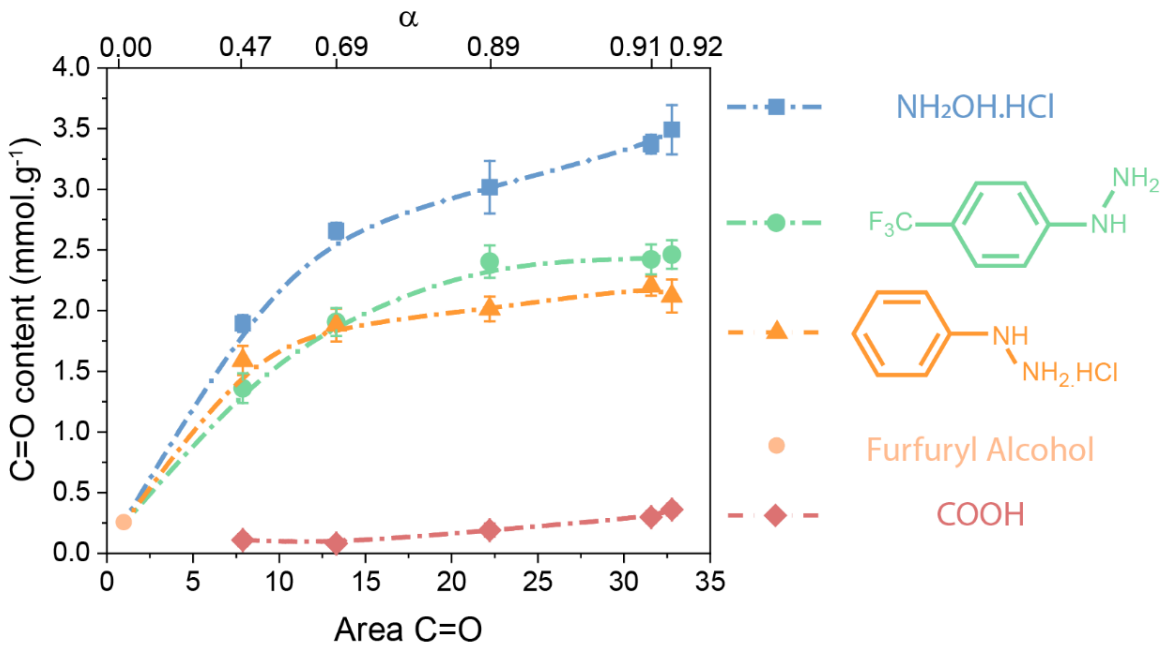

Figure 2.2-2. Carbonyls content (in $mmol.g^{-1}$) obtained for PFA+ (prepared with undistilled FA) from oximation with $NH_2OH.HCl$ (squares) or with $\Phi NHNH_2.HCl$ method (triangles) and from ^{19}F NMR quantification $CF_3\Phi NHNH_2$ (circle). Diamonds are for the acid content. The data are plotted against FTIR normalized C=O area (bottom abscissa axis) and DSC conversion degree (up abscissa axis). Error bars correspond to the standard deviation of triplicates.

The oximation and the ^{19}F NMR methods are in the same range in the first stage of polymerization. On the other hand, there is a clearcut difference at the end of polymerization. When $NH_2OH.HCl$ is employed, the carbonyl content continue to increase while a plateau is observed at the end of polymerization when the two phenylhydrazines are employed. Therefore, the nature and/or the size of the derivatizing agent is the most influencing factor on the quantification of carbonyl rather than the method itself (i.e. titration or quantitative NMR). It is likely that bigger derivatizing agent - i.e. $CF_3\Phi NHNH_2$ or $\Phi NHNH_2.HCl$ - with much more steric hindrance than the mobile $NH_2OH.HCl$ - will have more difficulty to react with carbonyls. This will be especially the case for the late phase of polymerization where carbonyls will become less accessible with the progressive increase of the cross-link density.

Presence of carboxylic acids was investigated trough the use of COOH blanks, as suggested by Faix et al. for acidic lignins. [319] As highlighted in Figure 2.2-2, a very low quantity of carboxylic groups (< 0.25 mmol.g^{-1}) is measured in PFA+. The COOH quantity slightly increases in the final phase of polymerization. Anyhow, their amount is too low to explain differences seen between $CF_3\Phi NHNH_2$ derivatization (^{19}F NMR method) and the oximation method with $NH_2OH.HCl$. The pinpoint of such large difference - especially at the end of polymerization could be somehow exploited to monitor the carbonyl accessibility especially when the network of PFA becomes denser.

Besides, it could be argued that the oximation method leads to further ring opening as it liberates HCl in the medium. However, $\Phi NHNH_2.HCl$ method exhibits a plateau in the same way as the $CF_3\Phi NHNH_2$ derivatization method. Liberated HCl is therefore not inducing further furanic ring openings in significant amounts.

On a side note, Constant et al. obtained 2.35 mmol.g^{-1} of C=O in industrial furanic humins using the ^{19}F method. [326] This is consistent with the most advanced PFA samples studied here (2.46 mmol.g^{-1} for PFA+ with α = 0.92).

During the polymerization of FA, (hemi)acetals and/or (hemi)ketals might form the carbonyls as alcohol and water are present in the present acidic system. Effect of (hemi)acetals or (hemi)ketals was investigated using bromoacetaldehyde dimethyl acetal as an acetal model and subjecting it to carbonyl quantification methods. Results from this investigations are reported in Table 2.2-1.

About 40 % of this acetal model reacted in the oximation method ($NH_2OH.HCl$) while less than 5 % reacted with the $CF_3\Phi NHNH_2$ derivatization method. When subjected to $\Phi NHNH_2.HCl$, 24 % of the acetal model reacted. On top of that, Constant et al. subjected 2-(diethoxymethyl)furan to $CF_3\Phi NHNH_2$ derivatization. No significant amount of hydrazone was found. [326] Theses results leave out the possibility that (hemi)acetal or (hemi)ketal formation as a possible explanation for the lower carbonyl content obtained by NMR.

Table 2.2-1. Data resulting from subjecting ketal model to carbonyl quantification methods.

Derivatizing agent	% of Bromoacetaldehyde dimethyl acetal reacted
$NH_2OH.HCl$	≈ 40 %
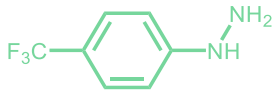	≈ 0 %
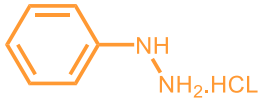	≈ 24 %

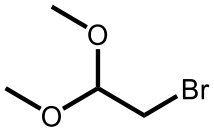

Bromoacetaldehyde dimethyl acetal

One could also argue the formation of pyrroles during the derivatization by $CF_3ΦNHNH_2$ and $ΦNHNH_2$.HCl. Indeed, Alvi et al. demonstrated that hydrazines can react with 1,4-diketones to form pyrrole-like structures. [331] In such case, two carbonyls would account as one when the by $CF_3ΦNHNH_2$ and $ΦNHNH_2$.HCl derivatizing agents are used. Hence, a model compound (2,5-hexanedione) was subjected to the ^{19}F NMR method. Figure 2.2-3 shows the restults of this experiment. The internal standard is present on the spectra (-62.2 ppm) but is not displayed on Figure 2.2-3.

In Figure 2.2-3, four peak can be distinguished. The one on the extreme left corresponds to $CF_3ΦNHNH_2$. The three other peaks are products of the reaction between $CF_3ΦNHNH_2$ and 2,5-hexanedione. When the three later peaks are integrated a C=O content of 17.0 mmol.g^{-1} is obtained and is equal to the theoretical one ($M_{2,5\text{-hexanedione}}$ = 114.14 g.mol^{-1}, with two C=O per molecule). From this it can be deduced that the ^{19}F NMR method does not induce the formation of pyrroles, at least in the conditions used here. Hence, pyrroles are not responsible for the inconsistencies observed in Figure 2.2-2. The presence of three peaks can be attributed to the various isomers of the product (Z/Z, Z/E and E/E). Separated ^{19}F chemical shifts for diastereoisomers was demonstrated by Constant et al. [326]

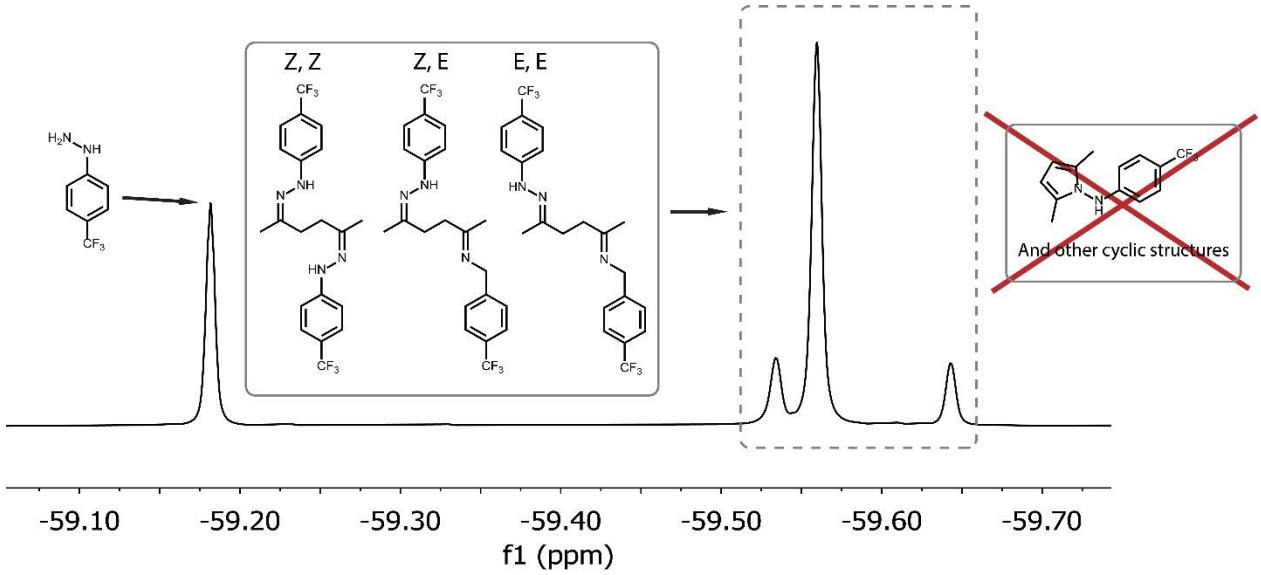

Figure 2.2-3. ^{19}F NMR spectra of derivatized 2,5-hexanedione

To further confirm the validity of the methods, quantitative ^{13}C solid state NMR (HPDEC) was carried out as a derivatization-free method. Spectrum of an advanced PFA+ (α = 0.92) is shown in Figure 2.2-4. The C3 and C4 furanic carbons (≈ 108 ppm) allow to approximate the proportion of furan ring.

When opened the C2 and C5 carbons of the furan ring will be transformed in two aliphatic carbons, considering an opening within the macromolecular chain. Therefore, the carbonyl content can be approximated using 208 ppm peak corresponding to the ketonic species. The integration of ketonic carbons at 208 ppm (13.6) rationalized to the integration from C3 + C4 furanic carbons - set to 100 - gives a carbonyl content of 3.4 mmol.g^{-1} for PFA+ at α = 0.92. These results are in perfect agreement with the oximation results (Figure 2.2-2) for which the carbonyl content is 3.5 ± 0.2 mmol.g^{-1} at α = 0.92.

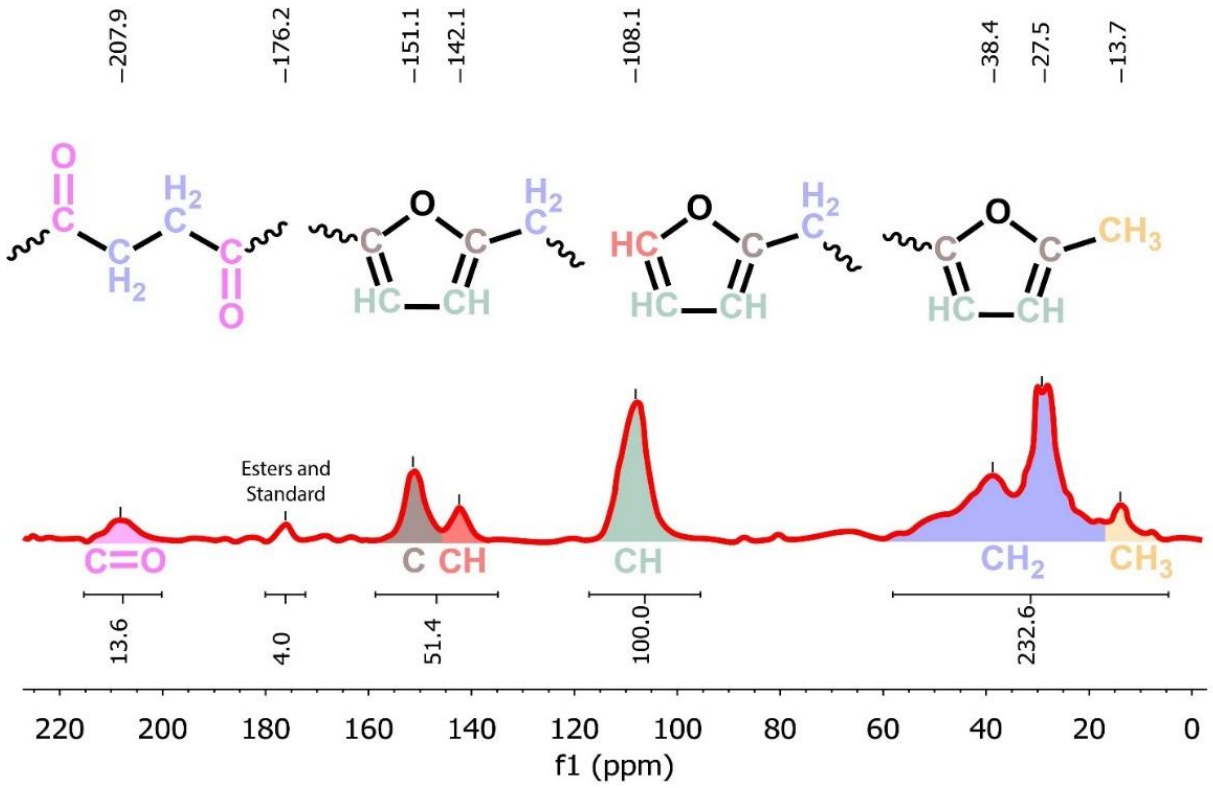

Figure 2.2-4. Quantitative ^{13}C solid state NMR (HPDEC) spectrum of a PFA+ (α = 0.92).

2.2.2 Degree of Open Structure (DOS) in PFA° and PFA+ systems

In this section the concept of degree of open structures (DOS) in PFA resins is introduced and employed to better visualize the impact of ring-opening reactions. Scheme 2.2-1 shows PFA structure obtained after self-polycondensation of FA units followed by inter-chains cross-links via Diels-Alder cycloaddition. Open structures with 1,4-diketones are also highlighted in Scheme 2.2-1. Assuming that furanic entity can lead to two carbonyl groups the degree of open structures in PFA can be estimated using in Equation 2.2-1.

$$Degree\ of\ open\ structures\ (DOS) = \frac{1}{2}.\frac{N_{C=O}}{N_{furanic}} \quad \text{Equation 2.2-1}$$

Where $N_{C=O}$ is the number of carbonyls (ketones) and $N_{furanic}$ is the number of furanic units. In the example of Scheme 2.2-1 there are C=O for 20 furanic units (N.B: the cycloadduct count for two furanic units) which thus give a DOS = 0.15. It means that 15 % of furanic units have been opened is this example

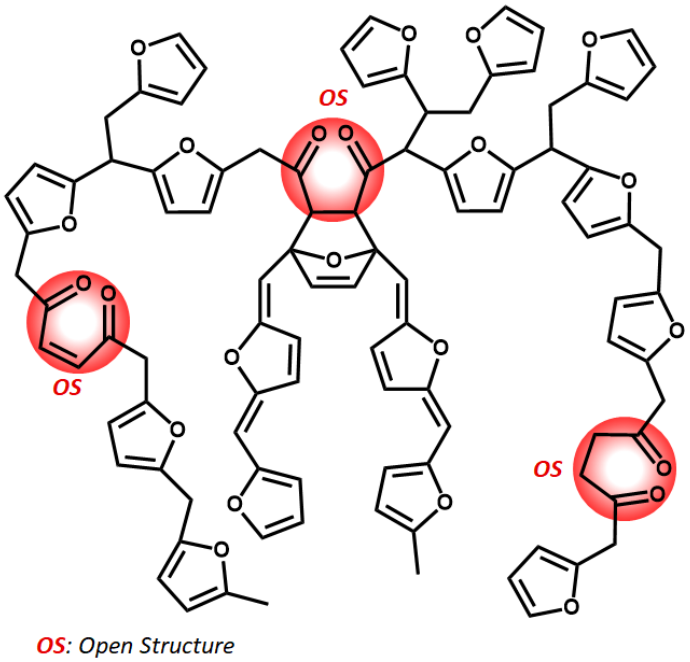

Scheme 2.2-1. Simplified scheme of PFA and its potential opened structures.

As highlighted in Scheme 2.2-1 and Equation 2.1-2, the DOS is a more visual concept than the carbonyl content per gram of PFA. The following section aims at comparing the DOS evolution during polymerization both in PFA+ system, i.e 50 % aqueous, and in a neat PFA° system. For this purpose, both titration and ^{19}NMR quantification were employed to quantify the DOS in PFA° and PFA+.

Figure 2.2-5 presents the DOS_{Titri} evolution for both PFA+ and PFA° as a function of the conversion degree α. PFA resins were either prepared with undistilled FA and distilled FA. First, as the oligomerization begins ($0 < \alpha < 0.40$) the DOS_{Titri} quickly rises to 0.05 - i.e. 5 % of furan ring opened - for both PFA° and PFA+. Then, the polymerization keeps going and carbonyls form with a steady rate for both systems. Interestingly, the DOS_{Titri} of both PFA° and PFA+ increase continuously for $\alpha > 0.20$ and this increase can be approximately linearly fitted.

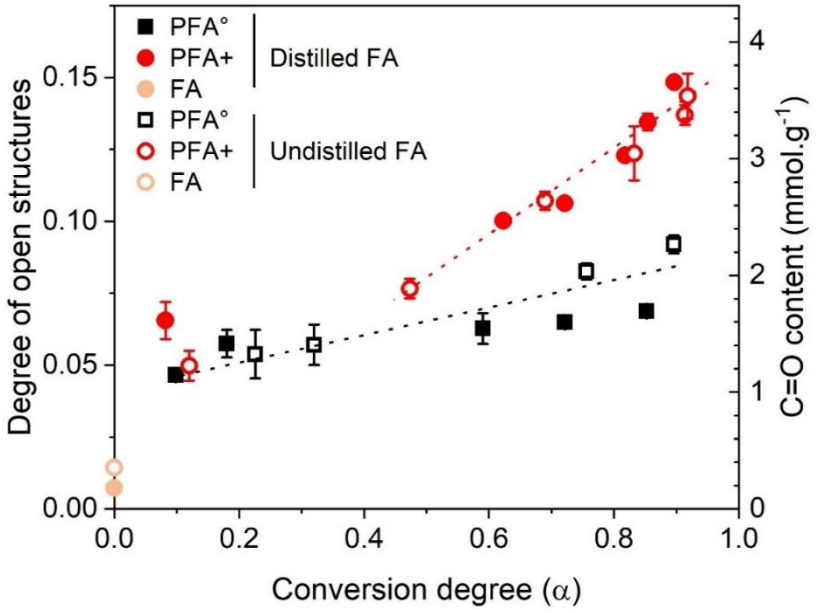

Figure 2.2-5. Evolution of DOS_{Titri} against the conversion degree for PFA° (black squares) and PFA+ (red circles). Open and solid symbols are for samples prepared with undistilled FA and distilled FA respectively. Dot lines represent the linear fits. Error bars correspond to the standard deviation of triplicates.

Overall, at a given conversion, PFA+ system exhibits higher DOS than PFA° (Figure 2.2-5). This difference is particularly marked for $\alpha > 0.20$ and suggest higher ring opening rate for PFA+. It therefore confirms that a polymerization in 50 % aqueous solution of FA will favor the formation of carbonyl groups. This difference can be explained by the increased rate of formation of furfuryl carbocations in polar solvents as shown by Kim et al. [289]

The formation of the furfuryl carbocation is a rate limiting step for the condensation reactions. Correlations can also be made with previous studies in which silylated furfuryl alcohol – furfuryloxytrimethylsilane - and furfuryl acetate were employed to avoid hydrolytic ring opening due to water produced during condensation reactions. [281, 276] Furthermore, Shi et al. also reported the importance of water in the formation of humins and hydrolytic furan ring opening. [332]

The DOS' increase throughout the polymerization (Figure 2.2-5) underlines that furan ring opening is a phenomenon occurring in concomitance with other reactions. Such conclusion agrees well with the non-sequential formation of PFA previously reported. [293]

Noteworthy is the difference obtained for the most advanced resinous PFA samples – i.e for $\alpha > 0.85$. DOS_{Titri} is about (0.14 ± 0.01) and (0.08 ± 0.02) respectively for PFA+ and PFA°. It indicates that there are more than 1.7 times more open structures in PFA resins when polymerization is conducted in water (50 % aqueous solution).

As shown in Figure 2.2-5, two batches (i.e. starting either from distilled or undistilled FA) for both PFA+ and PFA° were prepared and their DOS_{Titri} were compared. Inter-batch correlation can be done for PFA+ whose linear fit for $\alpha > 0.50$ has a rather good correlation coefficient ($R^2 \approx 0.95$). On the other hand, the goodness of the fit decreases for PFA° ($R^2 \approx 0.76$) indicating that inter-batch correlation is less relevant in this case or the impurities in FA lead to slightly more carbonyls in PFA° systems. The end-points of PFA+ are not well separated in Figure 2.2-5 when plotted as function of α. To circumvent this issue, the DOS_{Titri} of PFA° and PFA+ was plotted in Figure 2.2-6 as function of the overall C=O area (1650 - 1870 cm^{-1}). These areas have been determined from the FTIR spectra of PFA° (Figure 2.7-1) and PFA+ (Figure 2.2-1).

It is interesting to notice that the PFA+ system presents both higher DOS values but also larger normalized FTIR C=O area values than those of PFA°. This confirms that polymerization of FA in 50 % aqueous solution increases the occurrence of ring opening reactions and thus the amount of carbonyls. FTIR data gives a better vision of carbonyl formation in late polymerization stages as the six last points for PFA+ are much better separated when the area of carbonyls (Figure 2.2-6) is considered rather than the conversion degree (Figure 2.2-5). The simultaneous increase of both DOS_{Titri} and the normalized FTIR C=O area suggest that carbonyls keep being formed even in the rubbery state. These results highlight again the crucial role of water in ring opening reactions.

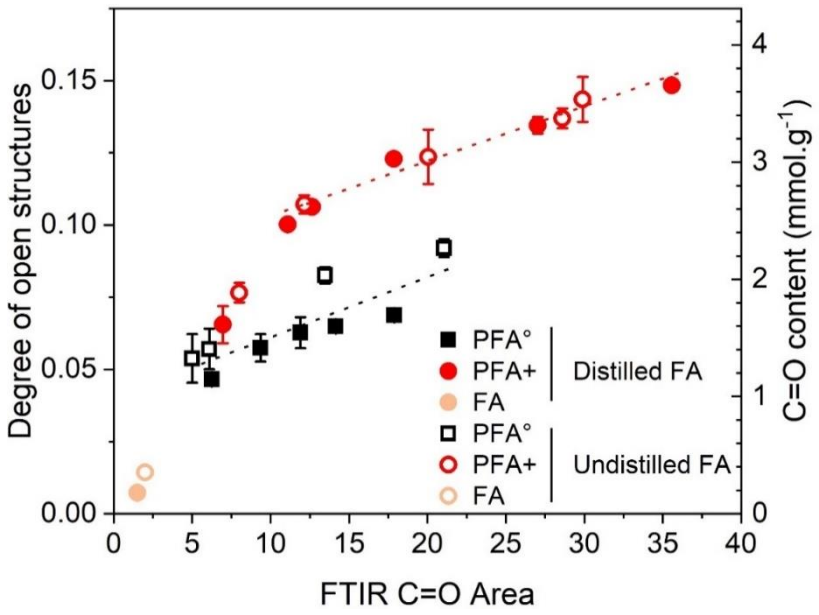

Figure 2.2-6. Evolution of DOS_{Titri} against FTIR normalized C=O area for PFA° (black squares) and PFA+ (red circles). Open and solid symbols are for samples prepared with undistilled FA and distilled FA respectively. Dot lines represent the linear fits. Error bars correspond to the standard deviation of triplicates.

Faix et al. performed a similar study on lignins. They obtained good linear correlation between carbonyl content and normalized FTIR C=O area ($R^2 \geq 0.98$) thus confirming the coherence between the oximation method and the FTIR spectroscopy. [319]

In the present study, a good correlation coefficient is obtained for PFA+ (employing the distilled and undistilled batches) for a part of the polymerization process. This underlines the existence of other phenomenons which affects either the normalized FTIR C=O area or the DOS or both. The presence of water in the samples could be an explanation as it might dilute the PFAs oligomers and increase normalized FTIR C=O area. Notwithstanding, contamination with water can be seen in FTIR with the broad peak at 1640 cm^{-1} appearing in the spectrum of PFA+ at α = 0.12 (Figure 2.2-1). Accordingly, such points have been removed from Figure 2.2-6. Moreover, samples with higher conversion degree PFA is highly apolar, leading to very low residual water. For PFA°, the deviation might lie in the presence of a shouldering around 1750 cm^{-1} (Figure 2.7-1). Indeed, such shape suggests that other carbonyl species are present in this system, possibly end-chain esters or lactones as previously postulated.[273, 283, 284] These species are not taken into account in the oximation method but are part of the normalized FTIR C=O area. Interestingly, this shouldering around 1750 cm^{-1} is absent in PFA+ systems. It might be caused by lactone opening or end-chain furan ring opening before lactone formation.

The evolution of DOS_{NMR} - either as function of α or C=O area - is presented in Figure 2.7-2 and Figure 2.7-3 and follow the same increasing trend as observed for the DOS_{Titri} (Figure 2.2-5, Figure 2.2-6). In agreement with the data of Figure 2.2-2 the DOS_{NMR} is lower than DOS_{Titri}. Considering all these data, the mean DOS_{NMR}/DOS_{Titri} ratio for PFA° is 0.57 ± 0.07 and this ratio increase to 0.73 ± 0.03 for PFA+. The gap between titration and ^{19}F NMR quantification is significantly more marked for PFA° than for PFA+. As explained in the first section, a high content of (hemi)acetal or (hemi)ketals in PFA° would increase the DOS_{Titri} and thus decrease the DOS_{NMR}/DOS_{Titri} ratio. On the other hand, the DOS_{NMR} might be more sensitive to steric hindrance around the carbonyls than the DOS_{Titri}. The higher gap between NMR and titration for PFA° would indicate that its carbonyls are generally less accessible than in PFA+. They may either be less accessible from a physical point of view (steric hindrance) or from a chemical point of view (protected ketals) or both.

On a side note, one could define a "FTIR conversion degree" using the heights of the disubstituted furans (1560 cm^{-1}) and the monosubstituted ones (1500 cm^{-1}). When these heights are extracted from a normalized spectrum and are used in a conversion degree formula such as Equation 2.1-4, Equation 2.2-2 is obtained.

$$\text{FTIR conversion degree} = \frac{H_{1560}}{H_{1560}+H_{1500}} \quad \text{Equation 2.2-2}$$

Using Equation 2.1-4 and Equation 2.2-2 a DSC conversion degree and an "FTIR conversion degree" can respectively be obtained. These conversion degrees were plotted against each either to give Figure 2.2-7. Interestingly, rather high linear correlation coefficient may be obtained ($R^2 > 0.987$), especially if low conversion degrees are not taken into account. Such method could be useful to quickly characterize batches of PFAs prepared in the same conditions.

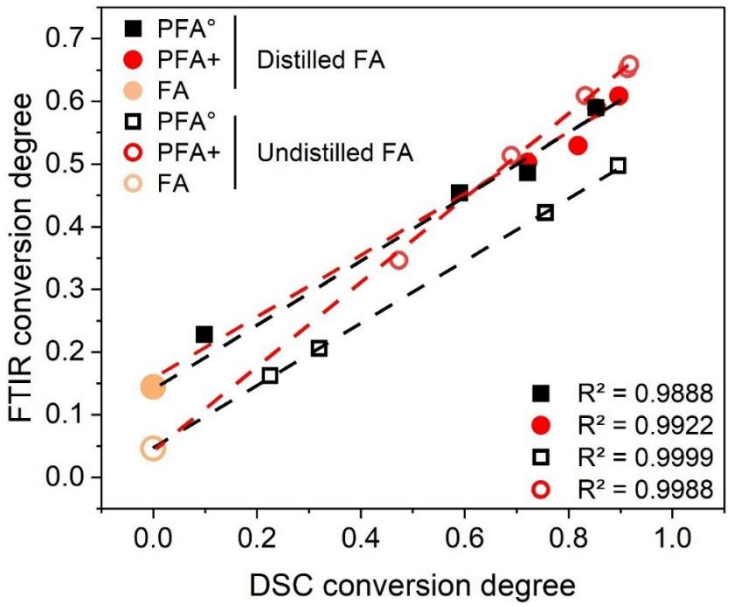

Figure 2.2-7. FTIR conversion degree as a function of DSC conversion degree for both PFA° (squares) and PFA+ (circles) both undistilled (open symbols) and distilled (filled symbols).

2.2.1 Conclusions section 2.2

The aim of this section was to investigate the degree of opened structures (DOS) within a PFA° - and in a PFA+ - MA intiated (i.e. in 50 % aqueous solution during polymerization stage). To do so, two carbonyl quantification methods were adapted to PFA. Results showed an linear increase of DOS both for PFA° and PFA+ all along the polymerisation. However the rate of DOS increase was much faster for PFA+ resulting in final resins containing about two times more open structures than polymerization without additional water (PFA°). This is consistent the starting assumption of Falco et al. that water promotes ring opening reactions. [283] This somehow highlights that, depending on conditions, the formation of carbonyl species can be controlled. Both quantification methodologies by means of wet titration and ^{19}F NMR spectral integration have agreed that DOS continously increase with the course polymerization but the carbonyl content is strongly dependent of the derivatizing agent's nature. Hinderred hydrazine employed for the ^{19}F NMR quantification lead to lower CO content compared to oximation with the small hydroxylamine hydrochloride. This somehow reflect the potential reactivity of these γ-diketones that are rather sensitive to the steric hindrance from the employed reagents or their protection under ketal forms. DOS_{NMR} were invariably lower than DOS_{Titri} and a DOS plateau was reached for DOS_{NMR} in late polymerization stages. Finally, results from derivatization-based methods were confirmed by ^{13}C quantitative NMR.

Overall, the present investigation showed that the DOS of PFAs – considered so far as a side reaction - could be somewhat controlled throughout the polymerization and maximized when using 50 % aqueous solution. The different pathways to determine the DOS can inform on the chemical availability of carbonyls within PFA. The following section is an investigation of the leverages available to control the ring opening reaction.

2.3 Carbonyl content in Lab-scale humins

This section is dedicated to the C=O content of lab-scale humins. Here, three kinds of humins, more or less condensed, were prepared. Figure 2.3-1 reports the FTIR (A) and ^{13}C ssNMR (B) of the lab-scale humins. Overall, the spectra of the humins are highly similar and display signs of C=O and furanic bonds.

In Figure 2.3-1A signals at ≈ 1000 cm^{-1} and ≈ 1500 cm^{-1} are more easily distinguished for the Hu3 sample. FTIR bands around 1000 and 1500 cm^{-1} may be attributed to furans. In the same manner Figure 2.3-1A shows signals around 150 and 110 ppm which are also typical peaks of furans. The Hu3 sample presents a 110 ppm peak clearer than the other humins. In addition, peaks around 70 – 80 ppm could correspond to C-O bonds, possible sugar ones. Finally, the most condensed humins, especially Hu3 show non-furanic C=C bonds between 120 and 130 ppm. A possible explanation could be the reaction of furans towards aromatics when exposed at high temperatures in the autoclave. However, further investigation is required to shed light on these humins' structure.

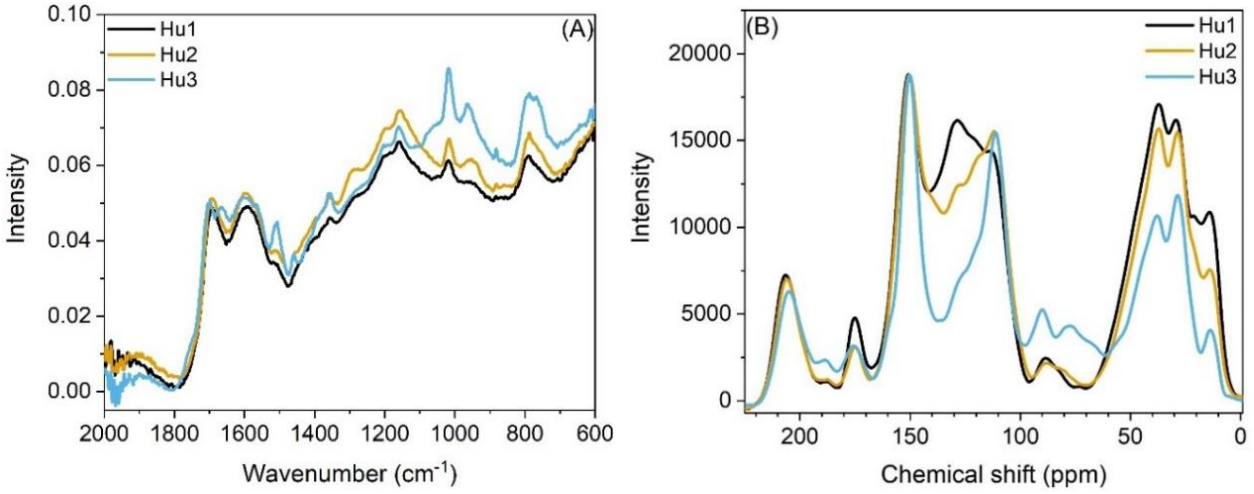

Figure 2.3-1. (A) Magnified FTIR spectra of lab-scale humins. (B) ^{13}C NMR (CPMAS) of lab-scale humins. Hu1 is more condensed than Hu2 which is itself more condensed than Hu3.

In PFA, it was shown that the potentiometric method required 24 h of oximation to reach completion (Figure 2.1-1). Hence, the same test was applied to two batches of Hu1. The results are compiled in Figure 2.3-2. In this Figure, the C=O content rises up to about 4.5 mmol.g^{-1} for the first 24 h for both batches. Yet, it then decreases to about 3.5 mmol.g^{-1} for higher oximation times. The origin of this inconsistency is not understood although the insolubility of humins or remaining sugars might play a role.

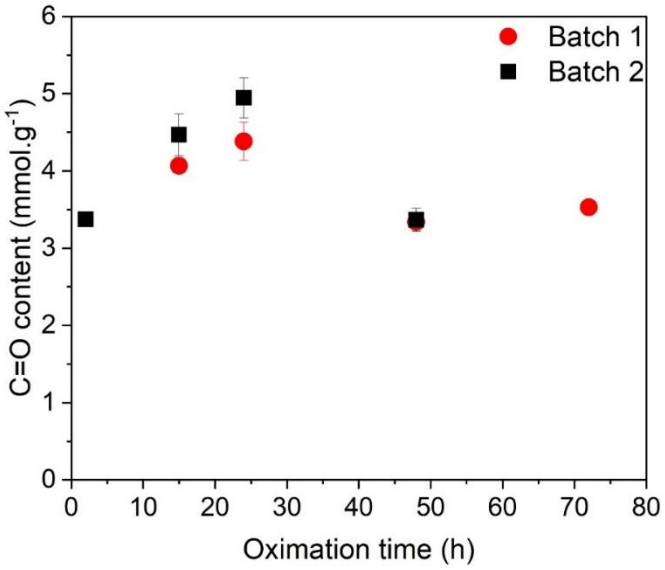

Figure 2.3-2. Dependency of the C=O content of two batches of lab-scale humins (Hu1) on the oximation time.

To compare the different types of humins, an oximation time of 24 h of was arbitrarely selected. The results of the quantifications are available in Figure 2.3-3. This figure shows little variation between Hu1 and Hu2. Thus, concentrations of H_2SO_4 between 0.1 M and 0.01 M have little influence on the C=O content in lab-scale humins. However, Hu3 presents a C=O content of about 7.0 mmol.g^{-1}, i.e about 1.5 times more than the other humins. Its seems that the softer synthesis conditions of Hu3 play a role here. A possible explanation could be the presence of not-fully consensed surgars. It could also be possible that the autoclave forces non-surgar carbonyls to consense. Yet, it is hard to draw definitive conclusions from this preliminary investigation.

Further research is required and Designs Of Experiments would be a very powerfull tool to explore the influences of parameters on the C=O content of lab-scale humins.

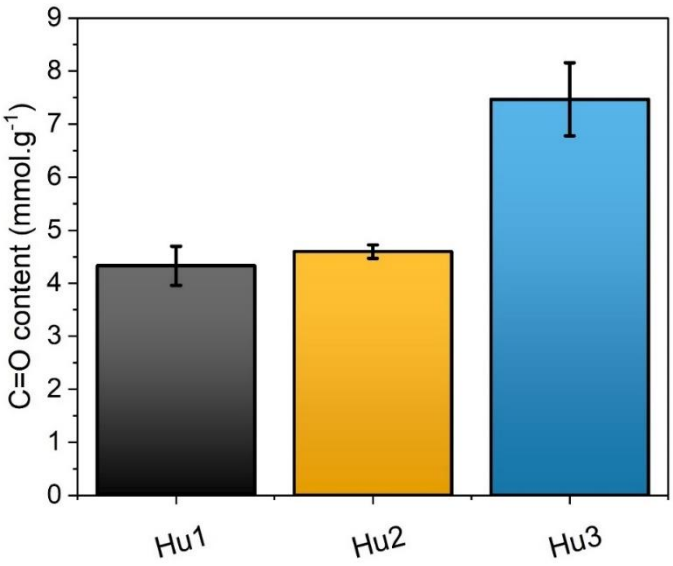

Figure 2.3-3. C=O content of three kinds of humins after 24 h of oximation. Hu1 is more condensed than Hu2 which is itself more condensed than Hu3.

Finally, several attemps of producing humin-based materials using the procedures developped in Chapter 5 were attempted. It was not possible to achieve materials using solely the lab-scale humins, most-likely due to their insolubility and highly consensed states. However, it might possible to integrate them in PFA-Humins systems. Another likely successful possibility would be to use consensed yet soluble humins.

2.4 Conditions affecting the carbonyl content in PFA resins

The main purpose of this work was to study the furan ring opening focusing on certain aspects such as the effects of the acidic initiator, the presence or not of additional water and its ratio on the ring opening. In addition, the last sub-section reports all the others means attempted to increase the C=O content in PFA.

First, the role of the acidic initiator on the furan ring opening was studied by comparing Brönsted initiators such as citric acid, oxalic acid, acetic acid, with Lewis initiators such as boron trifluoride, iodine, alumina or montmorillonite K10 (MMT-K10). Most have already been used in the past [180, 273, 286, 333]. A Brönsted superacid such as trifluoromethanesulfonic acid as well as initiators combining the two acidities such as cation exchanged montmorillonite with alkyl-ammonium and bismuth triflate were also employed. Indeed, cation exchanged montmorillonite (Org-MMT) displays a dual acidity which, as highlighted by Zavaglia et al. leads to an acceleration of the FA polymerization rate. [180] Therefore, the dual acidity of Org-MMT might arguably affect the ring opening occurring during polymerization. This goes also for bismuth triflate which was shown to promote the ring opening of FA to alkyl levulinates. [77] The effect of additional water on the ring opening was investigated as well.

It should be noted that the control of the conversion degrees of PFA prepared with different catalyst is no easy task. They can behave in completely different manners, especially the MMT and Org-MMT PFAs. In addition, the amount of catalyst can significantly vary depending on the catalyst. For example, 10 %w of Al_2O_3 was necessary to obtain a resin while Tf(OH) had to be diluted in water. Otherwise, the polymerization with Tf(OH) occurred instantly at room temperature. In addition, some catalysts were heterogeneous and could not be removed from the resins without altering it. For all these reasons, PFA° and PFA+, both MA based, serve as references.

2.4.1 Effect of the catalyst

As stated previously, different initiators were investigated. For the Brönsted type, citric acid and oxalic acid were chosen as they have already been used for preparing PFA, as well as acetic acid for its industrial accessibility [333].

A Brönsted superacid, namely trifluoromethanesulfonic acid (TfOH) was also investigated. As for the Lewis type, boron trifluoride in methanol solution was chosen for being in liquid state. Alumina, iodine and MMT-K10 have been used in the past [180, 182, 273, 286]. Organically modified Montmorillonites (Org-MMT) were also used to investigated the effect of combined Lewis and Brönsted acidity. The results of the investigations on the role of the initiator are shown in Figure 2.4-1 for the titration results and Figure 2.7-4 for the NMR results.

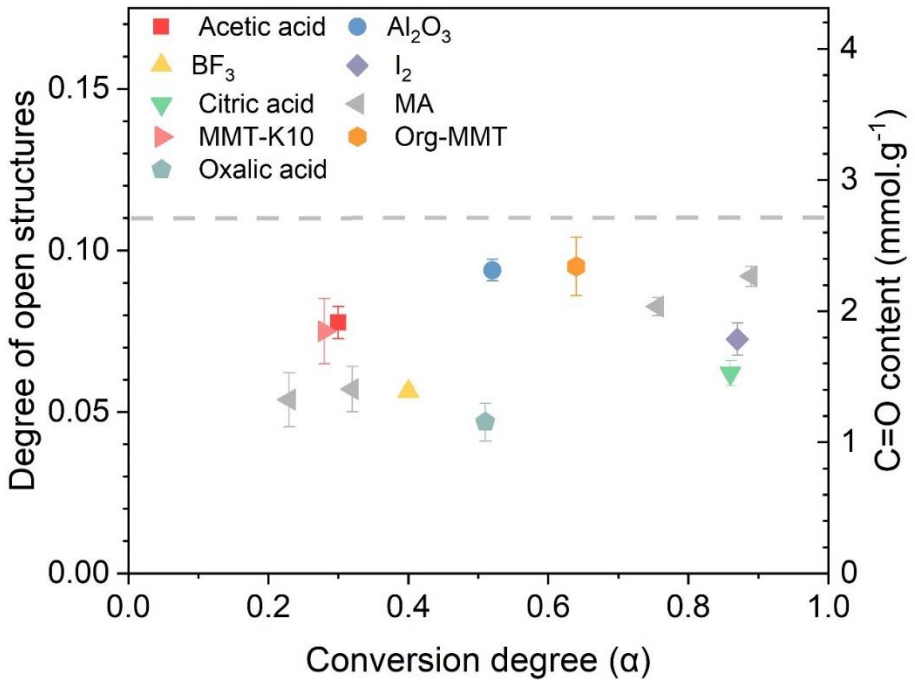

Figure 2.4-1. Comparison of the degree of open structures obtained from titration method synthesized with different initiators in function of the conversion degree.

The results plotted in Figure 2.4-1, suggest that the nature of acidic initiator (i.e. Lewis vs. Brönsted) does not particularly affect the DOS. Indeed, at a similar reaction progress, such as I_2 and citric acid or BF_3 and MA, Lewis and Brönsted acids do not notably stand out from one another. Neither do the combined acidity of Org-MMT. Moreover, in all cases the DOS_{Titri} were always below 0.10 for the PFAs prepared in neat conditions.

The results from the ^{19}F NMR method are available in Figure 2.7-4. A point worth noting is the undeniable difference between the titration and NMR results. They follow the same trend, however the DOS_{Titri} is always superior to the DOS_{NMR} as discussed in section 2.2.

These investigations confirmed that the DOS progressively increases with the conversion degree. However, the type of acidity does not particularly influence the DOS. Another aspect worthy of examination was the role of added water on the DOS.

2.4.2 Effect of Water in combination with catalysts

In order to determine whether the presence of additional water and its ratio affect the DOS two approaches were implemented.

First, the effect of additional water was studied by conducting several syntheses in which an array of initiators was tested with and without additional water in a same amount in the system, i.e. the initial water amount which will come in addition to the water generated during the polycondensation. The FA/water ratio was fixed to 50/50 as for PFA+ in section 2.2.

The results plotted in Figure 2.4-2 confirms that the presence of water does influence the DOS by increasing it. The ^{19}F NMR method in Figure 2.7-5 presents the same trend. Indeed, at a similar conversion degree the DOS is higher when the reaction was performed in the presence of additional water.

As stated, the results of this investigation show that the added water plays a role in the furan ring opening in agreement with both Falco et al. [283] and section 2.2. In addition to this investigation, it is clearly highlighted here that the increase in DOS is not strongly related to the acid initiator. In other words, all the systems show a DOS increase when additional water is present.

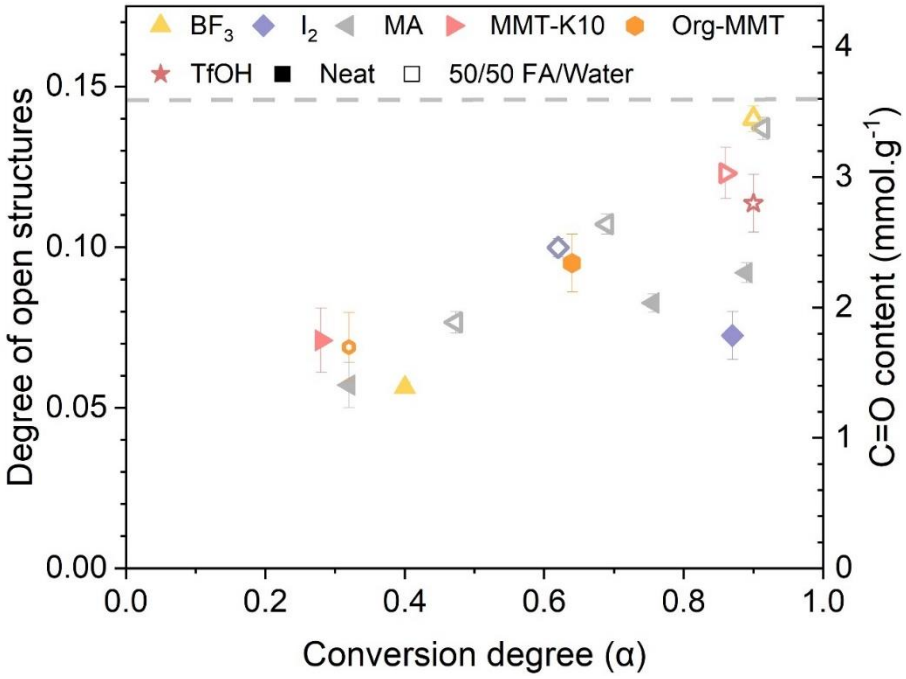

Figure 2.4-2. Comparison of the degree of open structures obtained by titration method and synthesized with different initiators with and without additional water (50/50 w/w) as function of the conversion degree.

2.4.3 The role of the additional water ratio

Here, several polymerizations were conducted by selecting only one initiator, namely maleic anhydride (MA) and changing the FA / additional water ratio, ranging from the neat PFA° (100/0) to 40/60.

Figure 2.4-3 exhibits the DOS_{Titri} as a function of the conversion degree for PFAs synthetized with more or less additional water. The ^{19}F NMR results are depicted in Figure 2.7-6.

Figure 2.4-3 and Figure 2.7-6 highlight that the DOS is continuously increasing with the conversion degree, independently of the FA/water ratio. The neat PFA shows the lowest DOS overall from the beginning to the near-end of the polymerization, i.e. $\alpha \approx 0.90$.

Regarding the water ratios, systems with less water (40/60 and 10/90) have slightly higher DOS than the 50/50 and 70/30 ratios at $\alpha < 0.80$. Nonetheless, at higher conversion degrees (i.e. $\alpha \approx 0.90$) , the gap shrinks around a DOS of 0.15. This is most likely due to the insolubility of PFA in water. Indeed, FA and water are miscible whereas above $\alpha \approx 0.20$ a demixion occurs as depicted in Figure 2.4-3. Thus, small, open and water-soluble oligomers might be not be taken into account in the DOS at low conversion degrees. Then, when the polymerization progresses, they would be integrated in the PFA phase leading to a final DOS of 0.15, i.e about 3.7 mmol.g^{-1} of C=O.

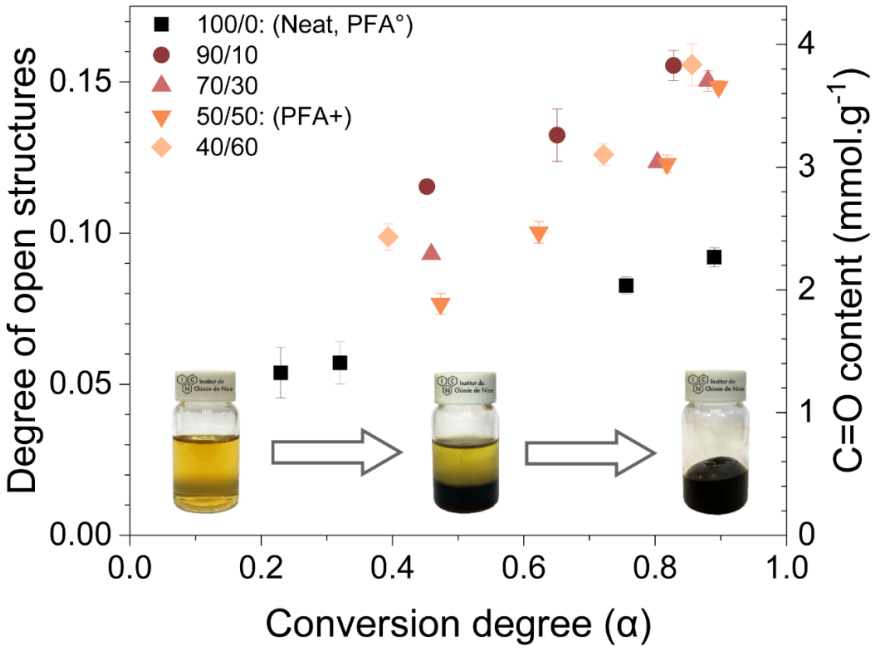

Figure 2.4-3. Comparison of the degree of open structures obtained with titration method and synthesized with different FA/Additional water ratios with in function of the conversion degree.

These investigations allowed to determine that adding water plays a role in the opening of the furan ring but the ratio of added water does not impact the DOS that is reached near the end of polymerization. Yet, lower amount of additional water such as 10 %w of water allows higher DOS at lower conversion degrees and thus lower viscosities. This may be exploited to maximize the C=O content of PFAs while remaining at a convenient viscosity.

2.4.4 Other attempts to increase the C=O content of PFAs

In this section, various complementary attempts to increase the C=O content of PFAs were conducted. The following experiments were rapid tests to check if any conditions yielded higher than usual C=O content. Most of the attempts reported in this section did not lead to significant increase of C=O content. The DOS was determined only with the potentiometric method and only the FTIR C=O area was used to compare the samples. The DOS_{NMR} and the DSC conversion degree were not determined here as they are more time consuming. The conditions of preparations of PFAs are reported in Table 2.7-2. The results of some test are reported in Figure 2.4-4, the values of PFA° and PFA+ may be used as reference lines.

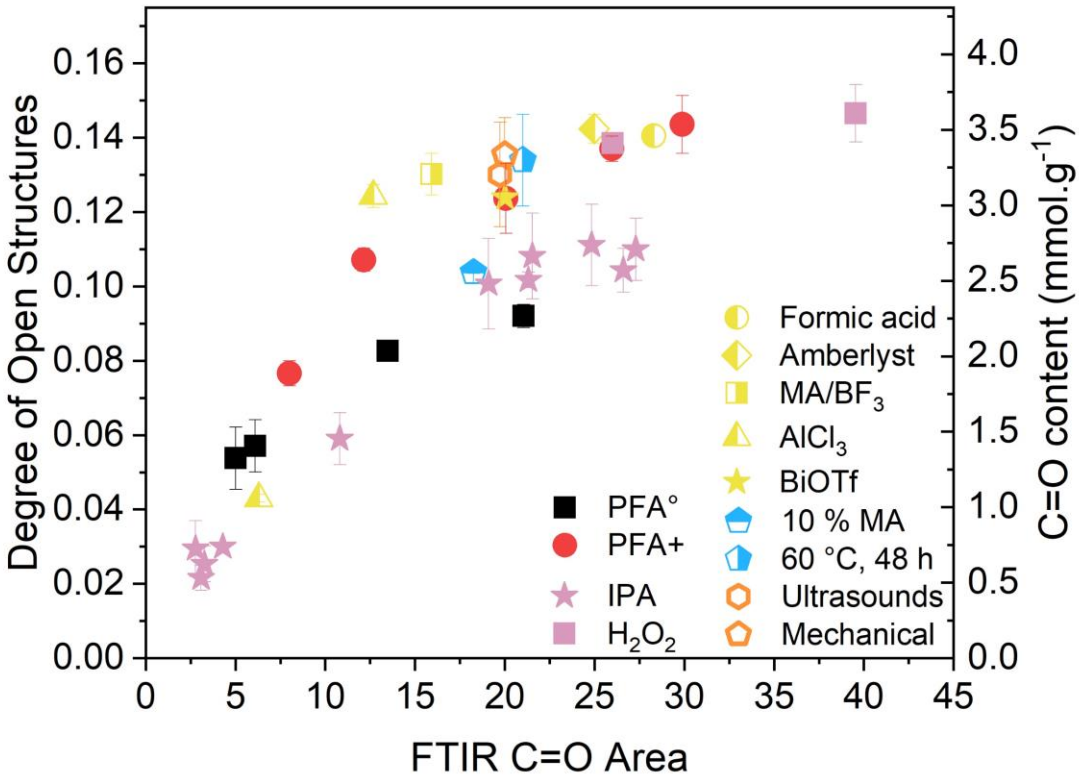

Figure 2.4-4. DOS and C=O content as a function of the FTIR C=O area of a multitude of PFAs.

First, authors reported that H_2O_2 promoted ring opening reactions in PFA. [201] Thus, the C=O content of such PFA was measured to check this claim. In Figure 2.4-4 the two "H_2O_2" samples showed rather high DOS but not so much higher than PFA+. However, the "H_2O_2" samples showed significant ester signals in FTIR which is unusual for PFAs prepared with 50 % additional water. A Baeyer-Villiger rearrangement may be responsible for this and may be exploited for derivatization purposes. It should also be noted that concentrated H_2O_2 strongly accelerate the polymerization of FA.

A series of catalyst and catalyst systems were tested in PFA systems with 50 % additional water (yellow symbols in Figure 2.4-4). The tests include mixture of Lewis and Brönsted acids (Bismuth triflate and a stoichiometric ratio of MA/BF_3). Formic acid, an Amberlyst and $AlCl_3$ were also tested. They all fit the PFA+ curves and thus does not improve significantly the C=O content.

In addition, the orange symbols in Figure 2.4-4 corresponds to a PFA prepared under ultrasonic solicitation and strong mechanical stirring. Figure 2.4-5 showcases the evolution of the aspect of PFA when prepared using only ultrasounds. It clearly shows that the ultrasounds can provide an excellent mixing of the phases when the pulses are ON. The synthesis was stopped when the apparatus reached overload due to the viscosity of PFA. The goal here was to try to overcome the demixion of water and PFA oligomers. However, both the ultrasounds and the mechanical stirring did not provide significant increase regarding the C=O content, in comparison with PFA+.

Tests were conducted using FA/MA/Water systems (50/50). One used 10 %w MA and the other 2 %w of MA but at a low temperature (60 °C) for a long time (48h). Both were in line with regular PFA+, after acid correction.

Initial solution (FA/MA/Water) | *After 6 min of ultrasounds (Left ultrasounds OFF, Right ultrasounds ON)* | *Final PFA (1 h 30)*

Figure 2.4-5. Picture of a PFA prepared using only ultrasounds.

A series of PFA were prepared using other solvent than water and mixtures of solvents and water. First, IPA was suggested by Falco et al. to promote the ring opening in PFA systems. Results of PFA/MA/IPA are displayed in Figure 2.4-6. The IPA PFAs are located in between PFA° and PFA+. Hence, if the IPA promotes ring-opening reaction it is either in small amounts or ketal species are formed or both.

Using a similar approach, PFA were prepared with solvent mixtures in an attempt to delay the demixion as much as possible. Mixtures of FA/MA/EtOAc/EtOH/water and FA/MA/Ethyl lactate/water were tested. However, the values of C=O contents were altered by the presence of the solvents.

To increase the C=O content of PFA systems, it was also considered to copolymerize FA and HMF together with MA as catalyst (2 % mol, based on the moles of furans). The samples were heated for varying time and temperature as the HMF highly disturbs FA's polymerization. Resins were sampled during their polymerization and their C=O content determined. The conversion degrees could not be determined by DSC as they were highly inconsistent.

Figure 2.4-7A reports the C=O content of resinous FA/HMF samples. It clearly shows that the higher the proportion of HMF the higher the C=O content. The FA/HMF resins were further heated and compression molding was performed.[i] Yet a C=O rich, HMF like viscous liquid, leaked during the compression even at low pressures. This was observed by smell and FTIR. Samples containing 75 % of HMF could not be molded at all. Samples were post-cured anyways and grounded before undergoing C=O quantifications. The resulting C=O content of post-cured FA/HMF are displayed in Figure 2.4-7B.

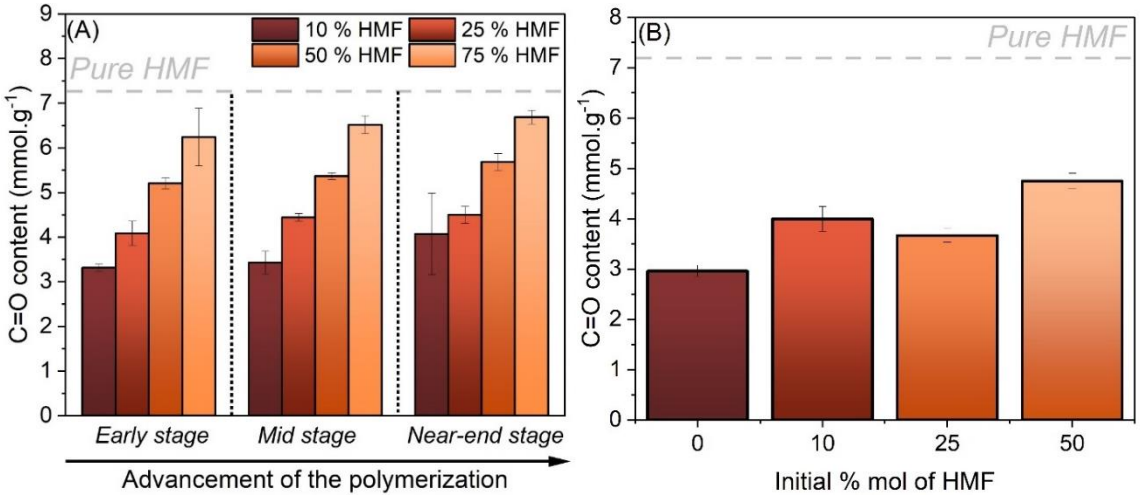

Figure 2.4-7. (A) C=O content of FA/HMF systems at resinous stages. (B) C=O content of FA/HMF samples cured, post cured and ground. All percentage are molar percentage considering only the furans.

[i] The temperature was set to 150 °C for 2 h. The pressure was varied between 3 and 25 bars. The post-curing was done at 150 °C for 3 h. The grinding was done with a ball mill. More details in chapter 5.

In Figure 2.4-7B, the C=O content increases with the proportion of HMF. The lower values for the 25 % samples may be due to the leaking issue. In addition, the C=O content in Figure 2.4-7 B are minimal values. They are minimized by both the leaking and the insolubility of the polymers, thus only the surface groups are quantified. Furthermore, the FA/HMF materials displayed poor properties, especially at high loads of HMF. The DMAs and TGAs of the samples are available in Figure 2.7-8.

In section 1.3.3 and more specifically Scheme 1.3-15 it what mentioned that the furan ring can be open through a combination of air dioxygen and light. To check this and investigate if UV light may increase the C=O content of PFA, a solution containing FA and 2%w of a photoacid[i] was prepared. The solution was coated on glass or aluminum pans and exposed to UV light[ii].

Figure 2.4-8 displays pictures taken during the polymerization. Interestingly, PFA first become green before further darkening which is unusual. Furthermore, after 2 hours of exposure a dark PFA is obtained with wrinkles as observed by other researchers. [261, 262]

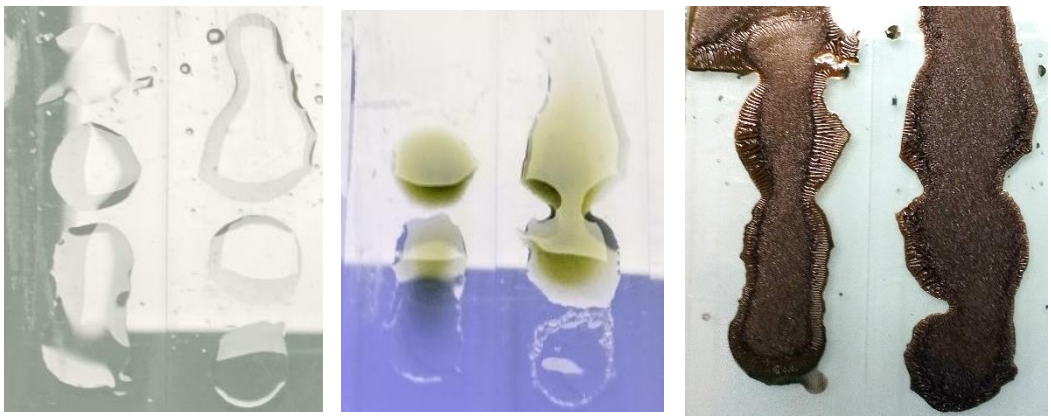

Initial solution *40 mins of exposure* *2 h of exposure*

Figure 2.4-8. Pictures taken over the polymerization of FA initiated by UV light.

[i] triarylsulfononium hexafluoroantimolate in 50 %w propylene carbonate
[ii] Power 30 W, wavelength 385-400 nm, about 1-2 cm between the light and the samples

In addition, two FTIR spectra of the samples were taken after two hours of exposure. One was the side facing the UV light and the other facing the glass, i.e somewhat protected from the UVs by PFA. The spectra are available in Figure 2.4-9. They are similar to the usual spectrum of PFA from 1450 to 1730 cm^{-1}. The most notable fact it the height of the C=O peak at 1715 cm^{-1} in comparison with the height of the furan peak at 1500 cm^{-1}. For the spectrum taken on the UV facing side, the C=O seems much more intense than the spectrum of the glass facing side. As a consequence, it may be possible to artificially increase the content of PFAs using UV systems. One could inspire itself from the synthesis of cyclobutane dicarboxylate from furylacrylic acid where the reagent is suspended in a solvent and exposed to UV light. [334]

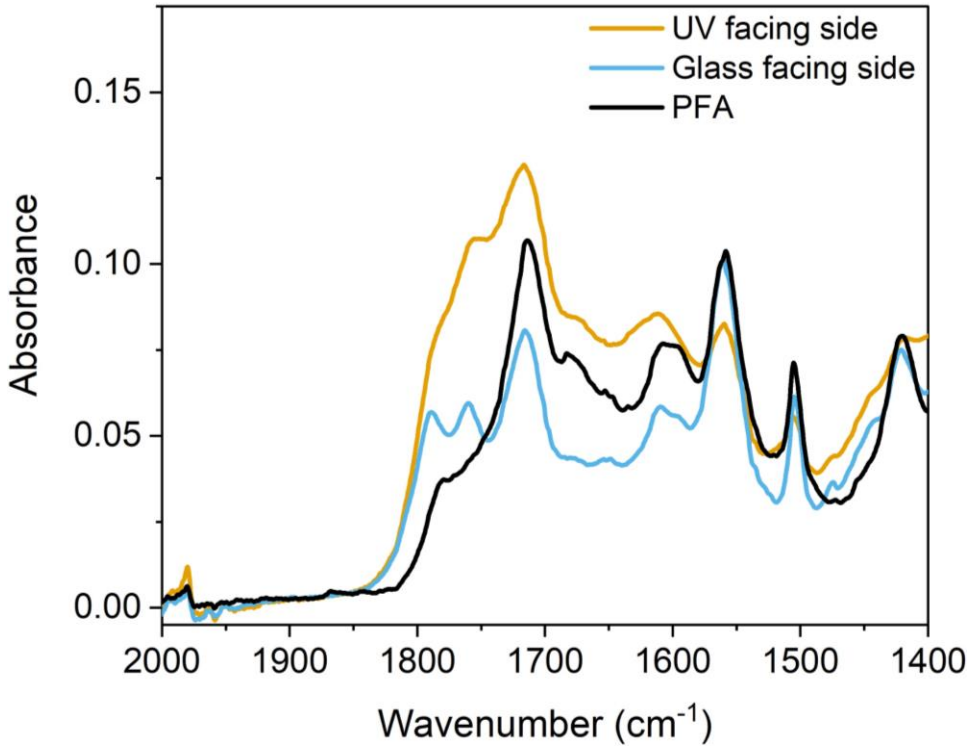

Figure 2.4-9. FTIR spectra of the UV initiated PFA, exposed two hours.

In the followings, other attempts of increasing the C=O content in PFA systems are briefly overviewed. In previous experiments, the approach was to increase the C=O content during the polymerization. Here, the approach was to first prepare a PFA+ and then expose it to various conditions to increase the C=O content without further polymerization.

In his book, P. Merion reported the Fenton reagent to open furans though an oxidative pathway. [316] The Fenton reagent is based on iron salts and H_2O_2. Pre-polymerized PFA resins were exposed, under magnetic stirring, to an aqueous solution of Fenton's reagent, a solution of Fe^{2+} salt alone and another in a solution of H_2O_2. In addition, similar resins were magnetically stirred in presence of water and another in presence of acidified water (TfOH). The DOS was measured before and after a 60 h exposition at room temperature. All tests were yielded equal of lower DOS values possibly due to the immiscibility of PFA and water.

Consequently, attempts in which PFA was dissolved in solvents were performed using THF, 1,4-dioxane or toluene. In addition, a small amount of water (about 10 %vol) and a strong acid (H_2SO_4 or Tf(OH)) were added. After refluxing for a few hours, the solvent was removed using vacuum and rotavapor, leaving PFA phase and yellowish water phase. The water was removed and the DOS was measured. The values were either equal to the initial PFA or lower. Hence, open furans are removed either by the rotavapor or were solubilized in the yellowish water.

Attempts at oxidizing PFA into carbonyls were also performed. A first one involving a pre-polymerized PFA and slightly acidified $KMnO_4$ was conducted. At room temperature, a highly vigorous reaction occurred and left a khaki PFA instead of the initial brownish PFA. This may indicate an oxidation of the conjugated moieties of PFA into carbonyls. It may be a way to increase the C=O content of PFAs although this method is labor intensive and means to mitigate the reaction speed are required. The uses of peroxides may also work.

Finally, it should be mentioned that during syntheses such as the PFA+ one, a demixion occur. The aqueous phase progressively evaporates to leave a yellowish liquid with a water-like viscosity. This liquid was recovered and left to evaporate. Its C=O content was measured and found to be 8.2 ± 0.3 $mmol.g^{-1}$ including 2.3 ± 0.4 $mmol.g^{-1}$ of COOH. Its FTIR spectrum available in Figure 2.7-7. This compound or mixture of compounds can also be observed when PFA+ are squeezed. Although its nature is unknown, Barr and Wallon, in 1971, observed a similar compound and characterized its NMR, melting point and performed elemental analysis. [274] Finally, this carbonylated compound can strongly interfere with the C=O content obtained from the quantifications, and one should be careful about this.

2.4.5 Conclusions control DOS

To conclude, few ways are at our disposal to control the C=O content of PFA systems.

Different acidic catalysts - spanning from Brönsted to Lewis acids and mixtures of both - were employed to initiate FA polymerization. The results point towards the fact that no specific type of acidity particularly promotes or reduces the DOS.

Then, the influence of the additional water content was examined and different initial FA/water ratios ranging from 100/0 to 60/40 were employed. When FA polymerization is not too much advanced (i.e. $\alpha < 0.8$), the DOS is quite influenced by the water ratio. This phenomenon was exploited in Chapter 5 to maximize the C=O content of PFAs while maintaining lower viscosities. For $\alpha > 0.8$, the DOS values are merging for all the FA/water ratio to an ultimate value of about 0.15, i.e about 3.7 $mmol.g^{-1}$. Only the neat FA (i.e. polymerized without any additional water) has much lower DOS (i.e. 0.09, 2.2 $mmol.g^{-1}$).

Finally, a series of other experiments were conducted. Polymerization in solvent systems, strong mechanical stirring and ultrasonication were attempted to mitigate demixion without significant improvement of the C=O content.

The possibilities of copolymerization of FA with HMF to artificially increase the C=O content were assessed. Although it allows a significant increase C=O content, this greatly diminished the properties of the material.

The use of UV-light was investigated as a mean to open furan ring through an oxidative pathway. Such method could work although the development of a procedure is required. Finally, it was unsuccessfully attempted to increase the C=O content of PFA prepolymers by hydrolysis an oxidation in solvents. If one desires to further increase the C=O content of PFAs, an oxidation either using UV light or oxidants might be the most promising routes.

2.5 Insight on the chemical structures of PFAs' carbonyls

All along this chapter, the hypothesis that all carbonyls result from the opening of furanic entities into alkyl 1,4-diketones was followed. Yet, the complexity of PFAs' polymerization process might induce production of several kind of carbonyls. This section is dedicated to giving insights on the chemical nature of carbonyls in PFA systems.

Insights on these carbonyls' nature can be given using the ^{19}F NMR spectra of derivatized PFAs. Figure 2.5-1 is an example of ^{19}F NMR spectra of $CF_3\Phi NHNH_2$ derivatised PFA° and PFA+. Figure 2.7-9 presents a more complete version of Figure 2.5-1, including various conversion degrees. It can be seen from theses spectra that the ketones in PFA are heterogeneous and at least five significantly different C=O are present in PFA. This possibly includes diastereoisomers. The spectra have many broad hydrazone peak overlaps. According to previous studies, carbonyl groups can be roughly classified using the chemical shifts of hydrazones having in mind that conjugated carbonyls are more upfield. [323, 324, 326] No statement can be made on the nature of carbonyls in PFA using Figure 2.5-1 and Figure 2.7-9 alone. Nevertheless, a significant proportion of conjugated carbonyls (i.e. more upfield hydrazones) can be highlighted in both system.

From the spectra in Figure 2.5-1, it can be deduced that aliphatic carbonyls (i.e. non-conjugated) such as 1,4-diketones or levulinate-like carbonyls are most likely present in both PFA° and PFA+. Indeed, levulinic acid's hydrazone has a chemical shift of -59.5 ppm (see ^{19}F spectra of derivatized LA in Figure 2.7-10) which is the major one in PFA°. However, PFA+ systems seem to have a larger extent of conjugated carbonyls. A plausible explanation for the presence of both aliphatic and conjugated carbonyls would be the co-existence of two pathways for furan ring opening, as illustrated in Figure 2.5-1. Literature reported hydrolytic ring opening of furan ring leading to saturated 1,4-diketones that were postulated by Conley & metil.[272] Nonetheless, unsaturated 1,4-diketones can also be formed through oxidation of furan ring. [335, 336] Such oxidation might be happening due of air dioxygen.

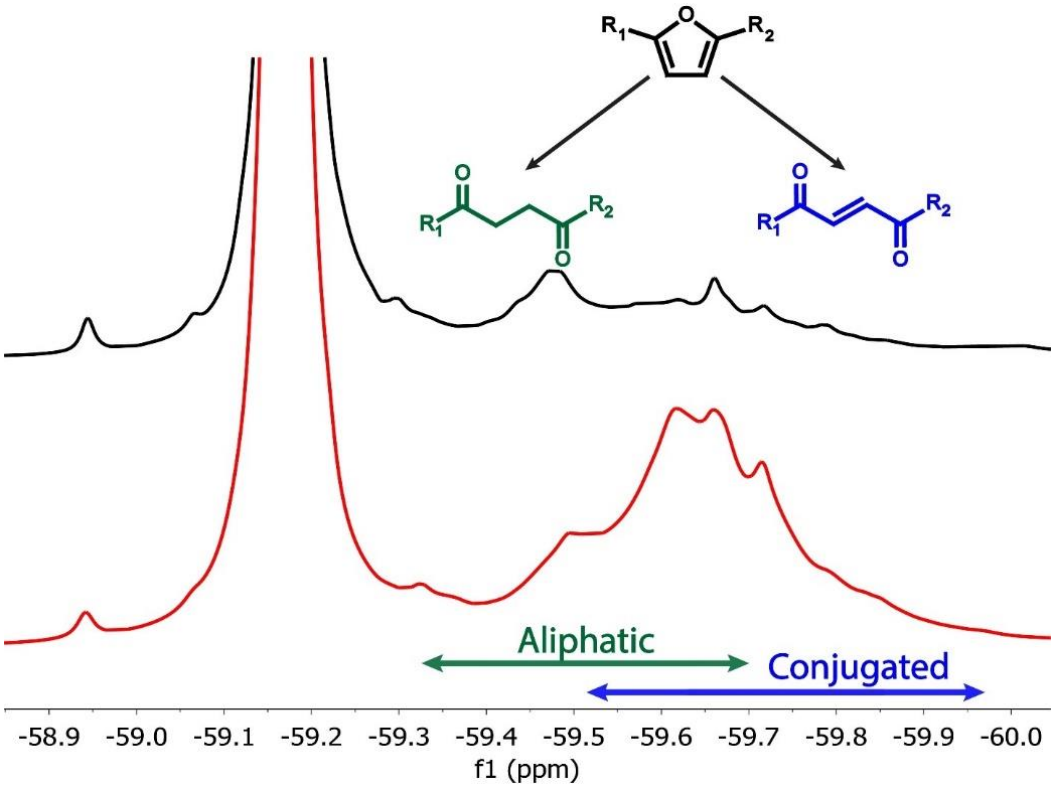

Figure 2.5-1. ^{19}F NMR spectrum of $CF_3\Phi NHNH_2$ derivatized PFA+ and PFA°.

To confirm this statement, a PFA+ resin ($\alpha \approx 0.80$) was left in open air environment for 2 months. A hard and dark crust formed at the surface. The C=O content of this surface crust was 3.87 ± 0.20 mmol.g^{-1} while the core resin (i.e. not exposed to air) was 3.04 ± 0.19 mmol.g^{-1}. It indicates that PFA exposed to long-term potential air oxidation has about 30 % higher C=O content than the heart. Moreover, Tondi et al. suggested a Diels-Alder reaction between unsaturated 1,4-diketones and conjugated sequence PFA to give a saturated 1,4-diketones adduct (schematized in Scheme 2.2-1) which would induce both aliphatic and conjugated carbonyls.[284] Finally, opened structures adjacent to conjugated moieties of PFA could as well explain the wide range of hydrazones chemical shifts evidenced in Figure 2.5-1.

In the past, it was highlighted several times that ketones are not the only carbonyls in PFA, esters groups are also present. [273, 283, 284] The FTIR spectra of PFA° and PFA+ at conversion degrees $\alpha \approx 0.5$ and $\alpha \approx 0.8$ are displayed in Figure 2.5-2. Both samples exhibit a C=O band at 1710 cm^{-1}. This band has been attributed to ketonic moieties. However, the neat PFA exhibits a shoulder around 1780 cm^{-1} which has been attributed to ester moieties [283, 284]. Figure 2.5-3 presents the ^{13}C NMR of the same samples. The peaks corresponding to ketones appear between 195-210 ppm. As shown in Figure 2.5-3 the sample PFA+ exhibits more peaks in this region compared to PFA°. In addition, in PFA+ there is at least five significantly different kinds of C=O in the ketone region. On the other hand, the chemical shifts attributed to esters are located between 160 and 178 ppm. PFA° shows more peaks attributed to esters compared to PFA+. In PFA+ at $\alpha \approx 0.8$, the 174 ppm peak is attributed to the COOH band from levulinic acid. Indeed, low levels of acid can be detected in such PFAs.

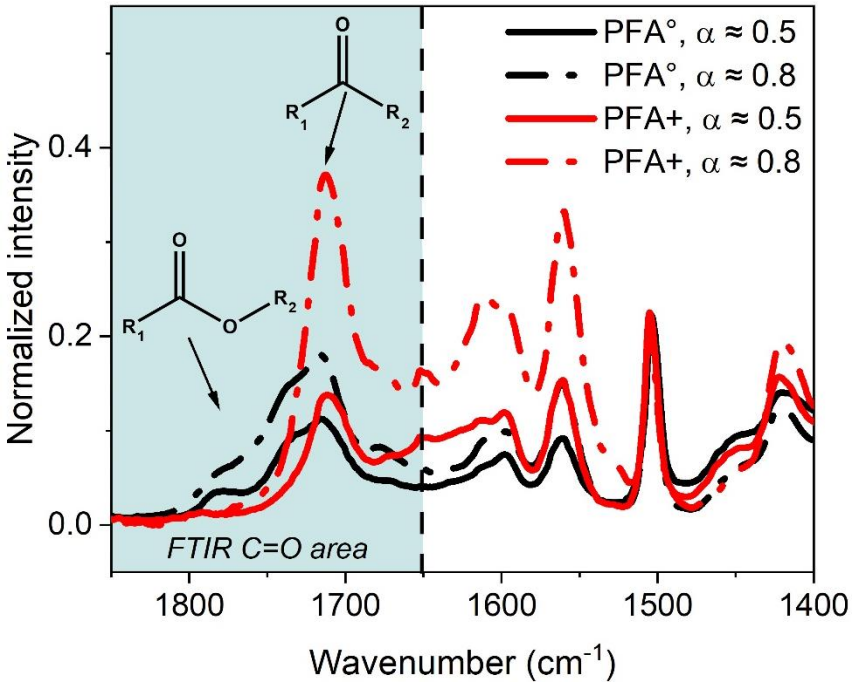

Figure 2.5-2**.** Normalized FTIR spectra of PFA+ and PFA° neat at $\alpha \approx 0.5$ and $\alpha \approx 0.8$.

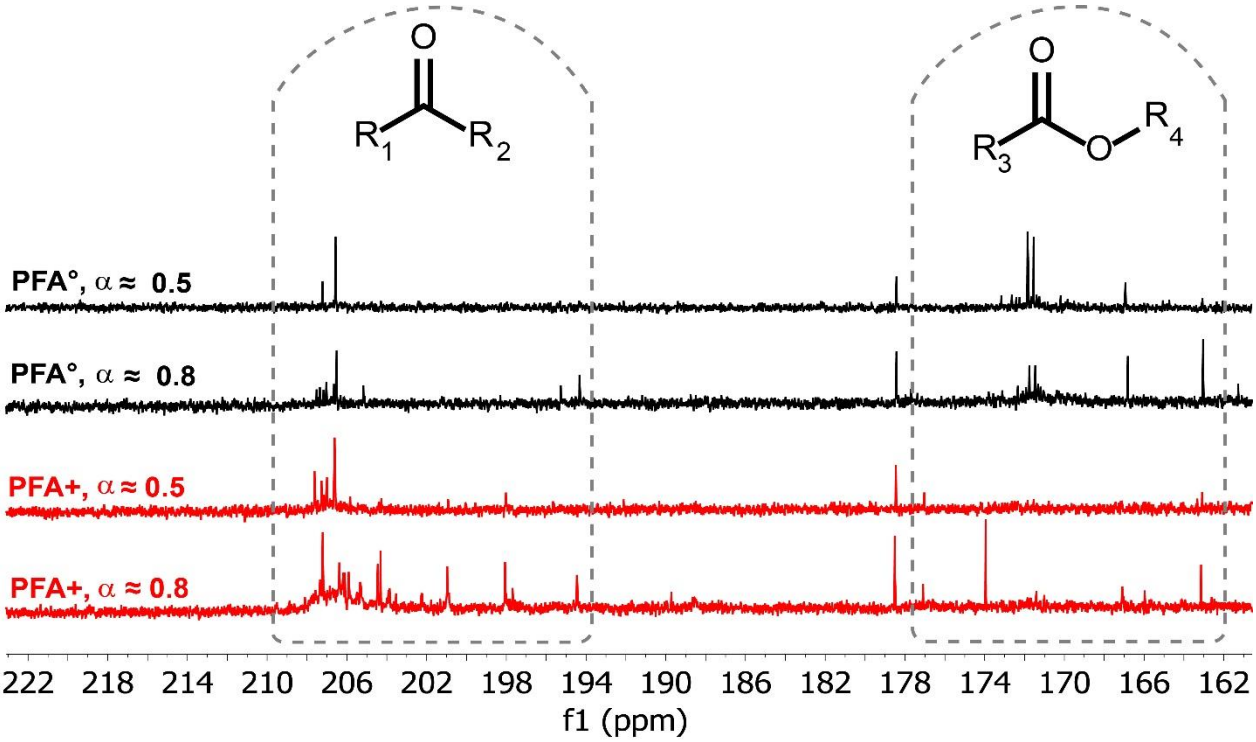

Figure 2.5-3. ^{13}C NMR spectra of PFA+ and neat PFA° at $\alpha \approx 0.5$ and $\alpha \approx 0.8$ with an accumulation of 6000 scans.

Figure 2.5-4 shows the DOS_{Titri} as function of the FTIR C=O area for all the investigated PFAs of this chapter and other prepared over the course of this thesis. A separation between PFAs prepared with additional water, the ones prepared in neat conditions and the ones prepared with additional IPA is portrayed in Figure 2.5-4. It is worth mentioning that both ketones and aldehydes functions are quantified by the oximation method but it is not the case for the ester function. However, it is rather difficult to discriminate the ketones/aldehydes from the ester functions when integrating the more or less broad carbonyl peak in FTIR. Accordingly, if only ketones or aldehydes are present in the systems, the C=O content should increase linearly with the FTIR C=O area. However, if other functional groups, such as esters, are taken into account in the C=O area, the DOS vs. the C=O area will not be linear. Moreover, in their work Wewerka et al. used alumina as a catalyst and identified lactones in the system [273]. In Figure 2.5-4, the data point of alumina catalyzed PFA (DOS 0.094; 30.4) is indeed in the ester bearing group.

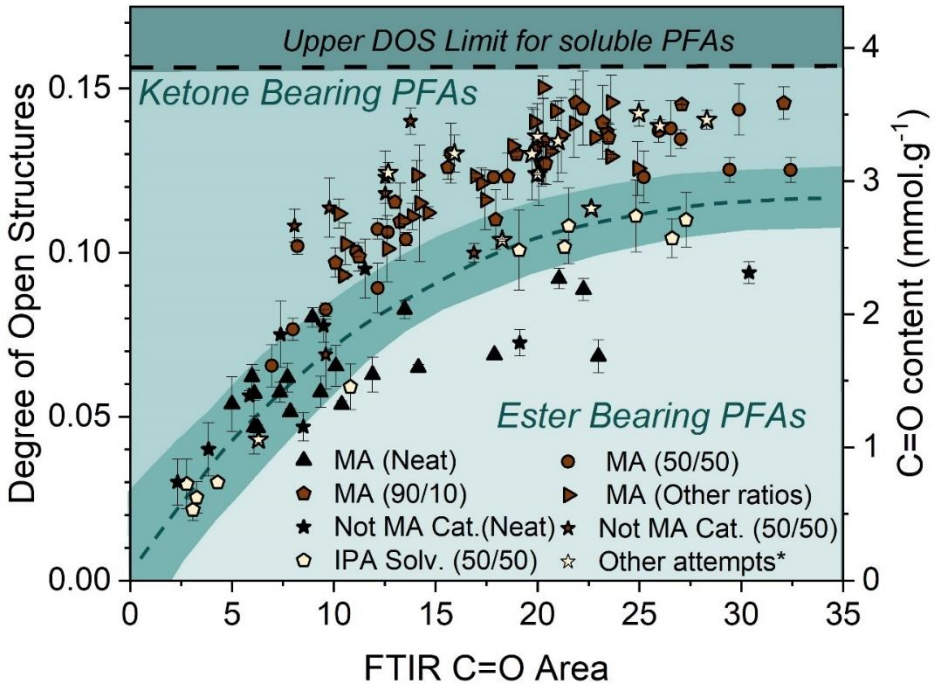

Figure 2.5-4: Degree of open structures obtained with titration method against FTIR C=O area for PFA synthetized in neat, aqueous and 50/50 IPA systems. PFA have been synthetized with aforementioned catalysts. *"Other attempts" include experiments of Section 2.4.4. The numbers, for example 90/10 correspond to the ratio of FA-Water or IPA if specified.

Regarding the PFAs prepared with 50/50 IPA, they also belong to the ester bearing groups in Figure 2.5-4 as observed by Falco et al. [283]. Yet, they have a higher DOS than the neat PFA. This suggests an opening of furan rings through the formation of compounds such as levulinates or lactones, thus increasing both the DOS and FTIR C=O area.

Finally, the ^{13}C NMR spectra of PFA+ in Figure 2.5-3 exhibits a significant number of carbonyl peaks from 194 to 210 ppm. Most of them are centered around 208 ppm which matches with 1,4-diketones. Similar peaks can be found in the neat PFA. However, at $\alpha \approx 0.80$ new peaks rise in the 194–205 ppm area, in PFA 50/50 only. This confirms the existence of other types of carbonyls containing species than 1,4-diketones in this system. These results suggest that additional water either prevents the formation of esters during FA polymerization or hydrolyses them or both.

To conclude, insights on the nature of the carbonyls contained in open structure of PFAs were given. The ^{19}F NMR spectra suggested that both alkyl and conjugated ketones coexist in PFA systems. Overall, at least five different types of C=O in the ketone region were observed by ^{13}C NMR in PFA+. The existence of esters in PFA resins was highlighted especially when FA polymerization was conducted without additional water. On the other hand, FA polymerization conducted with additional water rather highlighted the formation of ketonic groups in their opened structures and much less esters were identified.

2.6 Chapter 2: conclusions

This chapter had two initial goals. Develop C=O quantification methods adapted to PFA and explores the leverages available to tune the C=O content of PFAs.

First, this chapter aimed at the development of robust C=O quantification methods adapted to PFA systems. The C=O in PFA were quantified by potentiometric methods, ^{19}F and ^{13}C NMR. The potentiometric and ^{19}F NMR methods involved derivatization. Depending on the chemical nature of the derivatizing agent, the obtained C=O content might be higher ($NH_2OH.HCl$) or lower ($CF_3\Phi NHNH_2$). This was attributed to steric hindrance issues and/or the presence of protected carbonyl functions such as ketals. The quantifications methods were applied at different conversion degrees and highlighted a continuous increase of the degree of open structures during the polymerization of FA.

Secondly, this chapter aimed at exploring the leverages available to control the degree of open structures of PFA systems. The major factor allowing to increase the C=O content of PFA is the presence of additional water during the polymerization of FA. As little as 10 %w of water allows the highest C=O content. Overall, PFAs prepared with additional water exhibited a DOS maximum of 0.15, i.e about 3.7 $mmol.g^{-1}$. PFAs prepared in neat conditions were capped at a DOS of 0.09, i.e about 2.2 $mmol.g^{-1}$.

Finally, the spectrometric tools used in this chapter namely FTIR, ^{19}F and ^{13}C NMR highlighted the complexity of PFA. More specifically, an array of carbonyls is present in PFA, alkyl C=O, conjugated C=O and esters.

The next chapter adds a layer of complexity on the chemical nature of the carbonyls within PFAs. The structural investigation around PFAs' C=O is taken one step further using 2D NMR tools.

2.7 Supplementary Figures: chapter 2

Table 2.7-1. FA's polymerization conditions for Section 2.4.1 and 2.4.2 .

Catalyst	**% of catalyst (based on FA)**	**FA/Additional water ratio**
Citric acid	2 mol%	100/0
Boron trifluoride in MeOH (14%)	0.07 mol%	100/0
Oxalic acid	2 mol%	100/0
Acetic acid	2 mol%	100/0
MMT K10	2 wt%	100/0; 50/50
Org-MMT	2 wt%	100/0; 50/50
Alumina	10 mol%	100/0
Iodine	1 mol%	100/0; 50/50
Trifluoroacetic acid	0.1 mol%	50/50
Maleic anhydride	2 mol%	100/0; 70/30; 50/50; 40/60; 10/90

Table 2.7-2. Conditions for the preparation of the PFAs in Section 2.4.4.

Catalyst	**% of catalyst (based on FA)**	**Solvent**
H_2O_2	2 %w MA15%w of 30%w/v H_2O_2	FA/Water 50/50 (vol)
Seawater	2 %w MA	FA/Sea water, 50/50 (vol)
Formic acid	10 %w	FA/Water 50/50 (vol)
Bismuth triflate	1 % mol	FA/Water 50/50
Aluminium chloride	1.5 % mol	FA/Water 50/50
Amberlyst	0.5 %w	FA/Water 50/50
MA and BF_3	1 %mol MA and 1 % mol BF_3	FA/Water 50/50 (vol)
MA	2 %w MA	FA/Water, 50/50 (vol), Vigorous mechanical stirring
MA	10 %w MA	FA/Water 50/50 (vol)
MA	2 %w MA	FA/Water 50/50 (vol), sonication[i]
MA	2 %w MA	FA/Water, 50/50 (vol), 48 h at 60 °C

[i] Conditions: 15 s ON, 10 s off, 60% amplitude, 2 h using a Fisher scientific FB505 sonicator (500 W 20kHz)

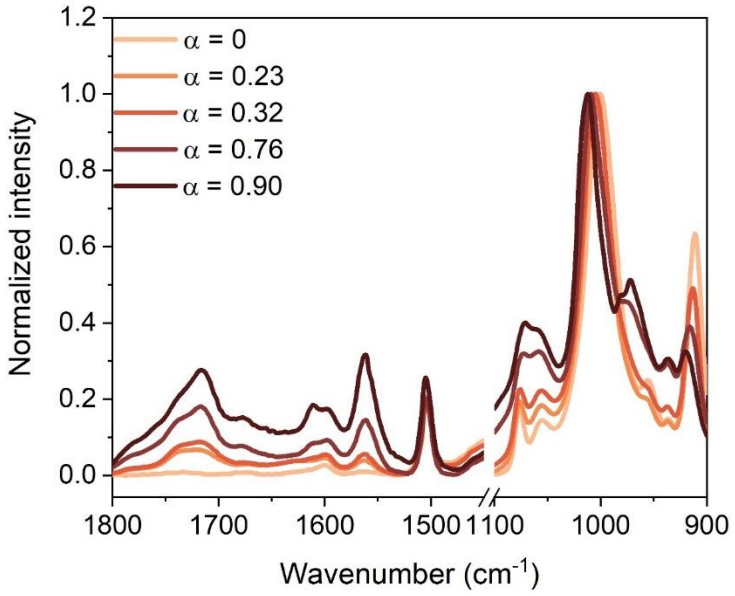

Figure 2.7-1. Normalized FTIR spectra of PFA° (starting from undistilled FA) as function of conversion. α = 0 corresponds to the initial spectrum of undistilled FA.

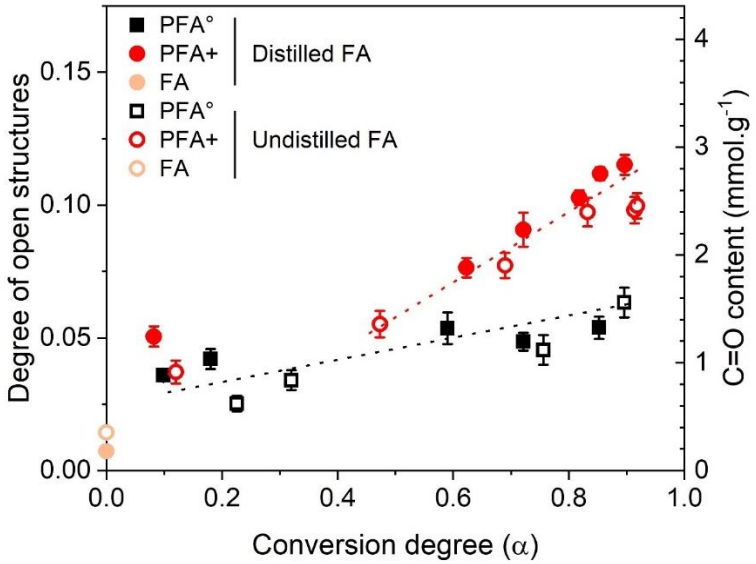

Figure 2.7-2. Evolution of DOS_{NMR} against the conversion degree; for PFA° (black squares) and PFA+ (red circles). Open and solid symbols are for samples prepared with undistilled FA and distilled FA respectively. Dot lines represent the linear fits. Error bars correspond to the standard deviation of triplicates.

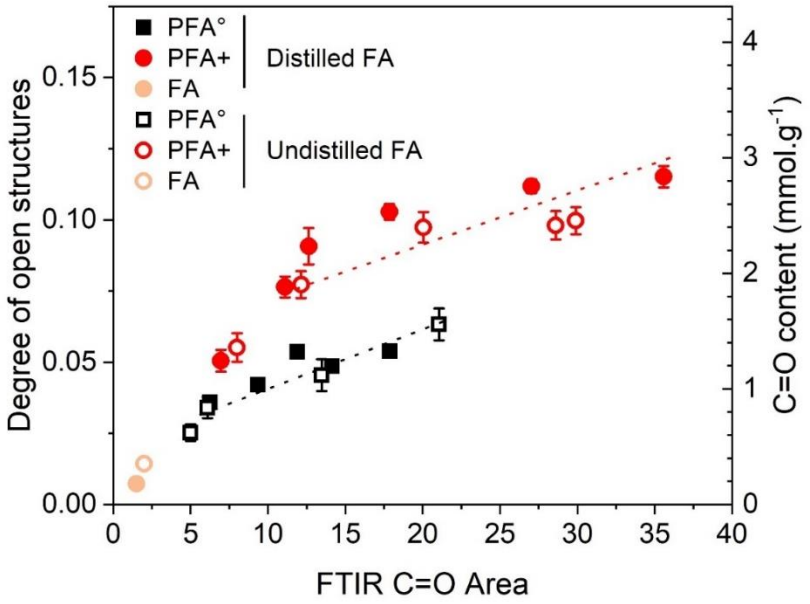

Figure 2.7-3. Evolution of DOS_{NMR} against the C=O area in FTIR, for PFA° (black squares) and PFA+ (red circles). Open and solid symbols are for samples prepared with undistilled FA and distilled FA respectively. Dot lines represent the linear fits.

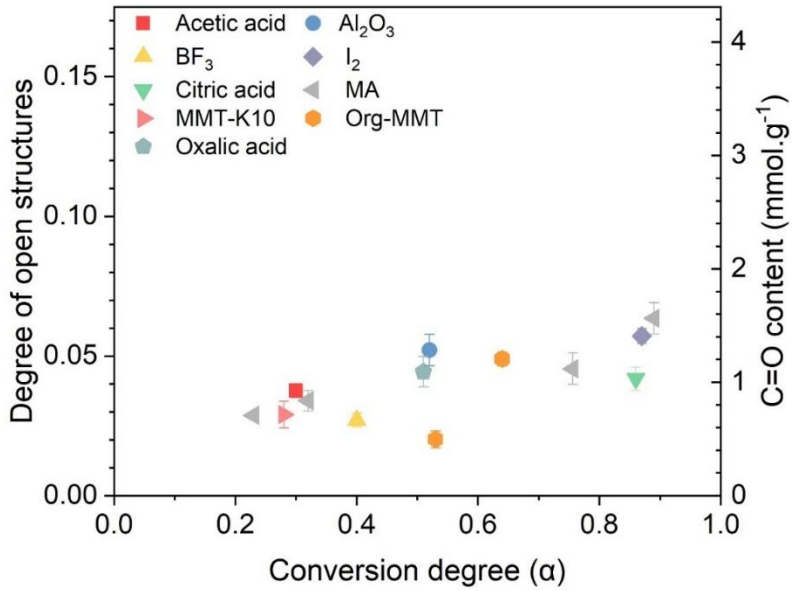

Figure 2.7-4. Comparison of the degree of open structures obtained from ^{19}F NMR method synthesized with different initiators in function of the conversion degree.

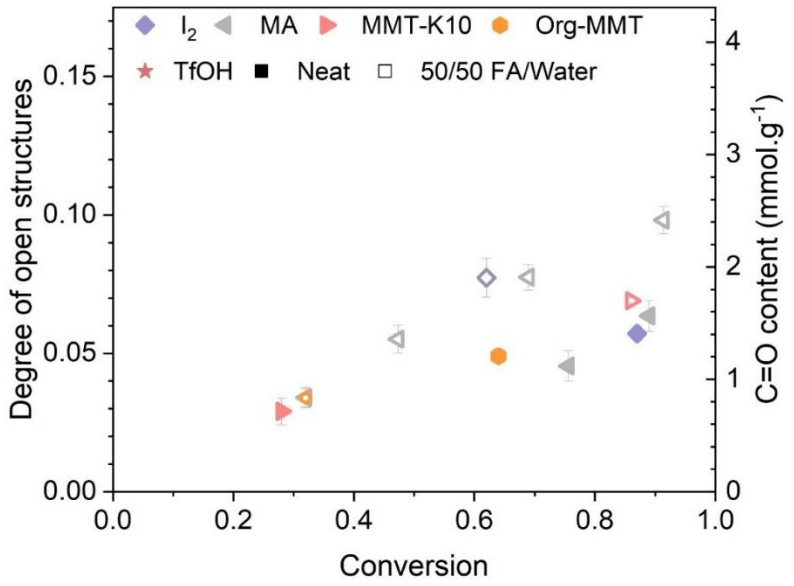

Figure 2.7-5. Comparison of the degree of open structures obtained ^{19}F NMR method and synthesized with different initiators with and without additional water (50 % w/w) in function of the conversion degree.

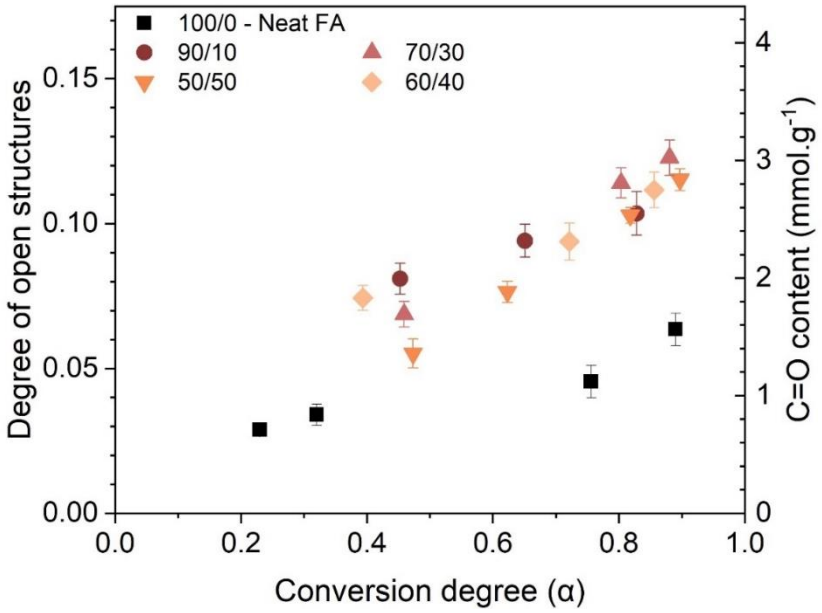

Figure 2.7-6. Comparison of the degree of open structures obtained with ^{19}F NMR method and synthesized with different FA/Additional water ratios with in function of the conversion degree.

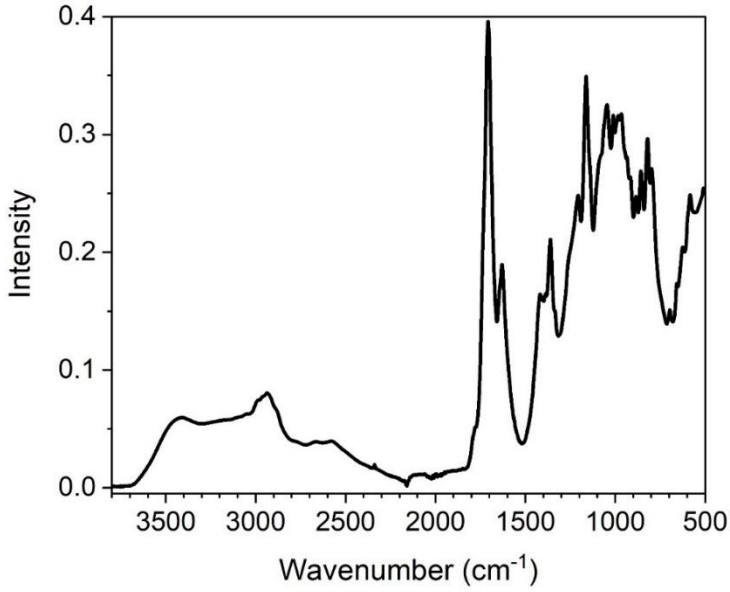

Figure 2.7-7. FTIR spectra of the yellowish liquid found in PFAs.

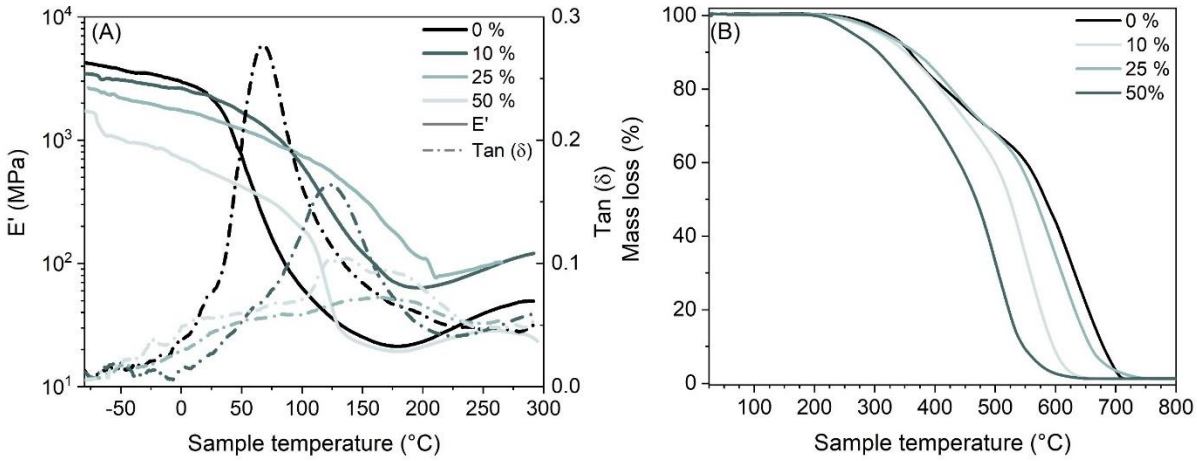

Figure 2.7-8. (A) DMAs scan of FA/HMF samples (2 °C.min^{-1}). (B) TGA scans of FA/HMF samples (10 °C.min^{-1}) under 50 mL.min^{-1} of air.

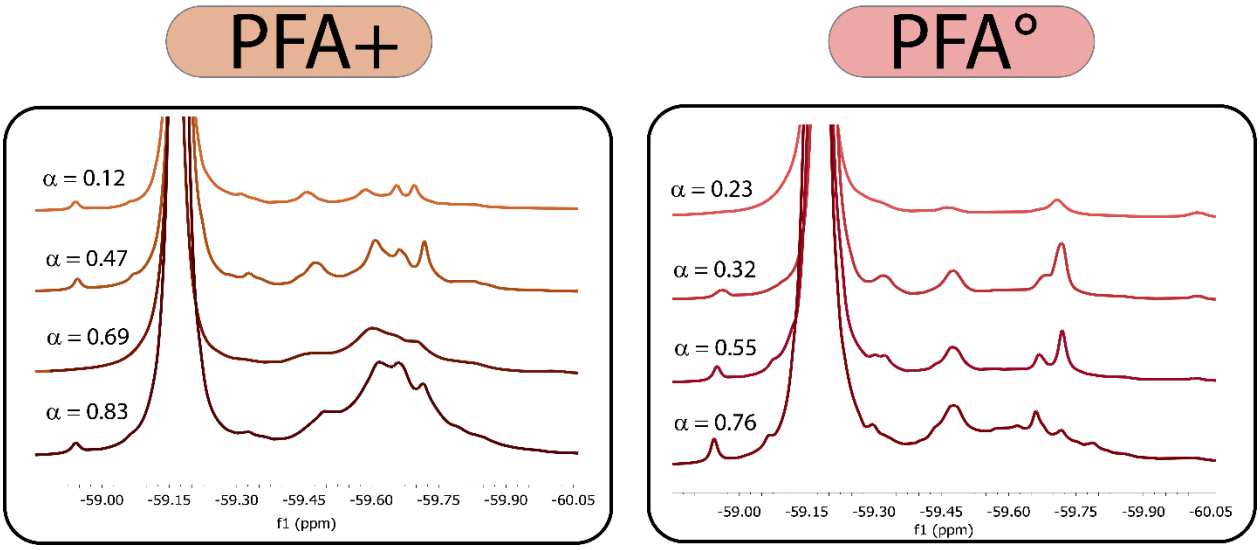

Figure 2.7-9. ^{19}F NMR spectra of PFA+ (left) and PFA° (right) at various conversion degrees.

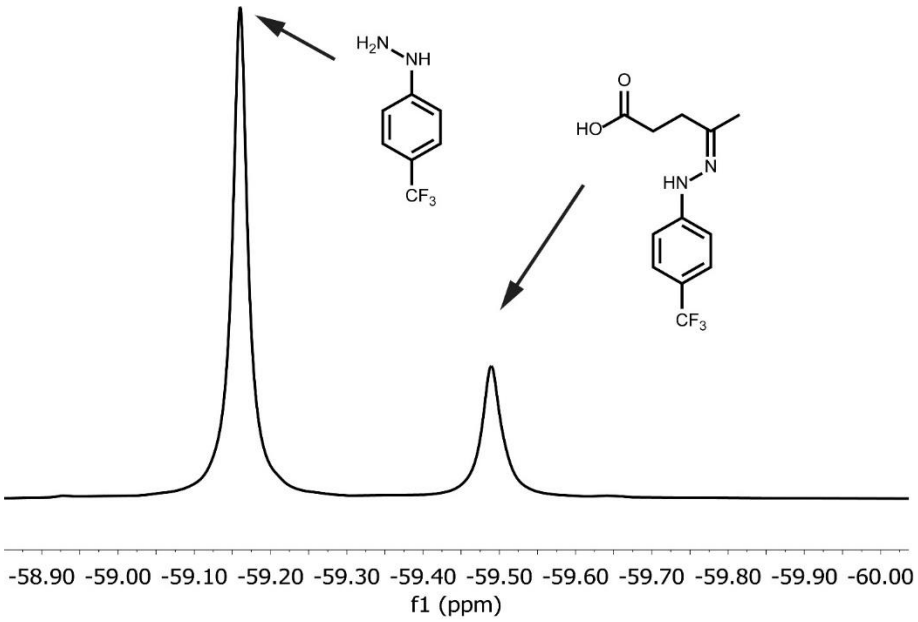

Figure 2.7-10. ^{19}F NMR spectrum of Levulinic acid derivatized with $CF_3\Phi NHNH_2$.

CHAPTER 3
The carbonyls in PFA: a structural investigation

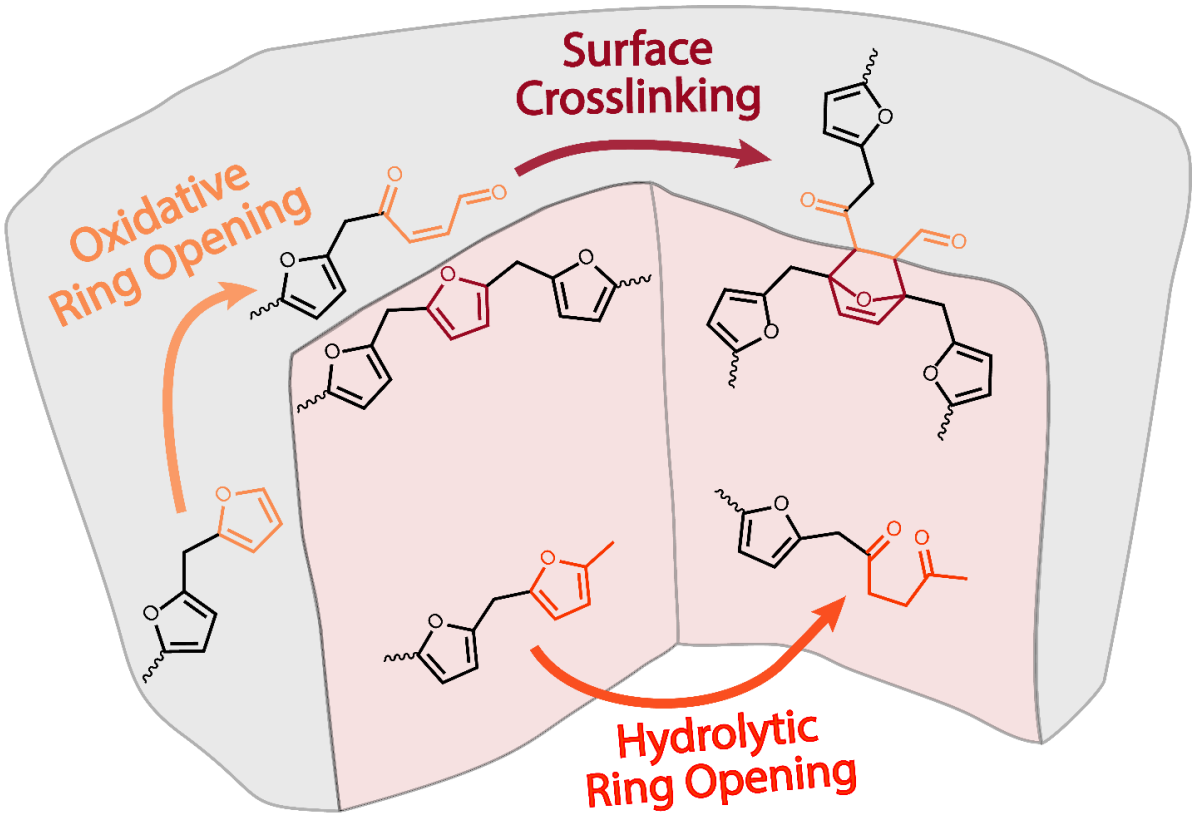

Based on:

Delliere, P.; Guigo, N. Revealed Pathways of Furan Ring Opening and Surface Crosslinking in Biobased Polyfurfuryl Alcohol. *Eur. Polym. J.* **2023**, *187*, 111869. https://doi.org/10.1016/j.eurpolymj.2023.111869.

and

Delliere, P.; Guigo, N.; Pizzi, A. Structural Variations in Biobased Polyfurfuryl Alcohol Induced by Polymerization in Water. *Polymers.* **2023**, *15* (7), 1745. https://doi.org/10.3390/polym15071745.

Chapter 1, reported investigations revolving around the chemical structure of PFA. Some of them used bidimensional NMR (2D NMR) for structural elucidation but never on PFA alone. To the best of our knowledge, bidimensional NMR was only employed to understand the nature of chemical links between PFA and other molecules such as lignin or epoxidized linseed oil. Furthermore, chapter 2 highlighted a diversity of carbonylated structures in PFA although their exact structure could not be elucidated.

Hence, the aim of this chapter is to deeply investigated the structure of PFA using modern NMR tools with a strong focus on the carbonyl products.

Section 3.2 is dedicated to the structural investigation of PFA+ using 2D NMR. The major known structural units are highlighted. In addition, the presence of several kinds of carbonyls is confirmed and new structures identified. This section also includes the quantification of functional groups by ^{1}H NMR in PFA+. In addition, the chapter 2 highlighted the formation of a C=O rich crust on the surface of PFA resins. This phenomenon is investigated in section 3.2.

Finally, section 3.3 deepens the findings of Section 3.2, this time by comparing a PFA° with a PFA+ with 2D NMR and MALDI ToF. Doing so should allow to identify reactions occurring only when additional water is added during the polymerization of FA.

3.1 Experimental section

Materials:

Furfuryl alcohol (96 %), maleic anhydride (99 %), and dimethyl terephthalate (*Trace*CERT®) were purchased from Sigma-Aldrich. DMSO-d_6 and D_2O were acquired from Eurisotop. All chemicals were used as received.

Preparation and characterization of PFA resins:

PFA+ and PFA° resins were synthetized and characterized as described in section 2.1. Their C=O content was determined by potentiometry and their conversion degree by DSC.

Nuclear Magnetic Resonance (NMR):

All NMR experiments were performed at 298 K on a Bruker Advance DRX 500 spectrometer equipped with a 5 mm PA DUL 500S2 C-H-D-05 Z probe. All the pulse sequences used were supplied by the manufacturer. The spectrometer operated at a frequency of 500.13 MHz for ^{1}H experiments and at 125.77 MHz for the ^{13}C experiments. The spectra were referenced to the DMSO peak (^{1}H 2.50 ppm; ^{13}C 39.52 ppm). About 100 mg of PFA resins were weighted and dissolved in 700 µL of DMSO-d_6. The exact masses were recorded for the quantification calculations.

^{1}H experiments:

^{1}H experiments were conducted the “zg” pulse program . For quantitative measurements, the spinning was turned off. As many different aldehydes are present in the system the T1 were not determined. However, a relaxation delay of 30 s was employed to ensure their complete relaxation. A total of 160 scans were accumulated. The presence of labile hydrogens under the areas of interest was checked by performing a control tube with PFA and D_2O. The areas of interest were free of labile hydrogens. To determine the concentration of aldehydes in PFA resins, two different approaches were used and are described thereafter.

Quantification using external standard:

The first quantification used dimethyl terephthalate as an external standard. About 2 mg of qNMR grade dimethylterephtalate (reference) were weighted on a Mettler Toledo microbalance XS3DU (d = 1 µg). Then they were dissolved in 700 µL of DMSO-d6.

On one hand, the reference spectrum of dimethylterephtalate was recorded using the previously described parameters and processed with Bernstein polynomial (order 3) baseline from 7 to 9 ppm. On the other hand, the spectra were recorded using the same parameters and the baseline was applied from 8.4 to 12.8 ppm to ensure accurate integration of the aldehyde peaks. If the baseline is applied on the whole spectrum, the area of the integrated peak would be highly overestimated as illustrated in Figure 3.5-1.

To determine the concentration of aldehydes within PFA resins, Equation 3.1-1 was used after adaptation from Soininen. [337] In Equation 3.1-1, *A* and *Ref* subscripts stand for the aldehydes and reference, respectively. *A* is the absolute area of the peaks which were integrated from 8.8 to 10.3 ppm for the aldehydes and from 8.0 to 8.20 for the reference. C_{ref} is the concentration of the reference, *n* the number of hydrogens responsible for the peak, V the volume of solution, and $m_{PFA}$the mass of PFA resin introduced in the tube.

$$Aldehyde\ content\ (mmol.g^{-1}) = C_{ref}\frac{A_A * n_{Href}}{A_{ref} * n_{HA}} * \frac{V}{m_{PFA}} \quad \text{Equation 3.1-1}$$

Quantification using the left-over furans:

The second approach used the furan rings in PFA as reference. For the calculation purpose, the macromolecular network of PFA was approximated as a repeating furfuryl unit (M = 80 g.mol^{-1}). In Chapter 2, such approximation was used to define the degree of open structures in PFA systems. In an opened furan, we assumed the formation of two carbonyls as the result of ring opening, thus giving Equation 3.1-2.

$$DOS = \frac{1}{2} * \frac{N_{C=O}}{N_{Furan}} = \frac{1}{2} * CO\ content * M_{(furfuryl\ unit)} \qquad \text{Equation 3.1-2}$$

Taking in account that only one aldehyde can be produced from one furanic entity, Equation 3.1-2 can be transformed into Equation 3.1-3.

$$Aldehyde\ content\ (mmol.g^{-1}) = \frac{N_{Aldehyde}}{N_{Furan}} * \frac{1000}{M_{(furfuryl\ unit)}} \qquad \text{Equation 3.1-3}$$

Then, $N_{Aldehyde}$ can be determined as the integrated area of all aldehydes in the NMR spectra, i.e from 8.8 to 10.3 ppm ($A_{8.8-10.3}$). The same can be done for N_{Furan} using the area from 5.6 to 7.0 ppm. This area corresponds to the two hydrogens, respectively in positions C3 and C4 of the furan ring. Thus, $N_{Furan} = 0.5 * A_{5.6-7.0}$. Therefore, Equation 3.1-4 is obtained. To measure $A_{8.8-10.3}$ and $A_{5.6-7.0}$ accurately, baselines were applied in the 8.4 – 12.8 ppm and 5.2 – 7.3 ppm, respectively.

$$Aldehyde\ content\ (mmol.g^{-1}) = \frac{A_{8.8-10.3}}{0.5 * A_{5.6-7.0}} * \frac{1000}{M_{(furfuryl\ unit)}} \qquad \text{Equation 3.1-4}$$

The relative proportion of aldehydes over all the C=O was calculated using Equation 3.1-5

$$Aldehyde\ \% = \frac{Aldehyde\ content\ (mmol.g^{-1})}{C=O\ content\ (mmol.g^{-1})} \qquad \text{Equation 3.1-5}$$

^{13}C NMR, HMBC and HSQC experiments:

The ^{13}C NMR spectra were acquired using the "zgpg30" pulse sequence, 20 000 scans and a relaxation delay of 2 s. The DEPT-90 experiments used the pulse sequence "deptsp90", 8 600 scans and a relaxation delay of 2 s. The DEPT-135 spectra were acquired using the "deptsp135" pulse sequence, 12 000 scans were accumulated, and a relaxation delay of 2 s was used.

The HSQC and HMBC are 2D NMR tools correlate ^{1}H and ^{13}C signals with each either on NMR maps. As illustrated in Scheme 3.1-1, HSQC correlates hydrogen and carbon one bond away while the HMBC correlation are for atoms two to four atoms away, without heteroatoms in between.

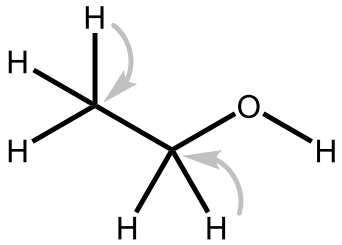

HSQC J^1 correlations

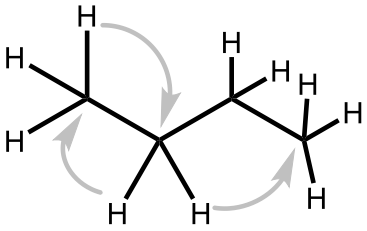

HMBC J^2 and J^3 correlations

Scheme 3.1-1. Correlations observed in HSQC (left) and HMBC (right).

For the HMBC experiments, the "hmbcetgpl3nd" pulse sequence was used with a relaxation delay of 2 s and 100 scans were accumulated. Finally, for the HSQC, the pulse sequence "hsqcedetgpsisp2.3" was used. 54 scans were recorded and a relaxation delay of 1.5 s was used.

MALDI ToF mass spectrometry

The samples were treated with a NaCl solution (1.5 µl of a 0.1 M) in a methanol/water mixture (1:1) to increase ion formation, and a drop placed on the MALDI target (3 mm diameter) steel plate and dried. The samples and the matrix were then mixed in equal amounts, and 1.5 µl of the resulting slurry was placed on the MALDI target and dried at 40 °C for 2 h before being analyzed. A matrix of 2,5-dihydroxy benzoic acid was used. Red phosphorous (500–3000 $g.mol^{-1}$) was used as reference for spectrum calibration. Finally, after evaporation of the solvent, the MALDI target was introduced into the spectrometer. The spectra were recorded on a KRATOS AXIMA Performance mass spectrometer from Shimadzu Biotech (Kratos Analytical Shimadzu Europe, Ltd., Manchester, UK). The irradiation source was a pulsed nitrogen laser with a wavelength of 337 nm. The length of one laser pulse was 3 ns. Measurements were carried out using the following conditions: polarity-positive, flight path-linear, 20 kV acceleration voltages, 100–150 pulses per spectrum. The delayed extraction technique was used applying delay times of 200–800 ns. The software MALDI-MS was used for the data treatment. The oligomers can appear in the spectra either corresponding to their molecular weight or to their molecular weight +23 $g.mol^{-1}$of the Na^+ ion derived from the NaCl used as enhancer. The spectra precision is of ± 1 $g.mol^{-1}$.

3.2 Strucural elucidation of the carbonyls in PFA+

As discussed in Chapter 1, the chemistry of FA-based resins is complex. Over the years, extensive research was conducted to elucidate the chemical structure of PFA. Starting in the forties with the work of Dunlop and Peters [270] who first proposed a succession of furfuryl units as the most dominant structure in PFA. In the following years, researchers attempted to shed light on the structure of PFA using gel permeation chromatography [273], monodimensional ^{1}H and ^{13}C NMR [274, 275, 280, 285] including ^{13}C solid state NMR. [278, 279] Model compounds [276, 281], vibrational spectroscopy [272, 288], ab initio molecular modelling [287, 289], MALDI-ToF [208], and combination of these [286, 293] were as well. Overall, these different works lead to the various PFA' structures depicted in Scheme 3.2-1, among others.

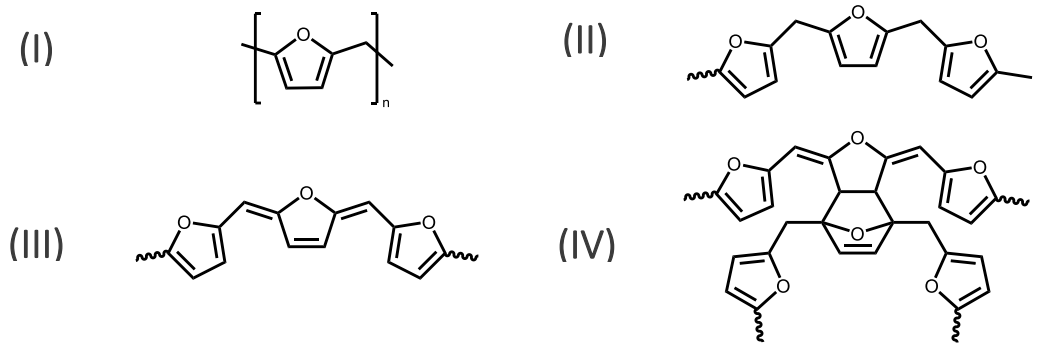

Scheme 3.2-1. Structures found in PFA.

Recently, a special emphasis was placed on side-structures within PFA after Falco et al. showed that the furan ring opening side-reaction can be used to tune the thermomechanical properties of PFA. [283] This study was followed by structural studies [284, 296] focused on the carbonyl moieties formed by hydrolytic furan-ring opening of PFA. These different carbonyl structures of PFA reported in the literature are displayed in Scheme 3.2-2. Furthermore, chapter 2 showed that up to 15 % of the furan rings in PFA can be opened. As developed later in chapter 5 the side reactions during FA polymerization offer new possibilities.

Hence, to extend the potential of PFA resins, deeper knowledge on these carbonyls is required. Indeed, while in the previous studies a number of open structures were reported, their origin and link with the macromolecular network were not thoroughly investigated. Hence, tools giving additional information than ^{1}H, ^{13}C and infrared spectroscopy are needed to better understand the connections between carbonyl structures and the network of PFA.

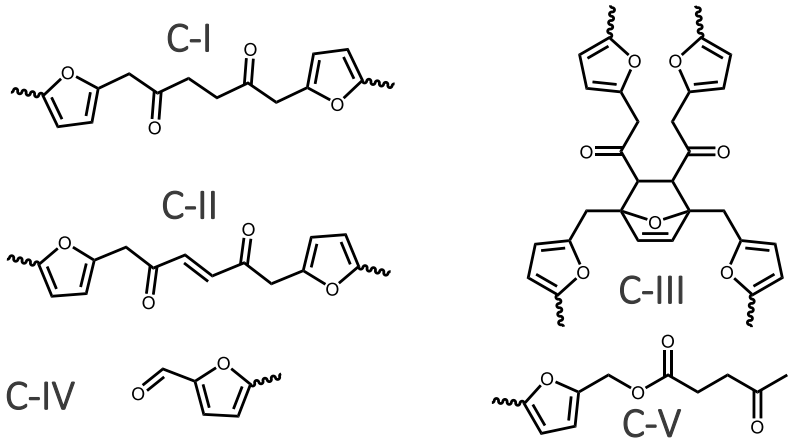

Scheme 3.2-2. Possible carbonyl-bearing moieties of PFA, according to literature. [272, 284, 289, 296]

Among the means dedicated to structural elucidation, bidimensional NMR has proven to be a powerful tool. Indeed, due to their growing industrial interest lignins and their derivatives have been extensively studied with these techniques. [338, 339, 340, 341] Nonetheless, to the best of our knowledge, bidimensional NMR was never used to elucidate the structure of PFA. Bidimensional NMR investigations were employed to determine interconnections between lignin and PFA [137, 295] or between epoxidized linseed oil and PFA. [224] Consequently, the focus of this section is to breakthrough knowledge on the structural elucidation of carbonyl moieties contained in PFA by means of bidimensional NMR and quantitative ^{1}H NMR.

3.2.1 General features in bidimentional NMR spectra

The main objective of this section is to identify the nature of the carbonyls within PFA+ and clarify their pathway of formation as well as their link to the macromolecular network. A PFA+ resin with a rather advanced conversion degree of 0.80 (based on FA polymerization), i.e when 80 % of the polymerization is completed, was chosen. This choice was driven by the high carbonyl content (≈ 3.0 mmol.g^{-1}) of the resin while it could be easily dissolved in DMSO-d6.

First, PFA was investigated with monodimentional NMR using a high number of scans to highlight the carbonyl moieties as their concentration is relatively low. The ^{1}H and ^{13}C NMR spectra are reported in Figure 3.2-1. The most intense signals have already been assigned in previous investigations. [274, 281, 286] The main structure of PFA (I) as well as the terminal methyl and furan are easily identified using 1D NMR. Nonetheless, many signals overlap with each other thus rendering unambiguous structural elucidation highly complex for structures such as the dihydrofurans of (III) or the carbonyl moieties of Scheme 3.2-1 and Scheme 3.2-2.

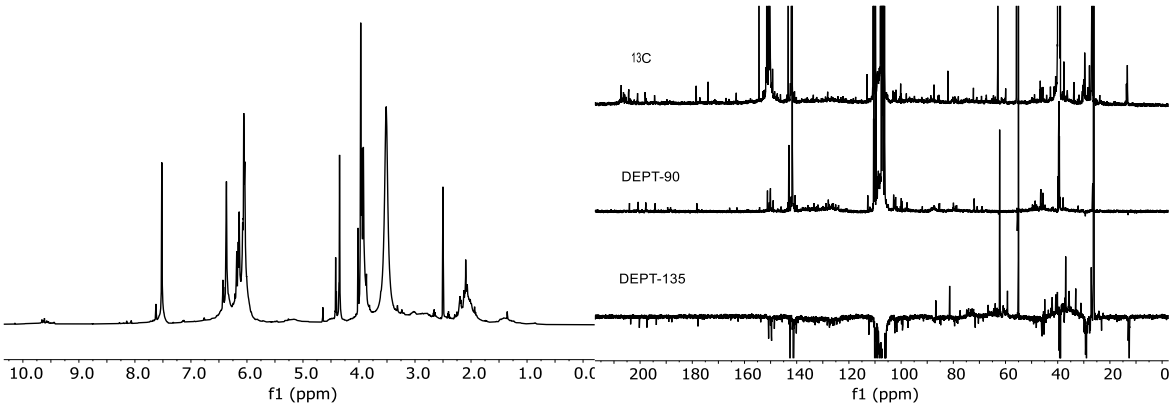

Figure 3.2-1. ^{1}H NMR spectrum of PFA (A), ^{13}C, DEPT-90 and DEPT-135 NMR spectra of PFA+ at a conversion degree of about 0.80.

To facilitate the interpretation of the spectra, bidimensional NMR was performed. First, the HSQC spectrum of PFA+ displayed in Figure 3.2-2 is first used to quickly review the main structures of PFA before focusing on the carbonyls.

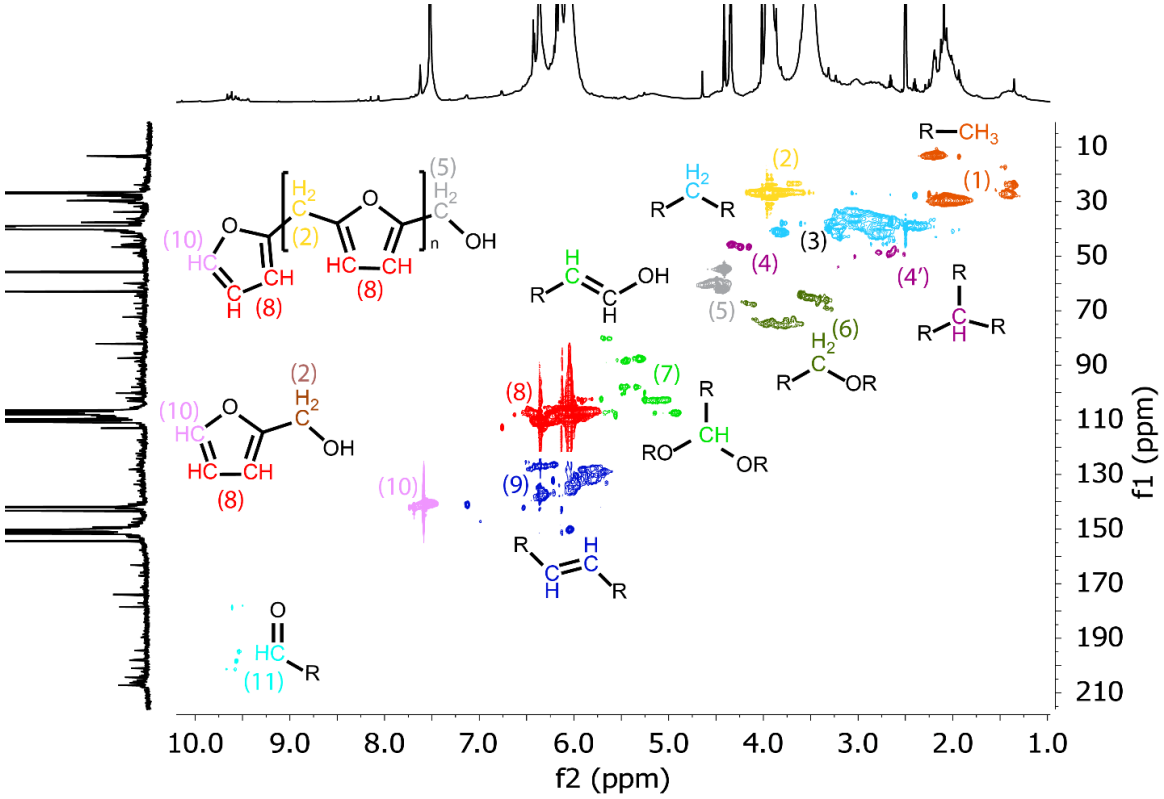

Figure 3.2-2. HSQC spectrum of a PFA+ resin with a conversion degree of about 0.80.

From Figure 3.2-2, the structure (I) of PFA and FA can be easily identified. The cluster (2) and (8) are respectively the methylene bridge and the C_3-C_4 of the furan ring. The cluster (5) is the CH_2-OH from FA or end-chain alcohols. [281] On one hand, the cluster (10) corresponds to the unsubstituted =CH of terminal furan. [281] On the other hand, the methyl groups at 10 ppm from cluster (1) have been identified as the methyl group of structure (II) formed concomitantly with the conjugated structure (III). [281] However, three kinds of methyl groups are observed in cluster (1). Structure (III) and (IV) are most-likely responsible for the cluster (9). Indeed, C=C bonds of alkenes are often comprised between 110 and 150 ppm. [330]

In previous reports, the HC=C hydrogen signal of (III) and (IV) could not be distinguished from the hydrogens in position 3 and 4 of the furan solely by ^{1}H NMR. The cluster (4') could correspond to CH of the Diels-Alder adduct of structure (IV). Cluster (4) might also be a sign of a methylene bridge, as depicted in Scheme 1.3-11 Another possibility for the origin of the other CH, i.e cluster (4), and the origin of the wide array of CH_2, i.e cluster (3), are discussed thereafter. The cluster (6) could be assigned to the ether structures formed by head-to-head condensation. It degrades to structure (I) by freeing formaldehyde, as shown in Scheme 3.2-3. [271] Although the liberation of formaldehyde is known since decades, to the best of our knowledge, it was never quantified.

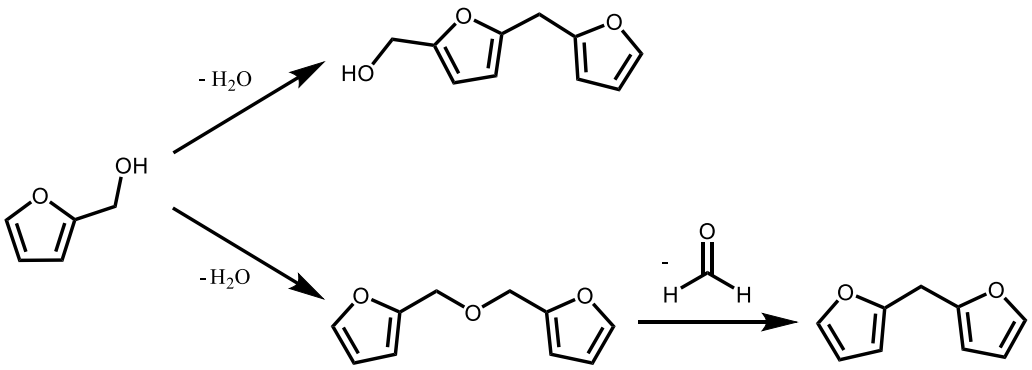

Scheme 3.2-3. Pathways for the acid-catalyzed condensation of FA. [271]

Regarding the rest of the spectrum, the cluster (7) highlights the presence of enols and/or ketal species. [330] Such note is of importance as these are derived from carbonyls and makes them less available for chemical reactions. Chapter 2 showed a gap between two quantification techniques. The first one was based on the derivatization of carbonyls by hydroxylamine hydrochloride followed by potentiometric titration. The second method, involved a derivation by a fluorinated phenyl hydrazine followed by ^{19}F NMR. Overall, the latter method yielded lower carbonyl content than the potentiometric one. This gap was mainly attributed to steric hindrance with a participation of ketal species. The data in Figure 3.2-2 outlines the fact that some carbonyls may not be directly available for derivatization. Indeed, the enol and ketals do not behave as carbonyls in terms of reactivity. Thus, a displacement of equilibrium from the enol/ketal towards the carbonyl may be required to fully exploit the potential of the carbonyl moieties in PFAs.

Interestingly, the presence of cluster (11) unambiguously highlights that aldehydes functions are present in PFA. Theses aldehydes can be seen in Figure 3.2-1 on the ^{1}H and DEPT spectra. At least seven types of aldehydes are present in the system. Their possible structures are discussed later.

Figure 3.2-3 displays a part of the HMBC spectrum of the same PFA+ as earlier. From this figure, the linear PFA and methylfuran from structure (I) and (II) can be found through cluster (6) and (8), respectively. In the followings, the existence of structures C-I to C-V from Scheme 3.2-2 are discussed using the HMBC spectra in Figure 3.2-3.

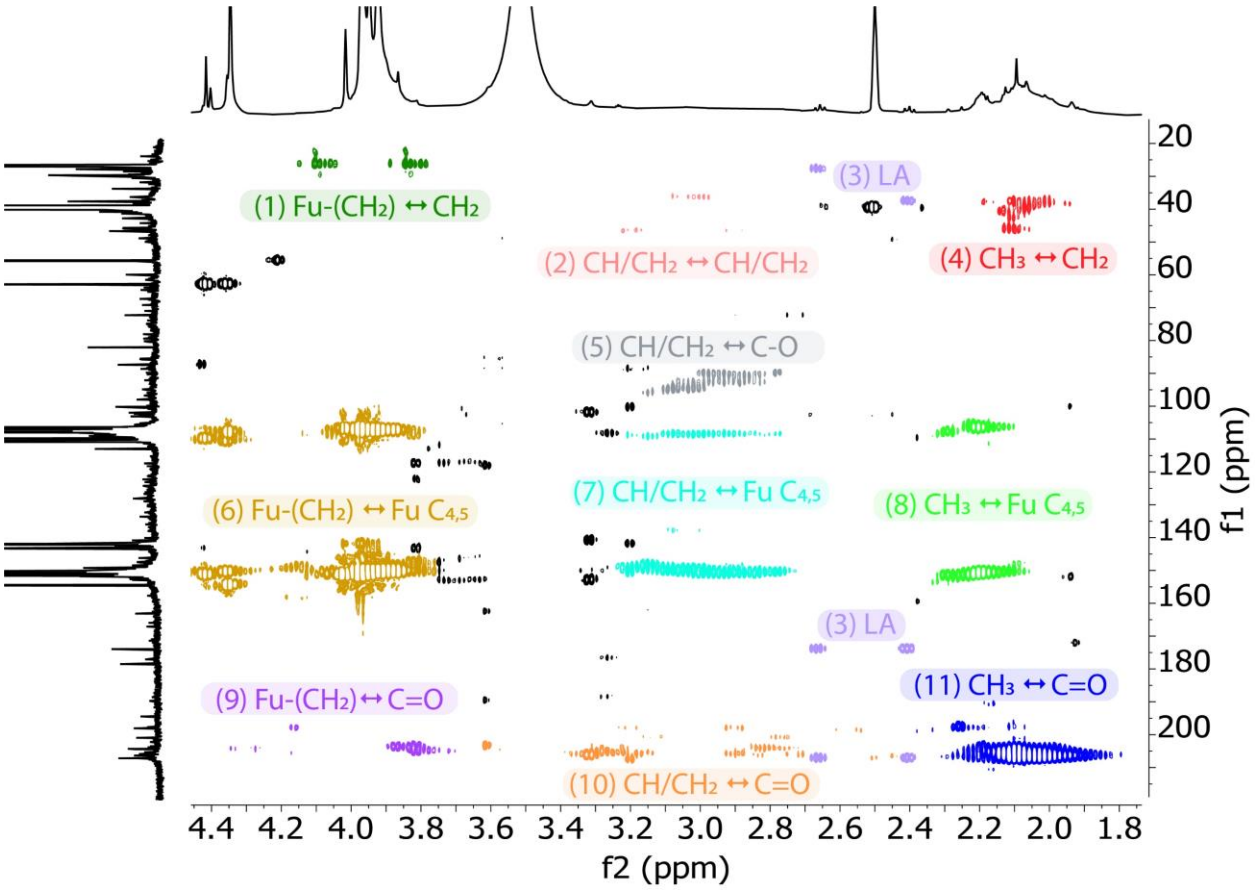

Figure 3.2-3. Magnified HMBC spectrum of PFA+ at a converion degree of about 0.80.

First, the clusters (3) form a spin system coherent with either levulinic acid (LA) or furfuryl levulinate (C-V). However, using potentiometric titration, about 0.15 $mmol.g^{-1}$ of COOH can be found in PFA+ at this stage of polymerization. Moreover, theses PFA+ do not show signs of COOR bands in FTIR (Figure 2.5-2). Hence, it is more likely that free LA molecules are responsible for cluster (3) rather than structure C-V. The cluster (10) at 2.8 ppm as well as cluster (9) at 3.8 ppm might correspond to structure C-I, postulated by Conley and Metil. [272] This kind of structure would emerge from the hydrolytic ring opening of furan within the chains of PFA.

The full HMBC spectrum of this sample is available in Figure 3.5-2 along with a magnification from 4.5 to 8.0 ppm in Figure 3.5-3. Only two clusters of **H**C= correlating to H**C=O** are observed. Moreover, the related carbon peaks - 194.2 and 197.8 ppm – are positive in the DEPT-90 spectra. Hence, these peaks are caused by aldehydes. In addition, Tondi et al. attributed a ^{13}C peak at 219 ppm to the structure C-II, which is not observed in our PFA. [284] Hence, structure C-II could not be observed here. Its existence cannot be completely ruled out as it could be in low concentration or masked as an enol or ketal. Other possibilities are that the formation of this kind of carbonyls could appear later in the polymerization or be dependent on the polymerization conditions. Finally, Tondi et al. reported that structure C-II would react with furans to give the Diels-Alder adduct C-III. The clusters (10) around 3.3 ppm might correspond to this structure.

The cluster (11) has been assigned as a methyl to ketone correlation. Indeed, only two aldehydes have chemical shifts between 200 and 205 ppm and it is unlikely to see methyl – aldehyde neighbors in PFA systems. The cluster (4) is linked to correlation between CH_2 and CH_3. Hence, a possibility for the origin of clusters (4) and (11) is the hydrolytic ring opening of methylfuran, structure (II), into structure C-VI, as depicted in Scheme 3.2-4. This hypothesis is backed-up by the cluster correlations Fu-(CH_2) with a CH_2 of cluster (1) and with a C=O of cluster (9). Furthermore, the CH_2 of cluster (10) around 2.8 ppm also point to structure C-VI. The CH_2 to CH_3 correlation is however not seen. Interestingly, the heterogeneity of cluster (11) is a good sign that these carbonyls are linked to the macromolecular chain rather than being parts of free molecules. These results are also consistent with section 2.5 where the presence of levulinic-like species was suggested by ^{19}F NMR

In chapter 2, the conditions of polymerization were varied to control the concentration of carbonyls in PFA resins. The degree of open structure (DOS) in all cases could not go above 15 % for soluble resins. If most of ring opening occurs in end groups i.e., either as in structure C-VI or as aldehydes, it is logical that the DOS is then limited to a certain extent.

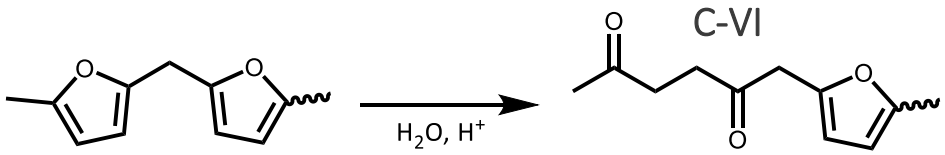

Scheme 3.2-4. Representation of the hydrolytic ring opening of terminal methylfuran.

3.2.2 Unexpected carbonyls

In the following, the focus is made on the aldehydes, using Figure 3.2-4A and B, extracts of HSQC and HMBC, respectively.

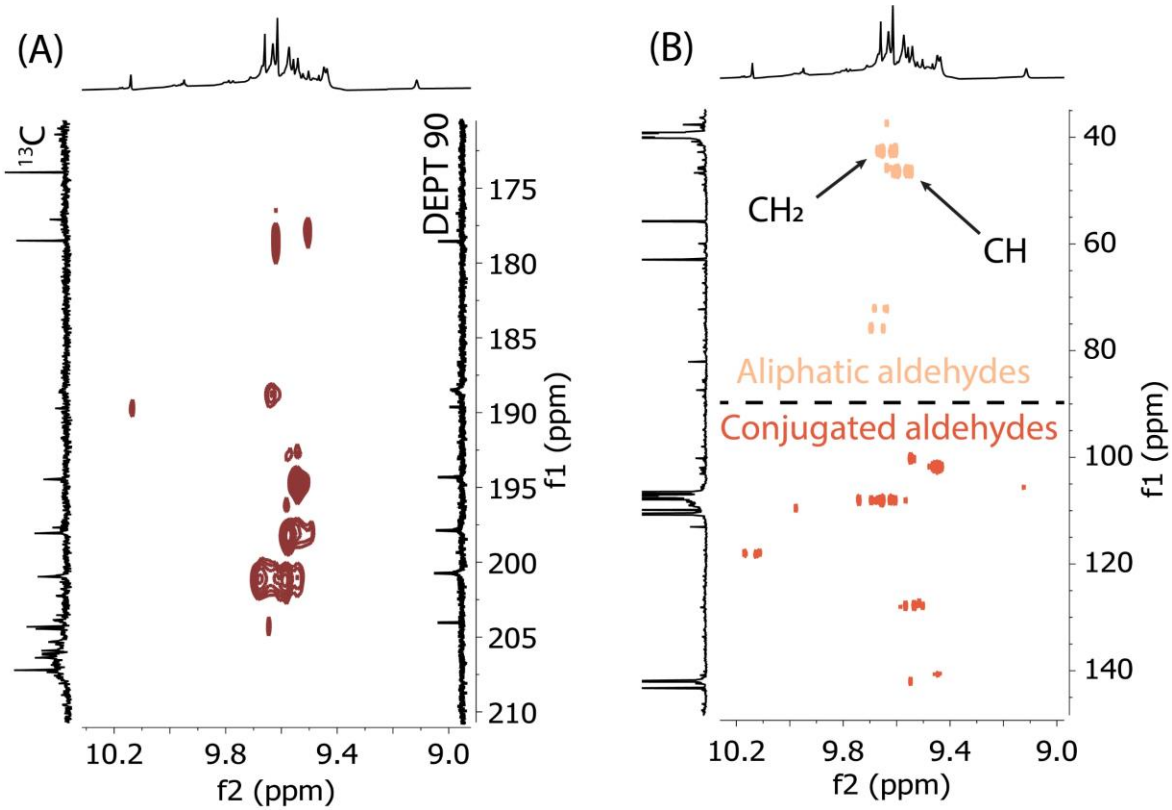

Figure 3.2-4. Magnification of the HSQC (A) and HMBC (B) of PFA+ at a converion degree of about 0.80.

First, the DEPT-90 spectra in Figure 3.2-1 reveals a positive peak at 178 ppm. The magnified HSQC spectra in Figure 3.2-4A corroborate that the peak at 178 ppm is an aldehyde. According to the literature, the chemical shift of C=O in furfural is about 178 ppm. [330] Thus, furfural or its derivatives such as structure C-IV are present in the system. Furfural comes as an impurity from the initial FA although some could also form though mild oxidation of FA during the polymerization.

However, a significant number of other aldehydes are present. According to the literature, the ^{13}C chemical shift of conjugated aldehydes is most often comprised between 175 and 200 ppm while aliphatic aldehydes are above 200 ppm. [330] In the HMQC extract of Figure 3.2-4B two groups can be identified. A first one, correlating with carbons below 90 ppm corresponding to aliphatic aldehydes and with conjugated ones above 90 ppm.

As both conjugated and aliphatic aldehydes are observed in PFA we conjectured some possible structures, they are reported in Scheme 3.2-5. The structure C-VII would emerge from the oxidative ring opening of a terminal furan, as in the first step of Achmatowitcz reactions. [342] Then, this conjugated aldehyde would be a suitable candidate for a Diels-Alder reaction with furans to yield the adduct C-VIII. Indeed, structure C-VII is a good dienophile with its two electron withdrawing groups. [343] The spectra's complexity and low concentration of aldehydes does not allow full assignment of the structure.

Despite this, the HMBC extract in Figure 3.5-3 show a **H**C=C with H**C=O** correlation at 7.16 with 197 ppm and 7.5 with 194 ppm. They could match with structure C-VII. Moreover, the HMBC of Figure 3.2-4B shows correlations of the aldehydes with carbons at 42.8 and 46.7 ppm which are CH_2 and CH, respectively. This figure also shows clusters around 75 ppm which is a match for quaternary carbons and thus, structure C-VIII. Also, the CH_2 cluster could correspond to a structure similar to C-IX. Indeed, Hu et al. reported the opening of furan into succinaldehyde when subjected to aqueous and acidic media. [344]

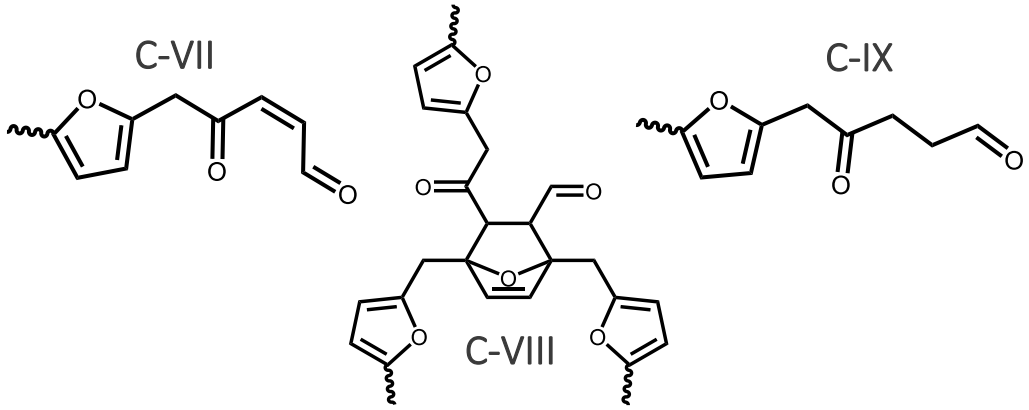

Scheme 3.2-5. Postulated aldehyde-based structures within PFA.

Subsequently to the identification of the aldehydes in PFA, their quantification was performed using ^{1}H NMR. Two methods were employed. The first one, referred as "external quantification" used dimethyl terephthalate as an external standard. The second method was based on the use of the hydrogen in position 3 and 4 of the furan ring and on the assumption that PFA's chains are a succession of furfuryl units. The results are compiled in Table 3.2-1 and illustrated by the ^{1}H NMR spectra in Figure 3.2-5.

Both Table 3.2-1 and Figure 3.2-5 show the gradual increase in aldehyde content during FA polymerization. The results are consistent between the two methods. The internal method has always a higher concentration of aldehydes. However, this is expected as the assumption made does not take in account open furans and Diels-Alder adducts. It should be noted that at the end of polymerization about 1/5 or 1/6 of carbonyls are aldehyde functions.

Table 3.2-1. Results from the aldehyde quantification experiments in a PFA+ system at different conversion degrees.

	External standard		**Left-over furans**	
Conversion degree (α)	**Aldehyde content (mmol.g^{-1})**	**Aldehyde Ratio**	**Aldehyde content (mmol.g^{-1})**	**Aldehyde ratio**
0.12	0.05	**0.04**	0.08	**0.06**
0.47	0.17	**0.09**	0.25	**0.13**
0.69	0.24	**0.09**	0.36	**0.14**
0.83	0.47	**0.16**	0.62	**0.21**

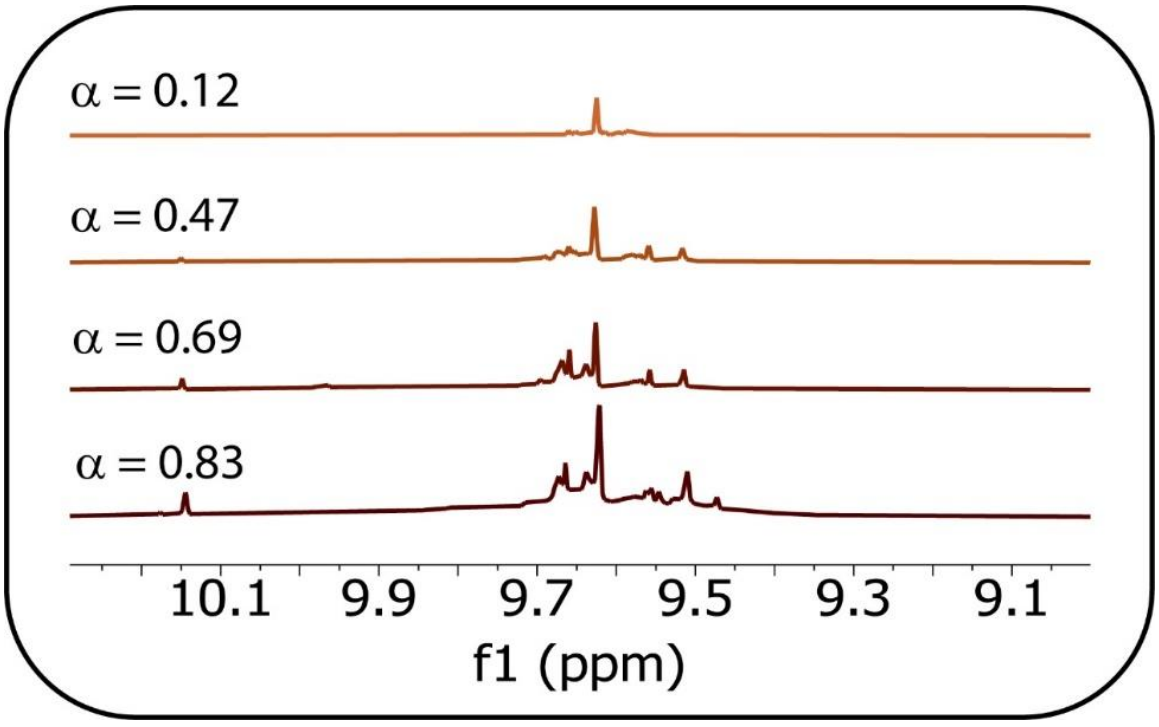

Figure 3.2-5. ^{1}H NMR spectra of the quantified PFA+ resins.

3.2.3 Origin of aldehyde formation in PFA

The literature can provide a few indications on the origin of these aldehydes. Indeed, some articles refer to the use of oxidative ring opening of furans to yield conjugated 1,4-dicarbonyls. [316, 345, 346, 347] In the case of furfuryl alcohol, the oxidative cleavage of the furan ring is often used in the Achmatowitcz rearrangement. Typical oxidants are Br_2, N-bromosuccinimide, m-chloroperoxybenzoic acid or H_2O_2. [342, 348, 349, 350] As well, few papers mention the use of dioxygen as an oxidant for the ring opening reaction of furans in photocatalyzed reactions. [351, 352, 353, 354]

In the past, Gonzalez et al. investigated the polymerization of FA under inter atmosphere or air. They did not find any significant influence of dioxygen during the polymerization. Yet, they noticed that their PFA would still be soluble after 14 months when conserved in vacuum sealed ampoules i.e., with a limited contact with air. However, their synthetized PFA would become insoluble after only few hours exposed to air environment. [280, 286] Moreover, if a PFA resin with a conversion degree of 0.80 (or more) is left in open air, a dark and hard crust forms as depicted in the photography of Figure 3.2-6. More specifically, in five minutes exposed to air, the red color shifts to black and the crust becomes hard in less than two hours. In addition, the C=O content of the crust was found to be up to 30 % higher than the heart of the resin in section 2.2.2.

Figure 3.2-6. Photography of a PFA sample immediately taken after cutting the sample.

These observations coupled with the previous HMBC experiments and sensitivity of furans towards oxidative cleavage led us to the potential pathways depicted in Scheme 3.2-6.

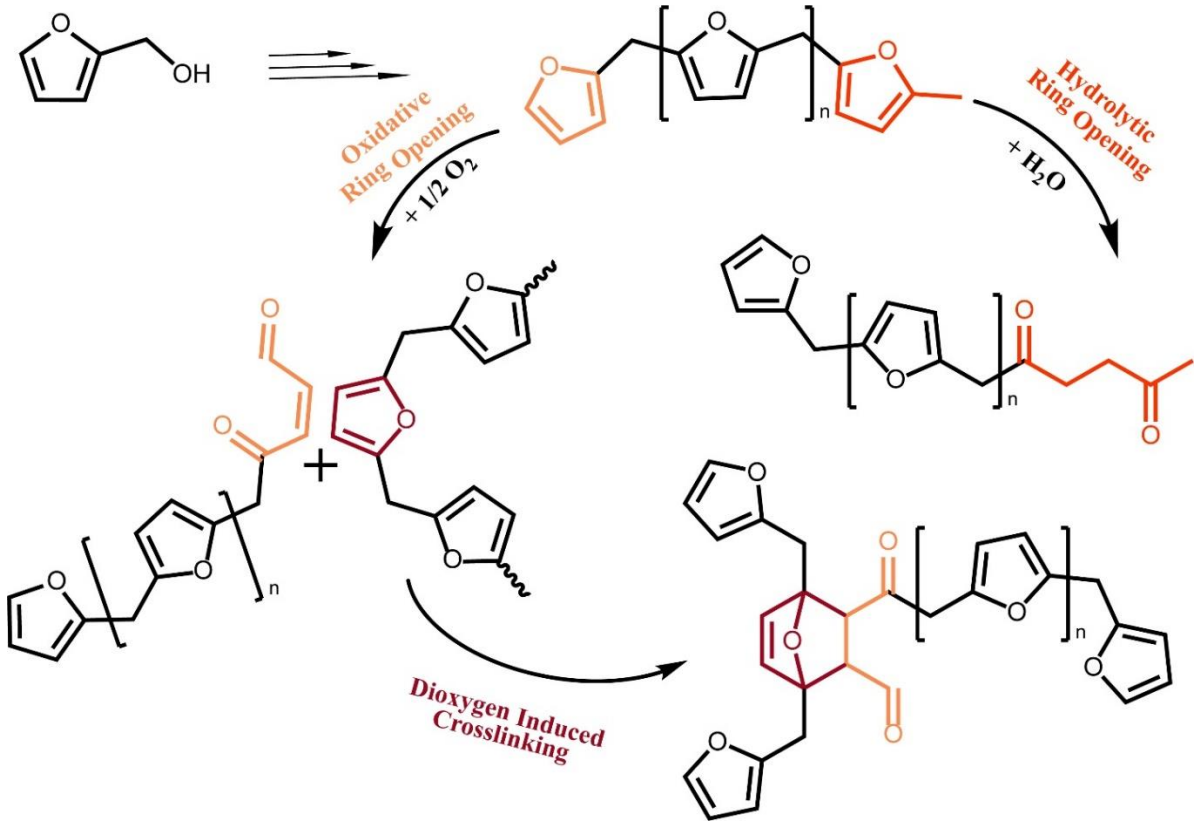

Scheme 3.2-6. Illustration of the two pathways proposed for end-chain ring opening in PFAs.

On the one hand, the methylfuran end-groups would open through hydrolytic ring opening (dark orange labelled furan in Scheme 3.2-6). On the other hand, the terminal furans would open through an oxidative ring opening when exposed to air (light orange labelled furan in Scheme 3.2-6). Then, the resulting conjugated aldehyde would react trough Diels-Alder cycloadditions with other furans to further crosslink the macromolecular chains and thus increasing the surface hardness.

3.2.4 Conclusion of section 3.2

This section shed new lights on the complex structure of PFA+ resins and – for the first time - with a special emphasis on carbonyls generated during FA polymerization.

The furan ring-opening reaction has been found to mostly occur on the terminal furans of PFA's macromolecular chains. Methylfuran end groups are opened into levulinic-like ketonic species while furan end-groups are opened into aldehydes. The NMR data confirmed that ketones are mostly non-conjugated and, on the contrary, aldehydes are rather conjugated. It was found that within all the formed carbonyls in PFA+, up to 20 % are aldehydes. The fact that most of the ring opening occurs on furan end-groups rather than furan rings embedded within the chain might explain why the degree of open structure remains somehow limited to about 15 % (3.7 $mmol.g^{-1}$) for soluble resins.

Finally, a pathway was proposed to explain the formation of a stiff crust on PFAs' surface. The dioxygen present in air induces an oxidative ring opening at the surface of PFA thus leading to conjugated aliphatic aldehydes. The dienophilic character of these opened end-groups is enhanced by the electron-attracting effect from the aldehyde. Therefore, they are prone to make additional crosslinks via Diels-Alder cycloadditions thus leading to the formation of a stiffer surface compared to the core material. The peculiar sensibility of PFA for surface oxidation can have useful and interesting consequences when designing its processability.

3.3 Structural comparison of PFA° and PFA+:

The aim of this section is to further apprehend the nature of the carbonyl groups in PFAs by comparing two types of PFA. The first one was prepared in neat conditions (PFA°), i.e., without additional water and a second one synthetized in 50 % aqueous solution (PFA+). The PFAs structures were compared using 2D NMR techniques (HMBC and HSQC) and ^{1}H NMR quantification. In addition, MALDI-TOF measurements were performed to further highlight the structural differences between the samples.

3.3.1 The CH_3 groups

First, HSQC experiments of PFA° and PFA+ resins were performed to highlight their main structural differences. For an easier comparison, resins with a conversion degree of about 0.80 were chosen. Figure 3.3-1 displays a magnification of the HSQC spectra of PFA+ and PFA° located on the methyl area. In Figure 3.3-1, PFA°(brown) is stacked above PFA+ (orange). The opposite viewpoint in which the PFA+ HSQC spectrum is shown in Figure 3.5-4. This magnification highlights the main types of methyl found in PFA. Three groups with significatively different chemical environments can be identified in soluble PFA resins.

The first group centered around 2.2/14 ppm can be attributed to the methylated furans as depicted in Scheme 3.3-1. The methylated furans are formed during the conjugations of furanic chains through the loss of a hydride ion. [281] Such methyls are observed in both PFA° and PFA+. Nonetheless, a larger dispersion of chemical shift occurs in the case of PFA+, thus suggesting a higher heterogeneity of the furanic structures in PFA+ resins. Another distinct group of methyls at 1.95/15 ppm is observed only in the case of PFA+. This cluster does not spread as much as the main one. Thus, it might belong to a free molecule (i.e. dimers, trimers) rather than to a group linked to the main macromolecular chains.

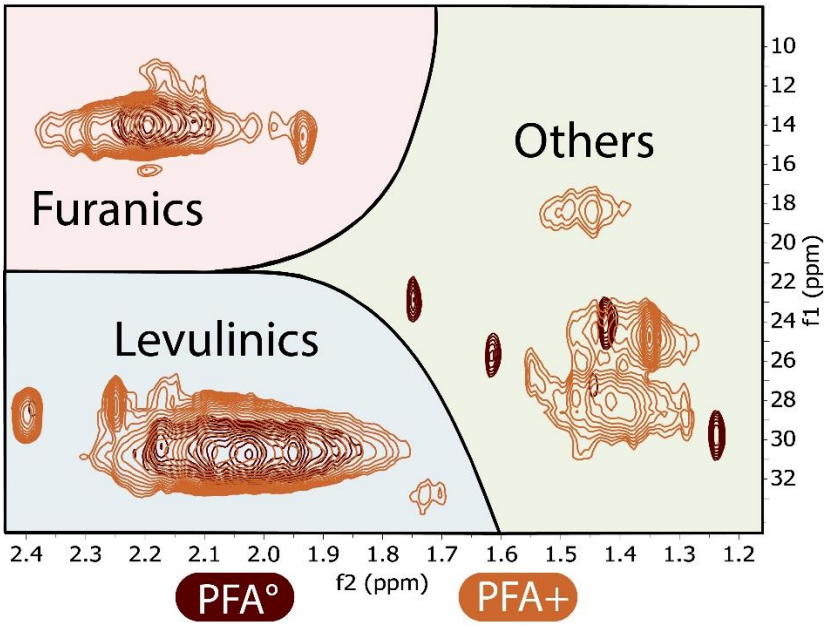

Figure 3.3-1. Magnified HSQC spectra of PFA+ (orange) and PFA° (brown) of the CH_3 area. The brown spectrum is stacked on blue the blue one.

A second group around 2.0/30 ppm is observed. In section 3.2 it has been attributed to levulinic-like structures (Scheme 3.3-1). This structure is believed to emerge from the end-chain hydrolytic ring opening of methylated furan units. Two other clusters of free molecules can be observed as well at 2.4/29 ppm and 2.25/28 ppm. The 2.4/29 ppm clusters are due to free levulinic acid. The nature of the 2.25/28 ppm cluster remains unclear.

Finally, on the right-hand side of Figure 3.3-1, five discrete clusters of methyls can be identified for the PFA° resins while three, much wider, clusters are observed in the case of the PFA+ resin. The ^{1}H NMR spectra in Figure 3.3-2 can help to better understand their nature with a focus on the 1.1 to 2.4 ppm. The PFA+ spectrum exhibits three broad methyl signals. The one at 2.2 ppm was assigned to the methylated furans and is found as well in the PFA° spectrum. An even broader signal is observed from 1.90 to 2.15 ppm. It was assigned to the end-chain levulinic units. While the two PFAs are at similar conversion degrees, the 1.90-2.15 ppm signal is much broader in the case of PFA+ compared to PFA°. This is consistent with the higher C=O content in PFA+.

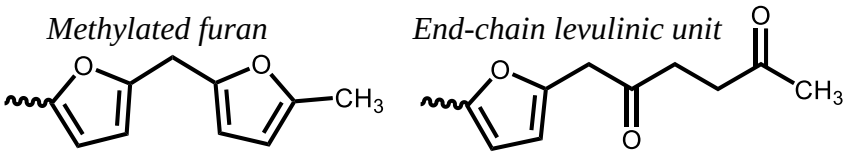

Scheme 3.3-1. Methyl groups found in PFA resins.

Moreover, the PFA+ spectrum displays a low intensity broad signal from 1.2 to 1.5 ppm. Such signal is not observed in the PFA° spectrum. Thus, it is obviously emerging from a water-induced side-reactions. The HMBC spectra in Figure 3.5-5, presents the methyl correlations observable for both PFA° and PFA+. The broad methyl signal from 1.2 to 1.5 ppm of PFA° correlates mainly with a peak around 106 ppm and to a lesser extent with peaks around 32, 43 and 156 ppm. Due to the overlapping with furan and CH_2 peaks, the nature of these methyls is hard to determine.

Instead of the broad 1.2 to 1.5 ppm signal, the spectrum of PFA° rather displays four well defined peaks at 1.24, 1.43, 1.63, 1.75 ppm. The chemical environment of the methyls behind these peaks is discussed later in section 3.3.5. Finally, both PFA° and PFA+ exhibit a methyl signal at 0.85 ppm, most-likely another side-reaction product. The 0.85 ppm methyl peak was also observed in a previous study. [280]

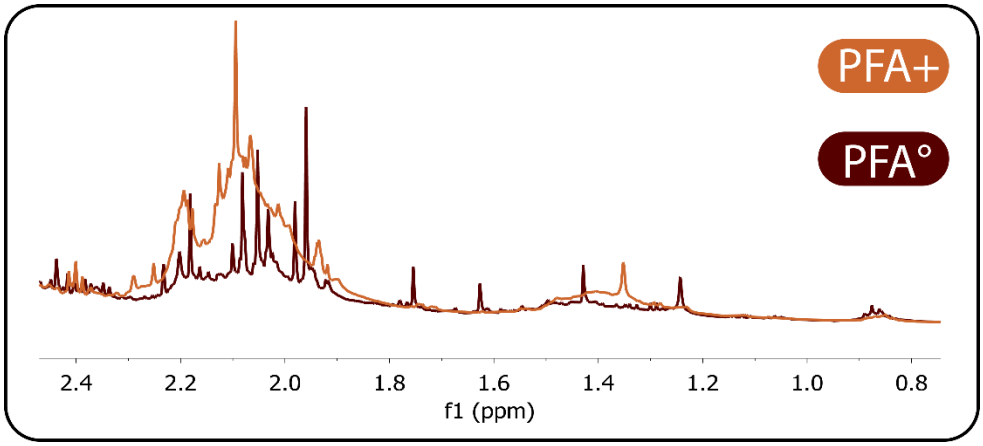

Figure 3.3-2. Magnified ^{1}H NMR spectra of PFA° (brown) and PFA+ (orange) at a conversion degree of about 0.80.

3.3.2 The CH_2 groups

In this section, the discrepancies between the CH_2 groups of PFA° and PFA+ are discussed.

Figure 3.3-3 displays a magnification of the HSQC spectra of PFA+ and PFA° centered in the CH_2 region. In Figure 3.3-3, the spectrum of PFA° is stacked above the one of PFA+, while the inverse situation (i.e., PFA+ above PFA°) ° is shown in Figure 3.5-6.

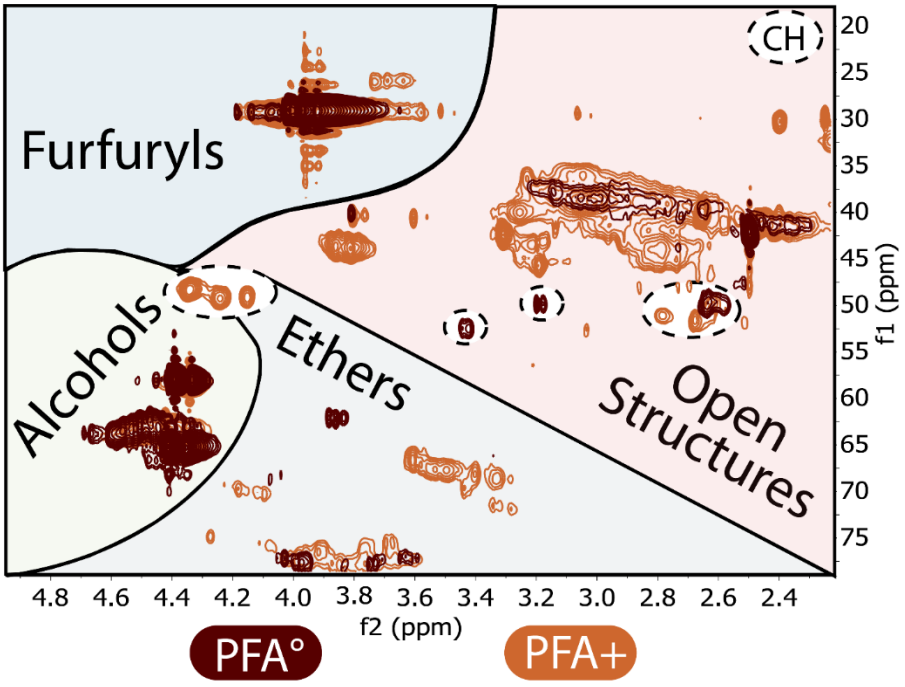

Figure 3.3-3. Magnified HSQC spectra of PFA+ (orange) and PFA° (brown) of the CH_2 area. The brown spectrum is stacked on top of the orange one. The clusters circled in black dashed lines are CH groups.

In Figure 3.3-3, four main types of CH_2 can be identified for both PFA+ and PFA°. The bottom-left one corresponds to furfuryl alcohol and its oligomers. The top-left group corresponds to the furfuryl units as shown in structure (I) of Scheme 3.2-1. [280, 281] For these two clusters, the spectra of PFA+ and PFA° superimpose nicely thus showing only few structural divergences regarding these moieties. Yet, small clusters around 3.7/28 ppm are observed on the PFA+ spectrum.

The bottom part in Figure 3.3-3 encompasses clusters that would match with ether functions. [330] The clusters around 3.8/75 ppm are common to both PFA+ and PFA° and are most likely the result of head-to-head condensation of furfuryl alcohol molecules. As depicted in Scheme 3.2-3. , such condensation is susceptible to occur and ultimately lead to furfuryl units by freeing formaldehyde. [281] A few other clusters are also visible on the PFA+ spectrum around 4.2/72 ppm as well as larger ones around 3.5/68 ppm and a small one at 3.9/62 ppm for PFA°. However, the exact nature of the molecules causing these correlations is difficult to point out.

The top-right group in Figure 3.3-3, displays CH_2 clusters that have been linked to carbonyl-based open structures, cf section 3.2.1. A very wide cluster 2.3-3.3/35-45 ppm is observed in the PFA+ spectrum. In the previous section, this cluster was attributed to the open structure of Scheme 3.3-2 and/or to the end-chain levulinic units of Scheme 3.3-1. In the case of PFA°, a similar, yet much narrower, cluster is observed.

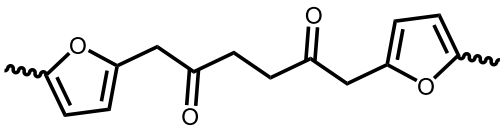

Scheme 3.3-2. Example of an open structure in PFA resins.

The carbonyl content of the studied PFA° is about 2.0 $mmol.g^{-1}$ while PFA+ contains about 3.0 $mmol.g^{-1}$ of carbonyls. Consequently, the intensity of the CH_2 neighboring the carbonyls in PFA+ should be higher than in PFA°. Also, a wider distribution of chemical shifts is expected as the chemical environment of CH_2 in PFA+ should be more diverse. The intensity and area of the ^1H signals from the CH_2 cannot be compared accurately due to a lack of proper baseline. Nonetheless, the HSQC spectra in Figure 3.3-3 displays a much higher heterogeneity of the CH_2 comprised between 2.2 and 3.3 ppm for PFA+, in comparison with PFA°. On top of that, the PFA+ spectrum displays clusters, mainly around 3.8/41 ppm, 3.3/40 ppm, 2,8/42 ppm and 3.2/43 ppm, which are not found in PFA°. Thus, introducing water in the initial reaction medium induces ring-opening reactions which are not occurring in a neat system.

Finally, the PFA° spectrum in Figure 3.3-3 displays CH clusters around 3.2/47, 3.4/50 ppm not visible on the PFA+ spectrum. Hence, the side-reactions occurring in a neat polymerization are of another nature than the ones occurring in aqueous systems. Theses sets of side-reactions might explain the influence of the reaction media on the polymerization of PFA. [180, 283, 301, 307]

3.3.3 The C=C and C-O bonds

In the following section, the differences in PFA+ and PFA° structures' of the C=C and the C-O areas are detailed.

Figure 3.3-4 depicts partial HSQC spectra of PFA° and PFA+ with PFA° on top of PFA+. The opposite situation with PFA+ on top of PFA° is available in Figure 3.5-7. In Figure 3.3-4, three groups of clusters can be isolated.

The top-left group corresponds to the C3 and C4 of furanic groups found in PFA, i.e., furfuryl units of PFA and FA.[281] As previously observed in Figure 3.3-3, the spectra of PFA+ and PFA° superimpose nicely for the furanic moieties.

The bottom-left group encompasses clusters matching with alkene groups. [330] They have been attributed to the conjugated structure of Scheme 3.3-3 and it's Diels-Alder adduct. The mechanisms leading to the conjugated structure and the Diels-Alder crosslinking were investigated in the past. [276, 281]

In Figure 3.3-4, the HC=C clusters at 6.3/137 ppm, 6.0/133 ppm and 5.8/130 ppm are common to both PFA systems thus suggesting an assignment to the structures in Scheme 3.3-3 and the left-over maleic acid. However, the PFA+ spectrum exhibits numerous clusters not observed in the case of PFA°. They might come from enolized carbonyl functions.

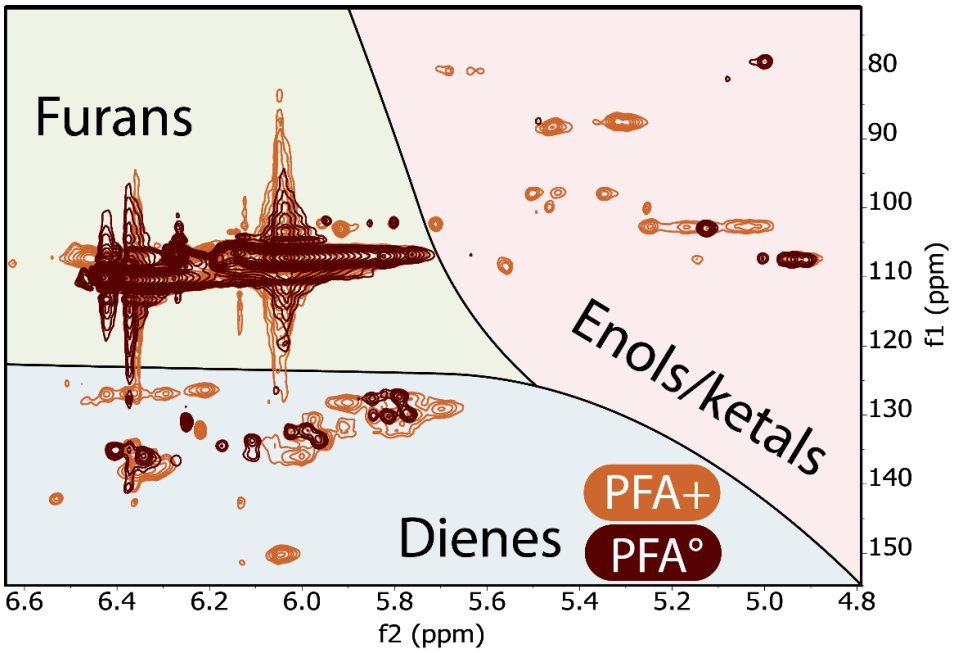

Figure 3.3-4. Magnified HSQC spectra of PFA+ (orange) and PFA° (brown) of the dienes and ethers areas. The brown spectrum is stacked on top of the orange one.

In top-right corner of Figure 3.3-4, the abundance of clusters is specific to PFA+ spectrum. Their chemical shifts are consistent with either enols or hydrated carbonyls. [330] This hypothesis is based on the fact that PFA° has very few clusters in this area which is consistent with a lower carbonyl content. Moreover, the quantification of carbonyls within PFA systems showed that longer derivatization time are necessary to fully quantify the carbonyls in PFA in comparison, for instance, with bio-oils [318] and lignins [319], cf section 2.2.

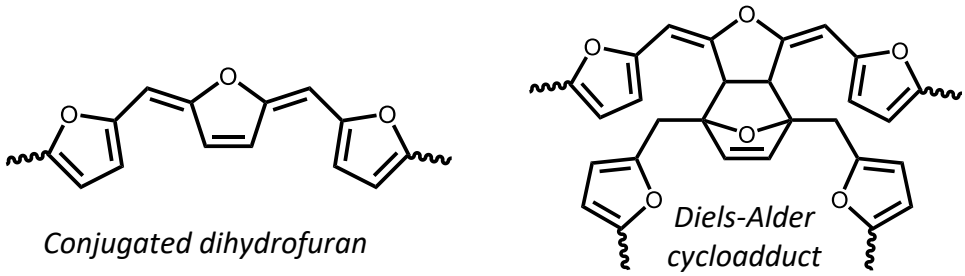

Scheme 3.3-3. Example of a conjugated moiety and the Diels-Alder adduct postulated in PFAs [281]

3.3.4 The aldehydes

In section 3.2, the presence of aldehyde groups in PFA+ was highlighted but no comparison was made with PFA°.

Figure 3.3-5 displays the HSQC spectra of PFA+ and PFA° focusing on the aldehyde region, with the spectrum of PFA° on top of the one of PFA+. The opposite situation is available in Figure 3.5-8.

In Figure 3.3-5, two populations of aldehydes can be identified in the PFA° system. The first one below 180 ppm can be identified as furfural and similar groups. Indeed, the chemical shift of the aldehyde group in furfural is around 178 ppm while other aldehydes are usually above 185 ppm. [330] It indicates that both PFA° and PFA+ bear aldehyde groups similar to the aldehyde of furfural.

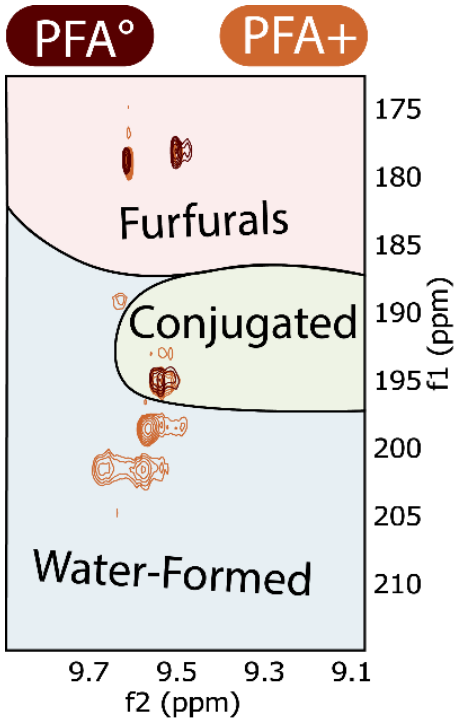

Figure 3.3-5**.** Magnified HSQC spectra of PFA+ (orange) and PFA° (brown) focusing on the aldehyde region. The PFA° spectrum is presented on top of the PFA+ spectrum.

Around 9.5/194 ppm, an aldehyde cluster is observed in both spectra. A previous study identified this cluster, depicted in Scheme 3.3-4, as the result of the oxidative ring opening of terminal furan units. It is believed that this conjugated aldehyde reacts through a Diels-Alder reaction with linear furans ultimately leading to a stiffening at the surface of the resin.

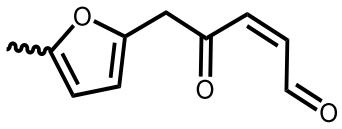

Scheme 3.3-4. Conjugated aldehyde resulting from the end-chain oxidative ring-opening of furans in PFA resins.

Finally, a third set of aldehydes is observed around 200 ppm for PFA+ only. Hence, the presence of additional water favors the formation of aldehydes during FA's polymerization. To further investigate the influence of water on the formation of aldehydes in PFA resins, they were quantified in PFA° resins employing the same methods ^{1}H NMR as previously done on PFA+.

Two methods were employed. The first one used dimethylterephtalate as an external standard. The second method employed the left-over furans as reference. This last method approximates the macromolecular network as a repetition of furfuryl unit. However, it does not require the sample mass for the calculations. The results are compiled in Table 3.3-1 and illustrated with the ^{1}H quantitative NMR spectra in Figure 3.3-6

Table 3.3-1. Results of the aldehydes quantification in the PFA° resin.

	External standard		**Left-over furans**	
Conversion degree (α)	**Aldehyde content (mmol.g^{-1})**	**Aldehyde Ratio**	**Aldehyde content (mmol.g^{-1})**	**Aldehyde ratio**
0.00	0.04	**0.21**	0.04	**0.20**
0.23	0.10	**0.07**	0.11	**0.08**
0.55	0.09	**0.05**	0.13	**0.07**
0.76	0.13	**0.07**	0.22	**0.11**

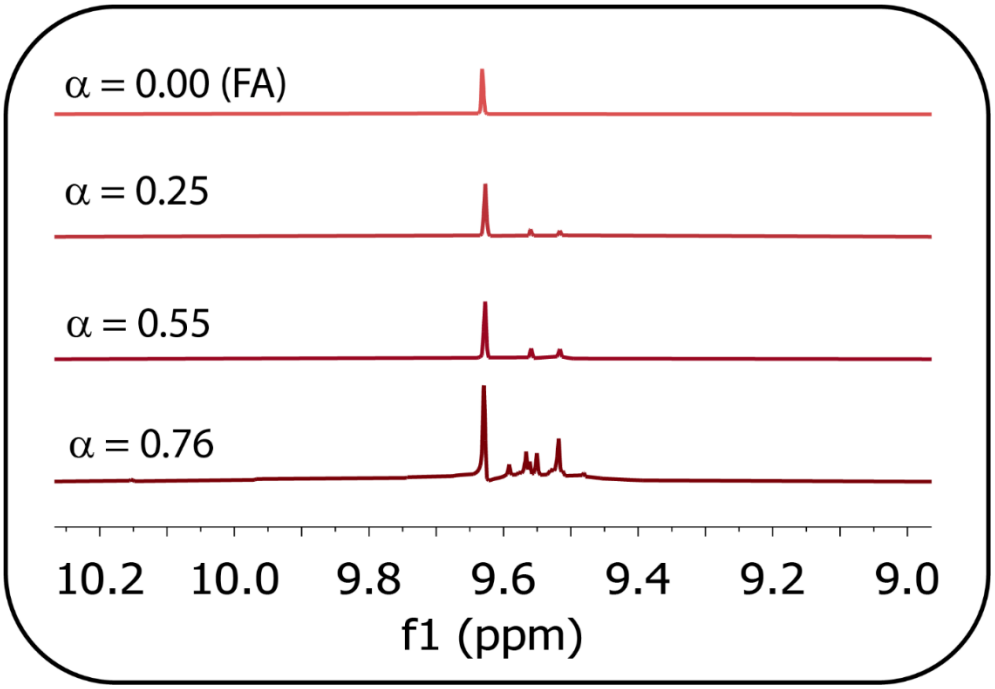

Figure 3.3-6. Quantitative ^{1}H NMR spectra of FA and PFA° resin focus on the aldehyde area.

In section 3.2.2 it was found that the concentration of aldehydes in PFA+ increase with the conversion degree, as well as the aldehyde ratio (over all the carbonyls). Table 3.3-1 reports a similar behavior for PFA°. With the method using an external standard, the aldehyde concentration increases very-slightly over time with the course of polymerization. Nonetheless, the aldehyde ratio remains steady during the whole polymerization of FA in the neat system. A similar trend is observed with the left-over furan method. Overall, PFA° comprised up to 0.13 mmol.g^{-1} of aldehydes, i.e., about 7 % of its carbonyls. In comparison, PFA+ resins comprise about 0.50 mmol.g^{-1} of aldehydes in resin with a conversion degree of 0.83 and about 0.20 mmol.g^{-1} of aldehydes for a resin with a conversion degree of 0.47. Consequently, polymerizing FA in a 50 % aqueous solution stimulates the production of aldehydes either from a water-based or an oxidative pathway.

3.3.5 The esters

To further emphasize the structural discrepancies between PFA° and PFA+, the ester functions are now discussed.

In the past, the existence of ester functions in a PFA network was mentioned numerous times. [183, 273, 283, 284, 296] and further confirmed in chapter 2. The lactone structure in Scheme 3.3-5 was proposed as the source of these esters. In the followings, the HMBC method was used to investigate their nature.

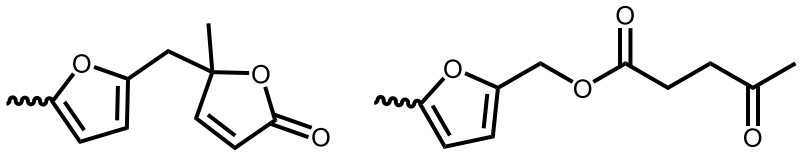

Scheme 3.3-5. Postulated ester functions within PFA. [273, 283, 284, 296]

Figure 3.3-7 displays the magnified HMBC spectrum of PFA°. As the concentration of esters is low and due to an overlapping with other signals, only few insights can be given. Figure 3.3-7 shows ^{2}J and ^{3}J correlations which matches well with the predicted chemical shifts of the lactone depicted in Scheme 3.3-5. The predicted chemical shifts were obtained from the "NMR predict" software from University of Lausanne "NMR DB" and are available in Table 3.5-1. [355]

The nature of the other methyl peaks in PFA° cannot be elucidated as easily. However, the peaks at 1.91, 1.75, 1.48 and 1.43 ppm all correlate with carbon peaks in the ester region, i.e from 150 to 185 ppm. The PFA+ HMBC spectrum in Figure 3.5-5, displays the 1.48/156 ppm and 1.91/172 ppm clusters as well. Nonetheless, the lactone is not observed in the PFA+ spectrum. This is consistent with previous work. Indeed, the FTIR spectra of PFA° resins exhibit the typical ester bands, cf Figure 2.7-1 and Table 1.3-3.

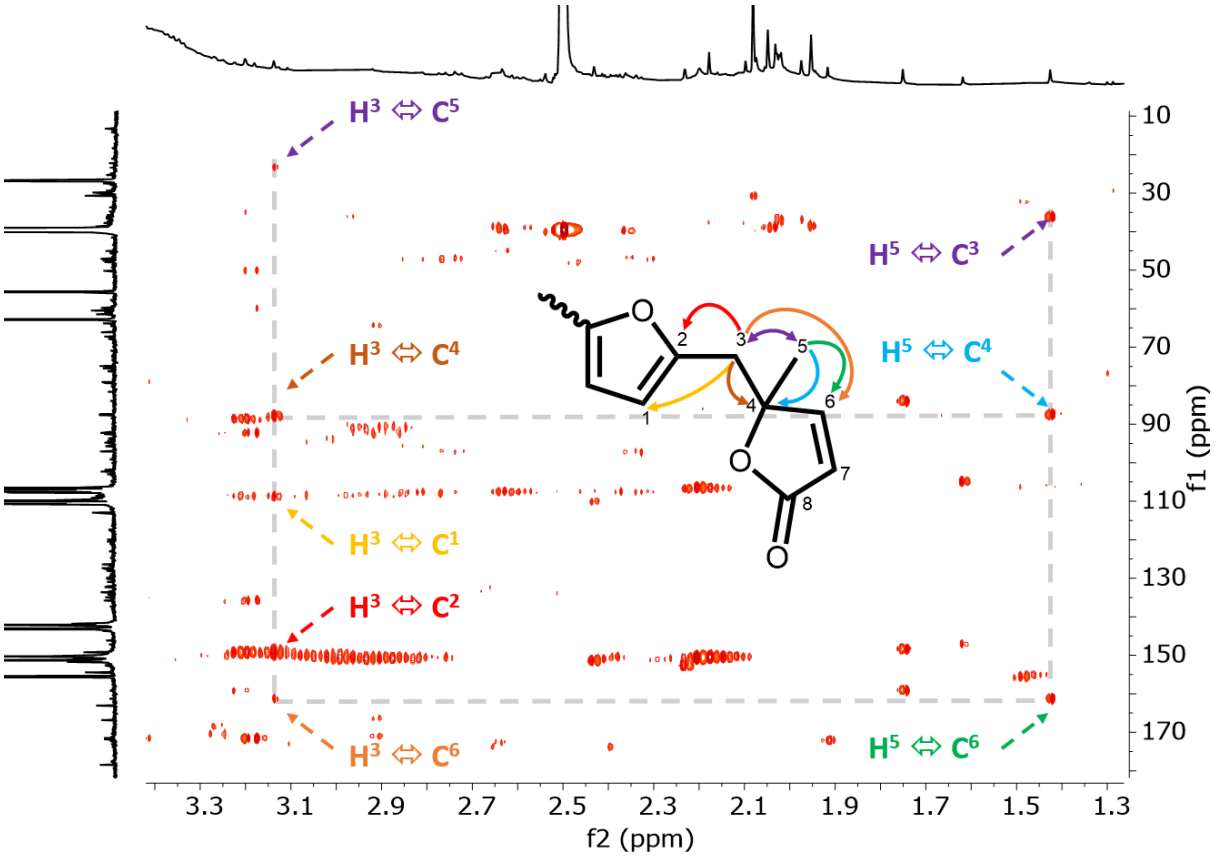

Figure 3.3-7. Magnified HMBC spectrum of PFA° at a conversion degree of 0.80.

Therefore, some of the esters in PFA° are terminal lactones or free molecules. The end-chain location of the lactones might explain why less aldehydes are present in the PFA° compared to PFA+. The presence of furfuryl levulinates is also possible although their signals might be overlapping with the ones of levulinic acid.

3.3.6 MALDI ToF analysis of PFA+ and PFA°

This section shows the MALDI ToF investigations to further support the findings of this chapter.

From the comparison of the MALDI ToF spectra in Figure 3.5-9 and Figure 3.5-10 and Table 3.5-2 there seem to be more open structures and ketone structures in PFA+ than in PFA°. This is suggested from the greatest abundance of the structures at 326-327, 334 and 574-576 g.mol^{-1} (Scheme 3.3-6). The structure of 326-327 g.mol^{-1} is in line with the open structure already found in the previous sections and shown in the simpler structure corresponding to the MALDI peak at 198 g.mol^{-1}. As depicted in Scheme 3.3-6, the 334 g.mol^{-1} and 574-576 g.mol^{-1} ones are also examples of oligomers which includes some open ketone structure. The two structures at 334 g.mol^{-1} and 574-576 g.mol^{-1} are also examples of how Diels–Alder rearrangement of furanic chains can participate in higher molecular weight oligomers.

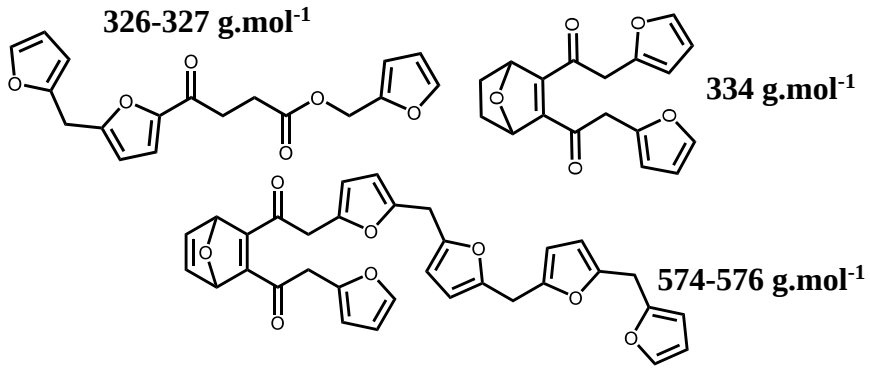

Scheme 3.3-6. MALDI ToF assignment of PFA° and PFA+.

For the 325 g.mol^{-1} the peak is much more intense in relation to the rest of the spectrum, and for the 334 g.mol^{-1} while the size is similar for the two PFA resins. PFA+ presents two peaks of equal height that indicates that the abundance of the structure is higher. The ketone carrying structure at 574-576 g.mol^{-1} has also a very much more pronounced peak for PFA+ and all its multiples are far more intense than in PFA°. The ketone structures at 360 and 440 g.mol^{-1} also present peaks clearly much more intense in PFA+. The structure at 361 g.mol^{-1} (including the 23 g.mol^{-1} for Na^+) is also one example of the structure determined in the NMR section (Figure 3.3-7).

There are other indications of this, the structures in Scheme 3.3-7.. The peak at 152 g.mol^{-1} in the PFA+ that it is smaller than the one of 154 g.mol^{-1} in PFA°. In PFA°, the peak at 154 g.mol^{-1} is closer to the non-ketone form (157 g.mol^{-1}).

152 g.mol^{-1} **157 g.mol^{-1}**

Scheme 3.3-7. MALDI ToF assignment of PFA° and PFA+.

There are several structures in which a charged atom is still present. One example is the peak at 161 g.mol^{-1} that could be interpreted as anyone of the two structures of Scheme 3.3-8.

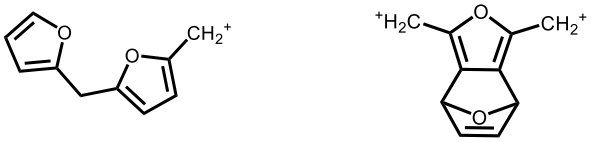

Scheme 3.3-8. MALDI ToF assignment of PFA° and PFA+ for the 161 g.mol^{-1} peak.

Both might be effectively present as well as being fabricated in the MALDI ToF experience itself. However, the presence of several other similarly charged structures at 176, 240-241, 481-483, and 496 g.mol^{-1} appear to indicate that these structures are not just a fabrication of the MALDI spectrometer.

The peak at 176 g.mol^{-1} (much stronger in PFA°) can be ascribed to two different structures contributing to the same peak (Scheme 3.3-9.). The much smaller residual of 176 g.mol^{-1} in PFA+ might be due to the open ketone structure. It could also be a dimer of FA. The peaks at 190 g.mol^{-1} and 192 g.mol^{-1}, assigned to the structures in Scheme 3.3-10, are also corresponding to ketonic structures from ring opening reactions.

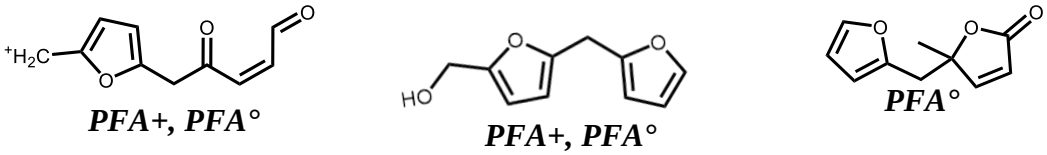

Scheme 3.3-9. MALDI ToF assignment of PFA° and PFA+ for the 176 g.mol^{-1} peak.

PFA+ ***PFA°***

Scheme 3.3-10. MALDI ToF assignment of PFA° and PFA+ for the 190 and 192 g.mol^{-1}.

At 190-191 g.mol^{-1}, with the right one far more likely than the left one, and the form at 194 g.mol^{-1} (Scheme 3.3-11). The behavior of the peak at 241-242 g.mol^{-1} is also interesting. This can be attributed to the two structures in Scheme 3.3-12. , both being likely.

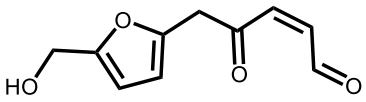

PFA+, PFA°

Scheme 3.3-11. MALDI ToF assignment of PFA° and PFA+ for the 190-191 g.mol^{-1} peak.

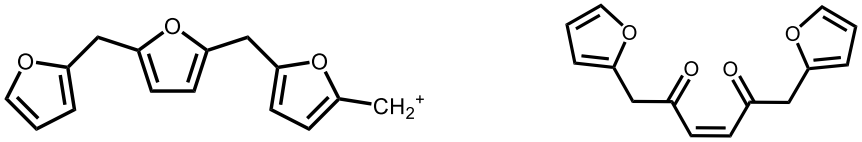

PFA+, PFA° **PFA+, PFA°**

Scheme 3.3-12. MALDI ToF assignment of PFA° and PFA+ for the 241-242 g.mol^{-1} peak.

Among the possible structures observed is also one structure identified in the NMR analysis in which the terminal unit of a furanic oligomer is a conjugated aldehyde resulting from the end-chain oxidative ring-opening of furans in PFA resins (Scheme 3.3-13.). This is observed at 404 g.mol^{-1} (no Na^+) and 428 g.mol^{-1} (with Na^+, presenting the structure in Scheme 3.3-13.)

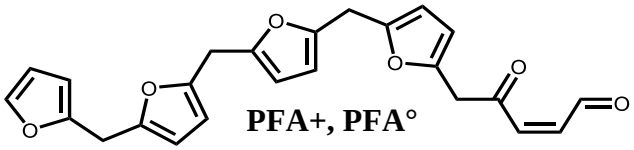

PFA+, PFA°

Scheme 3.3-13. MALDI ToF assignment of PFA° and PFA+ for the 404 g.mol^{-1} (no Na^+) and 428 g.mol^{-1} (with Na^+) peaks.

Finally, structure formed by Diels-Alder cycloadducts seem to be present in the examined PFA resins, with the peaks at 310, 318, 334 g.mol^{-1} (with Na^+), suggesting again more open forms in PFA+, 456 g.mol^{-1} (no Na^+) and 476-478 g.mol^{-1} (with Na^+), 470 g.mol^{-1} (no Na^+) and 493 g.mol^{-1} (with Na^+), 481-483 g.mol^{-1}and 496 g.mol^{-1} and 574-575 g.mol^{-1} (Table 3.5-2) such as the species at 456 g.mol^{-1} and 470 g.mol^{-1} as follows in Scheme 3.3-14.

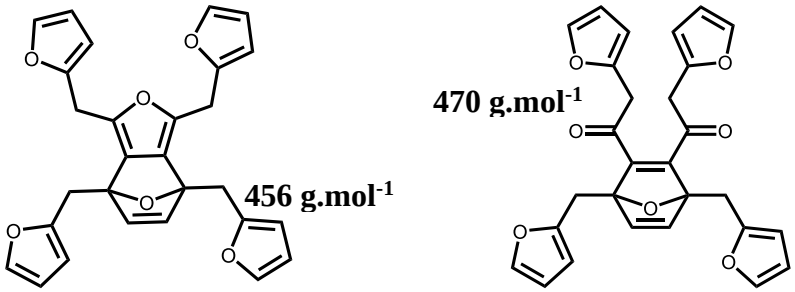

Scheme 3.3-14. MALDI ToF assignment of PFA° and PFA+.

3.3.7 Conclusions of section 3.3

In this section, the chemical structures of two types of PFA resins were investigated. The first PFA was prepared in neat conditions (PFA°) while the second one was prepared in a 50 %w aqueous solution (PFA+). To investigate the structures, both NMR and MALDI ToF were employed. Overall, the study highlighted a higher heterogeneity in PFA+ as exemplified by broader HSQC clusters. Such heterogeneities were attributed to water-induced reactions. They involve the formation of ketonic and aldehyde species. Moreover, it was further highlighted that the resulting ketones are sensitive to enolization and hydration. On the other hand, PFA° displays less ketone derivatives. In addition, the presence of aldehyde groups are about two times more important in PFA+ compared to PFA° thus indicating that polymerization in aqueous conditions favor their formation. Furthermore, the presence of lactone end-groups in PFA° was confirmed and it explains somehow the lower concentration of aldehydes for PFA°. Finally, the results from the MALDI ToF investigations corroborated the higher abundance of open-structures in PFA+ systems and helped to propose some potential structures.

3.4 Chapter 3: Conclusion

This chapter was dedicated to improving the understanding of the chemical structure of PFA, with a strong focus on carbonyl moieties. Quantitative ^{1}H NMR, bidimentional NMR (^{1}H-^{13}C) and MALDi ToF spectrometry were employed to reach this objective.

In section 3.2, the chemical structure of a C=O rich PFA+ was investigated. The NMR showed a predisposition of the terminal furan for ring-opening reactions. On one hand, the methyl furans open into levulinic-like moieties through a hydrolytic pathway. On the other hand, the monosubstituted terminal furan are sensitive to undergo oxidative ring opening to produce aldehydes. Quantitative ^{1}H NMR highlighted that up to 20 % of the total C=O in PFA+ are aldehydes.

Overall, whether they are aldehydes or levulinic end-chain units, the C=O in PFA seem to preferably form at the end of the macromolecular chains. This may be the reason why the carbonyl content of soluble PFAs could not be increased above 3.7 $mmol.g^{-1}$, i.e. 15 % of open furans.

Section 3.3 further supported the findings of section 3.2 by comparing a C=O enriched PFA+ with a C=O poor PFA°. The PFA+ exhibited a more heterogeneous structure than PFA°. The presence of esters in PFA° was once again observed and the presence of terminal lactone was confirmed. This further highlights the higher reactivity of terminal furans in PFA systems.

Finally, a new oxidation-induced surface crosslinking pathway was proposed in this chapter. This phenomenon gives birth to a hard crust on the surface of PFA resins. It is believed to emerge from the oxidation of terminal furans into conjugated 1,4-ketoaldehydes followed by a Diels-Alder cycloaddition. In the next chapter, the impact of this surface crosslinking on the properties of PFA materials is assessed.

3.5 Supplementary information

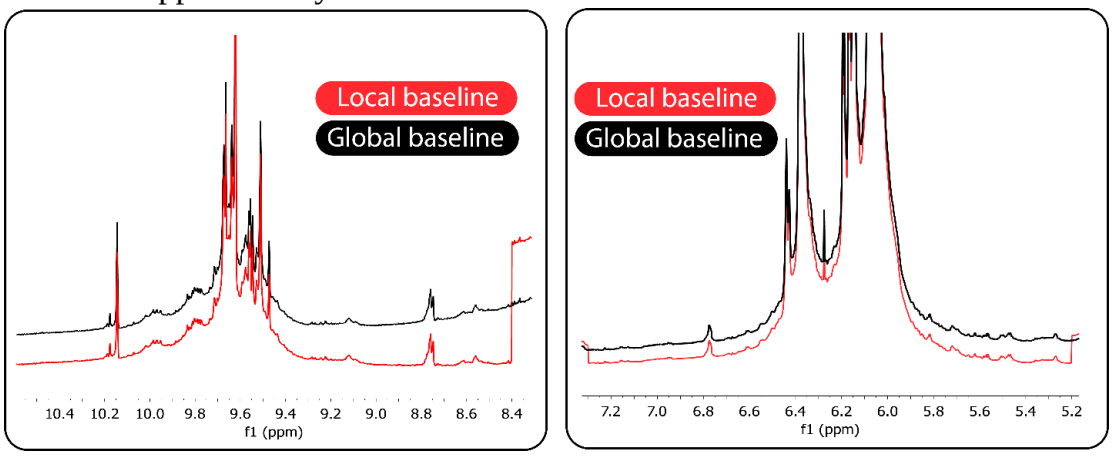

Figure 3.5-1. ^{1}H NMR spectra of a PFA resin, conversion degree of about 0.80, in blue with a baseline applied from 0 to 14 ppm and in red from 5.2 to 7.3 (Right) and 8.4 to 12.8 ppm (Left).

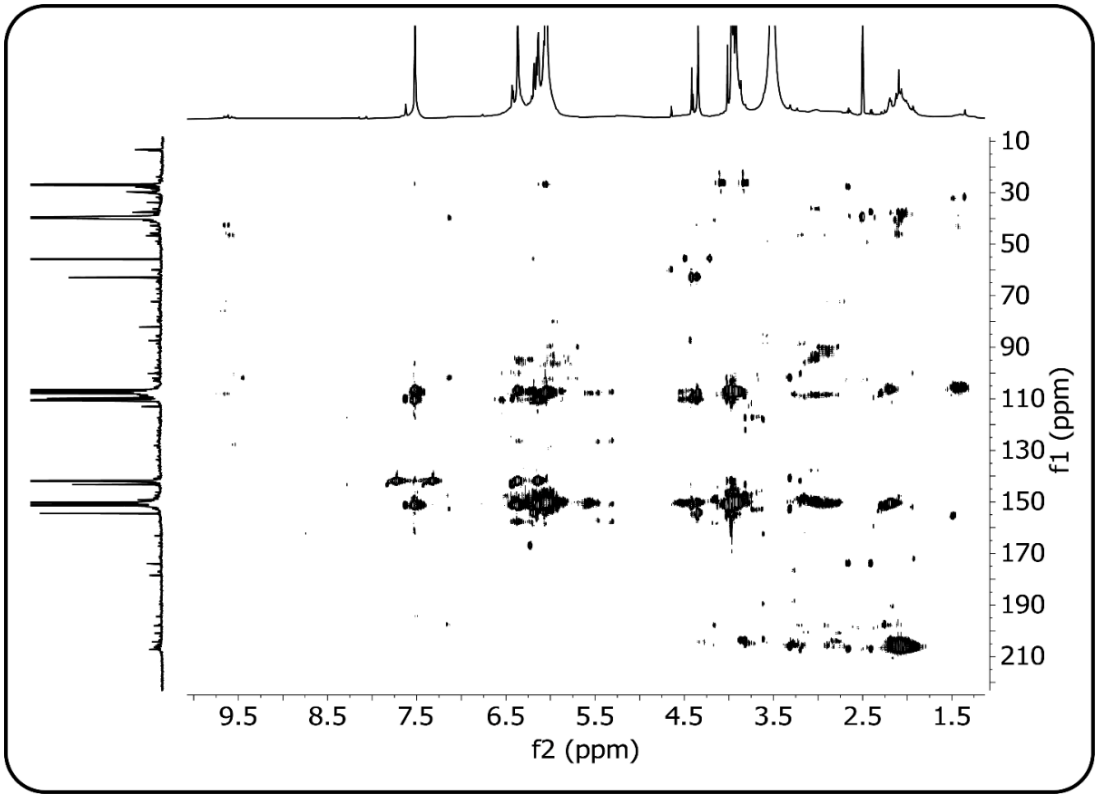

Figure 3.5-2. HMBC spectra of a PFA+ resin at conversion degree of about 0.80.

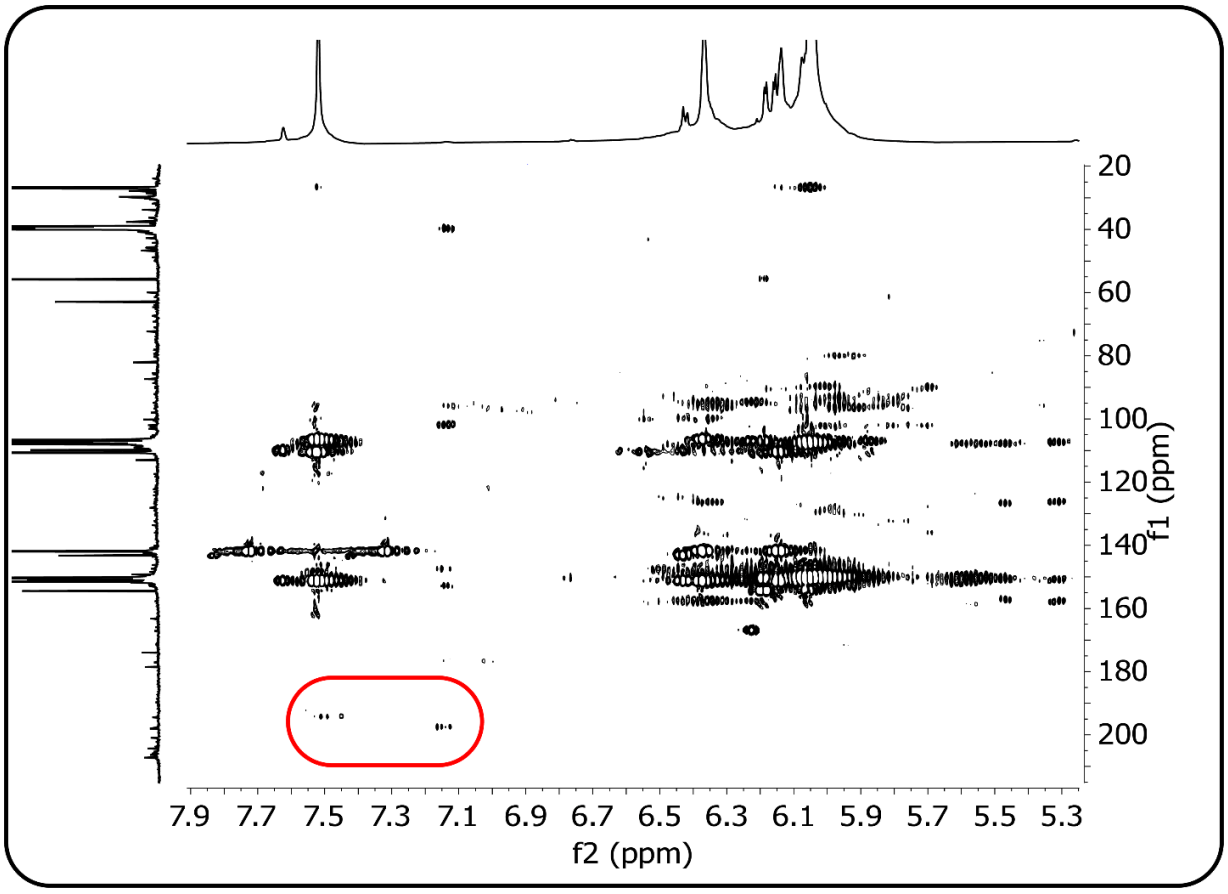

Figure 3.5-3. Magnified HMBC spectra of a PFA+ resin at conversion degree of about 0.80.

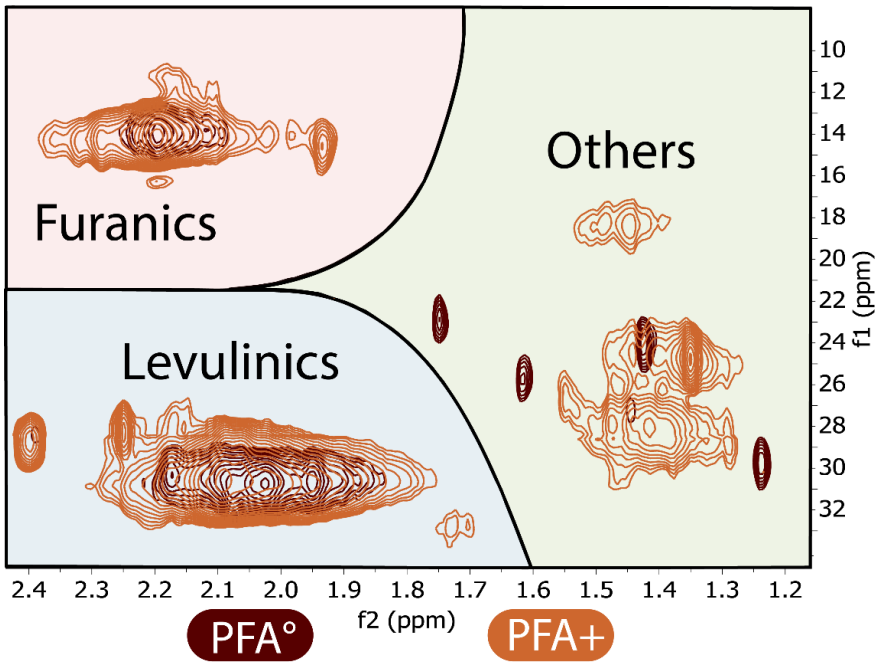

Figure 3.5-4. Magnified HSQC spectra of PFA+ (orange) and PFA° (brown) of the CH_3 area. The orange spectrum is stacked on top of the brown one.

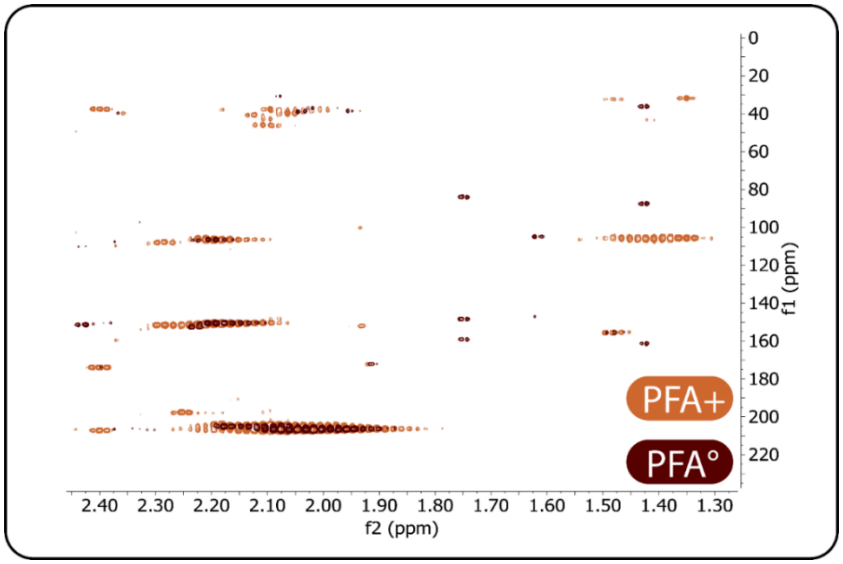

Figure 3.5-5. HMBC spectra of PFA° (brown) and PFA+ (orange) focusing on the methyls. The brown spectrum is on top of the orange one.

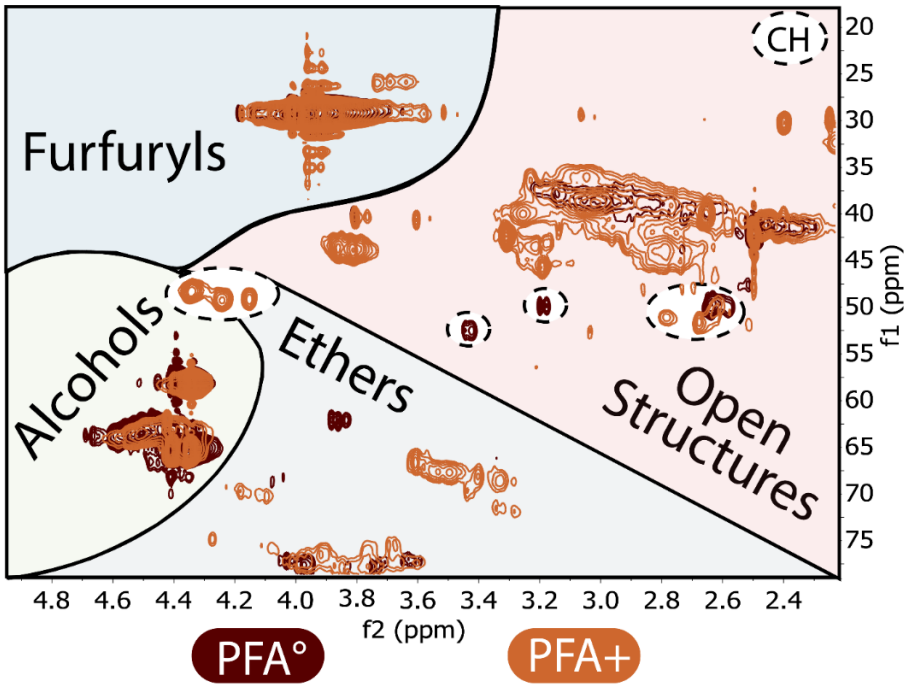

Figure 3.5-6. Magnified HSQC spectra of PFA+ (orange) and PFA° (brown) of the CH_2 area. The orange spectrum is stacked on top of the brown one.

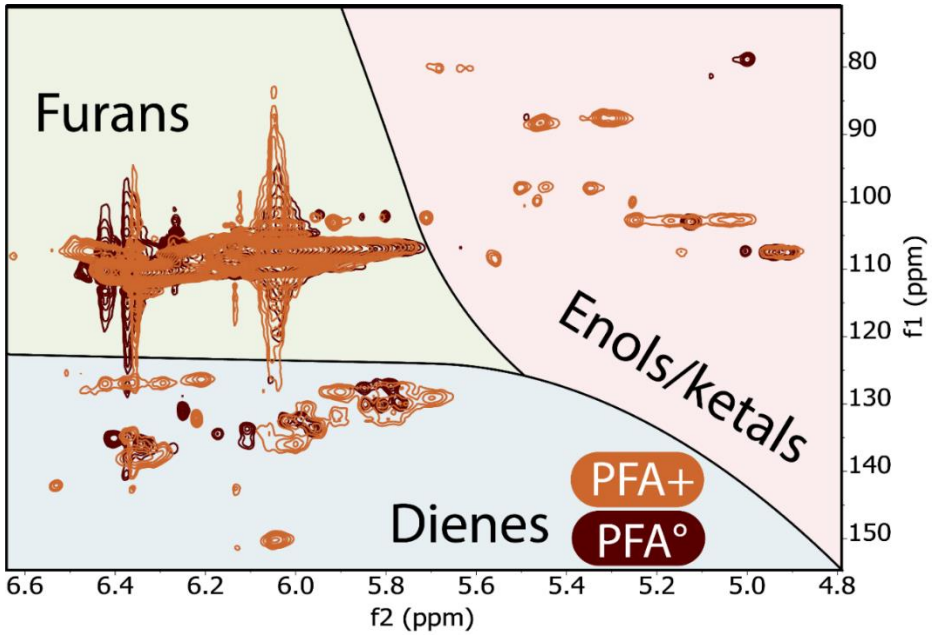

Figure 3.5-7. Magnified HSQC spectra of PFA+ (orange) and PFA° (brown) of the dienes and ethers areas. The orange spectrum is stacked on top of the orange one.

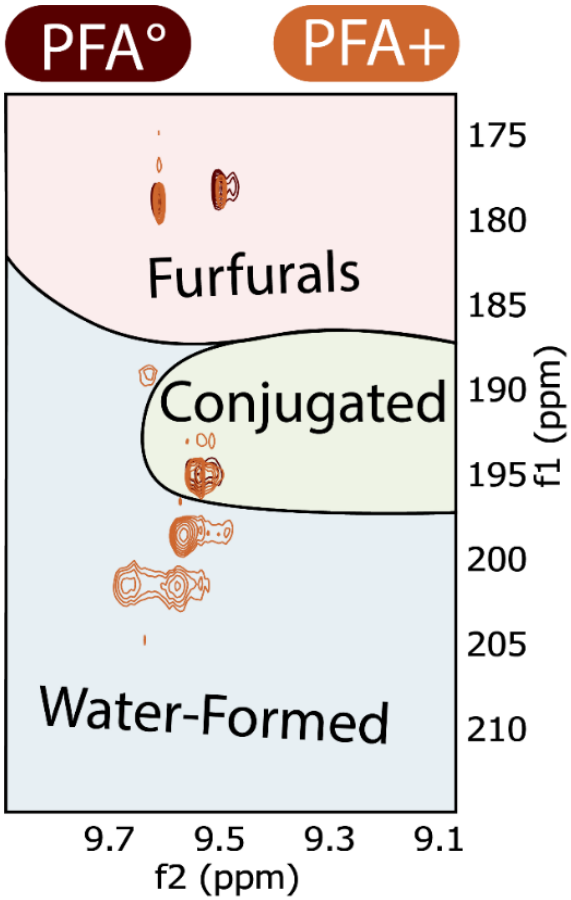

Figure 3.5-8. Magnified HSQC spectra of PFA+ (orange) and PFA° (brown) of the aldehyde area. The orange spectrum is stacked on top of the brown one.

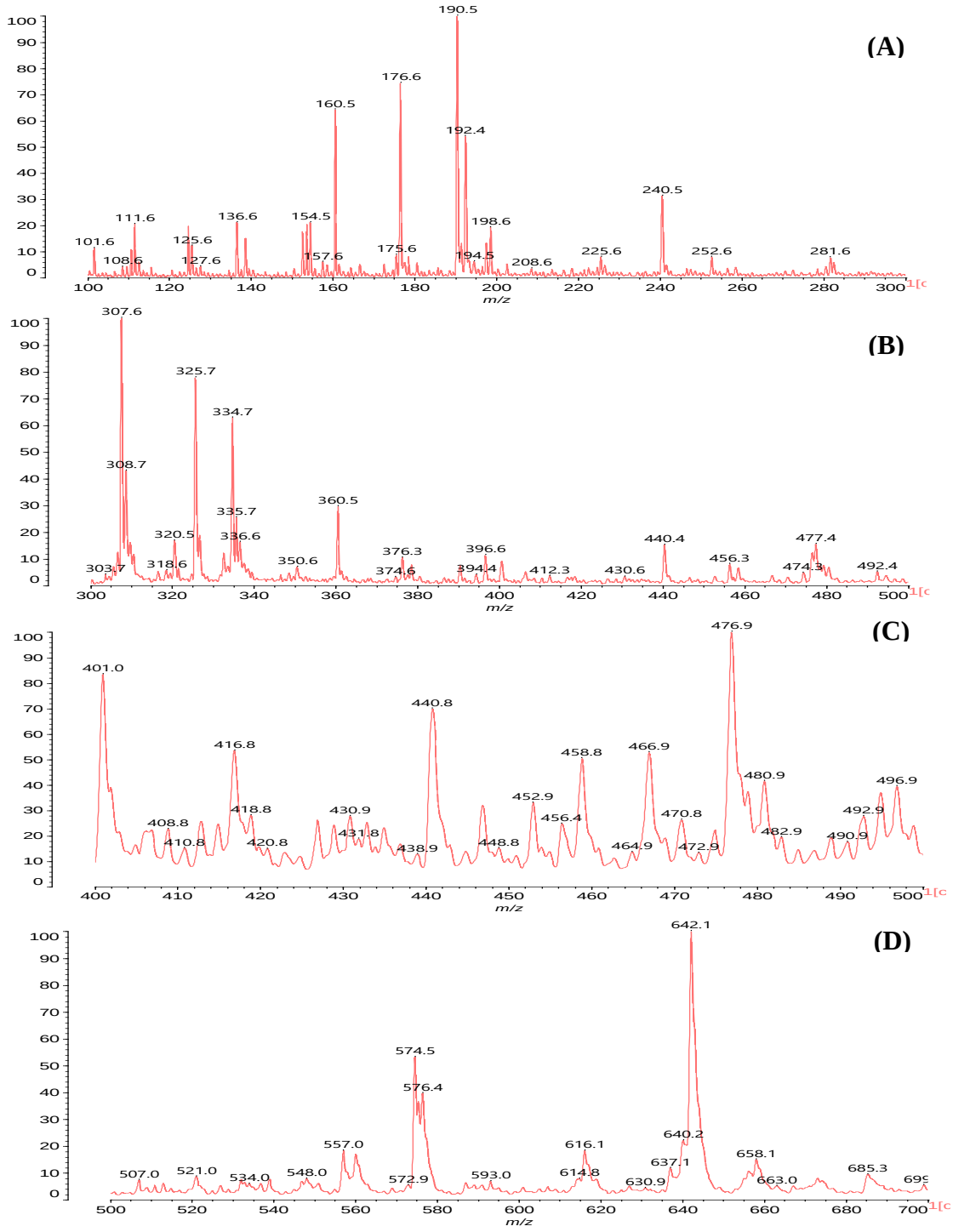

Figure 3.5-9. (A-D). MALDI ToF mass spectra of PFA°.

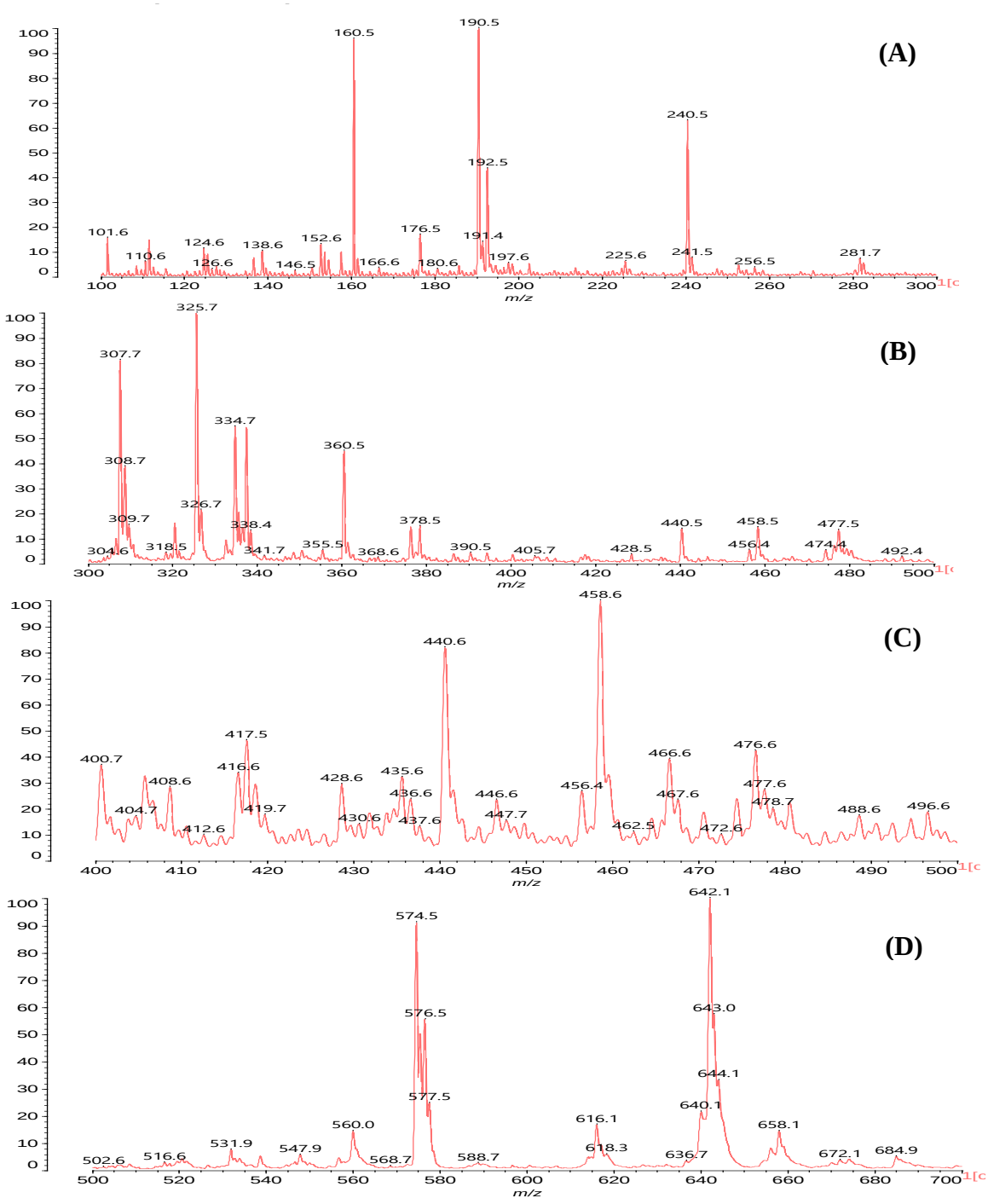

Figure 3.5-10. (A-D). MALDI ToF mass spectra of PFA+.

Table 3.5-1. ^{1}H and ^{13}C NMR predicted chemical shift of a furfuryl lactone unit.

N°	δ (^{1}H, ppm)	δ (^{13}C, ppm)
1	6.04	110.1
2	/	153.4
3	3.35	29.2
4	/	93.4
5	1.52	23.3
6	7.31	160.4
7	6.72	120
8	7	172.5

Table 3.5-2. Peak/structures possible assignments of the MALDI ToF spectra for PFA+ and PFA°.

152 g.mol^{-1} = 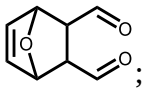 ; 157 g.mol^{-1} = 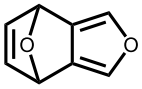

161 g.mol^{-1} = 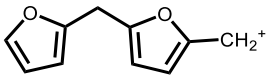 / 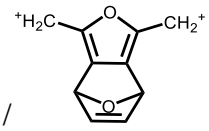

176 g.mol^{-1} = 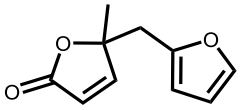 AND/OR 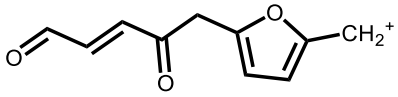

190 g.mol^{-1} = 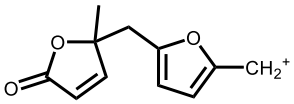 AND/OR 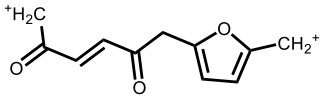

194 g.mol^{-1}= 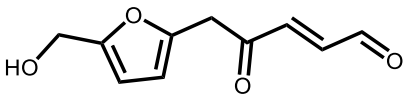

197-198 g.mol^{-1} = no Na^{+}, deprotonated 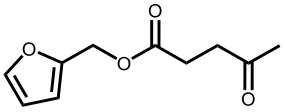

226 g.mol^{-1} = no Na^{+}, deprotonated 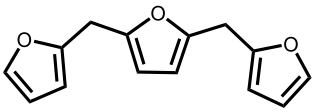

240-241 g.mol^{-1} = no Na^{+}, more present in PFA^{+} 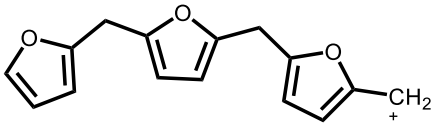

257 g.mol^{-1} = protonated no Na^{+} (in PFA+), and 281 g.mol^{-1}, with Na^{+} in both PFA+ and PFA°.

But more pronounced in PFA+ than in PFA° 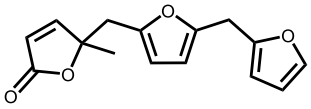

308 g.mol^{-1} = no Na^{+} 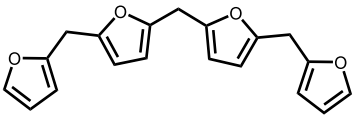

310 g.mol^{-1} =no Na^{+}, calc.310 g.mol^{-1}, and 334-335 g.mol^{-1}, with Na^{+} 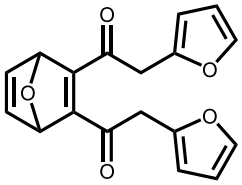

318.6 g.mol^{-1} = with Na^{+}, protonated 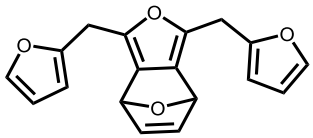

326-327 g.mol^{-1} =no Na^{+} (both in PFA° and PFA+), and 350 g.mol^{-1} with Na^{+} on in PFA° (small).Example of open structure of polyfuranics

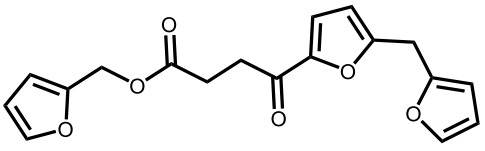 / 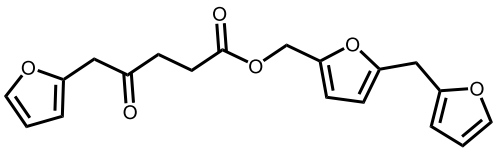

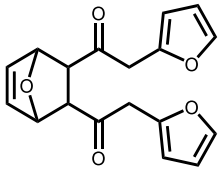

335 g.mol^{-1} = with Na^+, calc 321 g.mol^{-1}, showing more open forms in PFA+

336-338 g.mol^{-1} = no Na^+, Calc. 337 deprotonated, 338 g.mol^{-1} normal more present in PFA+,

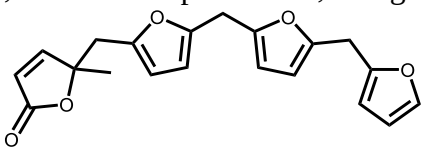

and 361 g.mol^{-1}with Na^+

404 g.mol^{-1} = no Na^+, and 428 g.mol^{-1} with Na^+, and example of an end-chain conjugated aldehyde resulting from the oxidative ring-opening of furans in PFA resins. It is present on PFA^+

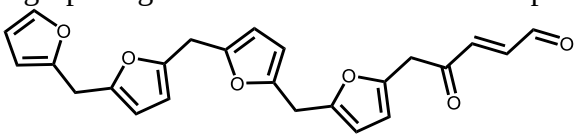

but not really distinguishable in PFA°.

456 g.mol^{-1} = no Na^+, protonated, calc. 455 g.mol^{-1}; 476-478 g.mol^{-1} with Na+, calculated 477 g.mol^{-1}

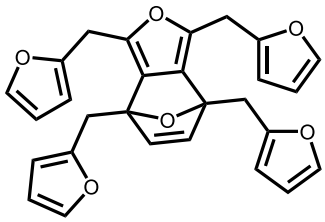

It shows that there are several more forms of this structure in PFA+.

All the above indicates that the open ketones forms predominate even in the Diels Alder structures.

470 g.mol^{-1} = no Na^+, and 493 g.mol^{-1} with Na^+

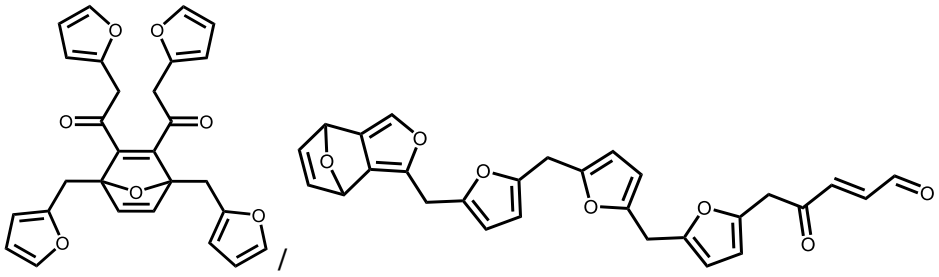

481-483 g.mol^{-1} = no Na^+, in PFA°

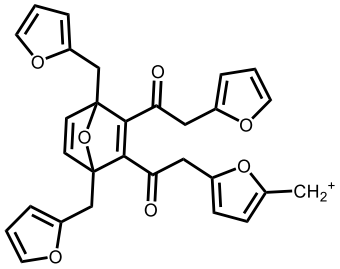

496 g.mol^{-1} = no Na^+ in both PFA° and PFA+, but more marked in PFA°

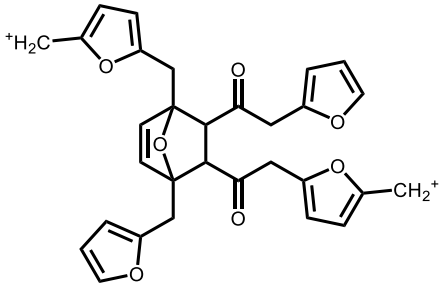

574-575 g.mol^{-1} = with $Na^{+,}$

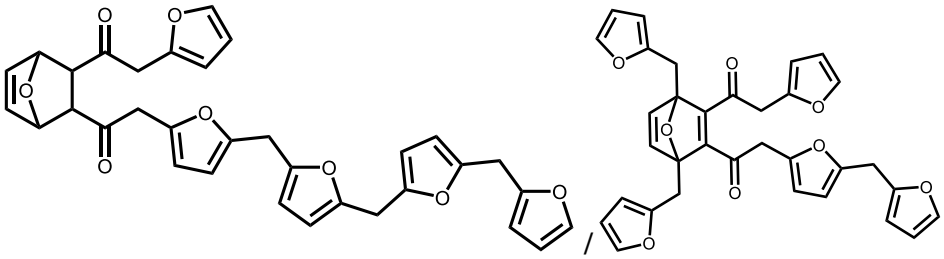

It is unnecessary to calculate and assigned higher oligomers structures as several isomer structures become possible.

CHAPTER 4
Oxygen-induced surface hardening and aromatization of PFA: origin and consequences

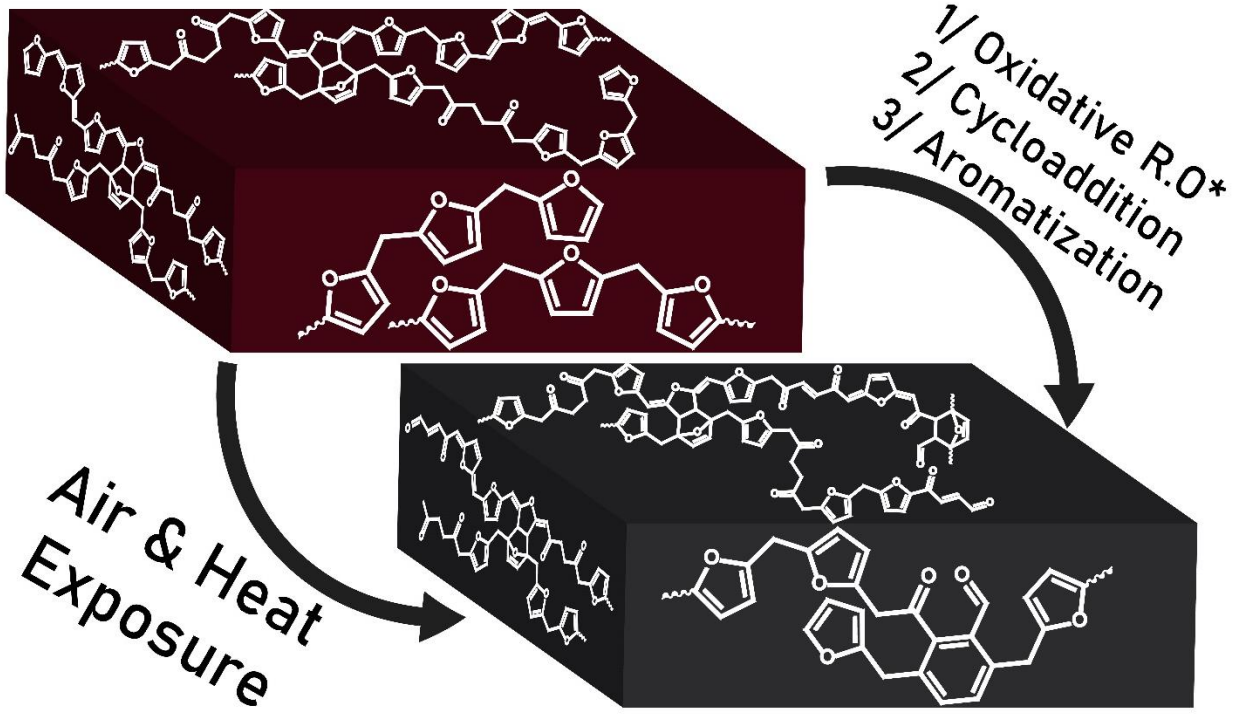

In chapter 3, an oxidation-induced surface crosslinking phenomenon was highlighted. This chapter aims at further understanding this phenomenon and its consequences on the properties of furan resins. To do so, two polymers were prepared under inert or oxidative atmosphere. The first one, called "PFA" was post-cured under N_2 to avoid any oxidation while the second one "Ox-PFA" was post-cured under air. To avoid any confusion, in this chapter the term furan resin is used to refer to PFAs in general, regardless of the post-curing conditions.

After the experimental section in 4.1, section 4.2 briefly describes the known chemical transformation occurring when furan resins are thermally treated.

Section 4.3 deals with the structure of PFA and Ox-PFA using spectroscopic technics coupled with elemental analysis, thermogravimetric analysis, aldehyde detection tests and C=O quantifications. The goal is to determine the functional groups present on the surface of furan resins.

Section 4.4 complements the pathway found in chapter 3 and highlights some of its consequences on the materials' properties. In addition, the thickness of this oxidized layer is determined.

Section 4.5 is dedicated to the kinetics of oxidation, hardening and degradation of furan resins. Finally, Section 4.6 deals with the macroscopic properties of oxidized and non-oxidized furan resins.

4.1 Experimental section

Materials:

Maleic anhydride (99 %), silver nitrate (99 %), fructose (97 %), aqueous ammonia (25 %), sodium hydroxide (97 %) and were bought from Merck. Furfuryl alcohol (96 %) and ethyl acetate (98 %) were acquired from Carlo Erba. Ethanol (96 %v) was purchased from VWR. The volumic purity of the N_2 used for the curing and TGA was superior to 99.995 %. All the chemicals were used without further purification.

Sample preparation:

The sample preparation procedure is summarized in Scheme 4.1-1.

To prepare the materials, a solution of furfuryl alcohol and maleic anhydride (100:2 mol) was first pre-polymerized. For this purpose, the mixture was heated at 100 °C for about 1 h 30 until a rubbery resin was obtained. The rubbery resin was then ground using a GT-300 ball-mill from Powtec. Two cycles at 1500 RPM for 2 mins were used. Prior to each cycle, the bowls were cooled down using liquid N_2. The resulting powder was vacuumed overnight at 40 °C to fully dry it. Then, the dried powder was compression-molded at 150 °C under 20-25 bars for 2 hours, resulting in a solid piece of polymer.

A fraction of the materials was then cut for the tensile tests using a dumbbell shaped cutter (ISO 527-2-1BB, cf picture in Figure 4.8-1) and parallelepipeds for dynamic mechanical analysis (DMA) and thermogravimetric analysis (TGA) experiments. The other fraction was ground using the ball-mill following the same protocol as described previously. Thereafter, both powders and pieces underwent either an oxidative atmosphere curing at 200 °C for 2 h 30 under air (named Ox-PFA) or an inert atmosphere curing at 200 °C for 2 h 30 (named PFA).

In the case of inert atmosphere curing, the oven was vacuumed then filled with N_2 then vacuumed and filled again with N_2. The 2 h 30 time refers to the time the samples spent at 200 °C and does not include the heating nor cooling times.

An isothermal DMA test was performed at 200 °C to ensure that 2 h 30 are enough to fully cure the samples. As well, a few pieces of Ox-PFA were sanded with 80 grit sandpaper to remove their top layers (≈ 200 µm).

On one hand, PFA and Ox-PFA pieces were subjected to DMA, tensile testing, gel content determination, Fourier-Transform Infra-Red (FTIR) spectroscopy and goniometry. On the other hand, PFA and Ox-PFA powders underwent C=O and COOH quantifications, TGA, oxidation onset temperature (OOT), elemental analysis, solid state nuclear magnetic resonance (ssNMR) spectroscopy, aldehyde detection, and FTIR spectroscopy.

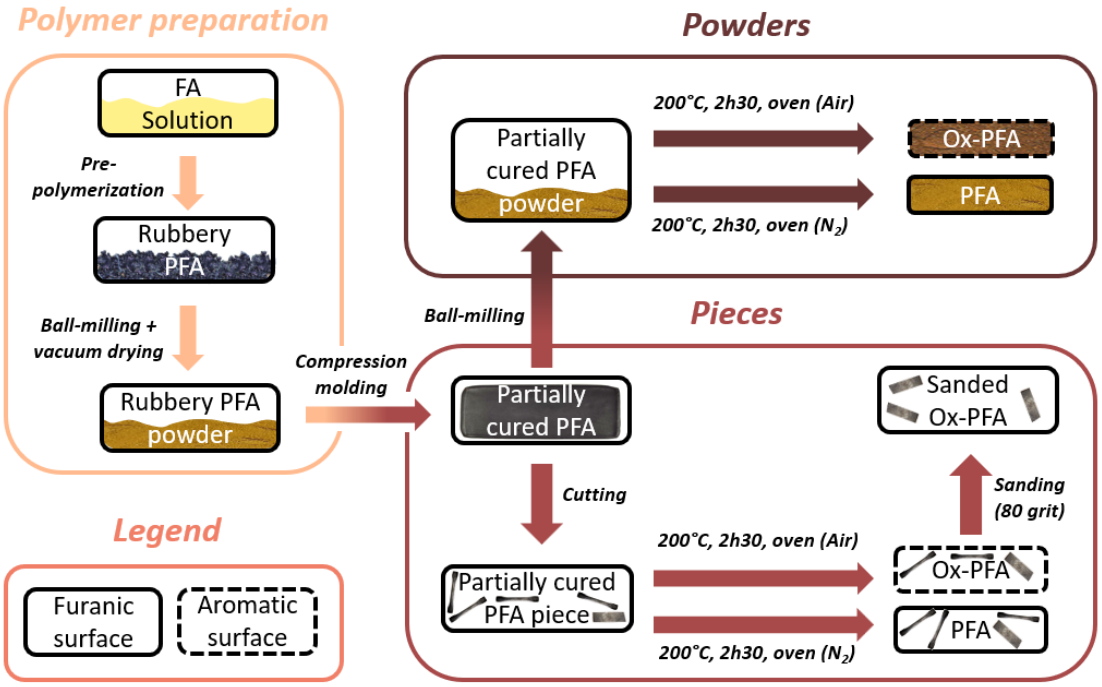

Scheme 4.1-1. Sample preparation procedure of PFA and Ox-PFA.

Spectroscopy:

The FTIR and ssNMR (CPMAS) spectra were acquired to the methods described in section 2.1. For the ssNMR, the spectra were referenced to the 151 ppm peak, i.e., the C=C of disubstituted furan rings. The height of this peak was set to 1 to compare PFA and Ox-PFA at a constant furan proportion. Such normalization could not be done on the FTIR spectra as the peaks overlapped with each either.

Elemental analysis:

The elemental analyses were conducted on a NCHS Thermo Electron Flash EA1112 from Thermo Fisher. About 1.5 mg of samples (powder form) were weighted in a flexible tin pan using a microbalance. After combustion, the gases were separated by gas chromatography and identified by a thermal conductivity detector. The resulting chromatogram was then integrated and the percentage of carbon and hydrogen were calculated. The oxygen content was deduced by subtraction.

Aldehyde detection (Tollens' reagent):

An aldehyde detection test was performed on PFA and Ox-PFA powders. This procedure was adapted from Malherbe et al. [356]. To do so, a 150 mL solution of 0.1 M silver nitrate in distilled water was prepared. Then, 2,4 g of sodium hydroxide were added, followed by 9 mL of 25 % ammonia solution. As a result, the reactions (1) to (3) occur.

$$AgNO_3 + NaOH \rightarrow AgOH + NaNO_3 \quad (1)$$

$$2\ AgOH \rightarrow Ag_2O + H_2O \quad (2)$$

$$Ag_2O + 4\ NH_3 + H_2O \rightarrow 2\ Ag(NH_3)_2^+ + 2\ ^-OH \quad (3)$$

Then, the reagent's quality was tested using about 15 mL of solution and 100 mg of fructose. A few minutes after the addition of fructose, a silver mirror appeared as the reaction (4) occurred. Upon shaking the silver mirror dissociates from the glass, revealing an orange solution. The silver mirror is a sign of the presence of aldehydes or alpha hydroxyketones. [356, 357]

$$R\text{-}CHO + 2\ Ag^{+} + 2\ ^{-}OH \rightarrow COOH + 2\ Ag^{+}\ H_2O \quad (4)$$

To test the presence of aldehydes in PFA and Ox-PFA, about 15 mL of the reagent and 400 mg of sample (powder form) were shaken and left to react for 24 h. A blank test was also conducted using only the tollens' reagent as it decomposes into Ag_3N over time as well as a fructose reference.

Thermogravimetric Analysis (TGA):

The TGA experiments were conducted on a TGA 851e apparatus from Mettler-Toledo. About 10 mg of samples were placed in 70 µL alumina pans. The temperature program started from 25 °C to reach 300 °C at 2 °C.min^{-1} under either 50 mL.min^{-1} of air or 50 mL.min^{-1} of N_2. Both PFA and Ox-PFA were subjected to these experiments (powder form). The experiments were duplicated. For kinetic analysis of the oxidation, heating rates of 1, 2, 4 and 8 °C.min^{-1} were employed. For kinetic analysis of the degradation, heating rates of 1, 2, 4, 8 and 16 °C.min^{-1} were employed.

Differential scanning calorimetry (DSC):

Oxidation Onset Temperature (OOT) experiments were performed on a DSC 1 from Mettler Toledo. The temperature program was adapted from Volpini et al. [358] The experiments were performed from 25 to 300 °C at 20 °C.min^{-1} under 50 mL.min^{-1} of air with 2-3 mg of sample in 30 µL open aluminum pan. The results are presented as the average and standard deviation of three experiments.

Dynamic Mechanical Analysis (DMA):

The DMA experiments were conducted on DMA 1 from Mettler-Toledo. The tensile mode was used. The temperature program started from - 80 °C to 300 °C at 2 °C.min^{-1}. The oscillation frequency was set at 1 Hz with a 0.1 % displacement amplitude. Both PFA and Ox-PFA were subjected to these experiments (piece form). These experiments were duplicated.

The curing time of 2 h 30 was determined using an isothermal experiment at 200 °C for 5 h. A strain amplitude of 0.1 % and a frequency of 1 Hz were used. The isotherm was preceded by a non-isothermal scan at 3 °C.min^{-1}, starting at 25 °C. The curve of the resulting *E*' as a function of time is available in Figure 4.1-1. For kinetic analysis of the hardening, heating rates of 0.5, 1 and 2 °C.min^{-1} were employed.

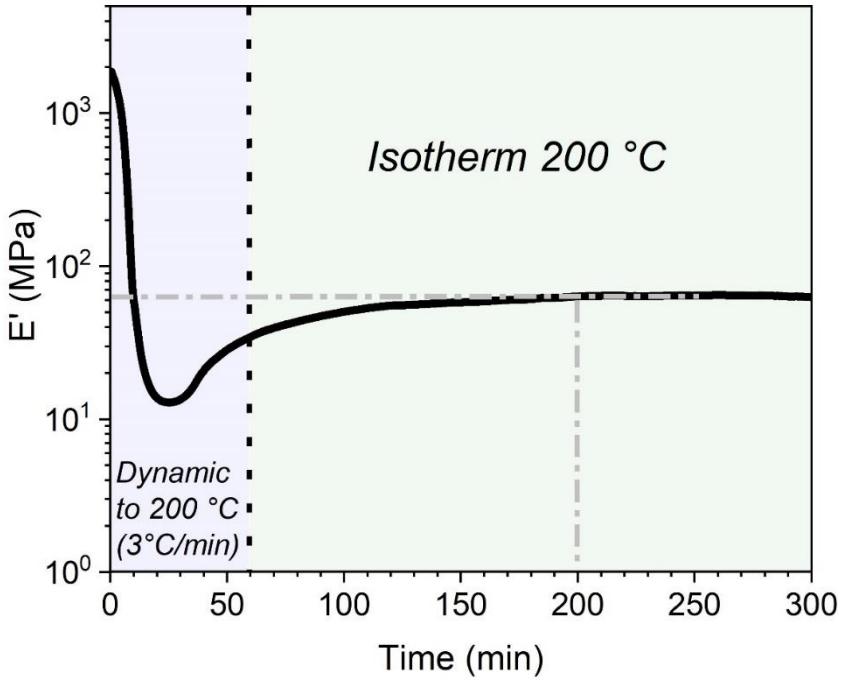

Figure 4.1-1. DMA curve used to determine the curing time of the PFAs.

Uniaxial tensile and Shore hardness tests:

To measure the tensile properties, a Shimadzu EZ-LX instrument was used. A load cell of 1 kN and a gauge length of 21 mm were used. The samples were cut in the dumbbell shape (ISO 527-2-1BB) using a dumbbell cutter prior to their post-curing. The crosshead's speed was set to 1 mm/min. The strain as well as the stress were recorded, and the curves were exploited using Origin 2021. PFA and Ox-PFA samples were tested seven times each. The hardness tests were conducted using a shore D durometer from Kern & Sohn GmbH. Overall, 10 attempts were performed at different spots on the samples. The results are presented as the average and standard deviations (i.e., error bars) from the repetitions.

Goniometry:

The contact angles were measured using a Goniometer dataphysics OCA25. Prior to analysis, the samples were preconditioned for 30 mins under the atmospheric conditions of measurement. A 5 µL water droplet was placed on the samples then a picture was taken by a camera a few seconds after the deposition of the droplet. Six measurements were taken for each sample. The results are presented as their average and standard deviation.

Carbonyl and carboxylic acid determination:

The C=O and COOH content were determined using the potentiometric method developed in section 2.1.

Gel Content:

To determine the gel content of PFA samples, rectangular pieces of about 150 mg were immersed in about 15 mL of ethyl acetate for 7 days at 25 °C. The ethyl acetate was then removed, the sample were washed two times with ethyl acetate. Then, they were vacuum dried at 40 °C overnight. Equation 4.1-1 was used to determine the gel content. In Equation 4.1-1, m_d stands for the dry mass while m_i corresponds to the initial mass of PFA or Ox-PFA. The gel content experiments were triplicated.

$$Gel\ fraction\ (\%) = (1 - \frac{m_i - m_d}{m_i}) * 100 \quad \text{Equation 4.1-1}$$

Scanning Electron Microscopy:

For scanning electron microscopy (SEM) observations, pieces of PFA samples were prepared as follow. From the fractured surface produced by the tensile test, cross section were cut with a razor blade and flat surfaces were prepared with a Reichert Ultracut E ultramicrotome. They were mounted on a SEM stub with carbon tape and subsequently coated with platinum (3 nm). SEM observations were carried out with a Tescan Vega 3 XMU scanning electron microscope (Tescan France, Fuveau, France) at an accelerating voltage of 5 kV.

4.2 Current knowledge about the chemical transformation of furan resins at high temperatures

As mentioned in section 1.3.1, furan resins are widely used as carbon precursors. To explain the chemical structure of the carbonaceous materials, the mechanisms of carbonization were thoroughly investigated. [359, 360, 361, 362, 363, 364] Scheme 4.2-1 reports example of structures found in carbonized furan resins. They mostly consist in a succession of aromatic rings that are more or less functionalized, depending on the carbonization conditions.

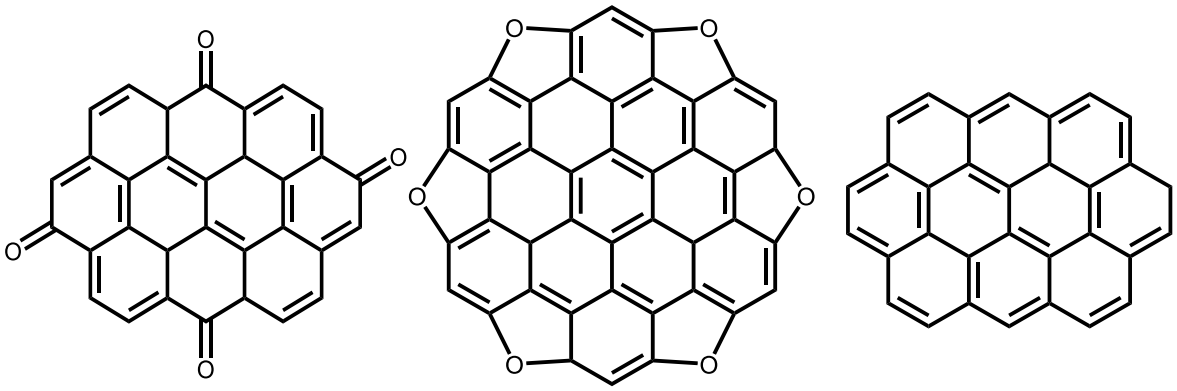

Scheme 4.2-1. Aromatic structures found in carbonized furan resins. [361, 362, 363, 364]

Furthermore, other authors attributed the aromatic structures of the carbonized resins as the result of the aromatization of the Diels-Alder adducts, as depicted in Scheme 4.2-2. [185, 365]

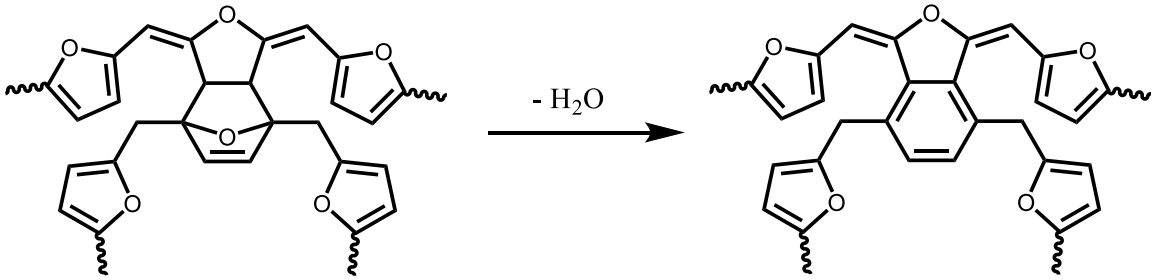

Scheme 4.2-2. Potential aromatization pathway of furan resins during carbonization. [185, 365]

To reach carbonaceous materials from furan resins, the researchers mostly worked at high temperatures, i.e., above 500 °C, and inert atmospheres. Only few studies investigated the starting temperatures of the aromatization. They found the aromatization starting point around 300 – 400 °C and more. [288, 359, 361, 364]

However, to the best of our knowledge, only one article reported the evolution of the chemical structures of furan resins at and above 200 °C under air. The authors observed significant changes in the FTIR spectra of the materials. They suggested the formation of carbonyls followed by chain scissions as shown in Scheme 4.2-3. [366]

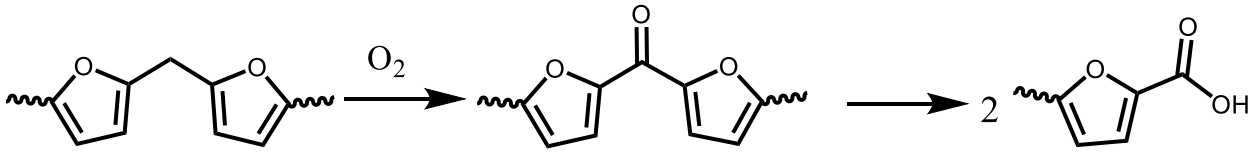

Scheme 4.2-3. Chain scission of furfuryl units according to Conley et al. [366]

A more recent article highlighted reactions occurring in the solid above 170 °C which led to an increase in Young's moduli of the material. [301] This is contradictory with the chain shortening suggested by Conley et al. Likewise, the temperature was too low to initiate the carbonization of the material.

The goal of this chapter is to shed new lights on the thermal phenomena occurring from 150 to 300 °C during the curing and/or post-curing treatment of furan resins. To do so, curing steps were performed under inert (N_2) and oxidative (air) atmosphere. The resulting materials were subjected to thermomechanical, spectroscopic analysis and kinetic computations to establish the structure-property relationships of the fully cured furan resins. The objective is to breakthrough knowledge on the aromatization of furanic resins i.e. the transformation of furanic moieties into benzenic moieties. The consequence of such amortization on thermo-mechanical properties are discussed.

4.3 Aromatization of furans: structural investigation

The goal of this section was to investigate the aromatization of furanic moieties within furan resins during their curing. For this purpose, two resins were prepared from the same batch and either a N_2 or an air atmosphere was applied during the post-curing step. They resulted respectively in PFA and Ox-PFA samples.

First, the chemical structure of these samples will be discussed using FTIR and ssNMR spectroscopies. Figure 4.3-1 displays the FTIR spectra of PFA and Ox-PFA. As a complement, the attributions of the main bands are reported in Table 4.3-1.

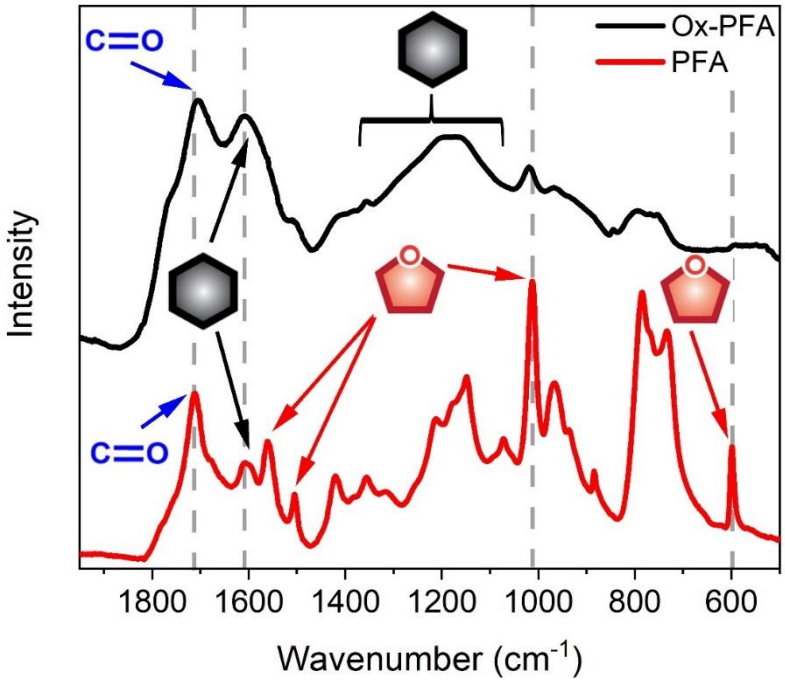

Figure 4.3-1. FTIR spectra of PFA (red line) and Ox-PFA (black line) in their powder form.

In Figure 4.3-1, the PFA spectrum exhibits the classical furanic bands respectively at 600, 1015, 1500 and 1550 cm^{-1}. In addition, the 1712 cm^{-1} band is also observed and it corresponds to the carbonyls from the furan opened-structures within the polymer.

Table 4.3-1. FTIR bands attributions of PFA and Ox-PFA.

	Wavenumber (cm^{-1})	Attribution	References
PFA	600	Furan ring: out of plane deformation	[292, 293]
	650-840	Multiple furanic bands (collective)	[292, 293]
	1014	2-sub: ring C-H in plane wag	[292, 293]
	1018	2,5-sub: ring C-H in plane wag	[292, 293]
	1505	2-sub: Furan C=C stretch	[292, 328]
	1560	2,5-sub: C=C stretch	[293, 328]
	1712	C=O stretch	[283, 288]
Ox-PFA	1060 - 1340	=C-H aromatic (in plane deformation)	[328, 360]
	1605	Aromatic CC stretch, C=C stretch	[328, 367]
	1705	C=O stretch	[328, 367]

However, in the Ox-PFA spectrum the furanic bands are either not observed (600 and 1500 cm^{-1}) or highly dimmed (1015 and 1550 cm^{-1}). Moreover, a broad signal is observed from 1060 to 1340 cm^{-1}. Furthermore, the 1600 cm^{-1} band is much more intense in the case of Ox-PFA relative to the furan peak at 1000 cm^{-1}. The 1060 – 1340 cm^{-1} and 1600 cm^{-1} bands match with aromatic vibrations, respectively =C-H and C=C. [288, 361, 360, 364] Likewise, the 1712 cm^{-1} band in PFA is shifted to 1705 cm^{-1}. Such shifting to lower wavelength could be linked to the apparition of more conjugated carbonyls [328, 330] In comparison with the furanic band at 1012 cm^{-1} the intensity of the C=O is much higher in the Ox-PFA spectrum than in PFA's. Figure 4.8-2 presents the magnified FTIR spectra of Ox-PFA and PFA from 2500 to 3400 cm^{-1}. For both samples, several bands superimpose in this area. Nonetheless, a COOH band is visible in the spectrum of Ox-PFA. In addition, both samples seem to exhibit traces of OH groups. Finally, a shouldered peak a 2650 cm^{-1} is distinguishable for both samples, especially in the case of Ox-PFA.

Vibrations in this area are typically attributed to C-H stretching of aldehydes (usually doublets). [328] Finally, Figure 4.3-2 displays pictures of PFA and Ox-PFA (powder form). Here, Ox-PFA is much darker than PFA. This observation is also consistent with a more conjugated chemical structure.

PFA *Ox-PFA*

Figure 4.3-2. Picture of PFA and Ox-PFA in their powder form.

In the past, the carbonization of PFAs into amorphous carbon was mostly studied under inert gazes [185, 361, 362, 363, 364]. To the best of our knowledge, only Conley et al. studied the chemical structure of oxidized PFA. They concluded with the formation of ketonic and carboxylic species while maintaining the furanic structure when the material was exposed 17 h at 200 °C under air as depicted in Scheme 4.2-3. Yet, Figure 4.3-1 shows an aromatic structure of the Ox-PFA sample while the PFA one is mostly furanic. Thus, the oxidative treatment involves the aromatization of the system on top of the formation of C=O in furan resins.

As the FTIR analysis only takes into account the surface of the sample, an Ox-PFA piece was crushed to investigate the internal structure of the material. Figure 4.8-3 shows the FTIR spectra of the surface of an Ox-PFA piece before and after being ground. Interestingly, the ground powder rather presents FTIR peaks of PFA instead of the aromatic ones observed on the surface of the Ox-PFA. Consequently, it can be logically deduced that the oxidative post curing treatment mostly affects the surface of the material.

Continuing on the chemical structures, ssNMR was used to investigate the different materials. Figure 4.3-3 displays the normalized ssNMR spectra of PFA and Ox-PFA. First, both spectra exhibit the typical peaks observed in PFA systems. Theirs attributions are available in Table 1.3-2. On both spectra, the 151, 108 and 27 ppm peak superimpose nicely, thanks to the normalization. Respectively, they correspond to the C_1/C_5 of disubstituted furans, the C_3/C_4 of furans and the CH_2 bridging the furans. (cf chapter 3) To ease the interpretation of the spectra, Figure 4.8-4A, B and C present magnifications of Figure 4.3-3.

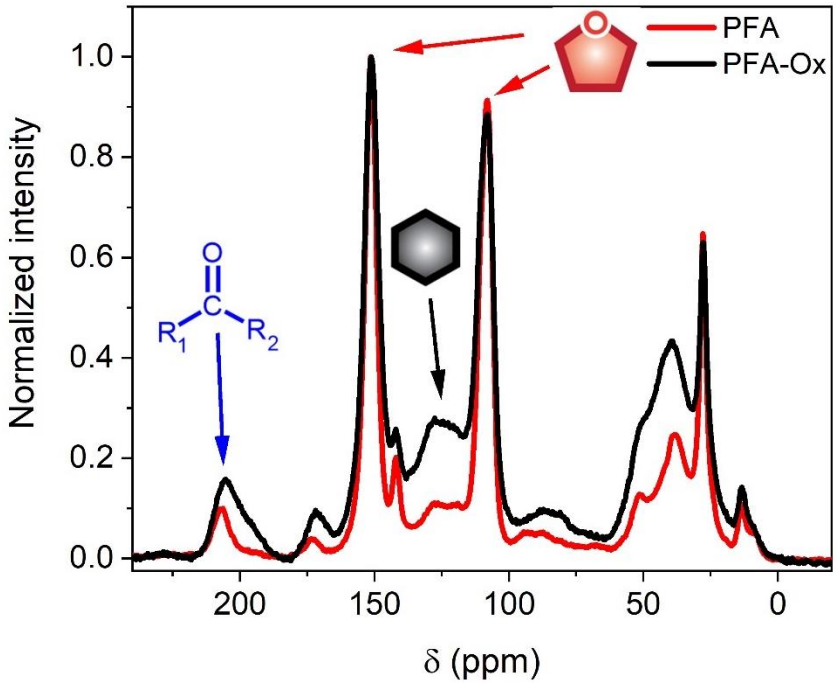

Figure 4.3-3. Normalized ssNMR spectra of PFA (red line) and Ox-PFA (black line) in their powder form. The spectra are normalized to the 151 ppm peak.

In Figure 4.8-4A the C=C area is magnified. The 151 and 108 ppm peaks of Ox-PFA are broader than the ones of PFA. Moreover, the peak at 140 ppm, i.e., corresponding to the C_5 of terminal furans, is less obvious in the case of Ox-PFA.

On top of that, the 115 - 135 ppm peak is both broader and more intense in the case of Ox-PFA. These signals have often been attributed to the Diels-Alder adducts of PFA, cf Table 1.3-2. However, they could also match with C=C bonds of aromatic compounds. [328] Similar C=C peaks have been observed in the case of carbonized furan resins. [361] The presence of aromatic C=C is consistent with the observations of the 1600 cm^{-1} and 1060 - 1340 cm^{-1} bands in the FTIR spectrum of Figure 4.3-1 and the darker color of Ox-PFA in comparison with PFA.

Figure 4.8-4B depicts a magnification of the CH/CH_2 area of the NMR spectra of PFA and Ox-PFA. Again, the Ox-PFA peaks are broader than the ones of PFA. This is especially the case of the 39 ppm peak. Likewise, the 51 ppm peak visible on the PFA spectrum appears more as a shoulder in the case of Ox-PFA. This shoulder was also observed in the case of carbonized furan resins. [361] These observations suggest once again a more heterogeneous structure of the furan resin if the post curing is performed under air rather than N_2.

Figure 4.8-4C focuses on the carbonyl region of the NMR spectra of Ox-PFA and PFA. Both spectra have two main signals around 208 and 170 ppm. The latter one corresponds to ester and/or carboxylic acid and is both broader and more intense in the case of Ox-PFA. Moreover, a slight shouldering towards lower chemical shifts is also observed which would be consistent with the conjugation of the COOH groups. The other peak at 208 ppm has often been attributed to 1,4-diketones emerging from the hydrolysis of the furan ring. Yet, chapter 3 showed that aldehydic species with a lower chemical shift can also form, especially when the furan resins are exposed to air. Here, the 208 ppm peak of PFA is both sharper and less intense than Ox-PFA. Besides, on the Ox-PFA spectrum a clear shouldering is visible from 185 to 200 ppm. This would be consistent with the presence of conjugated carbonyls (ketones or aldehydes). To confirm the presence of aldehydes, Tollens' tests were performed on the different samples and the pictures are shown in Figure 4.3-4.

Figure 4.3-4. Pictures from the Tollens test of the reference, fructose, PFA and Ox-PFA.

As the time of experiment was rather long for a Tollen's test (usually minutes), a reference using only Tollen's reagent as well as a reference with fructose were performed. The solution with only the Tollen's reagent did not change in color, only a small solid precipitate formed. This precipitate results from the decomposition of the silver complex into AgN_3. The test using fructose formed a silver mirror which fell from the glass upon shaking to expose a colored solution. Such phenomenon occurs when aldehydes are present in the system.

After the exposure of the PFA powder to the Tollen's reagent, a slight taint appeared without signs of silver mirror. In the case of Ox-PFA, the silver mirror could not be observed as well. However, the solution had a much deeper color, closer to the fructose test. Therefore, it would suggest the presence of aldehydes in the Ox-PFA sample. Hence, it is likely that the post curing in oxidative atmosphere induces the formation of aldehyde on the surface of the material. A positive Tollen's test could also be caused by the presence of α-hydroxyketones. [357]

The previous experiments only focused on qualitative analyses. To compensate for this, carbonyl and carboxylic acid quantifications were performed as well as elemental analysis. The results from the quantifications are compiled in Table 4.3-2.

Table 4.3-2. Results from the elemental analysis, C=O and COOH potentiometric titration.

	C=O ($mmol.g^{-1}$)	COOH ($mmol.g^{-1}$)	%C	%H	%O
Ox-PFA	5.46 ± 0.28	0.34 ± 0.05	65.6	4.0	30.5
PFA	3.20 ± 0.18	0.11 ± 0.01	72.1	4.7	23.2

Table 4.3-2 reports a C=O content about 1.7 times higher and a COOH content about 3 times higher for Ox-PFA compared with PFA. Additionally, the overall oxygen content of Ox-PFA is 1.3 times higher than PFA. Hence, the oxidative curing underwent by Ox-PFA incorporated oxygen in the material in the form of ketones/aldehydes and carboxylic acids. The presence of other oxygenated moieties is also a possibility.

In order to deeper understand the previously highlighted phenomena, thermogravimetric analyses were performed on PFA and Ox-PFA in their powder form. The samples underwent TGA under air and N_2 atmosphere. The curves are shown in Figure 4.3-5.

In Figure 4.3-5 the black lines correspond to the Ox-PFA samples. If the TGA is performed under N_2, the material will decompose later than if the TGA is performed under air. This behavior is usual for carbon-based material as the dioxygen in the air favorizes their decomposition.

However, in the case of PFA's, the TGA scan under inert atmosphere shows a continuous mass loss earlier than the one observed under oxidative atmosphere. Moreover, when the TGA of PFA is performed under air a mass gain of about 0.5% is observed from 180 °C to 225 °C in the experimental conditions. Thus, it supports an introduction of oxygen in PFA when it is exposed to air above 170 °C. As well, this phenomenon delays the degradation of the polymer. Therefore, this oxidized layer might protect the polymer from decomposition.

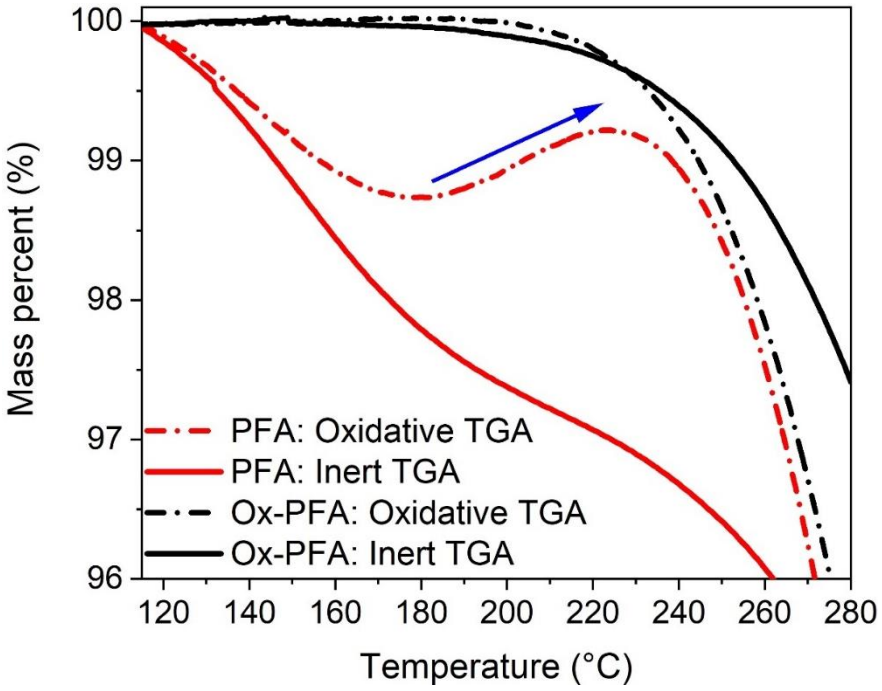

Figure 4.3-5. TGA curves of PFA (red lines) and Ox-PFA (black lines) in their powder form at 2 °C.min^{-1} from 25 to 300 °C. The dashed-dot lines correspond to the TGAs performed under air. The plain lines correspond to the TGAs performed under N_2.

To sum up, the atmospheric conditions (N_2 or Air) during the post-curing of a furan resin implies surface modification. The oxidative curing induces the formation of surface groups, including ketones, aldehydes, carboxylic acids and aromatics. Moreover, the FTIR spectra showed that very few furans are present on the surface of the material while the NMR proved that they are still in majority when considering the whole bulky material. Finally, the TGA supported that oxygen is incorporated in PFA in significant amounts when subjected to oxidative thermal treatment above 170 °C.

4.4 Origin of surface hardening

To further understand the effect of surface oxidation on the materials, three DMA experiments were performed. Both PFA and Ox-PFA samples were analyzed. In addition, an Ox-PFA piece was sanded prior to the DMA for removing the top surface layers of the material. Figure 4.4-1 presents the tan (δ) curves of these three samples.

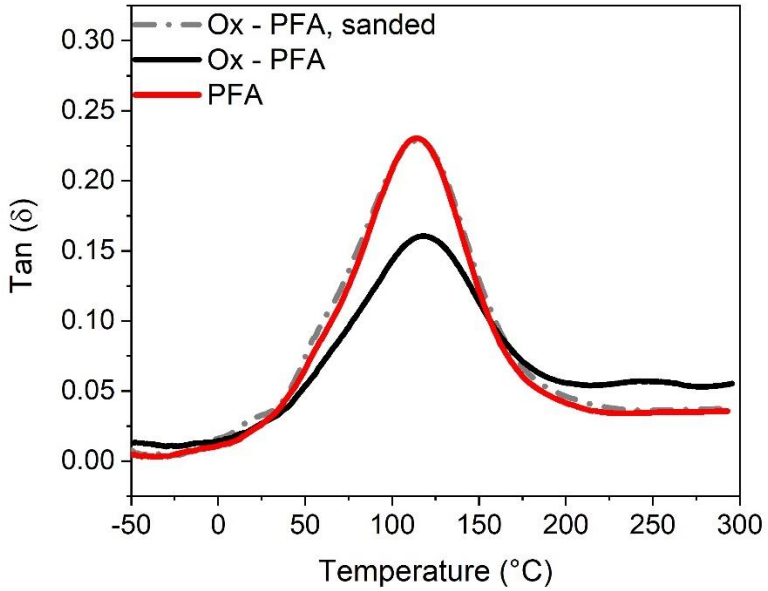

Figure 4.4-1. Tan (δ) curves from DMA experiments of PFA (red line), Ox-PFA (black line) and the sanded Ox-PFA (gray dashed-dot lines).

Figure 4.4-1 highlights few facts. First, the Ox-PFA has a maximum of tan (δ) of 0.16 while it increases to 0.23 for PFA (for similar peak-width). Thus, the surface oxidation induces a slightly lower damping capacity. In addition, the Ox-PFA has a T_g of 117 °C which is slightly higher than the one of PFA peaking at 113 °C. Secondly, the "Ox-PFA, sanded" curve superimposes nicely with PFA's. Thus, it confirms that the oxidation phenomenon is limited to a top surface layer. This implies that once the dioxygen reacted with PFA it becomes very difficult for the dioxygen molecules to enter into the core of the material and further react with other entities.

Hence, the top layer might, to some extent, act as a protection against further oxidation of the material. This could be a partial explanation for the well-known high thermal stability of the furan resins. In addition, it can be highlighted that the width of the tan (δ) peak remains constant, which suggests that the distribution of chain lengths is not or little impacted by the oxidative treatment. The elastic moduli curves of theses samples are highlighted in Figure 4.4-2.

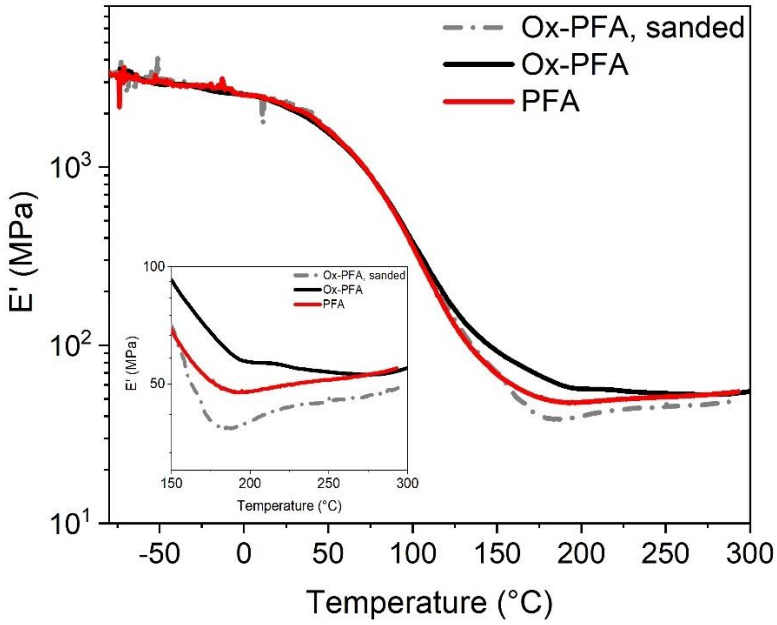

Figure 4.4-2. Elastic moduli vs. temperature obtained from DMA experiments of PFA (red), Ox-PFA (black) and the sanded Ox-PFA (gray dashed-dot lines).

The three samples have similar *E*' values in the glassy state. However, the *E*' curves of Ox-PFA and PFA diverge in the rubbery state. The magnification (inset Figure in Figure 4.4-2) highlights an increase in moduli from 180 °C for both PFA and "Ox-PFA, sanded". An increase of moduli after reaching the rubbery plateau can be the sign of a partially cured material or a graphitization phenomenon. However, Ox-PFA and "Ox-PFA, sanded" underwent the same preparation procedure and came from the same batch. The only difference was the sanding process of Ox-PFA (blue curve in Figure 4.4-2) prior to DMA.

On top of that, the temperature is too low for the graphitization to occur. As a consequence, it can be deduced that this final increase in E' might be linked to a crosslinking occurring at the surface of the material.

To further emphasize the correlation between the oxidation and increase in moduli, the TGA curve of Figure 4.3-5 has been put in perspective with the *E*' curve from Figure 4.4-2. This compilation is presented in Figure 4.4-3 for the PFA samples. The compiled curves from Ox-PFA are available in Figure 4.8-5.

Figure 4.4-3 displays the evolution of *E*' from the DMA along with the mass percent from the TGA as a function of the temperature for a PFA sample. These results have been presented and discussed separately earlier. Nonetheless, Figure 4.4-3 allows to clearly highlight the correlation between the mass gain in TGA, i.e., due to incorporation of oxygen, and the increase of *E*' in DMA, i.e., due to new crosslinks.

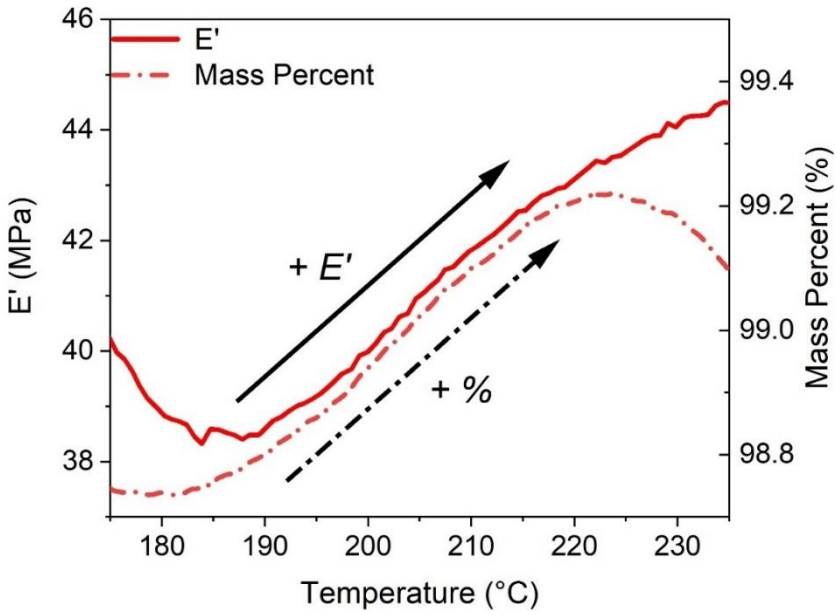

Figure 4.4-3. Magnified superposition of DMA (plain lines) and TGA (dashed-dot lines) of PFA. The same heating rate of 2 °C.min^{-1} was applied.

Based on the mechanism suggested in chapter 3 and the observations made here, a pathway for the surface crosslinking and aromatization of furans is proposed in Scheme 4.4-1. Upon exposure to air, the furan rings closest to the materials' surface can open into conjugated carbonyls. Hence, it explains the mass gain observed in TGA as well as the higher carbonyl contents. It is also possible that conjugated 1,4-diketone form following a similar process.

It is however challenging to determine the proportion of aldehydes and ketones. In either case, the resulting conjugated carbonyls are good dienophiles with their two electron withdrawing groups.[343] Consequently, they are likely to form Diels-Alder cycloadducts with the linear furans. Then, the aromatization would follow accompanied with a water release. As demonstrated earlier, this whole process seems to be limited to the surface.

The exact nature of the aromatized product is however unclear. The stability of the aldehydes is low, at least some of them might oxidize to carboxylic acid which could be followed by a decarboxylation.

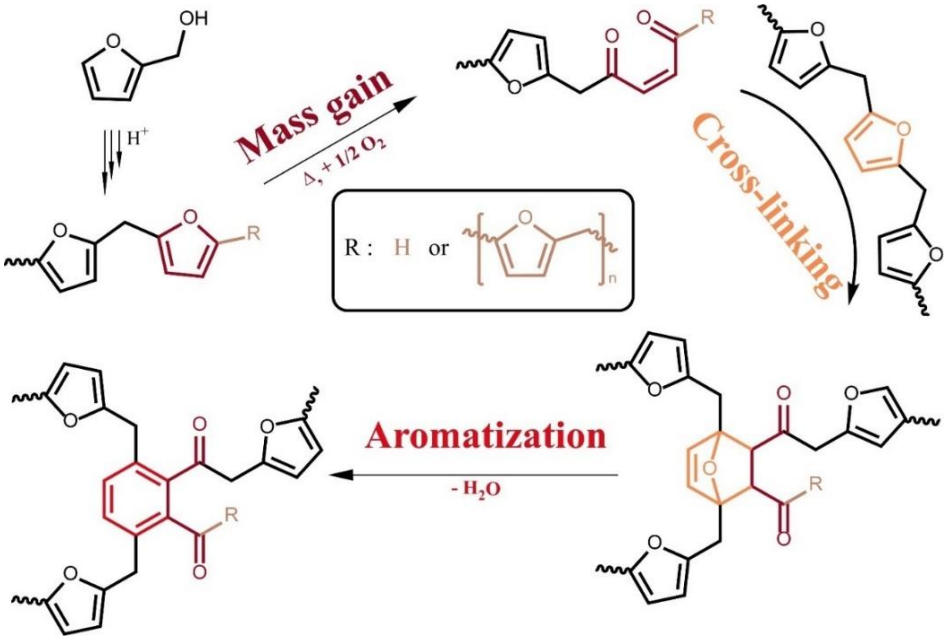

Scheme 4.4-1. Proposed mechanism for the crosslinking occurring sample's surface during post curing under air, based on the opening of furans.

To assess the thickness of the oxidized layer, SEM was performed. Figure 4.4-4 showcases the surface of relevant Ox-PFA and PFA samples. In both PFA and Ox-PFA, the heart of the material is constituted of a pattern resulting from the cutting process. Yet, near its surface, Ox-PFA displays “lines of circles” almost perpendicular to the surface as highlighted by white dashed lines. In PFA, this outer layer pattern is not so clearly visible nor organized although it appears different from the heart of the material. It should be noted that the sample preparation process with the microtome may induce edge effects. Thus, it may be a part of what is observed in Figure 4.4-4. Nonetheless, if an edge effect alone was responsible both PFA and Ox-PFA should present it, which is not the case here.

Based on about thirty measures, the thickness of the outer layers was averaged at 24.0 ± 4.5 µm for Ox-PFA. For PFA, the thickness of the outer layers was estimated to 3.6 ± 0.3 µm although it might be an edge effect caused by the cutting process.

This hypothesis is supported by the observations made on Figure 4.3-1. According to the FTIR spectra, the surface of PFA and Ox-PFA are chemically different. However, the spectrometer used in this study detects depths comprised between 0.5 and 5 µm depending on the wavenumber. More specifically, the penetration depth of the laser for ATR diamonds is typically around 2 µm at 1000 cm^{-1}. Hence, as furanic compounds only are detected in Figure 4.3-1 at 1000 cm^{-1} for PFA the thickness calculated earlier is not coming from an oxidized surface.

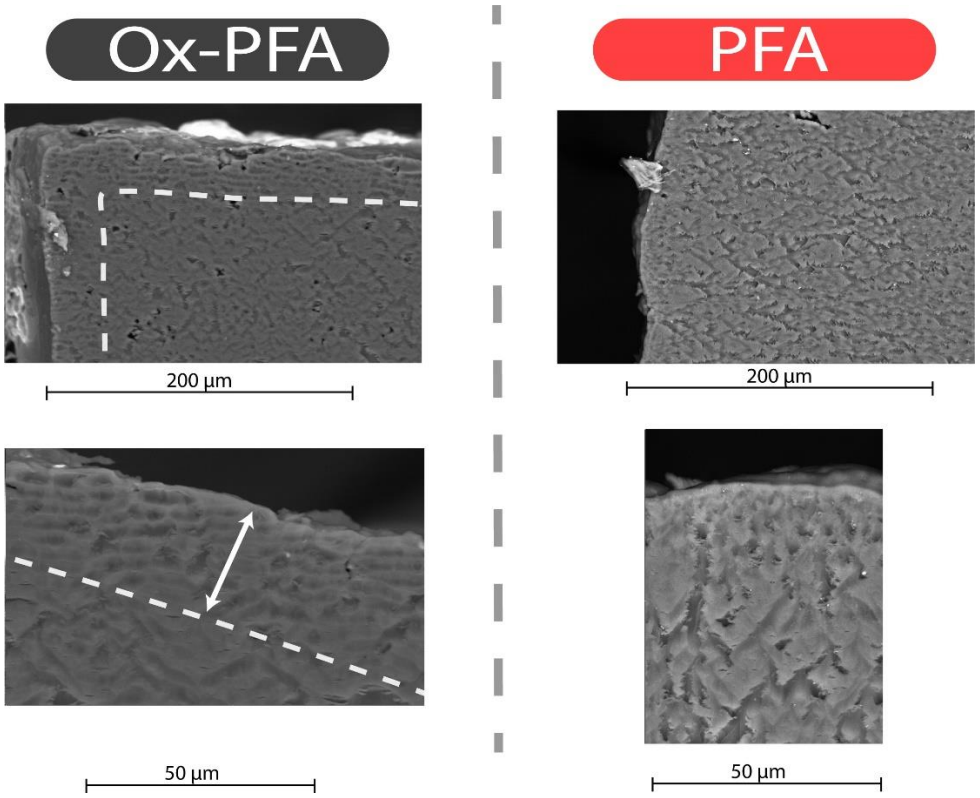

Figure 4.4-4. SEM pictures of Ox-PFA (left) and PFA (right). The white dashed lines highliths what was attributed to the oxidized layers. The white arrows is a representative example of how the thickness was measured.

To further confirm this thickness of the oxidized surface, one could perform several experiments. First, FTIR photoacoustic which is typically used to determine the thickness of coatings. Secondly, one could cut a flat surface with a microtome, create a map of chemical bonds with a Raman spectrometer and subject the same surface to SEM. Doing so may allow to visualize the aromatic C=C bonds on the outer layers of Ox-PFA.

4.5 Kinetics of oxidation, hardening and degradation

To better understand the aromatization phenomenon, experiments and kinetic computations for kinetic analysis were performed in accordance with the ICTAC Kinetics Committee Recommendations [368]. An advanced isoconversional method was used for this purpose and was described in previous papers [369, 370]. Figure 4.8-6, presents tha data obtained from DMA an TGA and Figure 4.5-1 depicts the dependence of the effective activation energy (E_α) with temperature (T) computed from these data for the reaction occurring when exposing PFA and Ox-PFA from 130 to 600 °C.

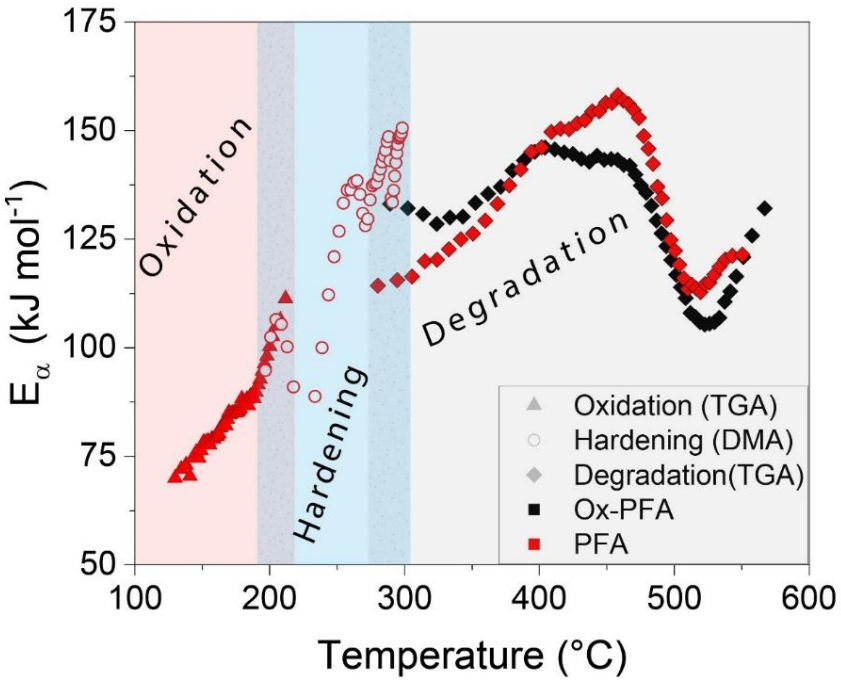

Figure 4.5-1. Dependence of the effective activation energy (E_α) with temperature (T).

In Figure 4.5-1, the first part (triangles) corresponds to the effective activation energy computed from mass of PFA during its oxidation (i.e., between ≈120 and 220 °C). The order of magnitude of the E_α is coherent with activation energies of the thermo-oxidative degradation of common polymers (PE, PP, PS 75 - 150 kJ.mol^{-1} [371]; bisphenol-based epoxies: 110 - 150 kJ.mol^{-1} [372, 373]). As PFA's oxidation is progressing, the E_α value increase which indicates that the process is increasingly difficult.

The end of PFA's oxidation superimposes nicely with the beginning of the surface hardening observed in DMA. The E_α obtained from the *E*' rise in DMA rises as oxidation proceeds. Then, as the temperature is increasing, the oxidation process is followed by a thermal hardening, which also presents increasing E_α values. This is coherent with the hypothesis emitted previously, i.e., the apparent difficulty encountered by dioxygen to penetrate the PFA's network. The end of the increase of *E*' is also coherent with the beginning of the degradation. The E_α of degradation of PFA and Ox-PFA are close and follow similar pathways, which indicates that the materials encounter the same degradation mechanisms once PFA has been fully oxidized.

Finally, Figure 4.5-1 shows that the effective activation energy at the beginning of the thermal degradation of PFA is slightly lower than the E_α of Ox-PFA's. As seen in Figure 4.3-5, oxidation of PFA is not complete once its thermal degradation starts. Thus, its oxidation degree is lower than for Ox-PFA and this perfectly corroborates the hypothesis of a lower stability of non-oxidated PFA.

4.6 Properties of PFA and Ox-PFA

The effect of the surface crosslinking on the mechanical properties of uncured furan resins was qualitatively reported in chapter 2 and 3. Uncured furan resins tend to form a hard crust richer in carbonyls than its core. In the followings, the properties of Ox-PFA and PFA will be compared to better apprehend the impact of the surface crosslinking on the material.

Figure 4.6-1 shows the tensile properties obtained on PFA and Ox-PFA samples. The elastic modulus of PFA is slightly lower than Ox-PFA, respectively 2.2 ± 0.3 GPa and 3.1 ± 0.3 GPa.

The elongations at break are of 1.2 ± 0.3 % for Ox-PFA and 1.9 ± 0.4 % for PFA while they have similar yield strength. In addition, the Shore D Hardness of Ox-PFA and PFA are slightly different. The higher *E*', lower elongation at break of Ox-PFA together with similar yield strength of the samples are consistent with the lower damping capacity observed for Ox-PFA in DMA. Overall, the effect of the surface crosslinking on the tensile properties of furan resins is rather limited. This surface crosslinking occurring in Ox-PFA make the material slightly stiffer and more brittle.

To complete this study, the gel content, contact angle and Oxidation Onset Temperature (OOT) of Ox-PFA and PFA have been determined. The results from these experiments are gathered in Table 4.6-1.

Table 4.6-1. Gel content, contact angle and OOT of Ox-PFA and PFA.

Sample	Gel content (%)	Contact angle (°)	OOT (°C)
Ox-PFA	92.4 ± 1.8	86.1 ± 2.7	253.6 ± 2.3
PFA	94.0 ± 1.5	85.3 ± 3.1	203.1 ± 3.1

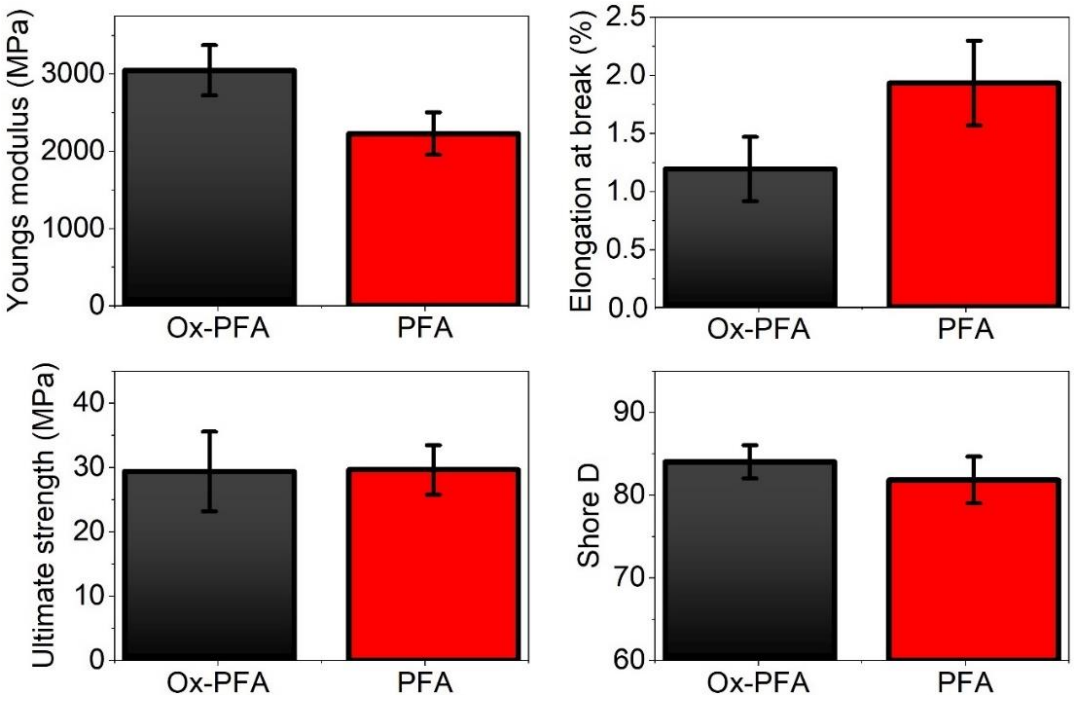

Figure 4.6-1. Tensile properties and Shore D hardness of Ox-PFA (black) and PFA (red).

The gel content was determined for both materials. Ox-PFA had a gel content of 92.4 ± 1.8 % while the one of PFA was of 94.0 ± 1.5 %. Hence, the resistance to solvents is not substantially affected by the oxidized surface layer. Furthermore, goniometry experiments were conducted on PFA and Ox-PFA. The analysis gave a contact angle of 86.1 ± 2.7 ° for Ox-PFA and 85.3 ± 3.1 ° for PFA. Thus, the hydrophobicity brought by the aromatization is most likely counteracted by the presence of oxygenated groups on the surface of the material.

Finally, the degradation temperature of Ox-PFA and PFA were evaluated using the OOT method. Figure 4.8-7 displays example of curves from the OOT determination, the results from three repetitions are compiled in Table 4.6-1. Ox-PFA yielded 253.6 ± 2.3 °C of OOT while PFA had an OOT of 203.1 ± 3.1 °C meaning that Ox-PFA is less sensitive to oxidation than PFA. Such results further emphasize the role of the aromatized surface layer of furan resins as it protects the material from further oxidation. The exotherm might also comprise the heat generated during the surface oxidation.

4.7 Conclusion

The formation of aromatic species, during the post-curing of furan resins was investigated. A furan resin was post-cured under N_2 to give PFA and was compared to a furan resin post-cured under air, i.e., Ox-PFA.

In terms of chemical structures, PFA presented the predominance of furanic structures. On the other hand, the Ox-PFA displayed signs of carbonyls, including aldehydes, as well as the presence of aromatic moieties. It was found that these groups are only located on the top surface. A mechanism was proposed to explain their formation. It involved the oxidative ring opening reaction of the furan ring followed by a Diels-Alder crosslinking and the aromatization reaction of the adduct. This process is accompanied by a mass gain and a rise of the *E*' in the rubbery plateau. From a thermomechanical point of view, this oxidative crosslinking is associated with a decrease of the damping capacity.

Overall, the observed oxidation process is limited to the surface, i.e., about 20 µm, and is protecting the material from further oxidation to some extent. Thus, such surface oxidation phenomenon might also explain the relatively high thermal stability obtained for furanic resins as highlighted by the kinetic study and OOT experiments. Finally, presence of an oxidized layer on the surface of PFA has little impact on the tensile properties of the material.

4.8 Supplementary Informations

Figure 4.8-1. ISO 527-2-1BB specimen (left) and dumbbell cutter (right).

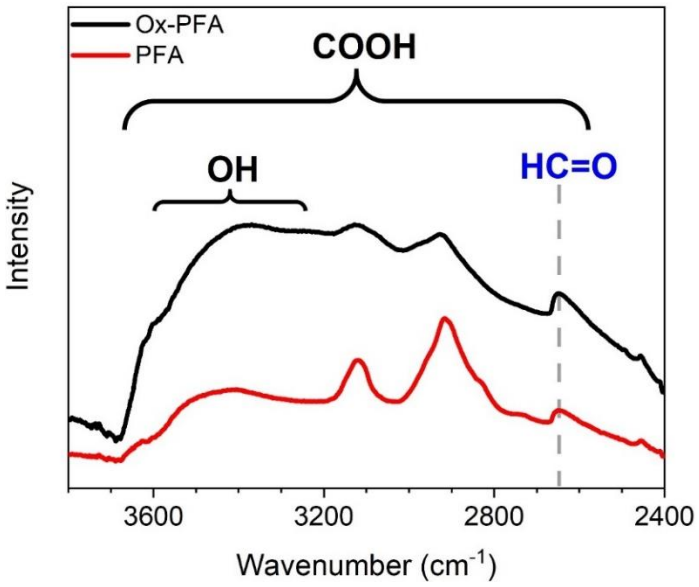

Figure 4.8-2. FTIR spectra of an Ox-PFA sample before (black) and after (red) magnified from 3700 to 2400 cm^{-1}.

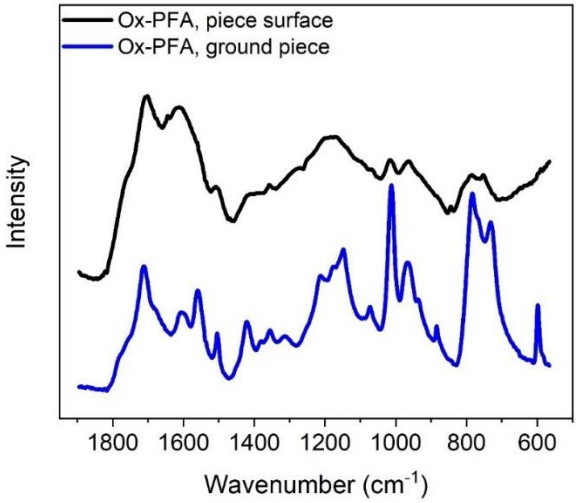

Figure 4.8-3. Magnified FTIR spectra of an Ox-PFA sample before (black) and after (red) being grinded by ball milling.

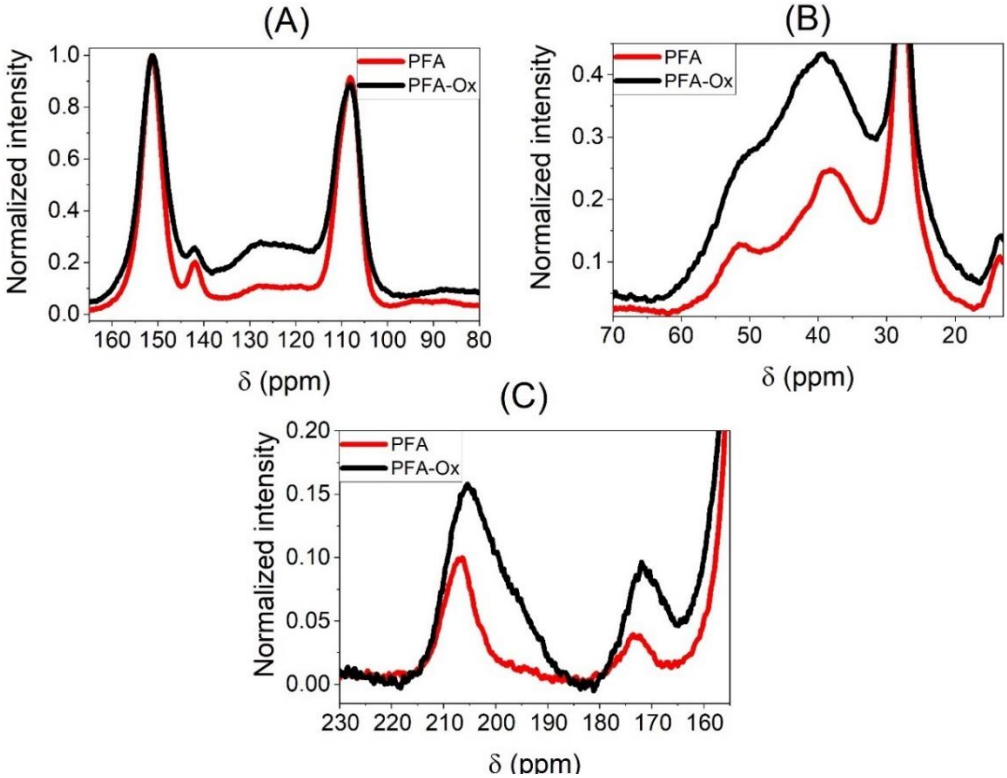

Figure 4.8-4. Magnified NMR spectra of PFA (red) and Ox-PFA (black) on the C=C area (A), alkyl area (B) and C=O area (B).

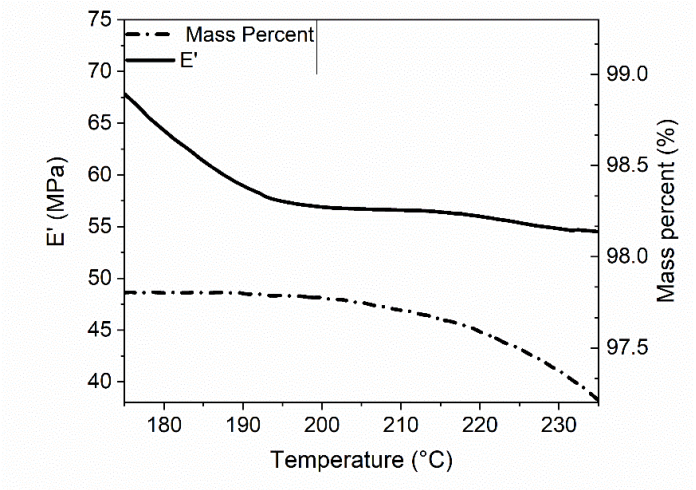

Figure 4.8-5. Magnified superposition of DMA (plain lines) and TGA (dashed-dot lines) of Ox-PFA.

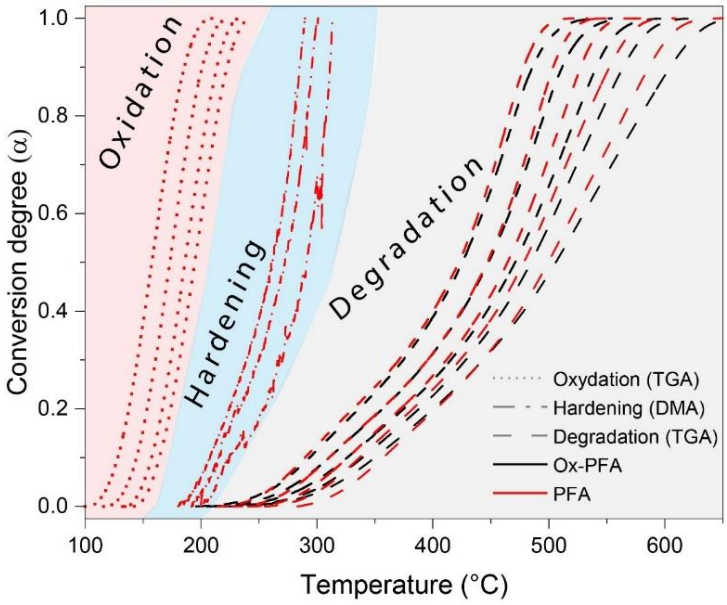

Figure 4.8-6. Extent of conversion (α) with temperature for PFA (red) and Ox-PFA (black). The dot lines correspond to the data calculated from the first mass variation in TGA, the dash-dot lines to the increase of *E*' in DMA and the dash lines to the TGA degradation at high temperature. All the experiments were performed under air.

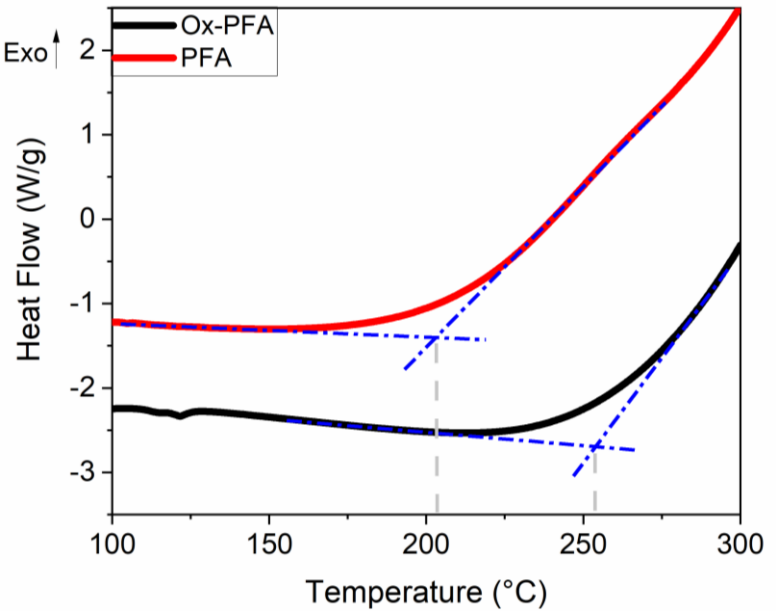

Figure 4.8-7. Curves from the oxidation onset temperature experiments of PFA (red) and Ox-PFA (black). The dashed lines guide the eyes to the onset temperature.

Chapter 5.
Exploring new horizons for poly(furfuryl alcohol) by exploiting side reactions

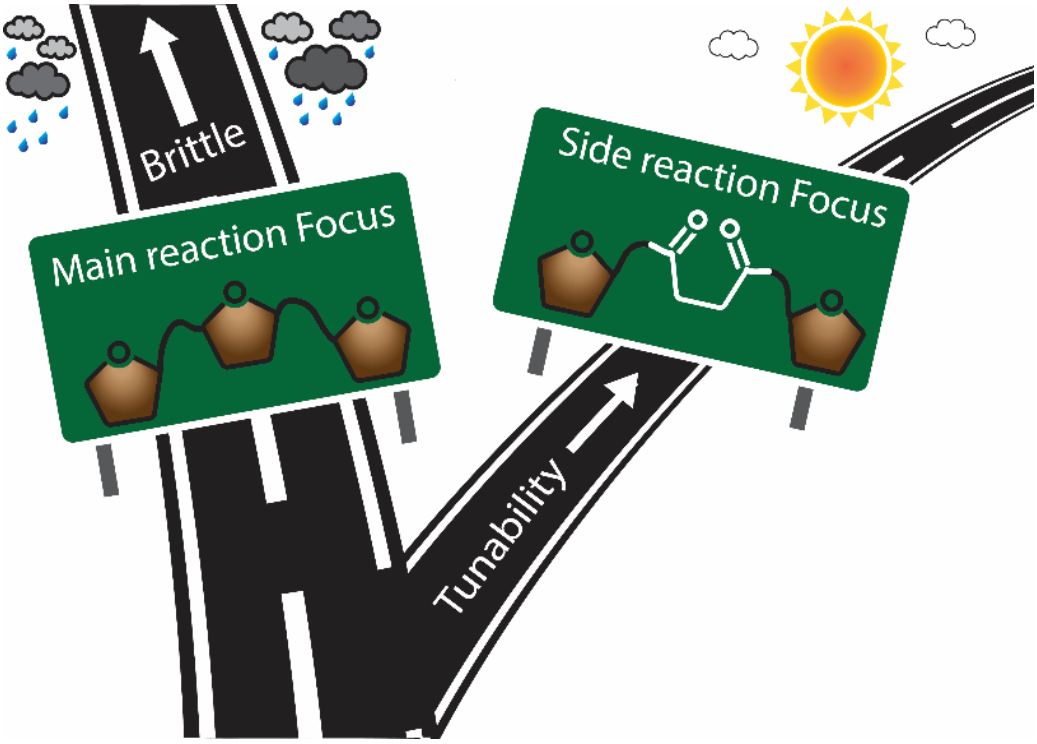

Based on

Delliere, P.; Guigo, N. Exploring New Horizons for Bio-Based Poly(Furfuryl Alcohol) by Exploiting Functionalities Offered by Side Reactions. *ACS Macro Lett.* **2022**, *11*, 1202–1206. https://doi.org/10.1021/acsmacrolett.2c00427.

Delliere, P.; Antonczak, P.; Guigo, N Impact of amine functionalization on poly(furfuryl alcohol) properties. *Polymer testing*. submitted**.**

In previous chapters, the C=O content of PFAs was quantified and somewhat optimized (chapter 2). In addition, their chemical environment was assessed (chapter 3) and an oxidation-induced surface crosslinking phenomena was observed and explained. Its impact on the properties of PFA materials was assessed (chapter 4).

In this chapter, the carbonyls presence in PFA are exploited to reach new materials with tunable properties. To do so, functionalization of carbonyls with amines was performed to give rise to PFA/Amine materials.

Section 5.1 regroups the experimental details common to all the sections. As the procedures vary between the sections, the experimental details specific to each section is reported directly inside the sections.

Section 5.2 consists in a preliminary study where Priamine 1071, a large and flexible amine, is employed as a softening agent. The chemical links between the amine and PFA are investigated. In addition, the dependency of the materials' properties as function of the amount of Priamine introduced is assessed together with a short stability and recyclability study.

Section 5.3 has two main objectives. The first one is to evaluate the influence of different amines' structures on the properties of PFA/Amine materials. The second one is to assess the impact of the curing atmosphere (oxidative, non-oxidative) on the properties of PFA/Amine materials.

Section 5.4 deals with the influence of several parameters on the properties of PFA/Amine materials. First the influence of the starting PFA's conversion degree, i.e., prior to the reaction with amines, is assessed. Then, the impact of the basicity of amines on the acid-catalyzed polymerization of FA is also discussed.

5.1 Experimental section, general

Materials:

Furfuryl alcohol (96 %), maleic anhydride (99 %), ethyl acetate (98 %), sulfuric acid (96.5 %) were supplied by Merck. Ethanol (96 %v) was acquired from VWR. Priamine 1071 was kindly provided by Croda (NH_2 content 3.39 mmol.g^{-1})

Maleic anhydride (99 %), urea (99.5 %) Jeffamine D-2000 (1.0 mmol.g^{-1} of NH_2), 2,5-bis(aminomethyl)furan (95 %), isophorone diamine (99 %) and hexylamine (99 %) were purchased from Merck. Ethyl acetate (99 %), 1,6-diaminohexane (98 %) and potassium hydroxide (99 %) were brought from Carlo-Erba. Huntsman provided the Jeffamine D230 (8.4 mmol.g^{-1} of NH_2) and VWR the ethanol (96 %v)

Preparation of PFA resins

PFA resins were prepared in batches constituted of 150 g of furfuryl alcohol (FA) in a 500 mL round-bottom flask, 17 g of water and 3 g of maleic anhydride. The components were mixed at room temperature until completely homogeneous. Then the flask was heated in an oil bath. The heating time and temperature varied depending on the conversion degree desired. More details are available in Table 5.1-1.

Table 5.1-1. Details regarding the unfunctionalized PFA pre-polymers (starting PFA).

Conversion degree (α)	Pre-polymerization time (80 °C)	Pre-polymerization time (120 °C)	C=O content (mmol.g^{-1})	Pre-curing time (130°C)
0.3	30 mins	/	2.4 ± 0.1	1 h 30
0.7	1 h 30	/	2.8 ± 0.1	50 mins
0.8	2 h 40	/	3.2 ± 0.1	40 mins
0.9	2 h 40	30 mins	3.62 ± 0.1	20 mins
0.95	2 h 40	2 h 30	4.6 ± 0.2	20 mins

Already reported characterization procedures

The determination of carbonyl contents (potentiometry), conversion degrees and acquisition of FTIR spectra were performed as in section 2.1. The elemental analyses were conducted as described in section 4.1. Conversion degrees and C=O content of PFA resins are reported in Table 5.1-1. ^{13}C NMR spectra were acquired following the procedure described in section 4.1.

Functionalization of PFA Resins and curing

The functionalization of PFA resins with Amines was performed as follows. The masses of amines were calculated using Equation 5.1-1 combined with Equation 5.1-2 or Equation 5.1-3. Batches were between 20 and 50 g. PFAs were dissolved in 150 mL ethyl acetate in a 250 mL round-bottom flask. The amines were diluted with 20 mL of ethanol and added slowly to the flask. The flask was placed in a heated oil bath under reflux and kept there for 4 hours to ensure conversion of ketones. The content of the round-bottom flask was poured into a crystal dish and left to evaporate overnight. The next steps are specific to each section and more details are given thereafter.

$$NH_2/C=O\ stoichiometric\ ratio = \frac{moles\ of\ NH_2}{moles\ of\ C=O} \quad \text{Equation 5.1-1}$$

$$m_{Amine} = \frac{Carbonyl\ content * m_{PFA} * NH_2/C=O\ stoichiometric\ ratio}{Amine\ content} \quad \text{Equation 5.1-2}$$

$$m_{Amine} = \frac{Carbonyl\ content * m_{PFA} * M_{Amine} * NH_2/C=O\ stoichiometric\ ratio}{Number\ of\ NH_2\ function} \quad \text{Equation 5.1-3}$$

Shore Hardness test

The hardness (Shore D) of samples thicker than 5 mm was measured with a Kern & Sohn GmbH durometer. Ten attempts were done on several spots of each specimen. The results are presented as the average and standard deviation of these attempts.

Thermogravimetric Analysis

A TGA 2 from Mettler-Toledo was used to investigate the degradation of the PFA/Amine materials under oxidative conditions. The scans started at 35 °C to reach 800 °C at a speed of 10 °C.min^{-1} under an air flow (50 mL.min^{-1}).

Dynamic Mechanical Analysis

DMA1 from Mettler-Toledo was employed to assess the thermomechanical properties of the samples. The tensile mode was used. The DMA scans started at -80 °C to reach 300 °C at a speed of 2 °C.min^{-1}. The oscillation frequency was set to 1 Hz along with 0.1 % displacement amplitude and a force amplitude of 0.1 N. The maxima of tan (δ) was assimilated as the glass transition temperature (T_g) of the materials.

Crosslink density was calculated using the Fox-Flory Equation 5.1-4 where E' represents the elastic modulus at T_g + 50 °C, T is the temperature and R is the ideal gas constant. [374, 375]

$$\nu = \frac{E'}{3RT} \quad \text{Equation 5.1-4}$$

Uniaxial tensile tests

The uniaxial tensile tests were conducted on an EZ-LX from Shimadzu. Excepted for section 5.2, ISO 527-2-1BB, specimens were tested with a 1 kN load cell, a gauge length of 21 mm and at a crosshead speed of 1 mm.min^{-1}. The stress and strain were recorded for seven measurements. The results are presented as the average and standard deviation of the attempts. The tensile toughness was calculated as the area beneath the stress (MPa) – strain (mm/mm) curve.

Gel fraction

Gel fraction experiments were performed by submerging about 80 mg of sample in 15 mL of ethyl acetate for 48 h at 25 °C. Then, the solvent was removed and the samples washed with ethyl acetate before undergoing a vacuum drying step for 16 h. The gel fraction was calculated using Equation 4.1-1 were m_i stands for the initial mass and m_d the dry mass.

$$Gel\ fraction\ (\%) = (1 - \frac{m_i - m_d}{m_i}) * 100 \quad \text{Equation 4.1-1}$$

Grinding procedure

A GT-300 Ball-Mill from POWTEC was used. The polymers were placed in the stainless-steel jars and cooled-down in liquid nitrogen prior to each cycle. This step is crucial if the T_g of the samples is below 40 °C. Otherwise, the samples stick to the jars and are not ground. The ball-mill operated at 1500 RPM for 2*2mins.

5.2 Preliminary investigations: Priamine 1071

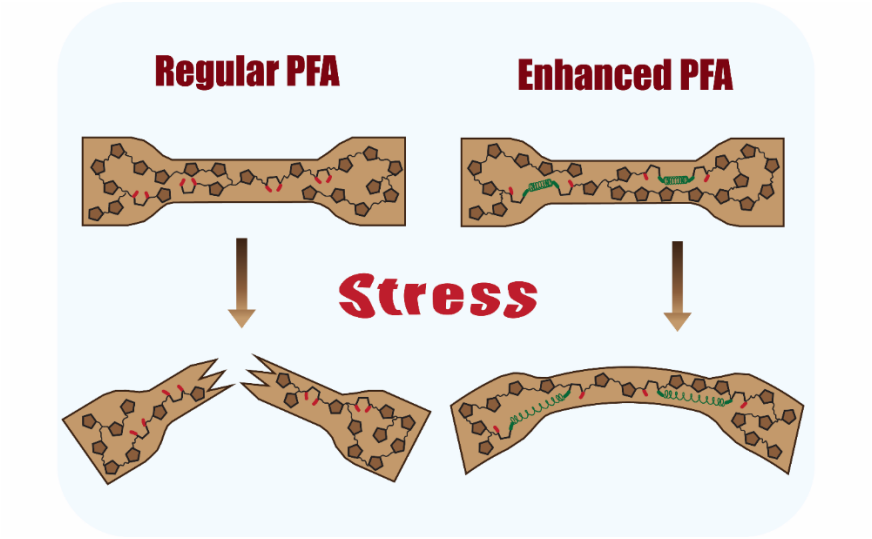

Figure 5.2-1. Section 5.2 graphical highlights

The aim of this section is to expand the possible applications of PFA. Therefore, advantage can be taken from the so-called "self-functionalizing" ability of PFA. Indeed, chapter 2 demonstrated a significant occurrence of carbonyl moieties in PFA. They are produced within the PFA's structure during the polymerization through ring-opening side-reactions. Consequently, these 'self-generated carbonyls' can be used as anchor points for further functionalization without prior oxidation, as needed for polysaccharides. [376, 377] Here, the focus is on the reaction between ketone and amine as a mean to tune the thermomechanical properties of PFA, with a focus on increasing the ductility of the material. To prove that PFA can be tuned via its open structures, a flexible C36 bio-based fatty diamine (i.e., Priamine 1071) was chosen to react with carbonyls. The formation of connections between PFA's carbonyls and primary amine-bearing flexible segments should impact the mechanical properties of PFA, which is known to be a very hard and brittle material. [183] Moreover, with between 100 and 1 000 tons manufactured or imported into Europe per year, the Priamine family belongs to the small group of commercially available bio-based amines.[378, 379] These Priamines are usually employed as epoxy cross-linkers [375], for polyamides [380], and as soft blocks in polyurethanes[381, 382], polymethacrylates[383] and polyimines.[384]

5.2.1 Experimental details specific to section 5.2

Section 5.2 was a preliminary study on the functionalization of PFA with amines using Priamine 1071. The preparation procedures were improved for the next studies.

The procedure for the preparation of samples for section 5.2 is illustrated in Scheme 5.2-1. Here, the PFAs had conversion degree 0.70. Table 5.2-1 reports the sample labels together with their proportion of PFA and Priamine 1071. Priamine 1071 will be labeled "PA".

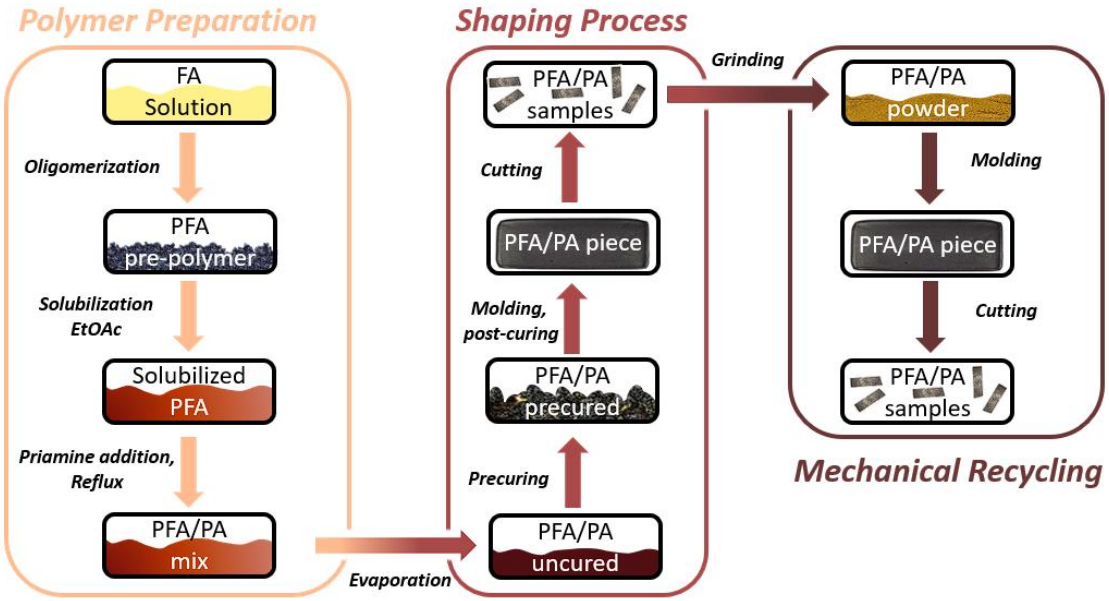

Scheme 5.2-1. Process of sample preparation relative to section 5.2.

Once evaporated, the PFA/PA were precured 50 mins at 130 °C. The samples were then compression molded at 150 °C and ≈ 10 bars for 2 h and post-cured in their molds for five additional hours. For the mechanical recycling, PFA/PA materials were ground using a ball mill and the powders were compression molded at 150 °C under 25-35 bars for two hours. For the uniaxial tensile tests, PFA/PA samples were cut in parallelepiped rectangles and a gauge length of 10 mm was used.

The determination of the T_g was performed using a DSC 1 from Mettler-Toledo. 5-10 mg of samples were introduced in 40 µL closed aluminum pans. The DSC was stabilized at -70 °C for 20 mins before increasing the temperature to 150 °C at 50 °C.min^{-1} under 25 mL.min^{-1} of air. The inflexion point was assimilated to the T_g of the polymers.

Table 5.2-1. Masses of compounds used for the functionalization of PFA with Priamine 1071.

Sample name	NH_2/C=O Stoichiometric ratio	Mass of PFA (g)	Mass of Priamine (g)	%w PFA
PFA	0	20	0	100.0
PFA/PA 0.1	0.1	20	1.8	91.7
PFA/PA 0.25	0.25	20	4.6	81.3
PFA/PA 0.5	0.5	20	9.2	68.5
PFA/PA 1.0	1	20	18.4	52.1

The stability of PFA/PA 1 towards hydrolysis was pursued by exposing 750 mg of powdered PFA/PA 1 to various conditions before drying and FTIR analysis. The test conditions included respectively exposure to water, acidic water (0.1 M), 50/50 %v ethanol/acidic water (0.1 M) and 50/50%v THF/acidic water (0.1 M). Sulfuric acid was used to acidify the water. All experiments were conducted for 2 hours under reflux. After filtering, washing and vacuum drying, the gel fractions were calculated according to Equation 4.1-1 and the powders were analyzed by FTIR spectroscopy. The conditions and gel fractions are reported in Table 5.2-2.

Table 5.2-2. Conditions used for the exposure of PFA/PA 1 to water and aqueous mixtures and gel fraction.

Sample Name	Volume of water (mL)	Volume of co-solvent (mL)	Gel fraction (wt. %)
EtOH/ Acidic water 0.1 M	12.5	12.5	93.7
THF/acidic water 0.1 M	12.5	12.5	92.3
Acidic water 0.1 M	25	0	91.1
Water	25	0	89.5

5.2.2 Structure-property relationship of Priamine functionalized PFAs

The NH_2/C=O stoichiometric ratio spanned from 0.1 to 1 and the thermo-mechanical properties of the modified PFA were assessed, with a special emphasis on the toughness. Scheme 5.2-2 schematically depicts the obtained thermoset and Table 5.2-1 regroups amounts of PFA and Priamine 1071 for this study.

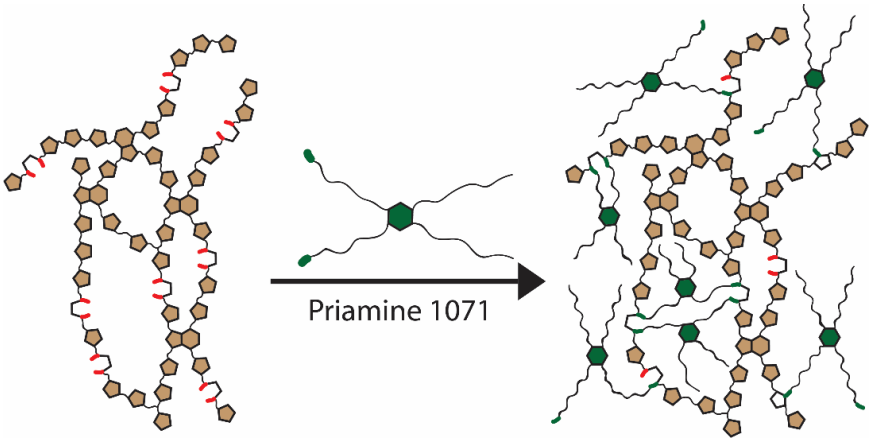

Scheme 5.2-2. Schematic representation of the imination of PFA - prepolymer by Priamine 1071.

First, the presence of C=N bonds was validated by means of Fourier-Transform Infra-Red spectroscopy (FTIR) and solid state ^{13}C NMR investigations. The spectra of cured resins are shown in Figure 5.2-2A (NMR) and Figure 5.2-2B (FTIR).

In Figure 5.2-2A, the intensity of the ketone peak at 208 ppm decreases when the stoichiometry of introduced Priamine increases. The peak at 171 ppm in PFA is attributed to ester groups (cf Table 1.3-2). In PFA/PA samples, this peak increases and is slightly shifted to 165 ppm. This is consistent with the formation of imines bonds in the 160-170 ppm region. [385, 386, 387, 388]

In Figure 5.2-2B, the carbonyl stretching band at 1710 cm^{-1} in PFA (cf Table 1.3-3) progressively decreases with the increasing addition of Priamine. This decrease of the C=O band is accompanied by the increase of the C=N band at 1656 cm^{-1}, thus showing the condensation of carbonyl and amine moieties into imines. [388, 389, 390, 391, 392, 393] The height ratio H_{1710}/H_{1656} was calculated and found to have a good linear correlation with the amount of Priamine introduced in the system, as depicted in Figure 5.6-1. However, a small amount of carbonyl is detected in PFA/PA 1 sample in both NMR and FTIR spectra. The fact that a small proportion of carbonyl remains unmodified can be associated with the steric hindrance of Priamine, as it has been shown in chapter 2(SECTION) that large derivatizing agents employed for the C=O quantification can have difficulties reaching carbonyl moieties within PFA. Carbonyls can also form after the functionalization of PFA through the oxidation route (chapter 4).

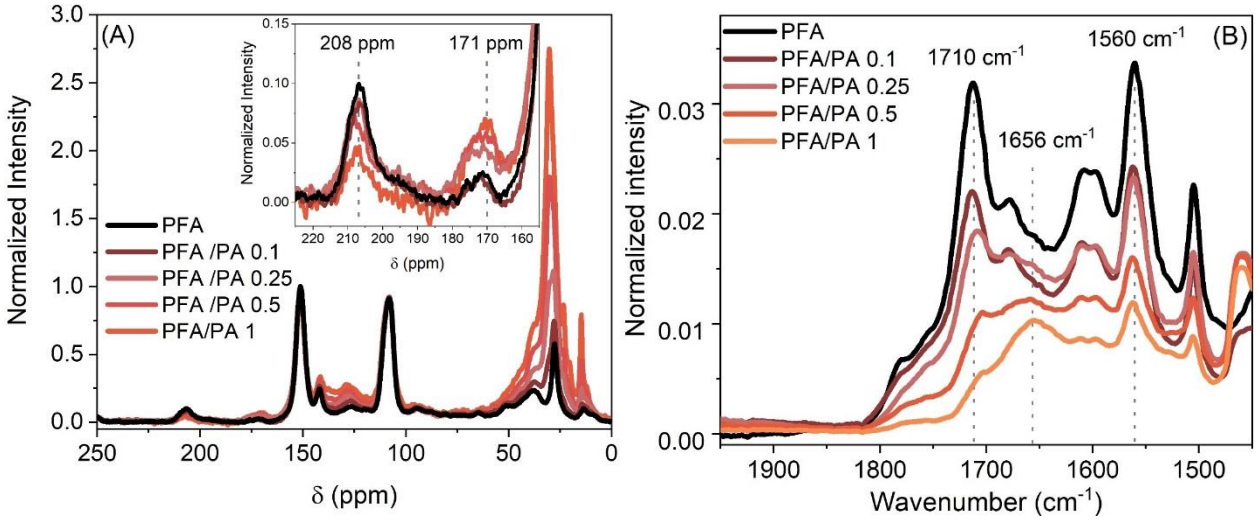

Figure 5.2-2. CPMAS ^{13}C Solid state NMR (A) and magnified FTIR (B) spectra of PFA and Priamine-functionalized PFA.

In PFA the hydrolytic and oxidative cleavage of the furan ring may yield a variety of carbonyl moieties, acetals and enols as highlighted in chapter 3. Some examples of PFA's carbonyls are depicted in Scheme 5.2-3. This array of structure may influence the nature of interactions between PFA and amines.

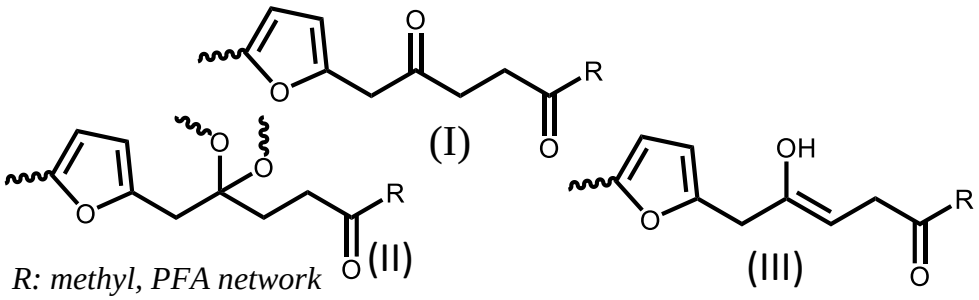

Scheme 5.2-3. Example of carbonyl moieties found in PFAs.

Earlier, it was proposed that the links between PFA and amines are only Schiff bases (C=N) on the basis of the appearance of a peak at 170 ppm in ^{13}C NMR and a FTIR band at 1656 cm^{-1}. Nonetheless, if the carbonyls in PFA were only based on the structure (I) in Scheme 5.2-3, their reaction with primary amines should yield pyrroles. Indeed, when a model compound such as 2,5-hexanedione is reacted with a primary amine the major product is a pyrrole, as depicted in Scheme 5.2-4. On the ^{13}C NMR spectra presented in Figure 5.2-2A, a slight shift is visible from about 125 ppm to about 130 ppm. The magnified ^{13}C ssNMR spectra in Figure 5.6-2 showcases this shift. Such shift could be consistent with the presence of pyrroles. However, determining the proportions of pyrroles compared to Schiff bases is very challenging as many functional groups are present in PFA/Amine systems which leads to overlapping signals.

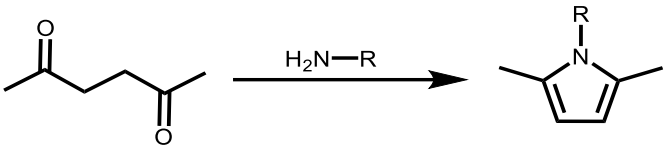

Scheme 5.2-4. Formation of pyrroles from 1,4-diketones through the Paal-Knorr reaction.

Taking into account the structures in Scheme 5.2-3, the reaction of the carbonyls with primary amines should yield the products highlighted in Scheme 5.2-5. The structure (I) is probably mostly yielding the pyrrole structure (IV) and structure (V) in minor proportions. Finally, the enol structure (VI) and ketal structure (VII) might be responsible for Schiff base bonds. In the following parts, the chemical links between PFA and amines will be referred as C=N as it englobes the possible reactions of amines with ketones, i.e both imines and pyrroles.

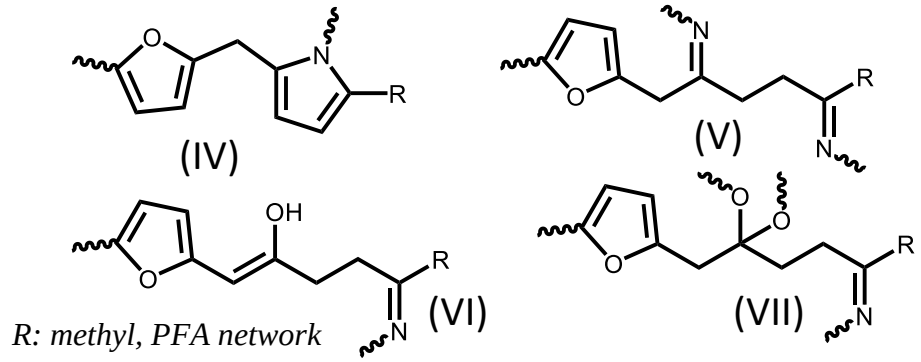

Scheme 5.2-5. Example of amine-derivatized carbonyl moieties in PFAs.

Following this spectroscopic confirmation that PFA was functionalized with Priamine, the rest of this section is dedicated to the evaluation of the thermomechanical properties. Typical stress-strain curves are depicted in Figure 5.2-3, which illustrates the progressive variations of properties using functionalization of high carbonyl content PFA with soft flexible segments. Thus, the mechanical properties of PFA resins can be tuned from a very brittle behavior for non-modified PFA towards a ductile behavior through Priamine modification (Figure 5.2-3). It thus opens the prospect to expand the portfolio of applications of PFA resins.

Figure 5.2-4 exhibits the elastic modulus, the glass transition temperature and the Shore D obtained for the different samples. Imination of PFA with Priamine creates an array of elastic moduli starting from 1 600 MPa for unmodified PFA to 20 MPa for PFA/PA 1 (E' at 20 °C DMA, extracted from DMA curves in Figure 5.6-3A). This decrease of moduli is directly linked to the T_g of the samples maximum of tan (δ), extracted from DMA curves in Figure 5.6-3B. Priamine's long aliphatic chains with intrinsic flexibility increase the free volume between chains and the possibility of molecular movements in the polymer.

The T_g of PFAs may also be extracted from DSC scans performed at high speeds. Figure 5.6-4 presents representative DSC scans of PFA and PFA/PA 1 along with the dependency of the T_g on the weight fraction of Priamine. The results follow the same tendency as in Figure 5.2-4.

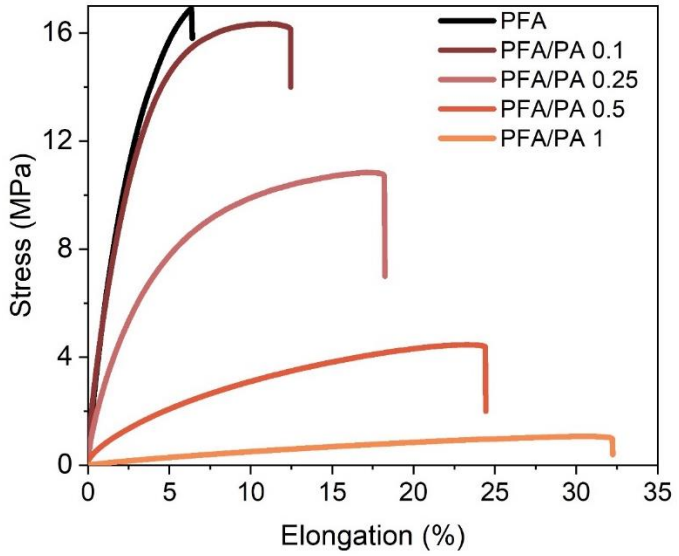

Figure 5.2-3. Examples of stress-elongation curves obtained from PFA and PFA/PA.

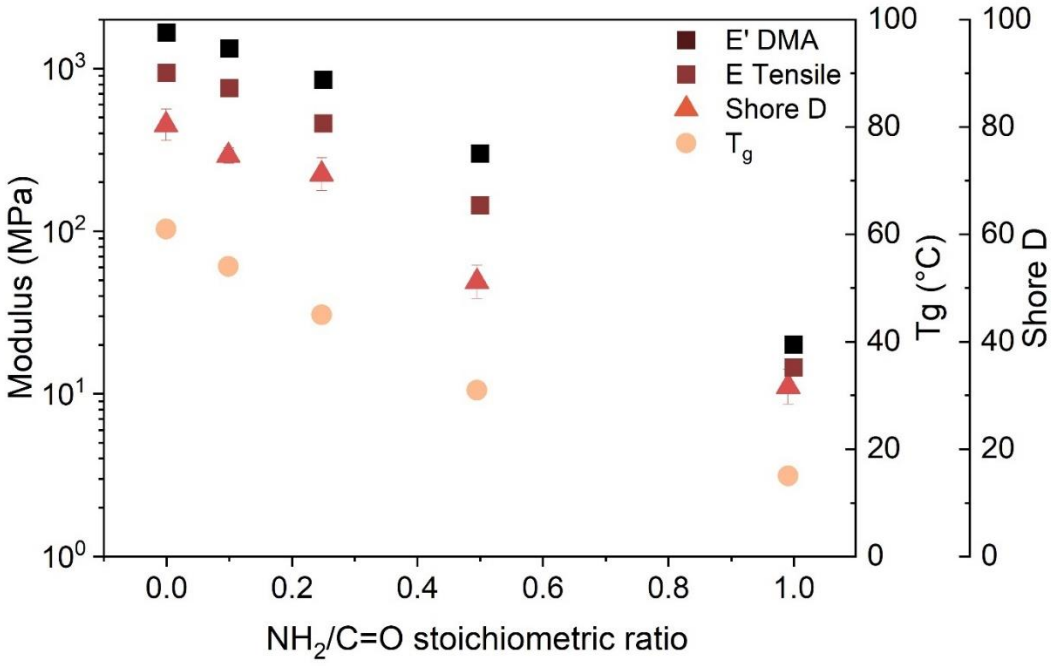

Figure 5.2-4. Variation of modulus (Young's and E' at 20 °C) and glass transition of Priamine-functionalized PFAs with the amount of Priamine introduced. The T_g was obtained from the maximum of the tan (δ) peak from DMA curves.

The above mentioned increase in flexibility is also well correlated with the Shore D measurements. Indeed, a large portion, i.e., from 80 to 30, of the Shore D range is covered by these systems, corresponding to extra hard for unmodified PFA to medium hard for PFA/PA-1.

Elongation at break and ultimate strength data were extracted from the stress-elongation curves to give Figure 5.2-5A and B, respectively. While classical PFA exhibits brittle behavior, i.e., ≈ 5 % elongation at break, the functionalization of PFA with Priamine allows it to reach up to ≈ 30 % elongation at break. This increase in ductility varies with the amount of Priamine introduced. However, such ductility comes with a decrease of the ultimate tensile strength, as can be seen in Figure 5.2-5B. Indeed, the ultimate tensile strength is reduced from 16 MPa to 1 MPa. Thus, the properties can be optimized to meet the requirements needed for a specific application.

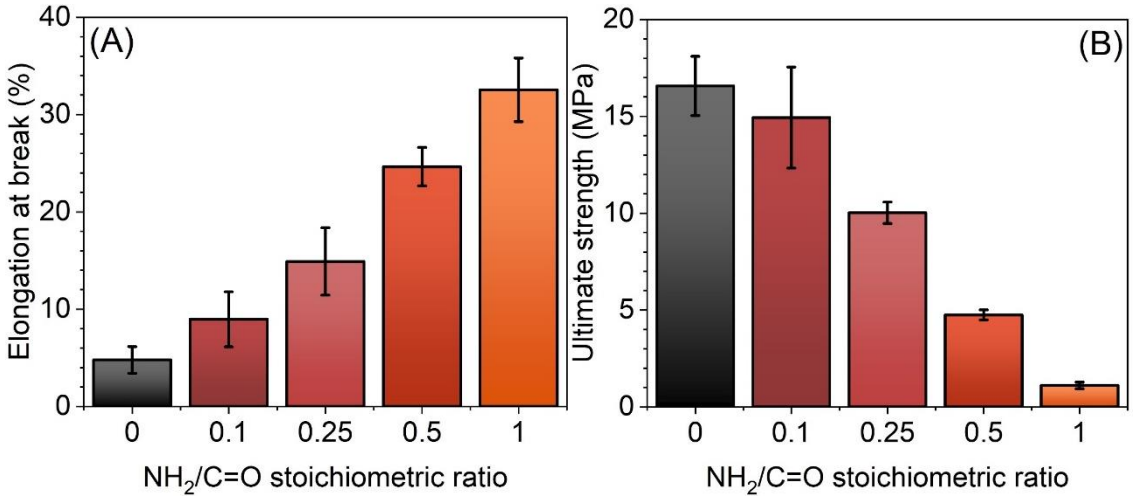

Figure 5.2-5. Variation of the elongation at break (A) and ultimate tensile strength (B) of Priamine-functionalized PFAs with the amount of Priamine introduced.

In their work, Pranger et al. [183] calculated the tensile toughness of PFA samples by integrating the area under the stress-strain curve, thus estimating the energy needed to break a cubic meter of PFA. Such an estimation is dependent on the crosshead's speed but remains a coherent metric with a fixed speed. Here, the tensile toughness of PFA and functionalized PFA are reported in Figure 5.2-6 along with the associated crosslink density obtained using the Flory-Fox law. [374]

Figure 5.2-6 depicts a bell-like curve of both toughness and crosslink density with peak values at 0.25 equivalent of NH_2. From the unmodified PFA to PFA/PA 0.25, the toughness rises from ≈ 0.5 $MJ.m^{-3}$ to ≈ 1.3 $MJ.m^{-3}$, thus more than doubling the energy needed to break the material. This behavior is closely related to the crosslink density, which also doubles (440 to 950 $mol.m^{-3}$). Therefore, the Priamine has a double effect on PFA system. First, at low concentration (i.e., 25 %mol) it mostly toughens the system by introduction of flexible crosslink nods. On the other hand, at higher concentration the plasticizing effect of Priamine 1071 takes over.

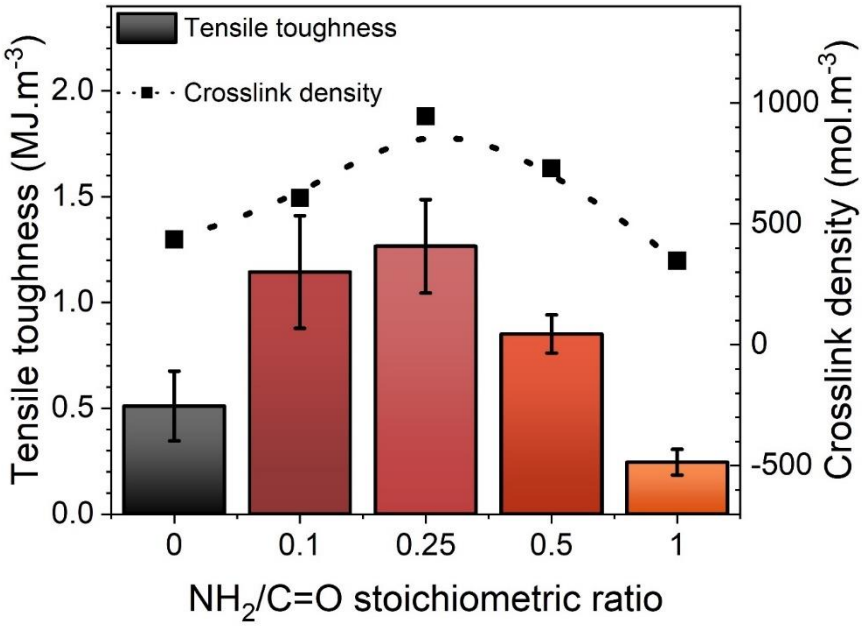

Figure 5.2-6. Variation of the tensile toughness and crosslink density of Priamine-functionalized PFAs with the amount of Priamine introduced.

5.2.3 Stability and Recyclability of PFA/PA

5.2.3.1 Stability of PFA/PA

In this section, the stability of PFA and PFA/PA samples was investigated. To do so, the thermo-oxidative degradation was assessed by TGA. The chemical resistance was first evaluated by the measurements of the gel fraction in ethyl acetate. In addition, the stability of PFA/PA 1 towards hydrolysis was checked.

The thermal resistance of the copolymers was assessed by TGA (curves in Figure 5.6-5) and the $T_{5\%}$ and $T_{10\%}$ were extracted and are reported in Table 5.2-3. The thermal resistance of PFA is maintained for all samples. Moreover, for the highest Priamine concentrations (PFA/PA 1) both $T_{5\%}$ and $T_{10\%}$ increase of about 40 °C compared to unmodified PFA.

Table 5.2-3. Degradation temperatures and gel fraction of PFA and functionalized PFAs.

Sample	$T_{5\%}$ (°C)	$T_{10\%}$ (°C)	Gel fraction (%w)
PFA	289	343	87.0 ± 0.4
PFA/PA 0.1	302	346	88.4 ± 0.4
PFA/PA 0.25	284	344	90.7 ± 1.0
PFA/PA 0.5	304	367	96.3 ± 1.3
PFA/PA 1	335	383	92.4 ± 0.1
Priamine 1071	312	346	0.0 ± 0

The gel fraction of the different samples was measured after 48 h immersion in EtOAc and the results are gathered in Table 5.2-3. The gel fraction increases from 87 wt% for PFA to 96 wt% for PFA/PA 0.5. It confirms that PFA is more cross-linked after functionalization with PA thus leading to higher stability in solvent. However, the slightly lower gel content for PFA/PA 1 (92 wt%) compared to PFA/PA 0.5 can be explained by its lower cross-link density (Figure 5.2-6) together with a facilitated swelling in the rubbery state (T_g PFA/PA 1 = 16 °C – Figure 5.2-4).

Imine groups can be hydrolyzed back to carbonyls. To highlight the stability of the newly formed imines, the PFA/PA 1 sample was exposed to different hydrolytic conditions (water, 0.1 M acidic water, acidic water/THF or acidic water/ethanol). Table 5.2-2 shows that the gel content after the different ageing remains very high (≈ 90 %w and above) and the released part is not correlated with the PA content (i.e 47.9 %w of PA in PFA/PA 1). Moreover, FTIR measurements conducted on the PFA/PA 1 samples and exposed to different hydrolytic conditions (Figure 5.2-7) did not show significant differences with the reference material. The imine band at 1656 cm^{-1} remains unaffected indicating that the hydrolysis did not occur in these relatively mild conditions. Only the sample exposed to 0.1 M acidic water showed a slight broadening of the imine band correlated with a slight increase of the carbonyl band (compared to the non-aged sample) suggesting a somehow limited hydrolysis or a modification of the imine environment.

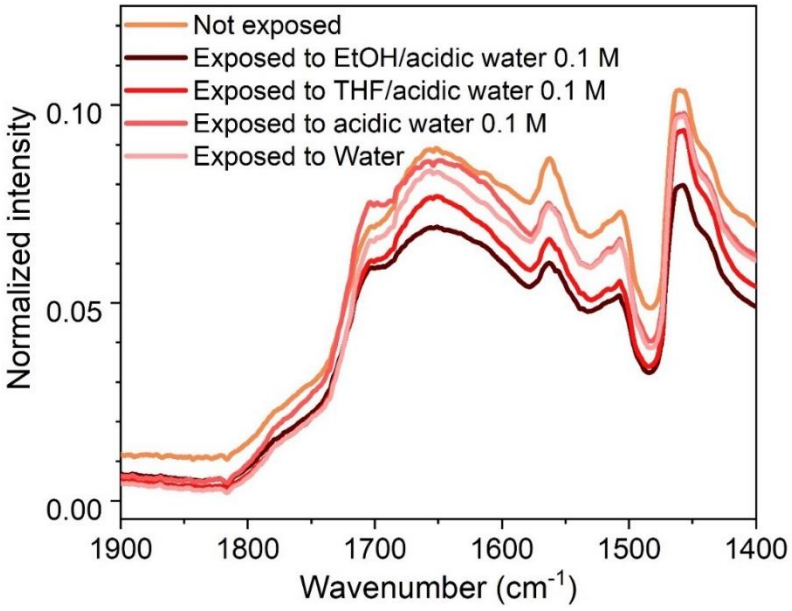

Figure 5.2-7. FTIR spectra of the PFA/PA-1 powder exposed to different hydrolytic conditions.

The PFA/PA 1 sample was immersed in water for respectively 2 and 6 days to highlight its water stability. The resulting DMA scans (Figure 5.2-8) shows that the α-relaxation peak and the rubbery behavior is not affected by the water exposure thus confirming the stability of imine bonds in mild conditions. Slightly lower glassy modulus and a slight increase of a secondary relaxation peak (maximum at -30 °C) are observed after progressive immersion in water that could have facilitated some local mobility (small plasticizing effect).

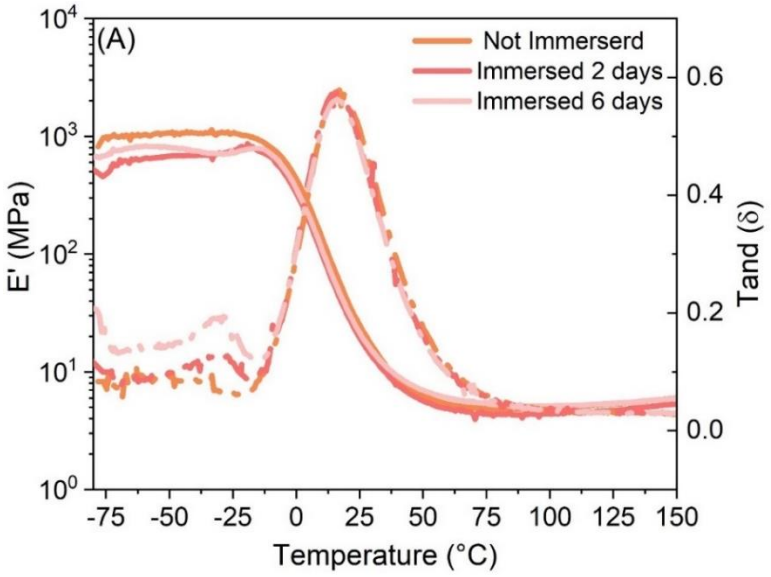

Figure 5.2-8. DMA scans showing *E*' curves (plain lines) and tan (δ) curves (dash dot lines). The samples are a non-immersed PFA/PA 1 sample, and a PFA/PA 1 sample immersed in water (25 °C) respectively for two days and six days.

Finally, a PFA/PA 1 sample was left to age for three months at room temperature in sealed bags. The DMA curves of a fresh and three months old PFA-PA 1 are available in Figure 5.2-9. The *E'* curve shifts towards higher moduli and the tan (δ) peak is both larger and less gaussian for the aged sample. In addition, the T_g of the aged sample is higher by about 20 °C. These results highlight either an uncompletion of the curing or other phenomena occurred during the ageing period. The latter hypothesis being supported by the non-gaussian shape of the tan (δ) peak which suggests an inhomogeneous macromolecular network.

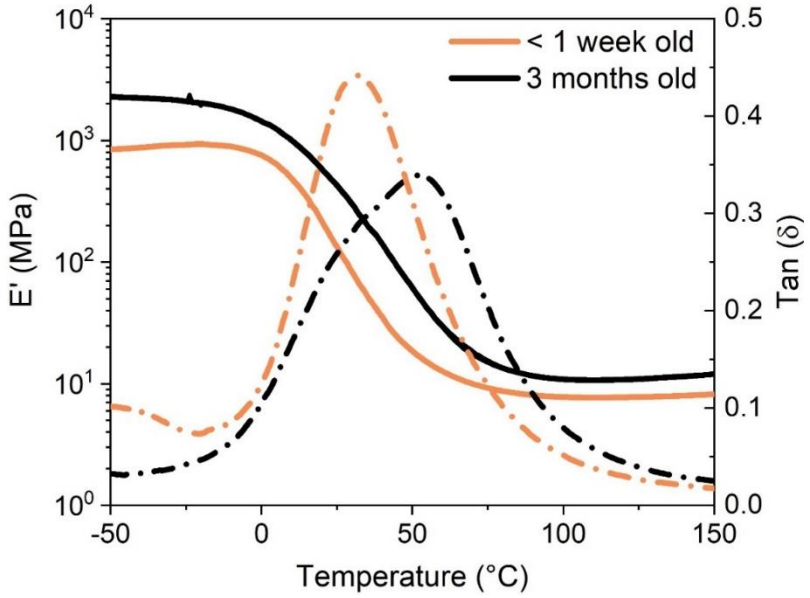

Figure 5.2-9. DMA scan of two PFA/PA 1 samples. The orange one is less than a week old and the black one is three-month-old. Plain lines correspond to the storage modulus and the dash-dot lines to the tan (δ).

5.2.3.2 Mechanical recycling of Priamine functionalized PFA

In this section, specimens of PFA and PFA/PA were ground with a ball-mill and the polymers were compression molded once again. The properties of the reprocessed specimens are briefly overviewed in the following. Unexpectedly, neat PFA showed a mechanical reprocessability.

Figure 5.2-10 displays the thermomechanical properties of the recycled PFA and PFA/PA samples. Over the reprocess cycles, the T_g of the polymers tended to increase by 5-10 °C at each cycle, excepted the PFA/PA 1. The *E'* at 20 °C from the DMA curves also tend to increase although the higher the Priamine content the lower the rise of *E'*. In addition, both the crosslink density and the hardness increased with the reprocessing. The samples were also subjected to tensile tests. The results are gathered in Figure 5.6-6.

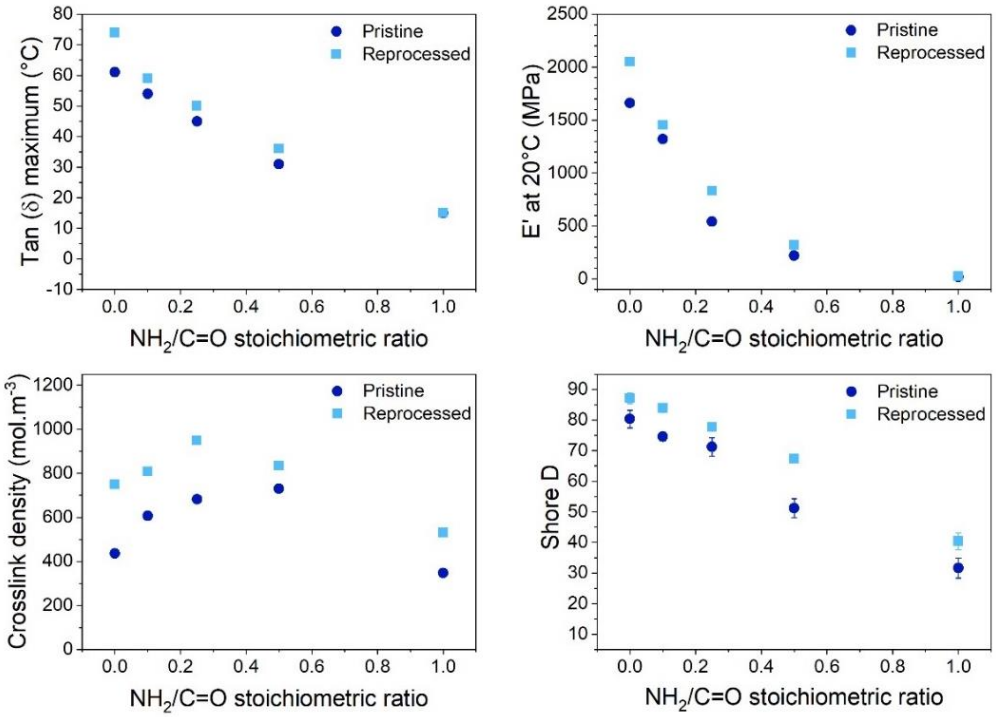

Figure 5.2-10. Mechanical Recycling PFA/PA: thermomechanical properties.

First, the successful realization of tensile test shows that PFA and PFA/PA cured at 150 °C and not aged can be reprocessed into cohesive samples. The Young's moduli of the samples behave similarly, as the *E'* at 20°C from Figure 5.2-10, i.e it increases after the reprocessing. This is less pronounced for higher amounts of Priamine. On the elongation at break, tensile toughness and ultimate strength it is hard to draw a conclusion as the standard deviation tend to overlap between the cycles. The exception being lower tensile toughness and ultimate strength for neat PFA.

To conclude on this part, it is possible to mechanically reprocess unaged PFA and PFA/PA if they were cured at 150 °C for less than 7 h. Yet, it is difficult to attribute this phenomenon to the presence of reversible reaction (imination, Diels-Alder). It could also very well be the presences of other, irreversible reactions, that did not occur during the fabrication of the materials (polycondensation, aromatization). The later hypothesis being more likely, especially as the DMA of PFA/PA 1 in Figure 5.2-9 shows a hardening of the polymer overtime and the fact that PFAs such as the one presented in Chapter 4 cannot be mechanically reprocessed as easily (cf annexes).

5.2.4 Conclusion Preliminary investigations

In summary, the aim of this section was to pave the way to use carbonyl moieties within poly(furfuryl alcohol) as a means to extend the possible applications of this thermoset. Indeed, PFA "self-functionalizes" during its polymerization though furan-ring opening. Consequently, chemically available ketones are ready to be the key to unlocking a latent potential for tunability.

In this work, PFA was treated with Priamine 1071. The resulting PFA/PA displayed a range of behavior from brittle to ductile. Elongation at break ranged from 5 to 35 % while tensile toughness could be doubled while maintaining the thermal resistance of PFA. Consequently, a fully bio-based and flexible thermoset with tunable properties can be prepared by exploiting the functionalities self-produced during polymerization.

However, further research is still needed to better understand the recyclability and variation of properties of Priamine-functionalized PFAs.

5.3 Effect of the amines' structure and post-curing environment

The aim of this section is to highlight the factors influencing the thermomechanical properties of the PFA/Amine materials. First, the influence of the amines' structure is studied. Additionally, the effect of the post-curing environment (oxidative or non-oxidative) is assessed.

In a first part, different amines bearing various structures were selected to understand to which extent the chemical structures of the employed amines (or urea) can impact the tunability of PFA resins (amine structures in Scheme 5.3-1). For this purpose, flexible and rigid amines were selected and their impact on the macromolecular network was assessed.

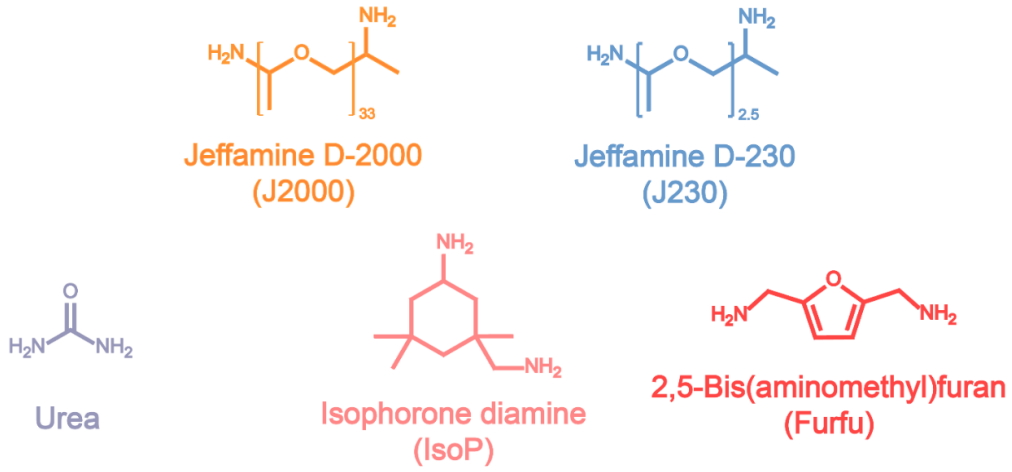

Scheme 5.3-1. Structures of the amines and urea selected for derivatization.

In a second part, the impact of the curing atmosphere (i.e inert or oxidative atmosphere) on the properties of PFA/Amine materials was evaluated. As demonstrated in the chapters 3 and 4, the furans located on the surface of PFA materials are sensitive to oxidative ring-opening. When exposed to air, these furans at the top-surface can open into conjugated 1,4-dicarbonyls. These conjugated carbonyls are prone to Diels-Alder cycloaddition with other furans in PFA. Consequently, additional crosslinking nods are created which induces a surface hardening. This process is accompanied by a darkening of PFA. Hence, the importance of this phenomenon on PFA/Amine properties was assessed.

Section 5.3 aims at understanding, the influence of the amines' structure on the properties of PFA/Amine materials. In addition, the influence of the post-curing environment (oxidative or inert) was assessed.

5.3.1 Experimental details specific to 5.3

In section 5.3, PFAs had a conversion degree of 0.80, i.e. 3.2 ± 0.1 mmol.g^{-1} of C=O. The sample preparation procedures used in section 5.3 are illustrated in Scheme 5.3-2. The synthesis of PFA/Amine materials were conducted as in described in section 5.1.

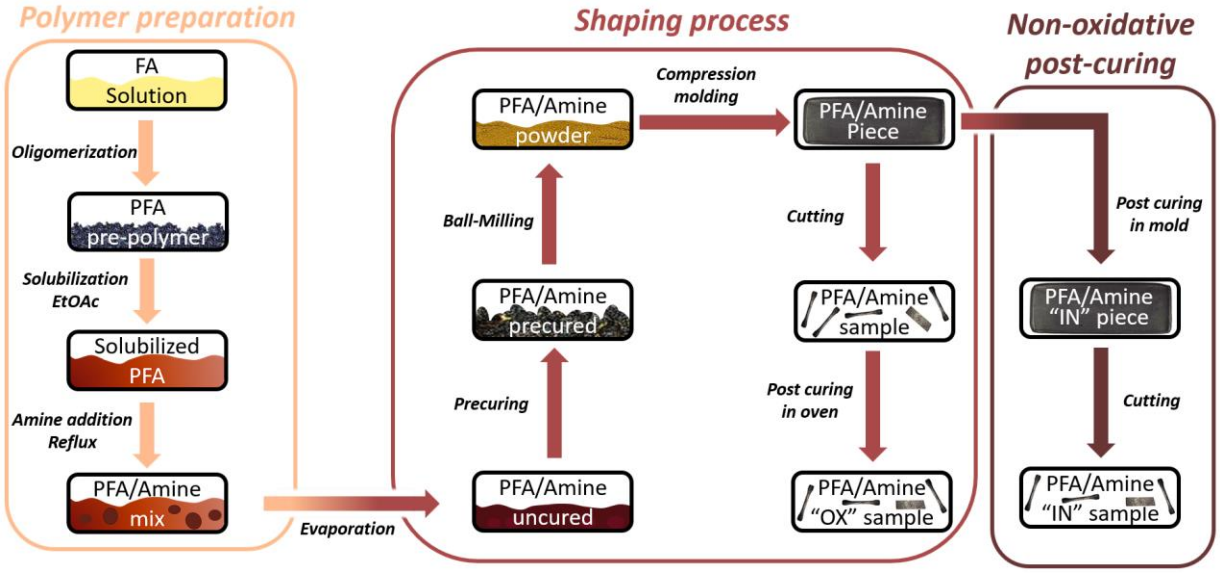

Scheme 5.3-2. Process of sample preparation relative to section 5.3.

Once the PFA/Amine solutions were evaporated and dried, the functionalized PFAs were heated at 130 °C in a forced convection oven for up to 90 mins with occasional stirring to reach the rubbery state. Then, the rubbers were ground using a ball mill. The powders were then compression molded at 150 °C under 25 – 35 bars for 2 hours in a heated press. The pictures in Figure 5.6-7 illustrate the molds, backing mold and heated press used for the experiments.

From here, two protocols were used. In most cases, the pieces were removed from the molds and cut in parallelepipeds for DMA, hardness and TGA measurements or in dumbbell shapes (ISO 527-2-1BB) using a specific cutter for the tensile tests (cf Figure 4.8-1). The cutting was performed at 150 °C to avoid breakage of the samples. Then, the specimens were post-cured in an oven at 150 °C for 3 hours.

In the second protocol, the samples were not removed from the molds and the post-curing was performed in the molds (150 °C, 3 h). Then the samples were cut using the same procedure. In the study, when comparing the first and second protocol, the terms "OX" and "IN" serve as distinction. If nothing is mentioned, the post-curing occurred in the oven.

5.3.2 Effect of the amine's chemical structure

Section 5.3.2 is dedicated to the influence of the chemical structure of the amines on the properties of PFA/Amine materials. Scheme 5.3-1 presents the selected amines and their abbreviation. Their molar masses ranged from 60 $g.mol^{-1}$ to 2 000 $g.mol^{-1}$. The selection included difunctional linear and cyclic amines as well as urea. The purpose of the larger aliphatic amines was to introduce flexibility in the macromolecular network. The aim of the shorter and cyclic ones was to potentially increase the rigidity of the network. It should be noted that the mass ratio of amines toward PFA is variable due to the large gap in molecular weight gap between the amines. Table 5.3-1 displays the mass percent of PFA for each sample.

The reaction between the C=O in PFA and the NH_2 was verified by means of FTIR spectroscopy in the same manner as in section 5.2. The magnified spectra of the PFA/Amine materials are available in Figure 5.3-1 and the spectra of pure amine are shown in Figure 5.6-8. Here, all the materials showed less intense C=O peak than the standard PFA. Most materials exhibited the formation of a C=N bond around 1650 cm^{-1}. This confirms the linkages between the amines and PFA. [328] Pyrroles are also likely formed as it was suggested by Mohajeri et al. in systems comprising an epoxy, an amine and a PFA. [219]

The case of urea is slightly more complex as other bonds than C=N and pyrroles are formed. [394] Nonetheless, the diminution of the C=O compared with the furanic C=C (1550 cm^{-1}) attest for interactions between PFA and urea. Even though the amines were introduced in stoichiometric amount with respect to the carbonyls, C=O signals are still visible in all the materials as in PFA/PA systems.

The properties of the PFA/Amine materials were assessed by DMA, TGA and shore D hardness. The corresponding DMA curves are available in Figure 5.3-2. Table 5.3-1 gathers data obtained from the evaluation of the DMAs and TGA scans and the Shore D values. The TGA scans of the materials and the pure amines are available in Figure 5.6-9 and Figure 5.6-10.

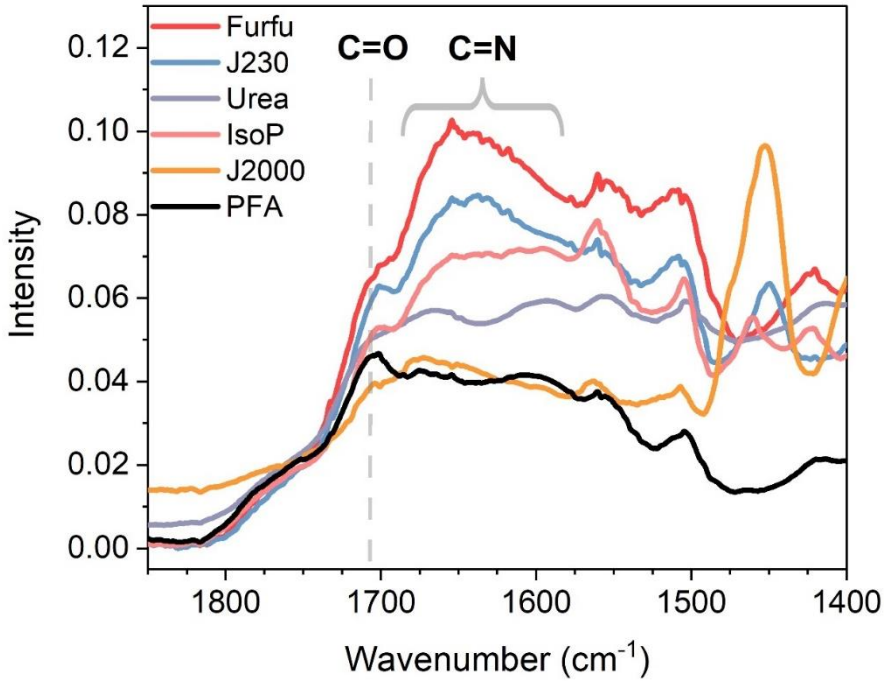

Figure 5.3-1. Magnified FTIR spectra of PFA reacted with several amines. The samples were prepared at NH_2/C=O stoichiometry.

In Figure 5.3-2, PFA/J2000 stands out from the other materials. The tan (δ) maxima of the PFA/J2000 is located at the lowest temperature (-44 °C). Moreover, the peak is at least three times higher than the other samples. Three orders of magnitude separate the *E'* value at 20 °C of PFA and the PFA/J2000 samples. According to Table 5.3-1, the shore D of the PFA/J2000 sample is about 8.5 times lower than the PFA's. Such behavior is consistent with the important amount of the flexible J2000 in the material (75 %w). Indeed, with such a high concentration of J2000, the macromolecular network of PFA is highly flexibilized. Finally, the $T_{5\%}$ and $T_{10\%}$ of the PFA/J2000 sample are about 10 °C lower than PFAs'. Thus, the good thermal stability of PFA is maintained although PFA represents only 25 %w of the total. Moreover, pure J2000 has a $T_{5\%}$ near 240 °C and a $T_{10\%}$ near 260 °C. So, PFA can also be seen as a thermal stabilizer when considering J2000 based materials.

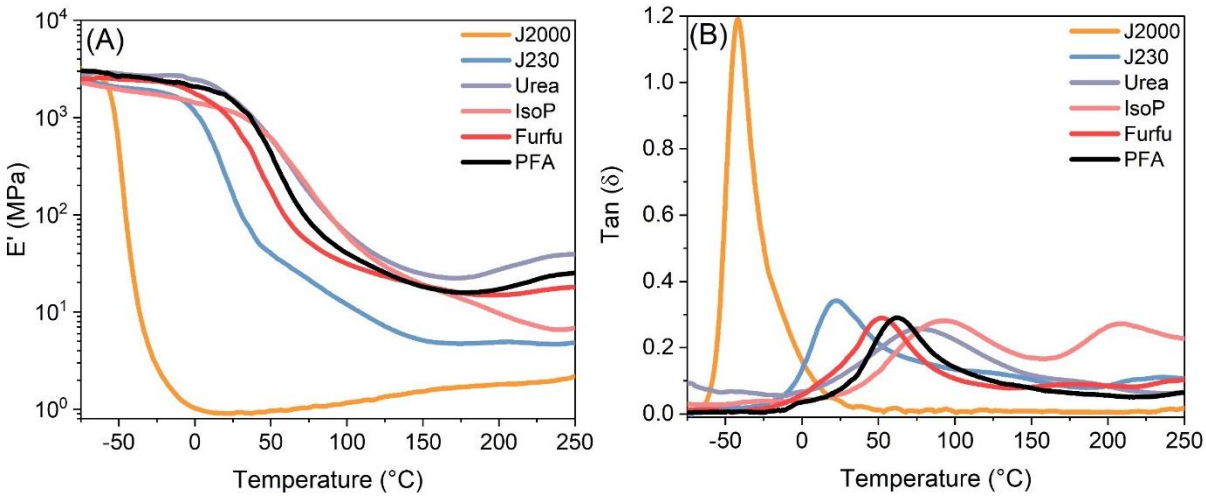

Figure 5.3-2. DMA Curves of the PFA/Amine materials, (A) *E*' and (B) tan (δ) curves. The samples were prepared at NH_2/C=O stoichiometric ratio = 1.

Table 5.3-1. Thermo-mechanical properties of the PFA/Amine materials. The samples were prepared at NH_2/C=O stoichiometry.

Sample	%w PFA	*E'* 20°C (MPa)	Tan (δ) maxima (°C)	$T_{5\%}$ (°C)	$T_{10\%}$ (°C)	Shore D
PFA/J2000	25	1.1	-44	319	350	9.6 ± 1.2
PFA/J230	72	280	20	322	356	49.1 ± 3.6
PFA/Urea	91	1800	76	284	332	79.3 ± 1.4
PFA/IsoP	79	1210	93	336	367	87.7 ± 1.8
PFA/Furfu	83	1130	52	341	364	80.4 ± 1.7
PFA	**100**	**1680**	**63**	**328**	**362**	**82.4 ± 2.1**

Regarding the other amines, both PFA/J230 presents lower T_g, *E*' at 20 °C and Shore D than PFA. However, as indicated by the $T_{5\%}$ and $T_{10\%}$ values, the thermal resistance of PFA is maintained despite the introduction of a less thermally resistant amine. Additionally, as shown in Figure 5.3-2, the rubbery plateau of PFA/J230 is lower than PFA's. Thus, J230 introduce some flexibility in the material. PFA/Urea shows a 13 °C increase of T_g together with a small increase of *E*' at 20 °C and no impact on the hardness, in comparison with PFA. Nonetheless, the $T_{5\%}$ of PFA/Urea is more than 40 °C lower than PFA's.

PFA/IsoP has a T_g that is 20 °C higher than PFA and a slightly higher hardness. Its *E*' value at 20 °C and at the rubbery plateau are lower than PFA's. Yet, the rubbery plateau of PFA/IsoP is reached around 230 °C while PFA's is reached around 175 °C. The thermal resistance remains unchanged. Finally, the PFA/Furfu sample has a lower T_g and *E*' at 20 °C than PFA. The properties PFA/Furfu remain close to PFA's.

In complement with the previous characterizations, the materials were subjected to uniaxial tensile tests. Figure 5.3-3 gathers data extracted from the tensile tests. Representative examples of the tensile curves are available in Figure 5.6-11. The results of the PFA/J2000 samples are not presented here. The samples were too soft for the tensile apparatus (*E*' at 20 °C ≈ 1 MPa). The samples were constantly damaged by the jaws of the apparatus. This induced early rupture of the specimens along the jaws.

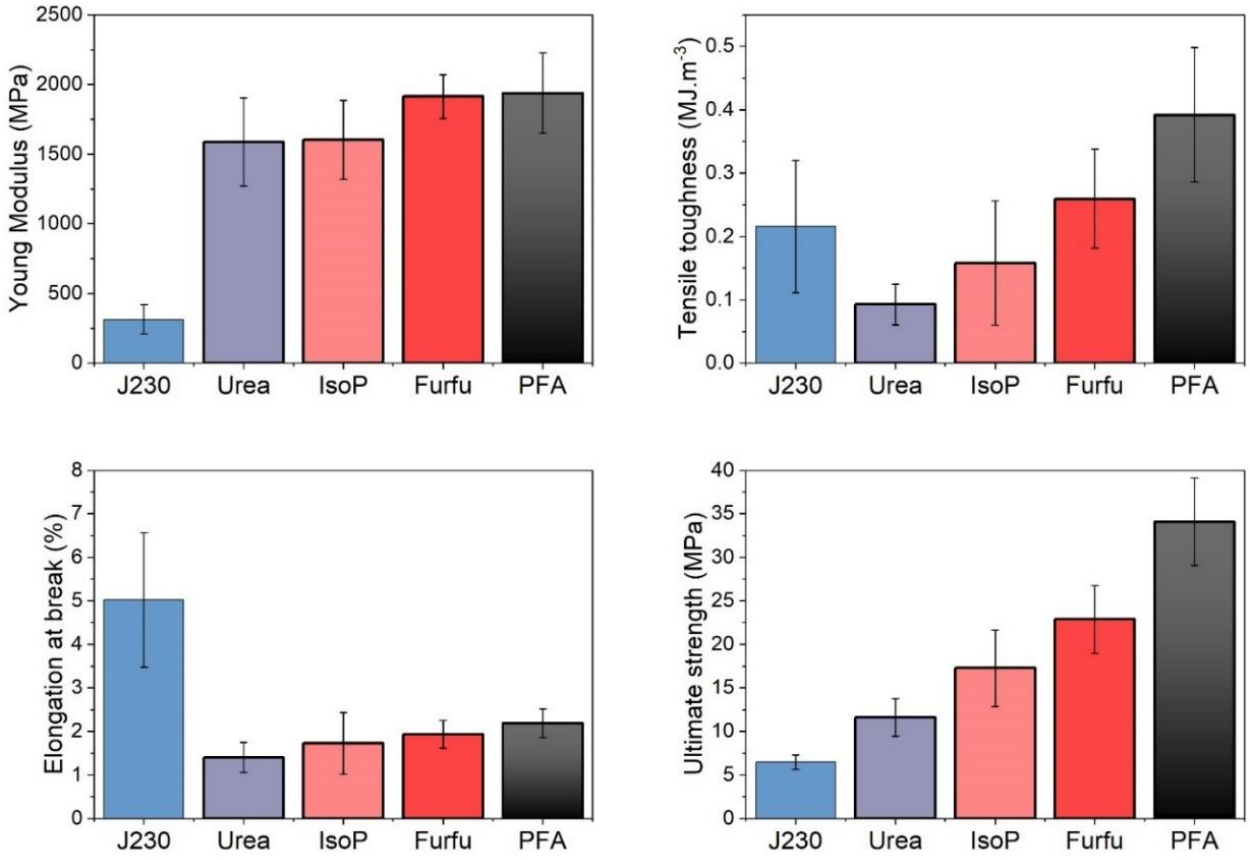

Figure 5.3-3. Tensile properties of the PFA/Amine materials. The samples were prepared at NH_2/C=O stoichiometry.

PFA/J230 showed significantly lower *E*' and ultimate strength than PFA while its elongation at break was doubled. This is expected as its T_g are lower than the T_g of PFA. PFA/Urea, PFA/IsoP, samples showed lower ultimate strength and tensile toughness than PFA. Their elastic moduli and elongation at break are close to the ones of PFA. The PFA/Furfu sample showed similar tensile behavior but even closer to PFA's.

Overall, when reacted with a PFA at a conversion degree of 0.8 and at NH_2/C=O stoichiometric ratio = 1, Urea and IsoP have negative effects on the tensile properties of PFA although they lead to an increase the T_g of the material. The introduction of these short amines has broadened the relaxation behavior of the materials and can be interesting for applications demanding low deformation. However, such short distance stiffening is not interesting when higher levels of deformation are needed. Interestingly, the more flexible amines such as J230 and J2000 increase the ductility of the material. This must be put in correlation with the weight percent of PFA in the samples (Table 5.3-1) which can be as low as 25 %w for PFA/J2000. The chemical structure of the amine also influences the properties of the material. The PFA/J230, and PFA/IsoP contain between 72 and 84 %w of PFA. Both samples retain the thermal stability of PFA. However, as their T_g are 70 °C apart, their mechanical properties measured at 24 °C are significantly different. Hence, at somewhat similar weight percent of amine, the chemical structure of the amine (rigid or flexible) has a strong effect on the mechanical properties of the material.

5.3.3 Consequences of PFA's surface hardening

During the post-curing steps, a surface hardening phenomenon was observed on some samples. This surface hardening was especially frequent and obvious in the case of ductile materials. Figure 5.3-4 depicts a representative example of a ductile sample which was post-cured in a forced convection oven and freshly cut along its length. As seen in Figure 5.3-4, the sample has a soft and brownish core while its surface is hard and dark. Such color and texture are highly similar to the one of the PFA resin in Figure 3.2-6. Hence, it suggests the intervention of the oxidation-induced surface crosslinking.

Figure 5.3-4. Picture of a PFA/J2000/0.3Eq/OX sample freshly cut along the length.

In chapter 3 and 4, it was mentioned that PFA is sensitive to surface oxidation and surface crosslinking when exposed to air. In the case of some PFA/Amine samples, a similar surface hardening phenomenon was observed. It is especially visible for ductile samples such as the one in Figure 5.3-4. To further investigate this aspect, PFA/J2000 samples were prepared at three NH_2/C=O stoichiometric ratios (0.1, 0.3 and 1.0). Two post-curing procedure were used in accordance with Scheme 5.3-2. For the first one, the post-curing occurred under air, i.e, in oxidative environment. In this case, the samples are labeled "OX". For the second procedure, the post-curing was performed in the molds, i.e., protected from air oxidation. In this case, the samples are labeled "IN". PFA references were also prepared following the two post-curing procedures. Figure 5.3-5 depicts the DMA curves of PFA and PFA/J2000 post-cured either in the oven or in their mold.

In Figure 5.3-5A, the *E*' curves of the reference PFA/OX and PFA/IN superimpose in the glassy state before the beginning of the glass transition. However, in the rubbery state, their evolution can be discriminated. PFA/OX exhibits a higher rubbery plateau and lower damping capacity than PFA/IN. These phenomena are specific to PFA and are linked to its ability to crosslink on its surface upon exposure to air. This oxidation-induced crosslinking was investigated in chapter 4 and is associated with a slight increase of *E*' when the material is in the rubbery plateau around 175 °C.

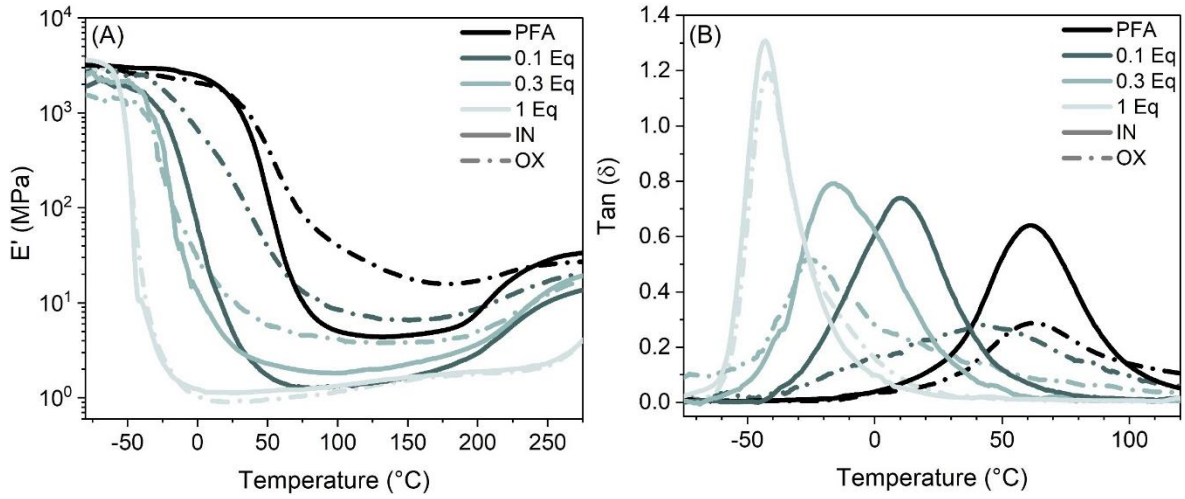

Figure 5.3-5. DMA curves, (A) *E'* and (B) tan (δ), of the PFA/J2000 materials post-cured either in the oven or in their mold. The plain lines correspond to samples post-cured in their mold (IN) and the dash-dot ones to samples post-cured in the oven (OX). The numbers in the legend correspond to the NH_2/C=O stoichiometric ratio.

For PFA/J2000/IN samples, the T_g decrease with the increase of the J2000 content. The T_g can reach very low value (up to -44 °C) for PFA/J2000/1Eq/IN. The drop of T_g is associated with more mobility of the chains and agrees with a lower rubbery plateau found for these systems compared to the reference (Figure 5.3-5A). Such behaviors are expected and coherent with observations made with a PFA/Priamine system in section 5.2.

Nonetheless, when comparing the post-curing conditions, the thermomechanical behavior strikingly differs. PFA/J2000/0.1Eq/IN has its tan (δ) maxima at 10 °C while the one of PFA/J2000/0.1Eq/OX is around 42 °C. The shape of the tan (δ) peak of PFA/J2000/0.1Eq/IN is also much sharper than its "OX" counterpart. In addition, the rubbery plateau of PFA/J2000/0.1Eq/IN is lower than PFA/J2000/0.1Eq/OX. Similar comments can be made on the PFA/J2000/0.3Eq/IN and "OX" although the gap between the DMA curves is tighter. Finally, in the case of PFA/J2000/1Eq/IN and OX, the curves are almost superimposed.

Thus, it can be deduced that PFA is responsible for both the crust on the samples and variation seen in the thermo-mechanical properties. Hence, high concentrations of PFA (between 50 and 75 %w) in the materials have a pronounced effect on the thermomechanical behavior variation between the "IN" and "OX" procedures. Vice-versa, for lower concentrations of PFA (≤ 25 %w), the effect is minimal and the samples show little to no crust. In complement, TGA and shore D hardness tests were performed. Figure 5.3-6 displays the results from these experiments along with the *E*' values at 20 °C obtained from the DMA curves of Figure 5.3-5. The TGA curves of the samples are available in Figure 5.6-12.

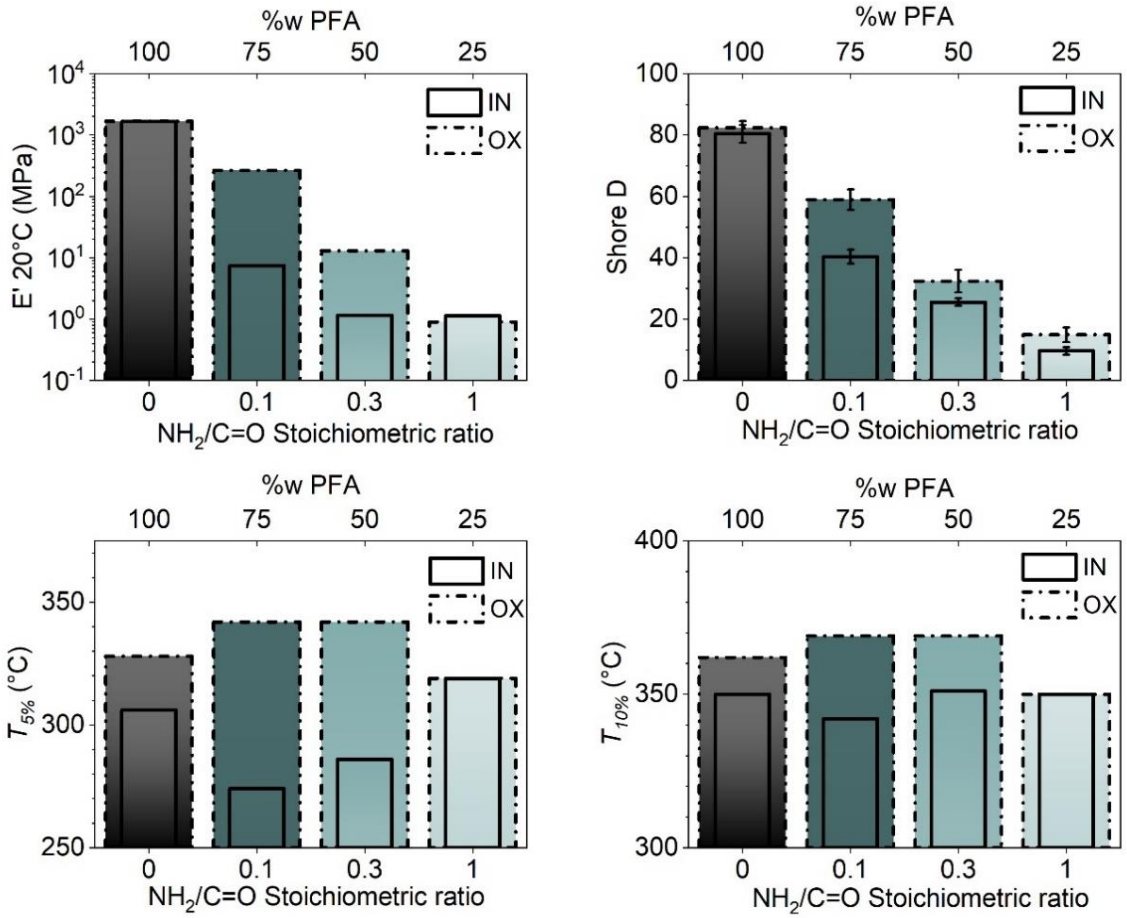

Figure 5.3-6. Dependency of the thermal and mechanical properties of the PFA/J2000 materials on the NH_2/C=O stoichiometric ratio, weight percent of PFA and post-curing environment. The post-curing was either performed in the oven (OX dash-dot lines) or in the molds (IN, plain lines).

In Figure 5.3-6 the *E*' at 20 °C obtained from DMA for the PFA/OX and PFA/IN are very close. The same conclusion also stands for PFA/J2000/1Eq samples. Nevertheless, for PFA/J2000/0.1 and 0.3 Eq, their *E*' at 20 °C are one to two orders of magnitude lower for the samples post-cured in inert conditions in comparison with the ones post-cured in a more oxidative environment. In this line, the hardness of PFA/J2000 samples is always higher in the case of the oven post-curing. This effect is especially strong for the PFA/J2000/0.1Eq samples which contain 75 %w of PFA. The PFA/OX and PFA/IN have similar hardness. However, their $T_{5\%}$ are about 20 °C apart. For PFA/J2000/0.3Eq/IN the $T_{5\%}$ is nearly 70 °C lower than its "OX" counterpart. For the PFA/J2000/0.1Eq/IN the effect is a little bit less significant with a $T_{5\%}$ about 55 °C lower than PFA/J2000/0.1Eq/OX. In addition, the two PFA/J2000/1Eq samples have similar $T_{5\%}$. For all the samples the $T_{10\%}$ values behave in a similar manner although the gaps between "OX" and "IN" are tighter.

To further study the impact of the crust formed in oxidative conditions, the PFA/J2000 samples were subjected to uniaxial tensile tests. As mentioned previously, the PFA/J2000/1Eq samples could not be tested. Figure 5.3-7 gathers the tensile properties of the samples and Figure 5.6-13 gives representative examples of the tensile curves of the samples.

First, the PFA/IN and PFA/OX demonstrate very similar tensile properties, only a slightly lower ultimate strength is noticeable for PFA/IN. Thus, the impact of this formed crust on neat PFA on its tensile properties is limited. This is in agreement with chapter 4. In the case of PFA/J2000/0.1Eq and PFA/J2000/0.3Eq the oxidized samples have much higher Young's moduli than the non-oxidized counterparts, by order(s) of magnitude. The same comment can be made about the yield strength. In complement, the elongation at break of these samples is three to five times higher in the case of the non-oxidative curing procedure. Finally, the tensile toughness is only impacted in the case of the PFA/J2000/0.3Eq samples.

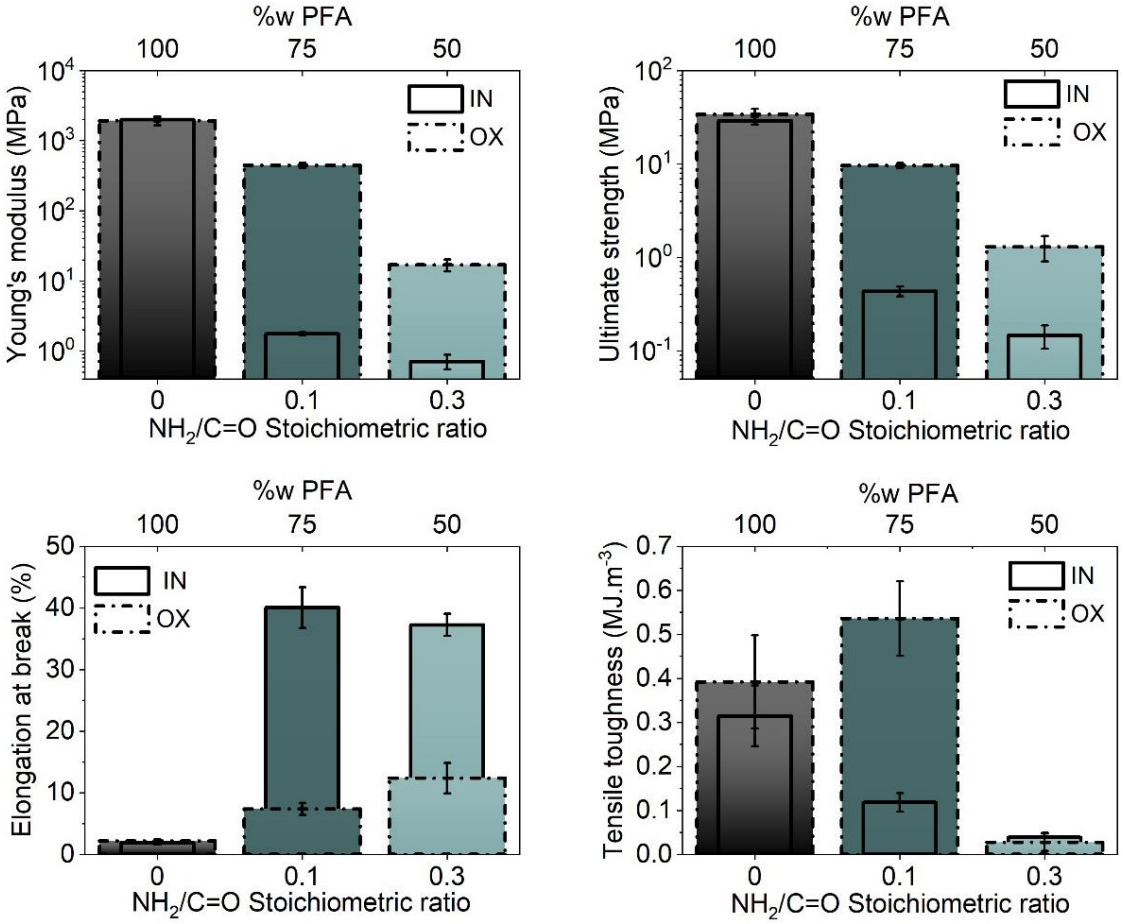

Figure 5.3-7. Dependency of the tensile properties of PFA/J2000 materials on the NH_2/C=O stoichiometric ratio, weight percent of PFA and post-curing environment. The post-curing was either performed in the oven (OX, dash-dot lines) or in the molds (IN, plain lines).

All these observations are direct consequences of the surface crosslinking ability of PFA. It increases the T_g of the materials by up to 30 °C. Hence, when the crust forms, the T_g is raised above the room temperature. Consequently, the tensile properties are tremendously impacted, the material shifts from ductile to brittle.

Finally, PFA/J2000/0.3Eq samples were post-cured in a forced convection oven at 200 °C for 2 h 30 to maximize the formation of this rigid crust. As demonstrated in chapter 4, with such time and temperature conditions, the polymer is fully cured. On the one hand, a sample was directly subjected to DMA. On the other hand, the crust of a sample was removed with a scalpel prior to the DMA. The resulting curves are available in Figure 5.3-8. The samples have thermomechanical behaviors highly similar to the PFA/J2000/0.3Eq/IN and "OX" in Figure 5.3-5. It further emphasizes the effect of the surface hardening and its limitation to a layer thinner than a sheet of paper (< 100 µm) and probably around 20 µm if this crust is similar to the one forming on pure PFA. In addition, the oxidation might also be the cause for the variations of properties observed on a fresh and a three-month-old PFA/PA 1 in Figure 5.2-9.

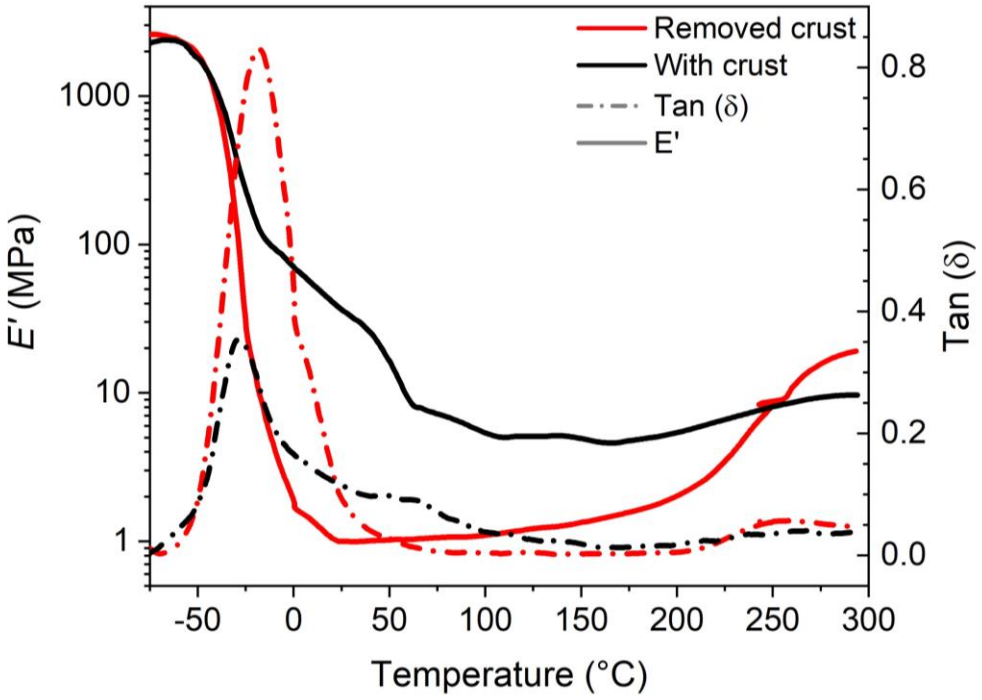

Figure 5.3-8. DMA curves of PFA/J2000/0.3Eq post-cured at 200 °C for 2 h 30 under air. The black lines correspond to a sample with crust (black). The red lines correspond to a sample without crust (removed with a scalpel). The plain lines correspond to the E' curves and the dash-dot ones to the tan (δ) curves.

To sum up, surface hardening ability of PFA's has a tremendous impact on the properties of the more ductile PFA/J2000 materials. The crust results from an oxidative ring-opening pathways followed by a cycloaddition and potentially an aromatization of the adduct. Although this phenomenon has a limited impact on PFA alone, the PFA/Amine material may undergo significant variation in their properties. Upon surface hardening, the T_g of the materials can increase to more than 25 °C due to this surface hardening. Therefore, the polymer may shift from a rubbery behavior at room temperature to a glassy one and the mechanical properties may shift from ductile to brittle.

Furthermore, the thermal degradation is significantly affected by the presence of this stiffer top-layer that leads to an increase of onset temperatures of degradation once the crust is formed. These effects are direct consequences of the unique reactivity of PFA. Thus, they are highly influenced by the weight percent of PFA in the materials. The dioxygen in the air plays a crucial role in the formation of the crust. Hence, if one wants to avoid its formation, protection from the air is required. Antioxidants and/or coating might be effective for that purpose.

5.3.4 Conclusions

In this section the C=O present in PFA were derivatized with difunctionnal primary amines. Three factors influencing the properties of PFA/Amine materials were investigated.

First, the effect of the amines' chemical structure was studied. Linear amines with long chains introduced flexibility in the material. The impact was especially significant for the larger amine, i.e, J2000. Materials based on rigid amines such as isophorone diamine gave materials with higher T_g than PFA. The impact of the amines on the thermo-oxidative degradation is limited in most cases.

Some of the PFA/Amine material presented the formation of a crust during their post-curing. This phenomena was investigated using PFA/J2000 materials at varying functionalization degree and post-curing environment (oxidative or non-oxidative). The materials post-cured in non-oxidative conditions were much more flexible than the ones post-cured in oxidative conditions. On similar samples, the post-curing environment can increase the T_g above room temperature. This ultimately leads to tensile properties – ultimate strength, Young's modulus- distant by orders of magnitudes. In addition, the oxidized PFA/J2000 samples presented superior thermo-oxidative degradation resistance as illustrated by an increase of $T_{5\%}$ of about 70 °C compared to material post-cured in inert conditions. In addition, if the crust is removed, the material recovers its flexibility. The formation of the crust results from an oxidation-induced surface crosslinking pathway specific to PFA described in chapter 4. It could not be avoided for pure PFA/Amine materials if the weight percent of PFA was superior or equal to 50 %w.

5.4 Effect of PFA's conversion degree and effect of the amines' basicity

The aim of this section is to further highlight the factors influencing the thermomechanical properties of the PFA/Amine materials. This section is divided in three parts. First, the precipitation of PFA upon reaction with DiHex in ethyl acetate is discussed. Then, the influence of the degree of polymerization of the starting PFA is evaluated. Finally, the last part deals with the impact of the amines' basicity on the acid-catalyzed polymerization of FA.

As discussed in this manuscript, the polymerization of FA is far from being straightforward. To better understand this section, major facts are recalled in the followings. Briefly, the polymerization of FA goes through two main chain lengthening pathways. They are reported in Table 5.4-1. The condensation reactions (Pathway I) are the first step of polymerization. Once a degree of polymerization of four to ten is achieved, a loss of hydride ion occurs and leads to conjugated 2,5-dihydrofurans. Then, the conjugated and non-conjugated moieties react together by Diels-Alder (Pathway II), thus providing crosslinking nods. Pathway II is believed to be the main source of crosslinking in PFA. [281]

Furthermore, if a PFA resin is exposed to air, the furan ring can open into conjugated 1,4-dicarbonyls, especially 1,4-ketoaldehydes. The conjugated carbonyls can then undergo a Diels-Alder cycloaddition with non-conjugated furans to yield oxidation-induced crosslinking nods (Pathway III). Pathway III is observable through a rise of elastic moduli starting around 175 °C. It should be noted that Pathway III was only observed at the PFA-Air interface and is limited to a thin layer (≈ 20 µm). Finally, the oxidation-induced cycloadducts may be aromatized if exposed to further air and heat, as discussed in chapter 4.

Table 5.4-1. Chain lengthening pathways during the polymerization of FA.

Requirement for the formation of the precursor	**Chain lengthening precursor**	**Chain lengthening product**	**Pathway**	**Reference**
Acidic medium + monosubstituted furan	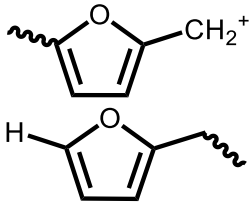	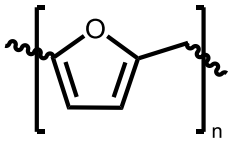	Acid-catalyzed polycondensation (bulk, surface) **(Pathway I)**	[281]
Hydride ion abstraction	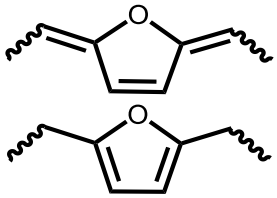	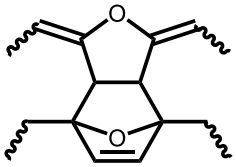	Diels-Alder cycloaddition (bulk, surface) **(Pathway II)**	[281]
Air-induced Oxidative ring-opening*	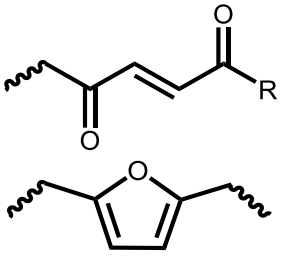	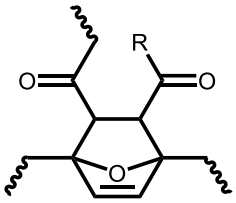	Oxidation induced crosslinking (surface only) **(Pathway III)**	[284], chapter 3

R: H, PFA network

**The monosubstituted furans are especially sensitive to this reaction*

Section 5.2 and 5.3 highlighted the potential of expanding the portfolio of applications of PFA materials trough functionalization of the C=O. Yet, there are still phenomena which need to be understood to fully exploit the potential of C=O in PFAs. For this purpose, two features of the materials were investigated in this study.

In a first phase, the impact of the conversion degree of PFA on the functionalization of its C=O, and consequently on the sample properties, was investigated. Indeed, the C=O content of PFA increase during the course of polymerization. Although highly polymerized PFA have the highest C=O content, their partial insolubility may hinder the C=Os' reactivity. Thus, PFAs at various conversion degrees ($0.3 \leq \alpha \leq 0.95$) were prepared, characterized and functionalized with 1,6-diaminohexane (DiHex).

In a second phase, investigations using a monoamine (hexylamine) and potassium hydroxide were conducted to assess the impact of the basicity on the polymerization and final properties of the materials. Indeed, the basicity of amines is in opposition with the acid-catalyzed polymerization of FA and it somehow impacts the final stages of the polymerization.

5.4.1 Experimental details specific to section 5.4

In section 5.4, the impact of the conversion degree of PFA before functionalization was studied using 1,6-diaminohexane (DiHex). In addition, the impact of bases on the polymerization was assessed. Accordingly, n-hexylamine (Hex) and potassium hydroxide (KOH) were employed.

The sample preparation procedures are illustrated in Scheme 5.4-1.

First, mixtures of FA comprising 10 %w of water and 2 %w of maleic anhydride were homogenized. The mixtures were then placed in a thermoregulated bath. To reach the desired conversion degrees the time and temperature conditions reported in Table 5.1-1 were used. The C=O content of these PFA prepolymers are also reported in Table 5.1-1. All the pre-polymers were soluble excepted the α = 0.95 specimen who reached vitrification. Thus, it was ground using a ball mill prior to functionalization.

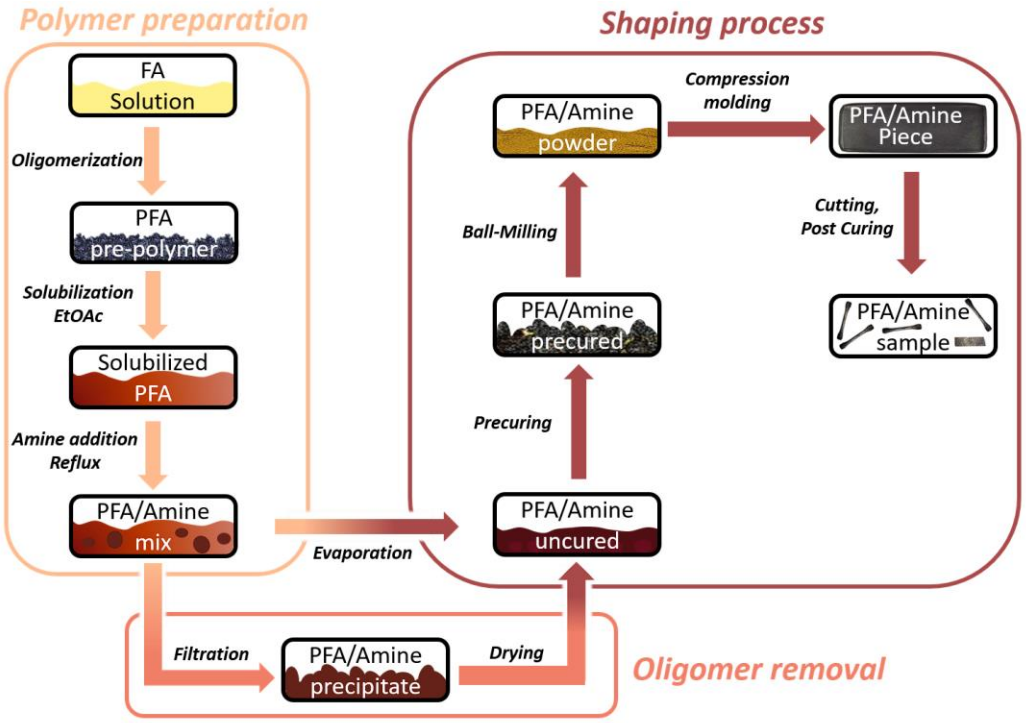

Scheme 5.4-1. Process of sample preparation relative to section 5.4.

To derivatize the C=O, about 30 g of PFA prepolymer were placed in a round bottom flask and dissolved in refluxed ethyl acetate (≈ 150 mL). In the case of PFA at α = 0.95, only swelling was achievable. Then, a solution of amine or KOH in ethanol (20 mL) was quantitatively transferred to the round bottom flask. Depending on the conversion degree of the resin and the amine type, precipitation may occur at this stage. The PFA/Amine solutions were refluxed for 4 h before being left to evaporate in a crystalizing dish for 24 h with occasional stirring to break any chunks or floating layer. In some assays, the precipitate was filtered and washed thoroughly with ethyl acetate before drying. In this case, the sample name was suffixed with the letter “p”. The yield of precipitate was calculated according to Equation 5.4-1. The washings were done with ethyl acetate.

$$Yield\ of\ precipitate = \frac{Mass\ of\ washed\ and\ dry\ prcipitate}{Mass\ of\ amine + Mass\ of\ PFA} \quad \text{Equation 5.4-1}$$

Once dried, the samples were heated at 130 °C in a forced convection oven for up to 90 mins to reach the rubbery state (precuring step). For some samples, i.e PFA/KOH, all the PFA/Hex and PFA/DiHex/α0.3/1Eq the precuring step required manual stirring. For the reference PFA and the PFA/DiHex, 20 mins at 130 °C without stirring were generally enough to reach rubbery state. Yet, PFA/KOH for example, required 90 mins at 130 °C with regular manual spatula stirring, i.e., exposure to air. Here the stirring was mandatory to reach a material. During this step the polymer formed a hard crust while its central part (or core) stayed soft. The crust needed to be broken to expose the soft core of the sample and allow it to reach rubbery state. This phenomenon is illustrated in Scheme 5.4-2.

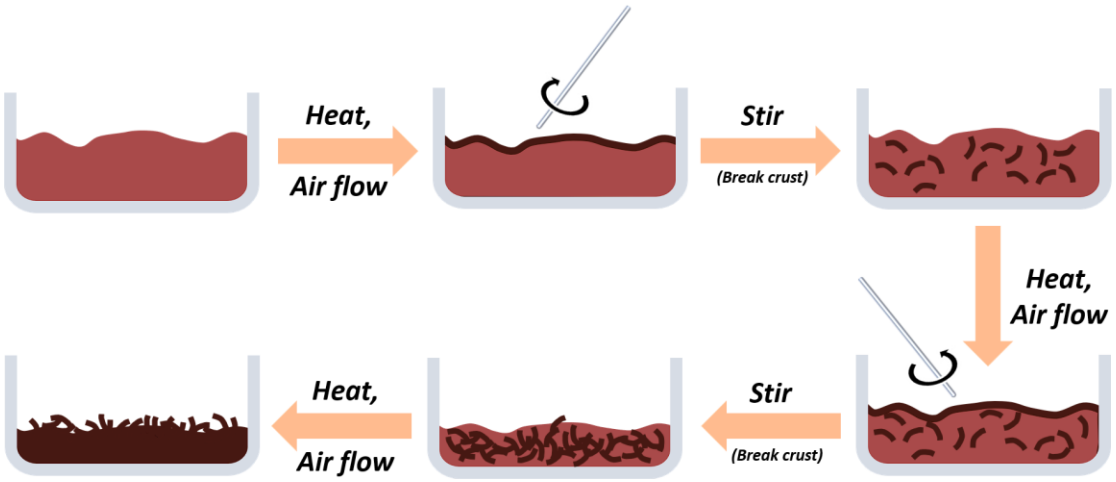

Scheme 5.4-2. Illustration of the formation of PFA/Hex and PFA/KOH crust during the precuring step.

Then, the procedure mentioned previously (section 5.1) was used to grind the rubbers. The precuring and grinding steps were crucial to obtain bubble free and homogeneous materials. The resulting powders were then molded under 25 – 35 bars at 150 °C and for 2 hours in a heated press. From here, the pieces were recovered from the molds and cut in various shapes. For DMA, hardness and TGA experiments parallelepipeds were used. For the tensile tests, dumbbell shapes (ISO 527-2-1BB) were used.

The cutting was done at 150 °C using with specific cutters. The heat is required to avoid fracture of the samples. Then, the materials were post-cured for 3 h at 150 °C in a forced-convection oven. To ensure proper interpretations, reference samples were prepared according to the same procedure using PFAs at α of 0.30, 0.80 and 0.95 without any amine or base. In these cases, the precipitation phenomenon was not observed. Figure 5.6-14 (DMA curves), Figure 5.6-15 (TGA curves), Table 5.6-1 (thermomechanical properties) and Figure 5.6-16 (tensile data) display the results from characterization of the neat PFA samples i.e prepared without amines but following the same protocols. As variations can be observed between the PFAs, the "PFA" data are presented as the average and standard variation of the three controls.

5.4.2 Phase separation phenomenon during the functionalization of PFA's C=O

When the carbonyls of PFA are reacted with difunctional primary amines, a phase separation may occur. This section is dedicated to this phase separation phenomenon in the case of PFA/DiHex.

The phase separation phenomenon is illustrated in Figure 5.4-1 with the example of PFA/DiHex/ α0.9. Pictures were taken at several step of the sample preparation and are presented in chronological order. During the synthesis, particles were observed in the flask together with a fluffy coating that readily formed on the flask surface as shown in Figure 5.4-1A. Figure 5.4-1B, C and D present photos of these particles before and after evaporation.

The evaporation process induces a darkening of the insoluble part with a formation of an external crust after long evaporation time (Figure 5.4-1D). These phenomena could be attributed to the drying process. Nevertheless, after the pre-curing step at 130 °C for 30 mins a hard and black solid (Figure 5.4-1E) is obtained which becomes orange-brown once ground (Figure 5.4-1F).

Then, after compression molding the samples become black again (Figure 5.4-1G). To explain such color variations, FTIR spectra of the samples in Figure 5.4-1(E) and (F) were acquired and are presented in Figure 5.4-2.

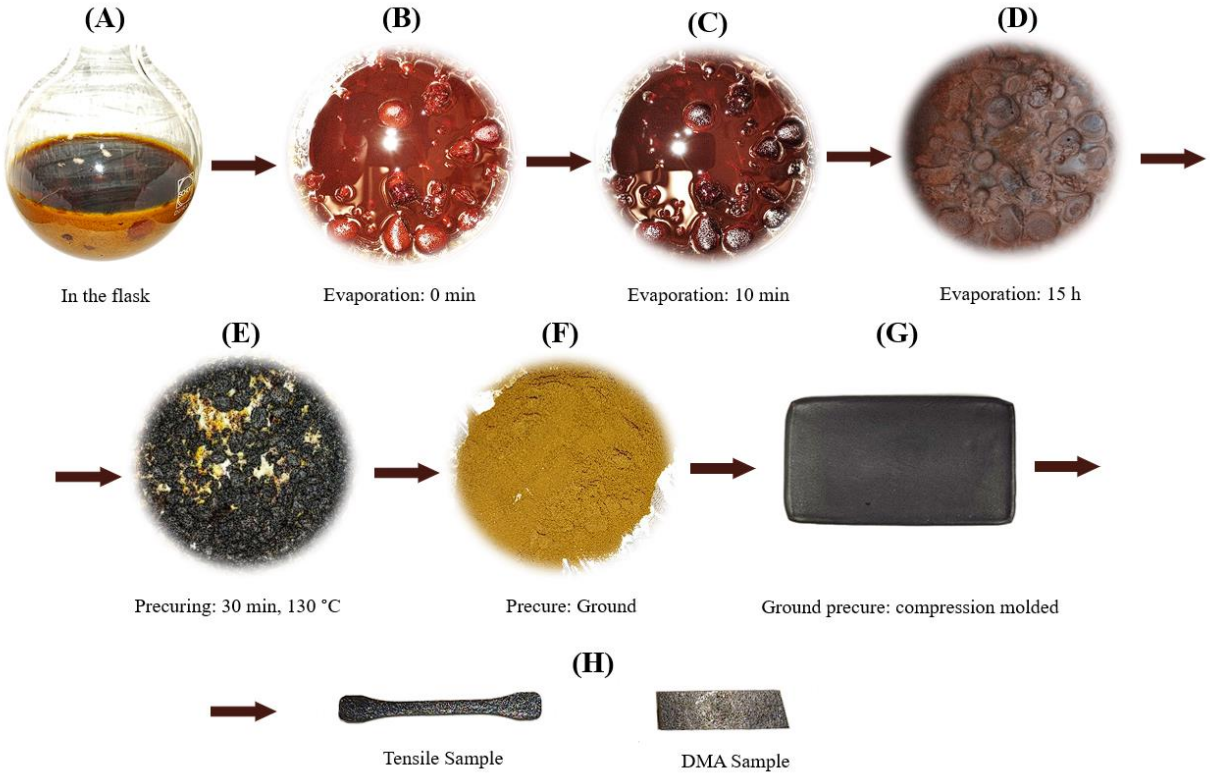

Figure 5.4-1. Pictures taken along the process of fabrication of PFA/Amine materials, case of PFA/DiHex, α =0.9, NH_2/C=O stoichiometry. The alphabetical order is also chronologic.

The magnified FTIR spectra in Figure 5.4-2 correspond to the precured sample of Figure 5.4-1 before -(E)-and after being ground -(F)-. In Figure 5.4-2 the bulky and black sample -(E)- exhibit bands attributable to C=O and C=C which are not visible on the ground sample, i.e., the orange-brown powder -(F)-. The presence of these bands is coherent with the surface oxidation detailed in chapter 4, Figure 4.3-1.

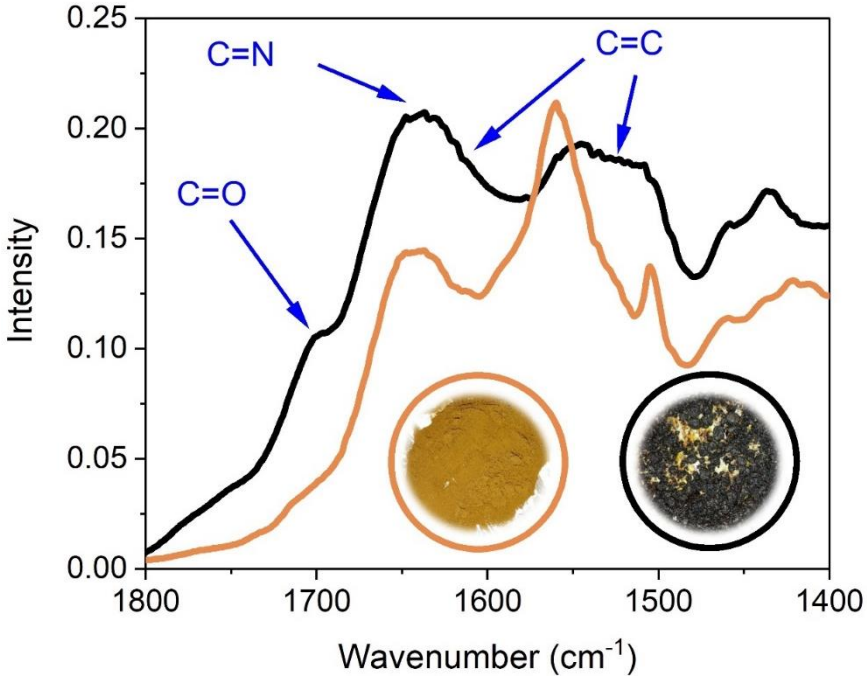

Figure 5.4-2. FTIR spectra of PFA/DiHex/α0.9 at the precured step before (black) and after grinding (orange). The samples were prepared at NH_2/C=O stoichiometry.

Finally, the yield of precipitate was evaluated as a function of the conversion degree of the starting PFA. Figure 5.4-3 depicts the mass ratio of insoluble part over the total mass of PFA and DiHex as a function of the PFA's conversion degree. Higher is the conversion degree and higher is the amount of insoluble part following a good linear correlation (R^2 = 0.989). This suggests that a minimal chain length – or crosslink density - is required for the macromolecules to make this phase separation. The origin of this separation is most-likely due to the formation the C-N bonds. Indeed, formation of additional bonds by introduction of the amine would imply longer macromolecules and/or a tighter network. Hence, the solubility of the polymer would decrease.

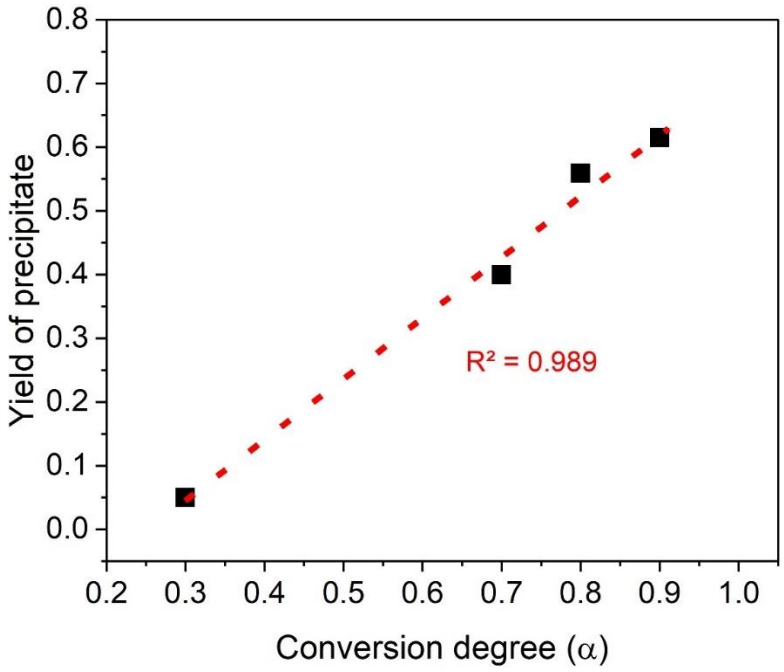

Figure 5.4-3. Dependency of the mass ratio of precipitate on the conversion degree of the starting PFA. The samples were prepared at NH_2/C=O stoichiometry.

To sum up, the reaction of PFA's C=O with difunctional primary amines in ethyl acetate may lead to the precipitation of the resulting polymers. The yield of precipitate is highly correlated with the conversion degree of the starting PFA. In addition, the yield of precipitate may be up to 65 %w in respect with the initial amount of reagents. Finally, the PFA/DiHex materials are sensitive to surface ring opening when exposed to air and heat. This may be a factor explaining the presence of residual carbonyl groups on the surface of PFA/Amine materials.

5.4.3 Effect of the conversion degree on the properties of PFA/DiHex

In this section, the thermomechanical properties of PFA/DiHex materials are discussed. In addition, materials prepared from the precipitated macromolecules alone were also assessed. They were labeled with a "p" suffix.

First, the successful derivatization of the C=O was checked by FTIR. The amount of C=O in a PFA resin can be assessed by comparing the height of the C=O peak at 1715 cm^{-1} versus the 1550 cm^{-1} peak, corresponding to the C=C of disubstituted furan. [292, 296, 328] Figure 5.4-4 displays the FTIR spectra of the PFA/DiHex materials. In this Figure, the C=O band at 1710 cm^{-1} in the PFA/DiHex samples is greatly diminishing in comparison with the furan band at 1550 cm^{-1}. Moreover, at C=N band around 1650 cm^{-1} is visible in the PFA/DiHex. [328] Finally, a small signal can be observed between 1510 and 1540 cm^{-1} for the PFA/DiHex. This may be attributed to pyrroles moieties. [328] Overall, Figure 5.4-4 showcases the successful reaction of PFA's C=O with NH_2 to yield either imines or pyrroles. The proportion of each is however hard to pin-point.

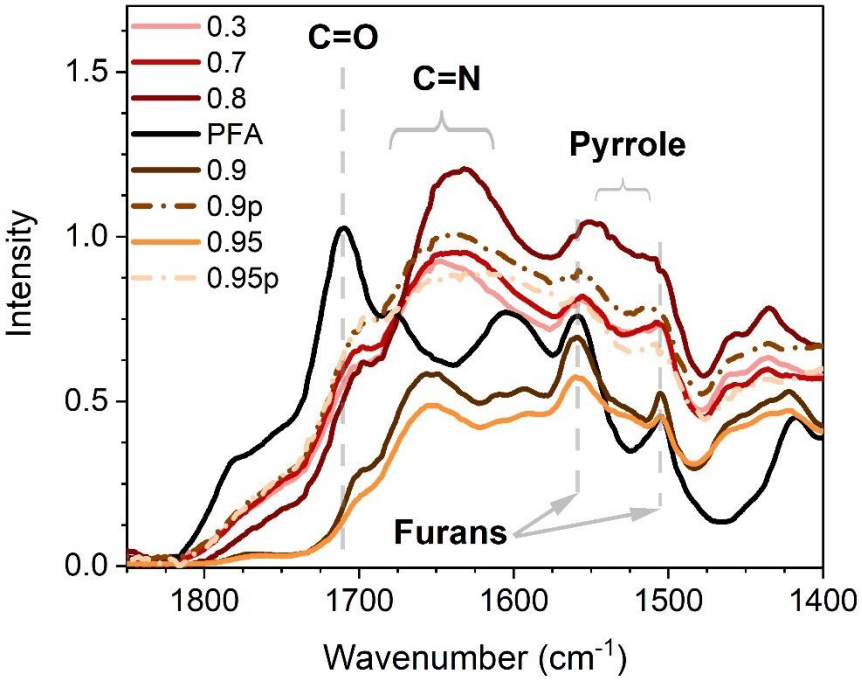

Figure 5.4-4. FTIR spectra of PFA/DiHex at NH_2/C=O stoichiometry using PFAs at different conversion degrees (0.3 to 0.95). The numbers in the legend indicate the conversion degree of each starting PFA. The letter "p" indicates that only the precipitated macromolecules were used (dash-dot lines). The reference PFA was prepared using a PFA at α = 0.8.

The thermomechanical properties of the materials were first assessed by DMA. The corresponding curves are displayed in Figure 5.4-5. To ease the reading, only one control (starting PFA at α = 0.8) is displayed in Figure 5.4-5. Additionally, Table 5.4-2 presents data extracted from the DMA, TGA and the Shore D hardness experiments. In Table 5.4-2, the data labeled "PFA" is the average and standard deviation of the three controls (α = 0.3; 0.8; 0.95). The TGA curves of the samples are available in Figure 5.6-17.

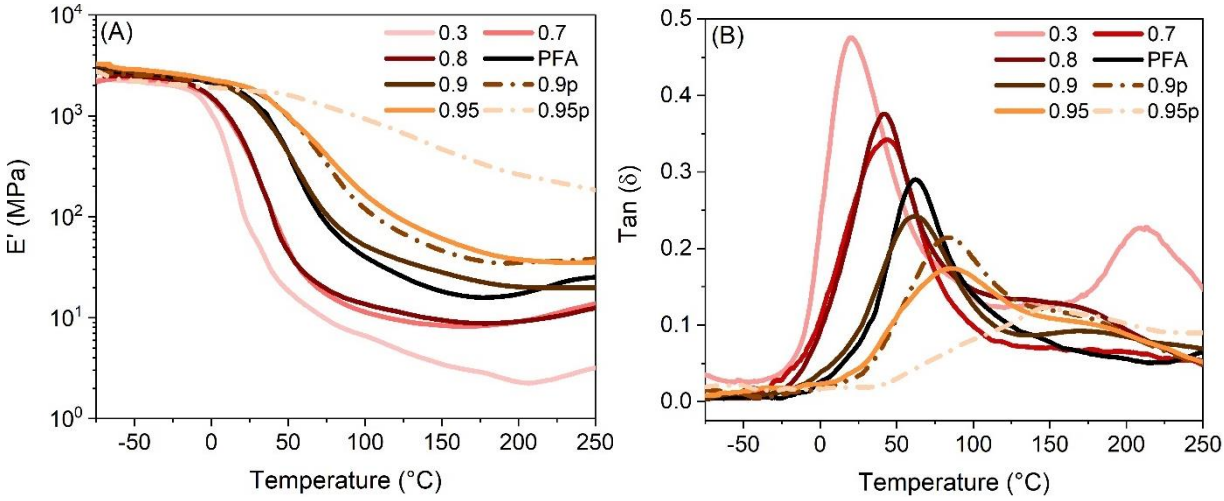

Figure 5.4-5. DMA curves, (A) E' and (B) tan (δ), of the PFA/DiHex prepared at NH_2/C=O stoichiometry and using PFAs at different conversion degrees (0.3 to 0.95). The numbers in the legend indicate the conversion degree (α) of the starting PFA. The letter "p" indicates that only the insoluble macromolecules were used in the preparation of the materials (dash-dot lines). The reference PFA was prepared using a PFA at α = 0.8.

In Figure 5.4-5, the *E*' curves of the samples prepared with PFAs at $\alpha \leq 0.8$ are all below the control PFA. Their surface of tan (δ) peak are higher than the one of reference PFA, thus it suggests a higher damping capacity for these samples. The sample prepared at a conversion degree of 0.3 (PFA/DiHex/α0.3) presents a T_g around 20 °C and consequently the *E*' value at 20 °C reach 160 MPa, i.e., about 100 times lower than the E' value PFA at 20 °C. The shore D hardness of this sample is also much lower than PFA's. Its $T_{5\%}$ and $T_{10\%}$ are about 30 °C lower than PFA.

Finally, a second tan (δ) peak is observed at 210 °C. Insights on the nature of this peak are given in the last section of this paper. The samples prepared at conversion degrees of 0.7 and 0.8 place themselves between PFA and the PFA/DiHex/α0.3. They are very close together apart from a higher $T_{5\%}$ and $T_{10\%}$ for PFA/DiHex/α0.8.

The PFA/DiHex/α0.9 sample is highly similar to PFA in most regards. Two small differences can however be highlighted. The $T_{5\%}$ and $T_{10\%}$ are increased by 5-10 °C and a secondary tan (δ) peak is observed around 175 °C. This peak is also visible on the PFA/DiHex/α0.8 curve. These differences are emphasized in the case of the PFA/DiHex/α0.95 sample. For PFA/DiHex/α0.95 the secondary tan (δ) peak at 175 °C appears more as a shouldering and its $T_{5\%}$ and $T_{10\%}$ are about 20 °C superior to PFAs'. The secondary tan (δ) peaks suggest a more rigid and heterogeneous macromolecular network than PFAs'. Such result is consistent with the higher diversity of chemical groups in PFA/DiHex materials.

Table 5.4-2. Thermal and mechanical properties of PFA/DiHex materials prepared with PFAs at various conversion degrees. The samples were all prepared at NH_2/C=O stoichiometry.

Sample's conversion degree (α)	%w PFA	*E'* DMA 20 °C (MPa)	Tan (δ) maxima (°C)	$T_{5\%}$ (°C)	$T_{10\%}$ (°C)	Shore D
0.3	88	160	20	296	334	38.4 ± 2.5
0.7	86	560	43	330	358	69.3 ± 2.5
0.8	84	600	42	341	369	69.8 ± 2.0
PFA (0.3, 0.8, 0.95)*	**100**	**1857 ± 575**	**66 ± 11**	**324 ± 7**	**359 ± 6**	**82.8 ± 2.2**
0.9	83	1560	62	345	370	85.0 ± 1.6
0.9p**	83	1940	84	329	367	83.9 ± 1.7
0.95	79	2050	86	358	386	86.2 ± 1.4
0.95p**	79	1780	145	335	374	88.6 ± 1.3

The PFA row comprises the average and standard deviation of three references prepared with PFA at α of 0.3, 0.8 and 0.95. The "p" suffix indicates that only the precipitated macromolecules were used in the making of the materials.*

To complete this part of the study, two samples were prepared using only the precipitated macromolecules (PFA/DiHex/α0.9p and PFA/DiHex/α0.95p). PFA/DiHex/α0.9p has a T_g 20 °C higher than its counterpart (PFA/DiHex/α0.9). This comes along with a higher *E*' at 20 °C but without significant variation of the hardness. The $T_{5\%}$ of PFA/DiHex/α0.9p is 16 °C lower than PFA/DiHex/α0.9 while their $T_{10\%}$ are close. Similarly, the PFA/DiHex/α0.95p samples shows a 10 - 20 °C diminution of $T_{5\%}$ and $T_{10\%}$ in comparison with PFA/DiHex/α0.95. However, the PFA/DiHex/α0.95p displays a much higher T_g (+60 °C), and higher hardness than PFAs. In addition, the PFA/DiHex/ α0.95p does not show a rubbery plateau in Figure 5.4-5 B. The *E'* of PFA/DiHex/α0.95p drops by about one order of magnitude upon passing it's T_g while the drop is of about two orders of magnitude of *E'* in the case of the non-precipitated sample.

These results suggested a higher crosslink density in the precipitated samples, possibly C=N crosslinks. To check this, elemental analyses were conducted. The results are displayed in Table 5.4-3. It clearly shows a higher proportion of nitrogen in the precipitated samples, about 1.4 times more than PFA/DiHex/α0.95.

Table 5.4-3. Elemental analyses of PFA and PFA/DiHex samples.

Sample	%C	%H	%N	%O
PFA	71.6	5.1	0	23.3
PFA/DiHex/α0.95p	71.4	6.6	5.6	16.4
PFA/DiHex/α0.95	71.0	6.1	3.9	19.0

Overall, PFA/DiHex from insoluble fractions have drastically different polymeric network than PFA. This is especially the case for the sample prepared with a starting PFA at α = 0.95. The most-likely explanation is a higher concentration of C-N bonds in the insoluble fraction. This results in a higher T_g (i.e., 145 °C) and *E*' in the rubbery state. Such high T_g might be achievable trough the removal of small, plasticizing oligomers and/or FA. The removal low molecular weight species is a good point to avoid future release of potentially harmful compounds during the lifetime of a material or its recycling. Yet, it comes at the cost of a slightly reduced resistance to thermo-oxidative degradation. The cleavage of C-N bonds might be responsible for this.

PFA/DiHex samples were subjected to tensile tests. Figure 5.4-6 displays a summary of the tensile data. Figure 5.6-18 presents representative examples of the tensile curves. In Figure 5.4-6, the PFA columns comprise the average and standard deviation of three reference materials prepared with PFAs at α of 0.3, 0.8 and 0.95. The data of each reference PFA is available in Figure 5.6-16.

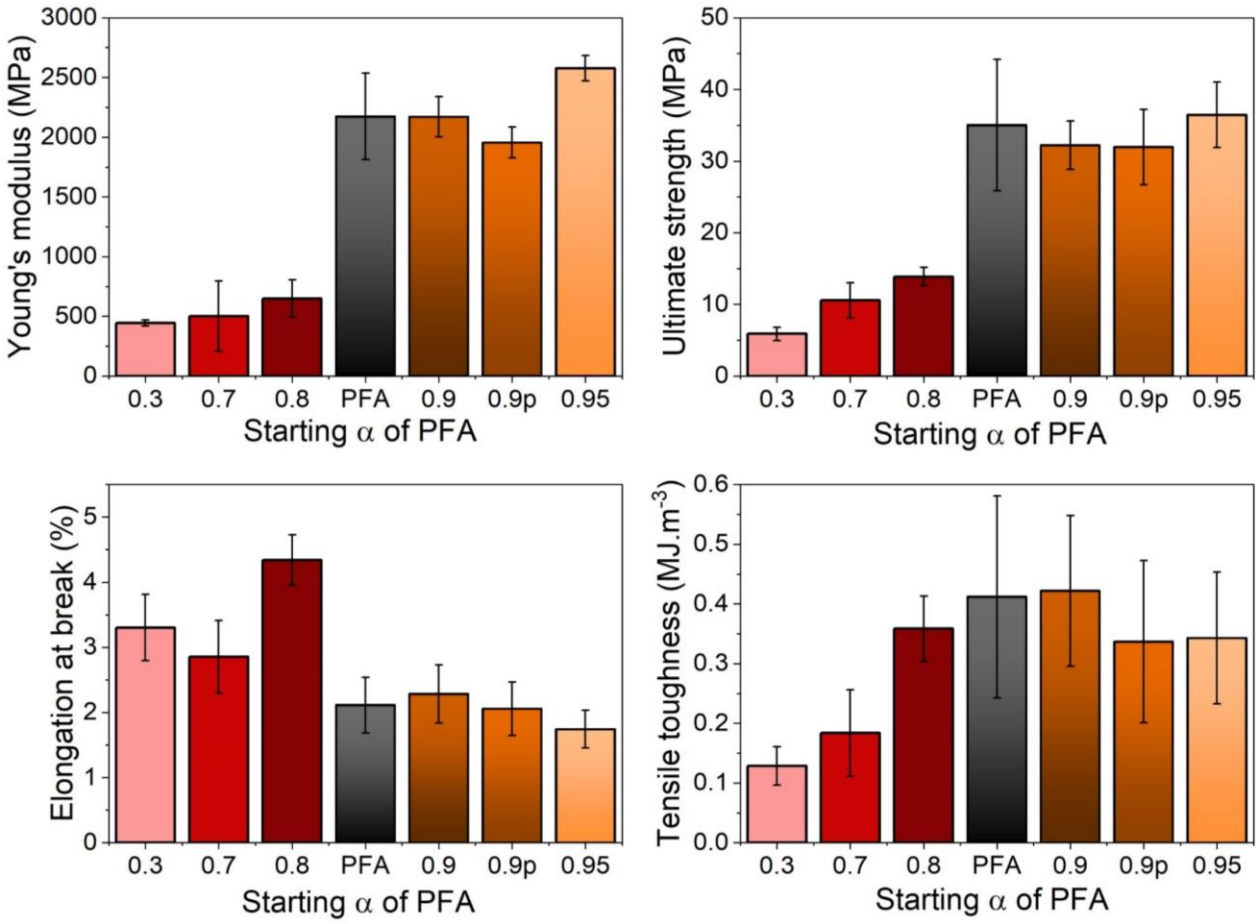

Figure 5.4-6. Tensile data of the PFA/DiHex at NH_2/C=O stoichiometry using PFAs at various conversion degrees (0.3 to 0.95). The "p" suffix indicates that only the precipitated macromolecules were used. The "PFA" columns comprise three references prepared with starting α of 0.3, 0.8 and 0.95.

For the PFA/DiHex samples prepared with a PFA at $\alpha \leq 0.8$, Figure 5.4-6 shows a much lower *E'*, ultimate strength and tensile toughness than the PFAs. The elongation at break of these samples is, however slightly increased, in comparison with PFAs.

Regarding the PFA/DiHex/α0.9 and PFA/DiHex/α0.95, little differences are observed. The tensile properties of PFA/DiHex/α0.95p could not be studied. The *E'* at temperature 150 °C and above of this sample is too high for it to be cut by the dumbbell cutter.

To sum up, 1,6-diaminohexane (DiHex) can be easily reacted with PFAs at conversion degree between 0.3 and 0.95 and materials can be obtained. PFA/DiHex samples prepared with a PFA at α between 0.3 and 0.8 showed significantly diminished T_g, in comparison with PFA. Yet, they remained brittle and their thermal resistance was also decreased in some cases. The origin of their brittleness is discussed in the next section.

The PFA/DiHex samples prepared with PFA at $\alpha > 0.8$ showed thermal and mechanical properties close to standard PFA, with slightly higher T_g, $T_{5\%}$ and $T_{10\%}$. Finally, during the synthesis of the PFA/amine materials, phase separation may occur. Materials were prepared using only the precipitate. The resulting specimens, especially PFA/DiHex/α0.95p, displayed much higher mechanical properties at temperatures between 100 and 250 °C than all the other samples. This improvement however comes with a compromise on the starting degradation temperatures that are attributed to the cleavage of C-N bonds.

5.4.4 Effect of bases on the polymerization of FA

The aim of this section is to better understand the impact of the basicity of amines on the polymerization of PFA. In this section, the polymerization of PFA was quenched with potassium hydroxide (KOH) and n-hexylamine (Hex). Even though the polycondensation reactions were stopped, crosslinked materials could still be obtained. Mechanistic insights on the crosslinking of quenched PFAs are given. Finally, the properties of a PFA quenched with KOH (PFA/KOH) and PFAs modified with hexylamine (PFA/Hex) at varying functionalizing degrees are investigated.

After being processed and shaped, the reference PFA, PFA/KOH and PFA/Hex samples were analyzed by DMA. Figure 5.4-7 reports the DMA scans of PFA and PFA/KOH. In Figure 5.4-7, the PFA sample exhibits a rise of *E'* beginning at 175 °C. This rise of *E'* is an indication that the Pathway III of Table 5.4-1 is occurring during the DMA scan, in agreement with chapter 4.

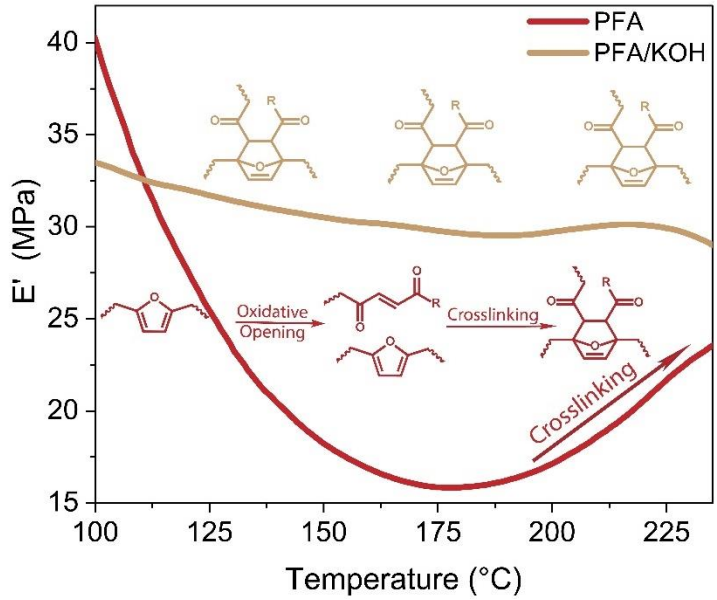

Figure 5.4-7. Magnified *E'* dependency on the temperature of PFA and PFA/KOH. The PFA/KOH was prepared at $^{-}$OH/C=O stoichiometry. The samples were prepared using a starting PFA at α = 0.8.

However, PFA/KOH displays a *E'* plateau starting around 100 °C. Therefore, the following conclusions can be drawn. First, even if the polycondensations are stopped at α = 0.8, a crosslinked polymer is still achievable (PFA/KOH). Secondly, the plateau of *E*' in PFA/KOH indicates that a full oxidation of the furans on the surface of the material occurred prior to the DMA scan (i.e. during the sample's preparation). This suggest that the oxidation-induced cycloadducts are widely present in PFA/KOH.

They are most-likely forming during the pre-curing step where air exposure is required to achieve a material. Hence, it suggests that the final crosslinking in PFA/KOH mostly occurs through the Pathway III. It is likely that the Pathway II also occurs, provided a sufficient amount of 2,5-dihydrofuran are present in the medium. In addition, an attempt to prepare a PFA/KOH using a resin at α = 0.3 was also performed. However, a material could not be obtained using the temperature conditions of this study (150 °C). Possibly because the condensation reactions were stopped too early in the polymerization process.

The followings are dedicated to the functionalization of PFA with a monoamine (Hex). The NH_2/C=O stoichiometric ratio was varied between 0.1 and 1, using a starting PFA at α = 0.8. The DMA curves of the PFA/Hex samples are available in Figure 5.4-8.

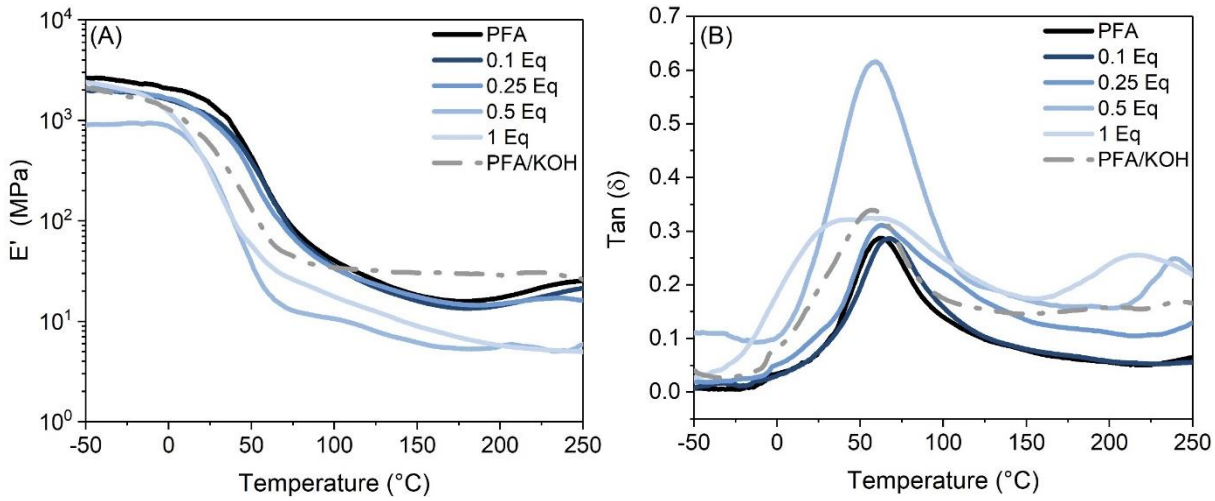

Figure 5.4-8. *E'* (A) and tan (δ) (B) dependency on the temperature of the PFA/Hex samples, PFA/KOH and PFA. The numbers in the legend correspond to the functionalization degree of the C=O. The samples were prepared with a starting PFA at α = 0.8.

In Figure 5.4-8A and B, the curves of PFA and PFA/Hex/0.1Eq are almost superimposed. The curves of PFA/Hex/0.25Eq are also close to PFA's until the tan (δ) maximum where the curves diverge. Regarding PFA/Hex/0.5Eq, its tan (δ) peak is both higher and wider than PFA's. Furthermore, after 150 °C its values of tan (δ) matches the ones of PFA/KOH (tan (δ) ≈ 0.15). Regarding the *E'* curve of PFA/Hex/0.5 Eq in Figure 5.4-8A, a plateau is observed starting at 175 °C. Finally, the PFA/Hex/1Eq displays a continuous decrease of *E'* on the studied range of temperature. Its tan (δ) values are close to PFA/KOH after the main tan (δ) peak. Furthermore, a secondary tan (δ) peak around 210 °C is observed. Overall, the behavior of the *E'* and tan (δ) curves of the PFA/Hex/0.5 and 1 Eq are somewhat similar to PFA/KOH. Hence, it is likely that the basicity of the NH_2 group interacts with the polymerization of PFA. The continuous decrease/plateau of *E'* of the samples with the highest proportion of hexylamine suggest that hardening through Pathway III occurred. In addition, the hexylamine might also plasticize the macromolecular network, thus yielding lower *E'* in the rubbery plateau than PFA and PFA/KOH.

Finally, Figure 5.4-9A and B display the DMA curves of PFA/Hex/1Eq (=PFA/Hex/ α0.8/1Eq) and PFA along with two samples from the previous section prepared with a difunctional amine, i.e., 1,6-diaminohexane (DiHex). Here, PFA/DiHex/α0.8/1Eq and PFA/Hex/ α0.8/1Eq have the same concentration of NH_2 groups. In Figure 5.4-9A, their *E'* curves are almost superimposed until 150 °C. After 150 °C the curve of PFA/Hex/ α0.8/1Eq keeps decreasing while the one of PFA/DiHex/α0.8/1Eq show a rise in *E'*. Hence, during its curing, PFA/DiHex/α0.8/1Eq did not fully oxidize through pathway III. It is likely that the difunctionality of DiHex induces C-N crosslinking. Thus, to reach gelation the PFA/DiHex/α0.8/1Eq does not need pathway III. On the contrary PFA functionalized with monoamine (PFA/Hex/α0.8/1Eq) need a crosslinking through Pathway III to reach gelation as the polycondensation are stopped by the basicity of the amine and no C=N crosslinking occured. In a similar way, PFA/DiHex/α0.3/1Eq has little functionalized C=O and cannot undergo polycondensations. To fill this lack of crosslinking nods, the polymer needs to be oxidized to crosslink through Pathway III. Hence, Pathway III acts as a last resort option when PFA cannot crosslink through Pathway II or C=N crosslinking.

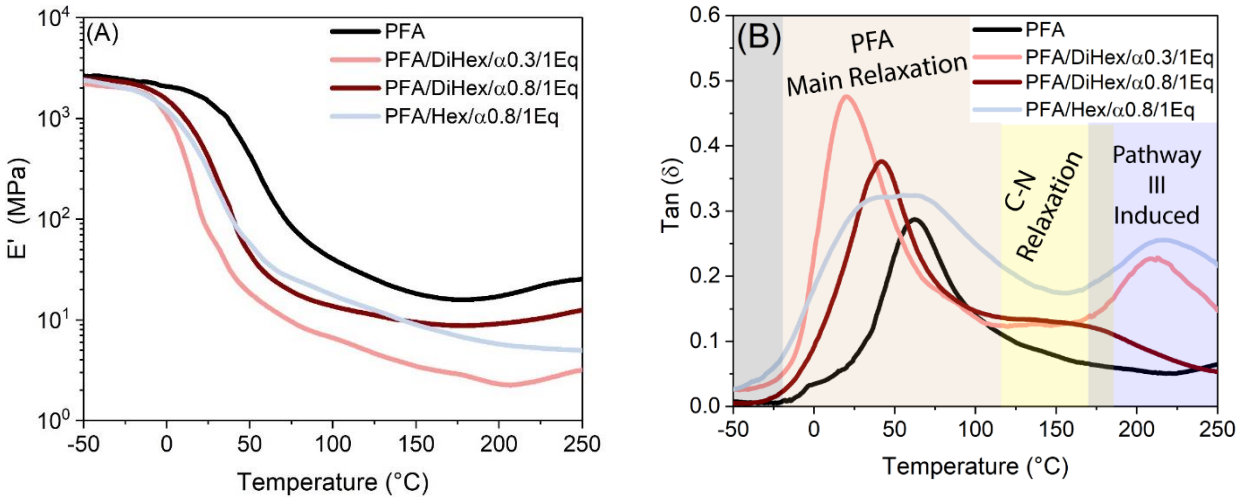

Figure 5.4-9. DMA curves, *E'* (A) and tan (δ) (B) of several PFA/Amine samples along with PFA. All the samples were prepared at NH_2/C=O stoichiometry.

In addition, in Figure 5.4-9B, PFA/DiHex/α0.8/1Eq displays a shouldering of the tan (δ) peak around 160 °C not seen in PFA/Hex/ α0.8/1Eq. Hence, the tan (δ) peak at 160 °C is most-likely linked to the relaxation of chains crosslinked by C-N bonds. Finally, in Figure 5.4-9A and B, PFA/Hex/ α0.3/1Eq behaves similarly as PFA/Hex/ α0.8/1Eq. Its *E'* continuously decreases and the secondary tan (δ) peak at 210 °C is observed. The 210 °C peak is associated with an increase in the *E'* and it might be somehow linked to the additional cross-links produced by pathway III.

In PFA/DiHex/ α0.3/1Eq, its C=O content was much lower than samples prepared with a starting PFA at a conversion degree of 0.8. Hence, a minimal concentration of C=O is required to produce PFA/DiHex materials with minimal intervention of pathway III.

5.4.5 Thermal and mechanical properties of PFA/KOH and PFA/Hex

As discussed earlier, it is possible to achieve PFA materials even if the polycondensation reactions were quenched with KOH and monoamines at a conversion degree of 0.8. Achieving PFA materials in such conditions is possible thanks to the oxidative surface crosslinking pathway (Pathway III of Table 5.1-1). In the followings, the properties of these materials are investigated.

Table 5.4-4 regroups data obtained from the DMAs, TGA and Shore D measurements of the PFA, PFA/Hex and PFA/KOH samples. The TGA curves are available in Figure 5.6-19.

Table 5.4-4. Thermomechanical properties of the PFA/Hex and PFA/KOH materials. All the samples were prepared using a starting PFA at $\alpha = 0.8$.

Sample	%w PFA	*E'* DMA 20 °C (MPa)	Tan (δ) maxima (°C)	$T_{5\%}$ (°C)	$T_{10\%}$ (°C)	Shore D
PFA	100	1680	63	328	362	82.4 ± 2.1
1 Eq KOH	85	690	57	235	300	Not measurable
0.1 Eq Hex	97	1250	68	327	361	85.4 ± 1.7
0.25 Eq Hex	93	1160	60	333	362	82.7 ± 3.0
0.5 Eq Hex	86	652	57	327	357	79.0 ± 2.9
1 Eq Hex	76	420	53	338	352	Not measurable

First, the PFA/KOH sample displays poor properties and very brittle behavior. The brittleness of the samples forbade the Shore D measurements, even on thick samples. The $T_{5\%}$ and $T_{10\%}$ values indicate a decrease of thermal stability for PFA/KOH in comparison with PFA.

Regarding the PFA/Hex samples, the PFA/Hex/0.1 and 0.3 Eq have properties close to PFA although their *E'* at 20 °C are lower. The PFA/Hex/0.5 and 1 Eq samples have significantly lower *E'* at 20 °C than PFA. The $T_{5\%}$ and $T_{10\%}$ of the PFA/Hex materials are almost identical to PFA's.

Finally, Figure 5.4-10 regroups data extracted from the tensile curves of PFA, PFA/Hex and PFA/KOH. Representative examples of the tensile curves are available in Figure 5.6-20.

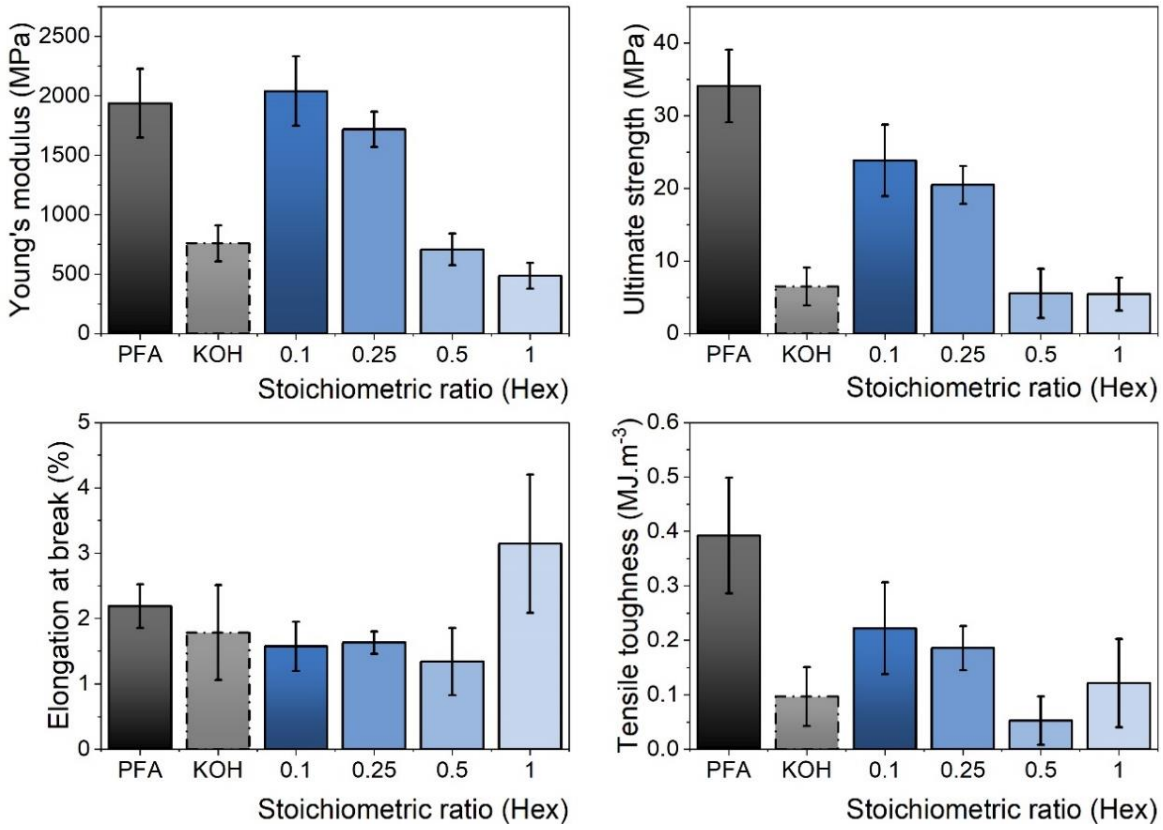

Figure 5.4-10. Tensile data of the PFA/Hex at varying NH_2/C=O stoichiometry PFA-KOH was prepared at $^-$OH/C=O stoichiometry. All the samples were prepared using a PFA at $\alpha = 0.8$.

The brittleness of PFA/KOH is highlighted through much lower yield strength elongation at break and Young's modulus than PFA. For the PFA/Hex samples, the properties progressively decrease with the increasing amount of hexylamine in the material, in coherence with the previous observations. Overall, although materials are achievable, introducing monoamines or KOH in a PFA at $\alpha = 0.8$ results in a loss of mechanical properties, especially at the highest NH_2/C=O stoichiometric ratios. The main reason behind this is likely the quenching of the final polycondensation reactions. Therefore, the loss of properties might be circumventable by the use of PFA at higher conversion degrees ($\alpha \geq 0.9$) to minimize oxidation-induced crosslinking (Pathway III).

To sum-up, the fabrication of PFA materials using monoamines is feasible. However, the basicity of the amine stops the condensation reactions. The obtention of a thermoset is nevertheless achieved through the oxidation-induced crosslinking pathway (Pathway III of Table 5.4-1). As a consequence, the materials display lower mechanical properties compared to PFA. In the case of PFA/KOH, the loss of properties might also be linked to the amount of salt remaining in the material (≈ 15 %w)

In the PFA/Diamine materials the lack of polycondensation might be counteracted by the formation of C-N crosslinks. Hence, if one desires prepared PFA/Monoamine materials, it is highly suggested to use PFA with conversion degrees higher than 0.9 and preferably higher than 0.95 although solubility issues will be encountered.

5.4.6 Conclusions:

To conclude, in this section the C=O in poly(furfuryl alcohol) (PFA) resins were reacted with primary amines to form PFA/Amine materials. The influence of the conversion degree of the starting PFA on the materials' properties was investigated. In addition, the effect of bases on the acid-catalyzed polymerization of FA was assessed.

The influence of the conversion degree (α) of the PFA used in the preparation of the materials was evaluated using 1,6-diaminohexane (DiHex). PFAs with at α comprised between 0.3 and 0.95 were studied. For $\alpha \leq 0.8$, the condensation reactions of FA and oligomers were compromised by the basicity of the amines. Hence, the resulting material showed poor mechanical properties and little increase of flexibility. For $\alpha \geq 0.9$ the PFA/DiHex materials had properties close to PFA. In addition, during the functionnalization of the C=O by NH_2 a phase separation occured. The yield of precipitate may be up to 65 %w of the reagents weight. This insoluble phase was isolated and compression molded. The resulting material displayed a T_g of 145 °C although its thermal degradation resistance was slightly decreased in comparison with PFA. Hence, the use of the precipitated product is reccomended to produce high T_g bio-based materials. In addition, the use of PFA with $\alpha \geq 0.9$ should be prefered to produce rigid PFA/Amine material.

The second part of the study involved the reaction of PFA with hexylamine to assess the effect of monoamines on PFA. Briefly, the resulting material showed decreased properties as the amount of hexylamine was increased. A reference PFA was also prepared using potassium hydroxide (KOH) as a polycondensation quencher. Although obtaining a hard and cohesive PFA in such conditions is achievable, it results in a brittle material. Hence, the basicity of the amines might prevent good mechanical properties by stopping the polymerization of PFA's oligomer if the conversion degree of the starting PFA is too low ($\alpha \leq 0.8$). The obtention of a PFA material with little polycondensation reactions is feasible through the oxidation-induced crosslinking. Such crosslinking pathway would be favored if the polycondensation are stopped and the pre-polymer exposed to enough air and heat.

5.5 General conclusion of chapter 5

The aim of this chapter was to extend the possible applications of PFAs trough functionalization of the C=O within PFA with primary amine to form imines and pyrroles.

First, a proof a concept was conducted in section 5.2. Priamine 1071, a flexible bio-sourced fatty amine was reacted with the carbonyls PFA. By varying the stoichiometric ratio of Priamine, the properties of the materials could be drastically modified. A stoichiometric ratio of one C=O for one NH_2 decreased the T_g by 40 °C which multiplied the elongation at break by seven while maintaining the thermal resistance of PFA and decreasing its ultimate strength, Young's modulus and hardness. In addition, the stability of Priamine functionalized PFAs towards hydrolysis in mild condition was confirmed.

Section 5.3 and 5.4 were dedicated to understanding the factors influencing the properties of the PFA/Amine materials.

Section 5.3 investigated the influences of the amines' structure. As expected, rigid amines decrease the mobility of the polymeric network while flexible ones increase it. In this section, the impact of the post-curing environment was also assessed. Briefly, if flexible PFA/Amine materials are exposed to air during their post-curing the samples form a crust which can tremendously impact the properties of the material by shifting their T_g from below to above room temperature. This crust is believed to take its origin from the oxidation-induced surface crosslinking detailed in chapter 3 and 4. The impact of the crust was the most pronounced for PFA weight fraction between 75 and 50 %w in a PFA/Jeffamine D2000 system.

Section 5.4 focused on the influence of the conversion degree of PFA prior to its functionalization with an amine together with the impact of the amines' basicity on the acid-catalyzed polymerization of FA.

The conversion degree of PFA was found to be of major importance, especially when rigid materials are targeted. In addition, precipitation may occur during the functionalization of PFA with amines. The precipitate may be isolated and processed into a high T_g material (T_g > 140 °C). To produce rigid materials, a conversion degree of 0.9 or above is recommended.

Regarding the effect of the amine's basicity, a C6 monoamine and potassium hydroxide were employed as models to avoid C=N crosslinking. This section highlighted the possibility of reaching a material from a PFA prepolymer even though the polycondensation are stopped at a conversion degree of 0.8. This it likely possible thanks to the oxidation-induced surface crosslinking of PFA (pathway III).

5.6 Supplementary

5.6.1 Supplementary information for section 5.2

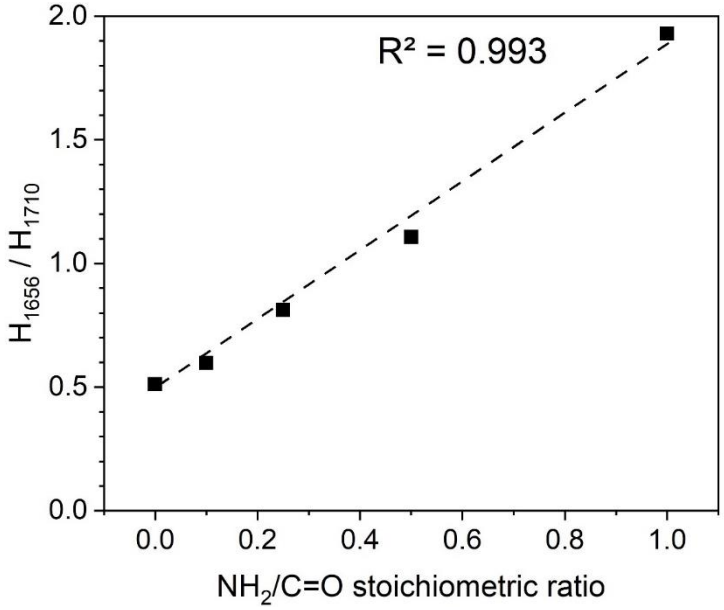

Figure 5.6-1. Height ratio of the 1656 cm^{-1} over the 1710 cm^{-1} band from the normalized FTIR spectra against the NH_2 equivalents introduced.

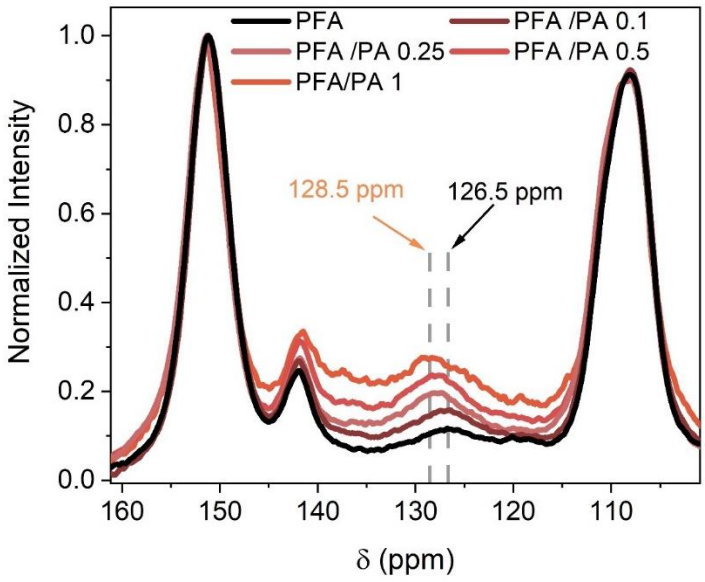

Figure 5.6-2. Magnified ^{13}C ssNMR spectra of PFA/PA samples

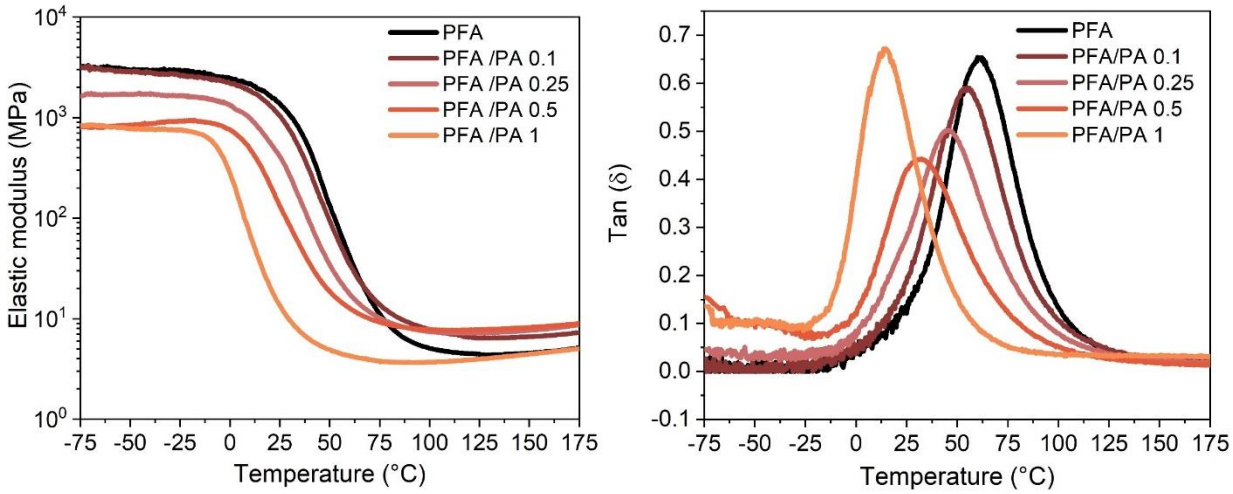

Figure 5.6-3. Elastic moduli from the DMA curves of PFA and PFA functionalized with Priamine 1071

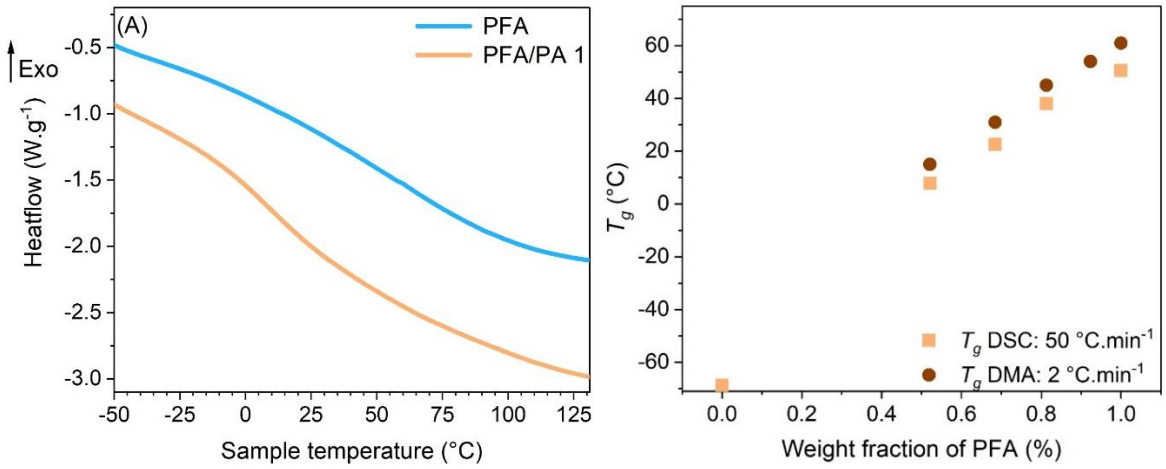

Figure 5.6-4. (A) DSC scan of PFA and PFA/PA 1 at 50°C.min^{-1}. (B) Dependency of the polymers' T_g from DMA (2 °C.min^{-1}) and T_g from DSC (50 °C.min^{-1}) on the weight fraction of PFA.

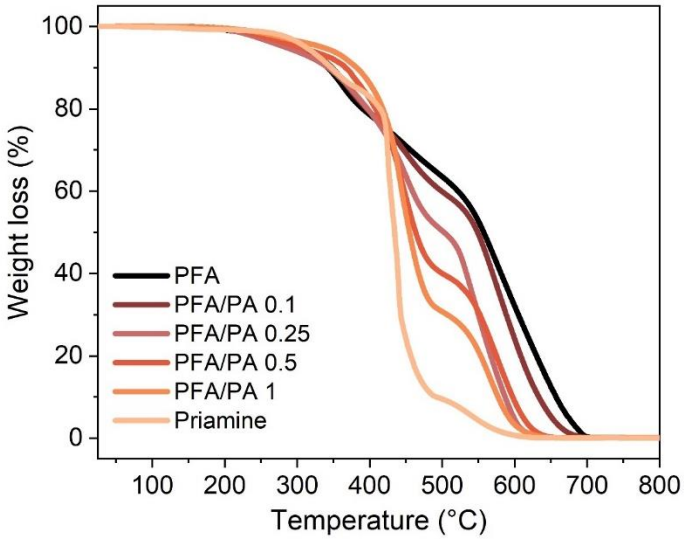

Figure 5.6-5. TGA curves of PFA, Priamine 1071 and PFA functionalized with Priamine under oxidative conditions.

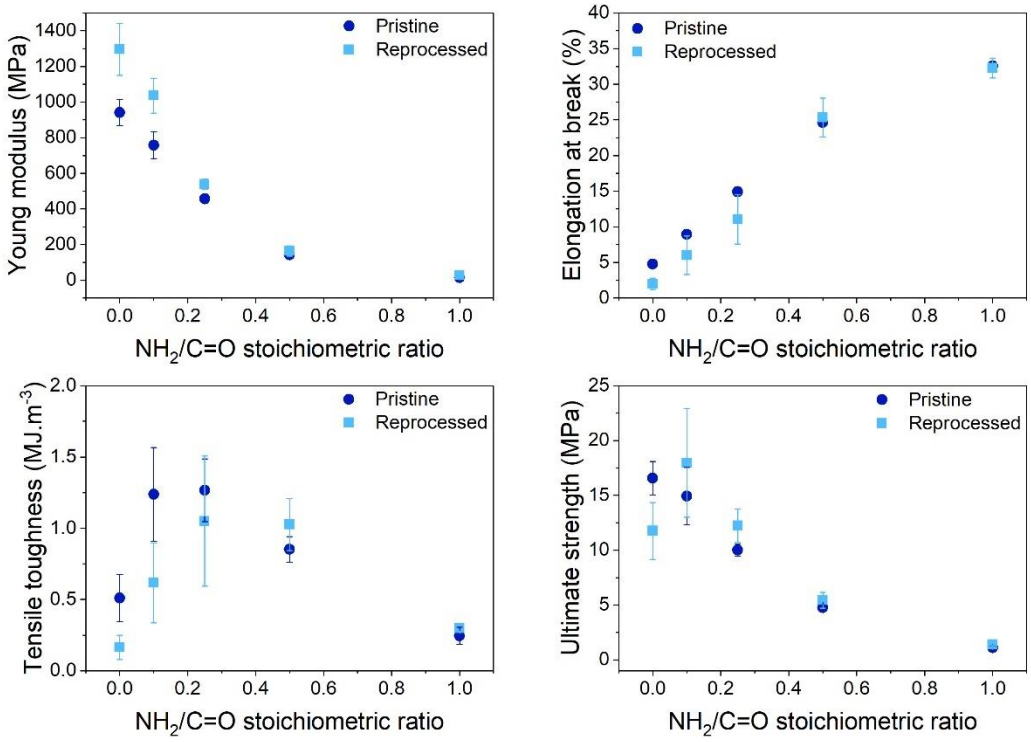

Figure 5.6-6. Mechanical Recycling PFA/PFA: tensile properties

5.6.2 Supplementary information for section 5.3

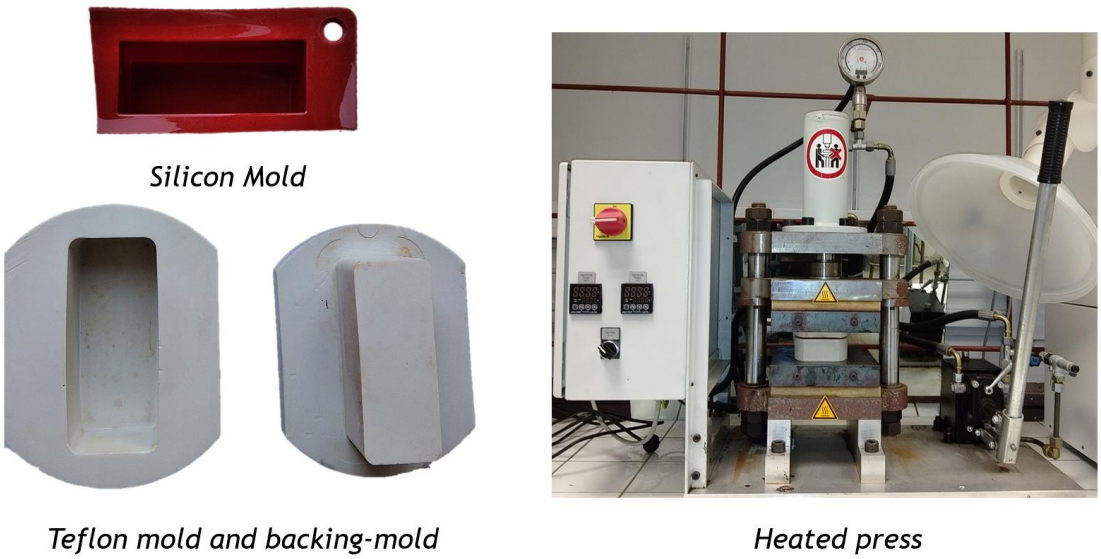

Figure 5.6-7. Picture of the molds, backing mold, and heated press used for the preparation of the materials

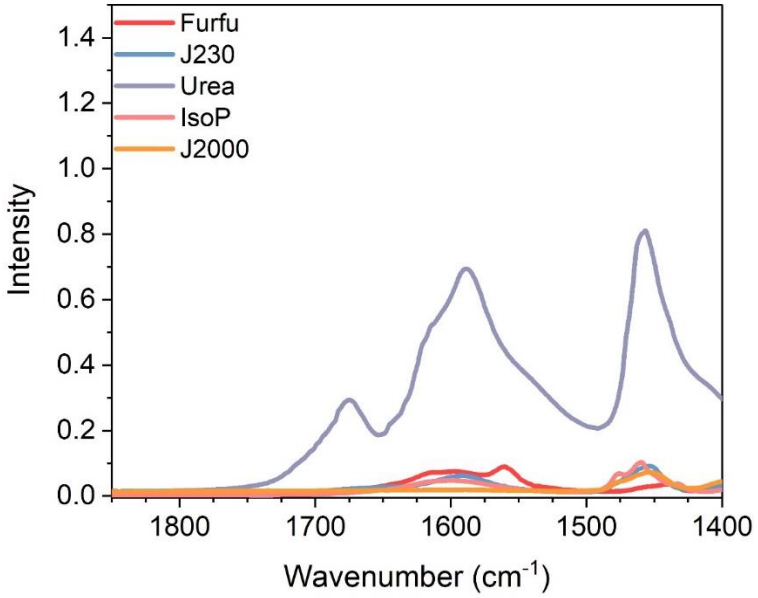

Figure 5.6-8. Magnified FTIR spectra of the amines used in the study. The samples were prepared at NH_2/C=O stoichiometry.

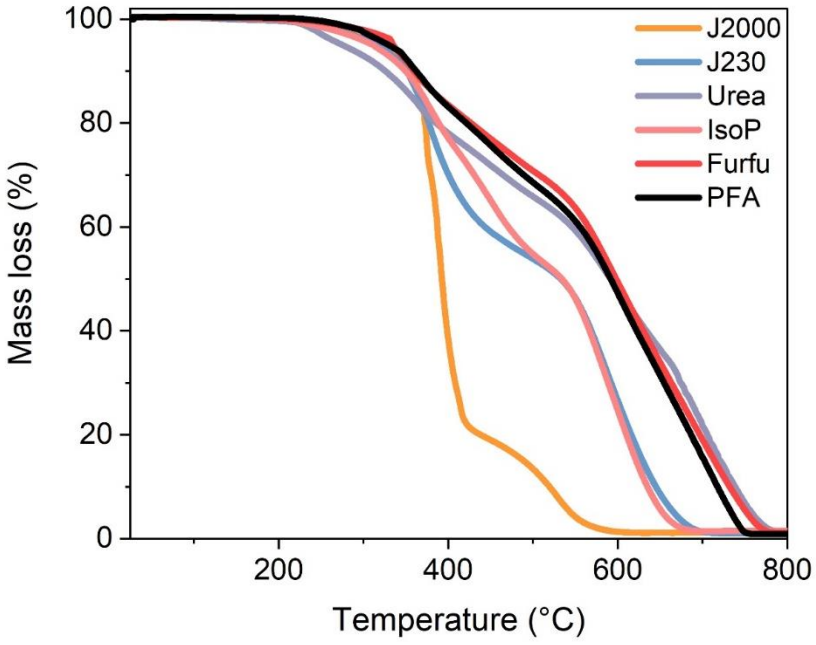

Figure 5.6-9. TGA curves of the PFA/Amine materials under oxidative atmosphere. The samples were prepared at NH_2/C=O stoichiometry. The TGA were performed under air flow.

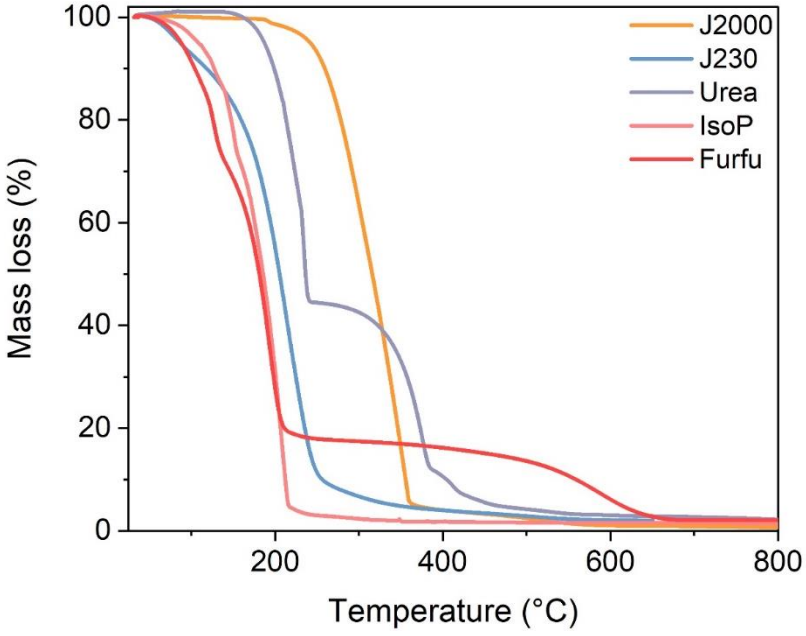

Figure 5.6-10. TGA curves of the pure amines under air flow.

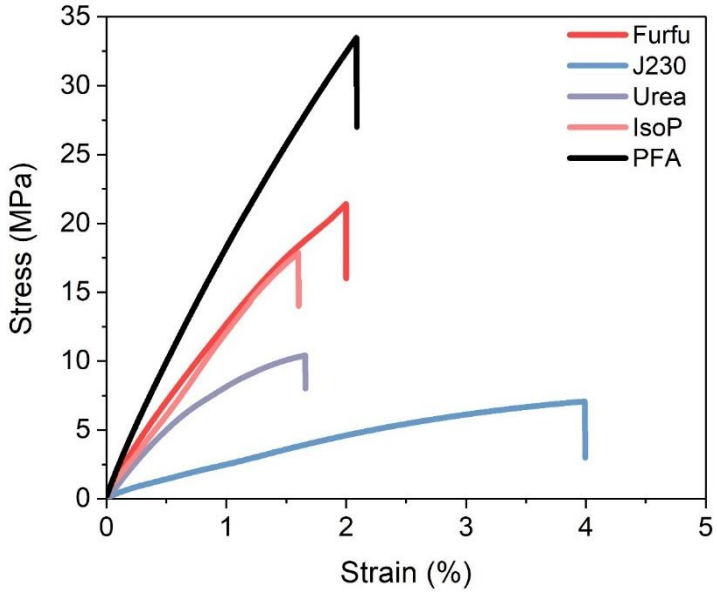

Figure 5.6-11. Examples of tensile curves from PFA reacted with several amines. The samples were prepared at NH_2/C=O stoichiometry.

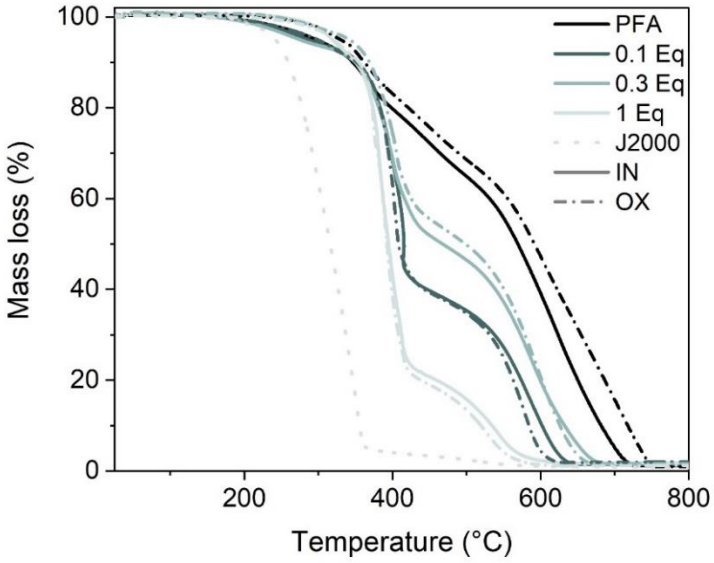

Figure 5.6-12. TGA curves of pure J2000 (dot line) and PFA/J2000 at varying NH_2/C=O stoichiometry post cured in the oven (OX, dash-dot lines) or within the mold (IN, plain lines). The numbers in the legend are the NH_2/C=O stoichiometric ratios. The TGAs were performed under air flow.

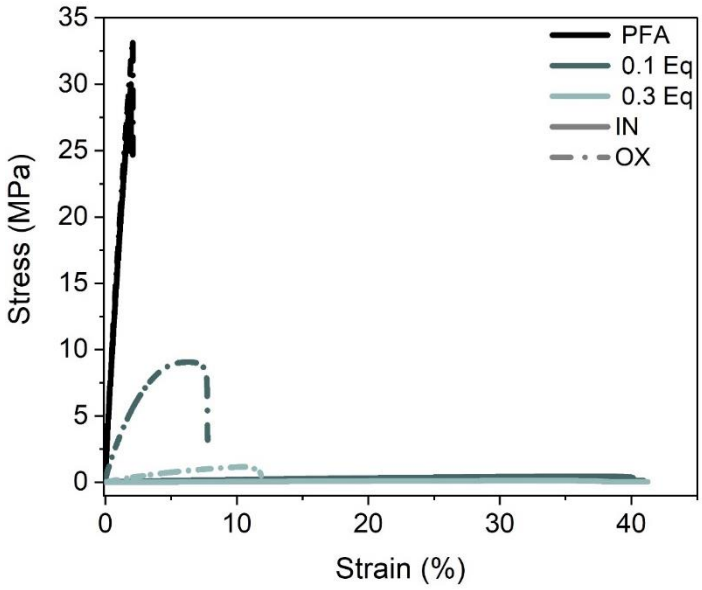

Figure 5.6-13. Examples of tensile curves of the PFA/J2000 at varying NH_2/C=O stoichiometry post cured in the (OX, dash-dot lines) or within the mold (IN, plain lines). The numbers in the legend are the NH_2/C=O stoichiometric ratios.

5.6.1 Supplementary information for section 5.4

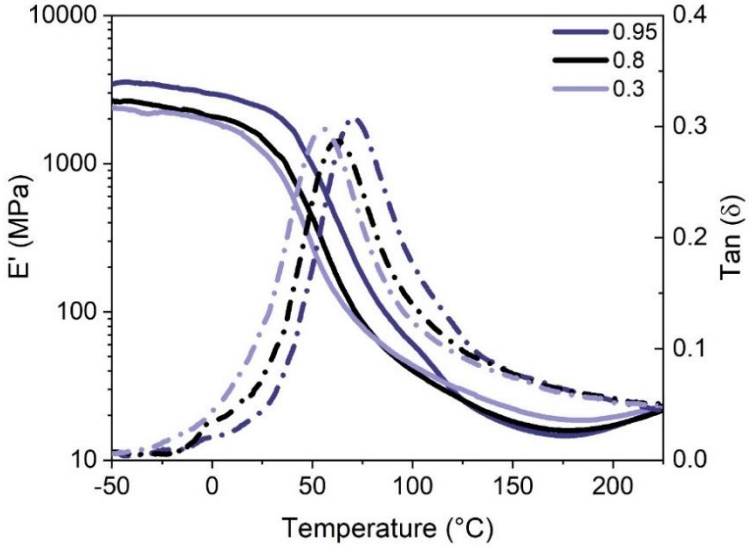

Figure 5.6-14. DMA curves of the reference PFA materials prepared with PFA at various conversion degrees (numbers in the legend). The plain lines are the E' curves and the dash-dot lines the tan (δ) curve.

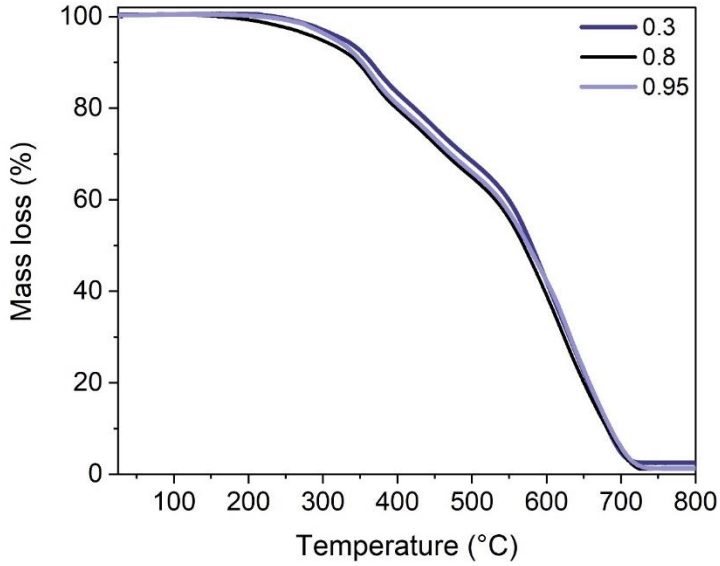

Figure 5.6-15. TGA curves of the reference PFA materials prepared with PFA at various conversion degrees (numbers in the legend). The plain lines are the E' curves and the dash-dot lines the tan (δ) curve.

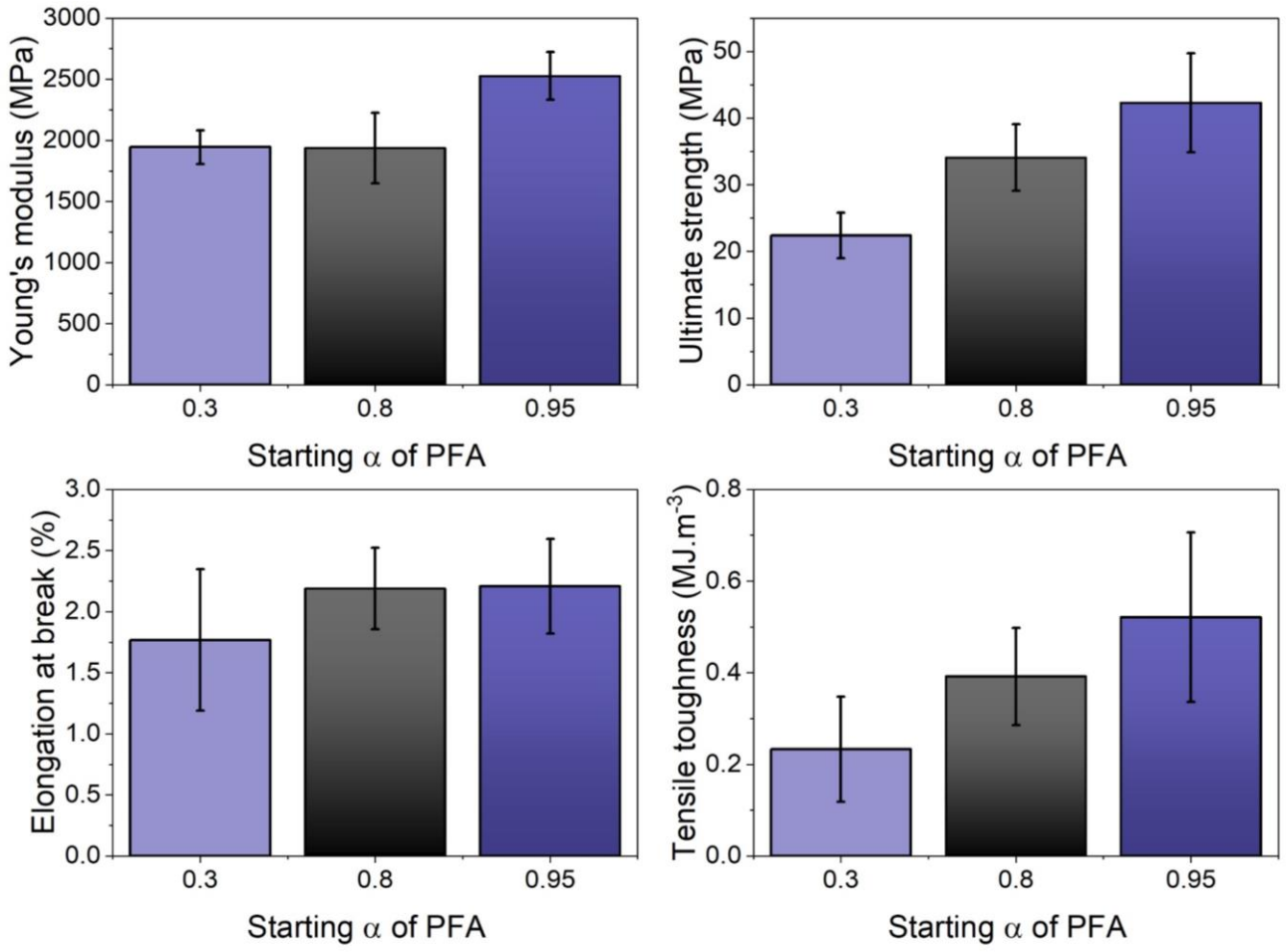

Figure 5.6-16. Tensile data of the reference PFA materials prepared with PFA at various conversion degrees.

Table 5.6-1. Thermomechanical properties materials prepared with starting PFAs at various conversion degrees.

Starting α of PFA	E' DMA 20°C (MPa)	Tan (δ) maxima (°C)	$T_{5\%}$ (°C)	$T_{10\%}$ (°C)	Shore D
0.30	1390	56	316	352	83.8 ± 2.9
0.80	1680	63	328	362	82.4 ± 2.1
0.95	2500	78	329	364	83.2 ± 2.6

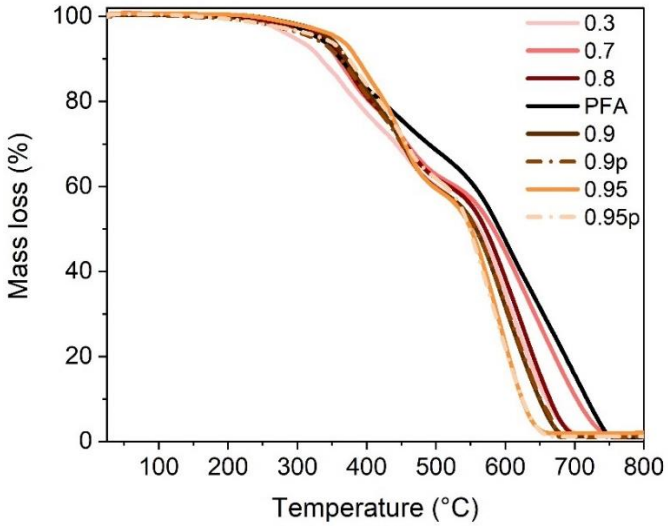

Figure 5.6-17. TGA curves of the PFA/DiHex at NH_2/C=O stoichiometry using PFAs at different conversion degrees (0.3 to 0.95). The numbers in the legend indicate the conversion degree of each starting PFA. The letter "p" indicates that only the precipitated macromolecules were used (dash-dot lines).

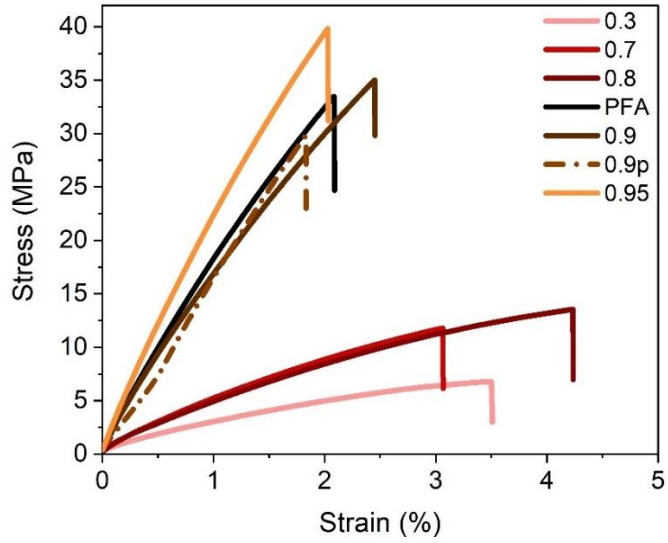

Figure 5.6-18. Examples of tensile curves of the PFA/DiHex at NH_2/C=O stoichiometry using PFAs at different conversion degrees (0.3 to 0.95). The numbers in the legend indicate the conversion degree of each starting PFA. The letter "p" indicates that only the precipitated macromolecules were used (dash-dot lines).

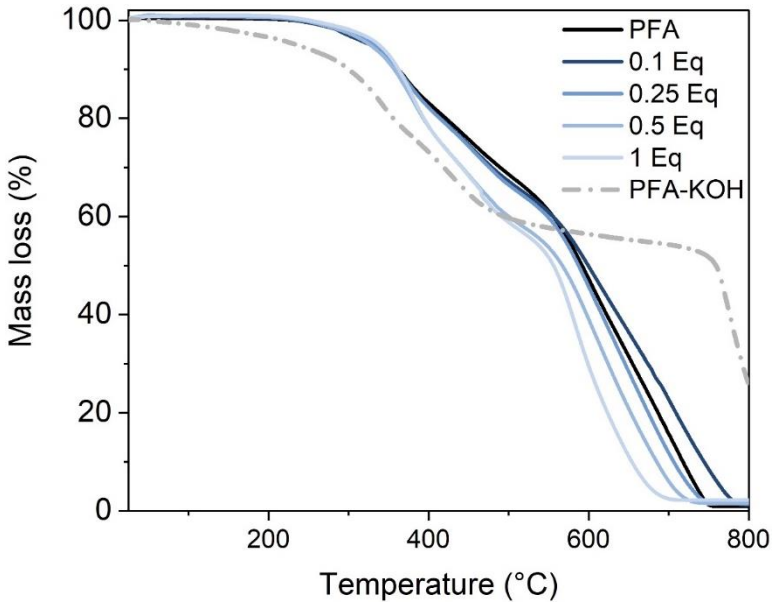

Figure 5.6-19. TGA curves of PFA/Hex samples at varying NH_2/C=O stoichiometry. PFA-KOH was prepared at $^-$OH/C=O stoichiometry. All the samples were prepared using a PFA at $\alpha = 0.8$.

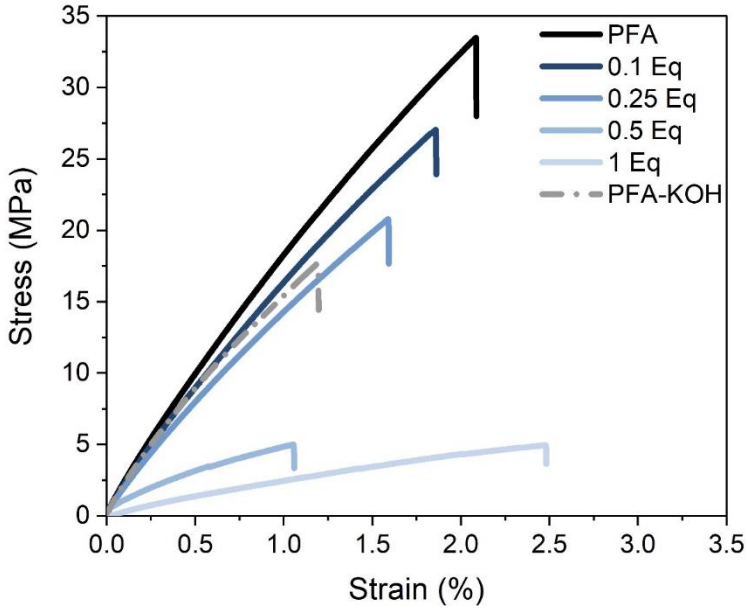

Figure 5.6-20. Representative tensile curves of PFA/Hex samples at varying NH_2/C=O stoichiometry. PFA-KOH was prepared at $^-$OH/C=O stoichiometry. All the samples were prepared using a PFA at $\alpha = 0.8$

Conclusions and perspectives

5.7 Conclusions

In the introduction, our dependency to petroleum-based products was highlighted. One possibility to tackle this issue is to use renewable resources to manufacture materials. In this line, furfuryl alcohol (FA), a widely synthetized from crop wastes, can be employed to manufacture high-performance materials. Indeed, when FA is exposed to an acidic medium, it polymerizes into poly(furfuryl alcohol) (PFA).

During its polymerization, (PFA) undergoes a furan ring opening side-reaction leading to carbonyls. Although PFA has been studied since the mid-20th century, the furan ring opening was often disregarded. This thesis aims at probing the possibilities offered by this "side-reaction". Hence, the major goals of this thesis were to quantify, control and take advantage of this side-reaction. Ultimately, the aim was to give an extent of tunability to this biobased thermoset by functionalizing its carbonyls.

First, chapter 1 reported the current knowledge on the application, structure and general features of PFA. Chapter 2 answered the following questions. *How can the carbonyls in PFA be quantified? Can the quantification be performed in an accurate and reproductible manner ? When do the carbonyl form during the polymerization? What are the leverages available to control the ring-opening reaction ?*

The carbonyls in PFA can be quantified by at least three methods. Potentiometry, quantitative ^{19}F and ^{13}C NMR can be used for this purpose. The method used can inform on the chemical availability of the carbonyls within PFA (steric hindrance, ketals, stabilized enols). The carbonyls tend to form at a steady rate during most of the polymerization. Finally, the most efficient way to act on the carbonyl content of PFA was to introduce additional water from the beginning of the polymerization (PFA+).

Indeed, at a given conversion degree, a neat PFA (PFA°) comprise about 2.2 $mmol.g^{-1}$ of C=O, a PFA+ prepared in aqueous condition has nearly two times more carbonyls, i.e. 3.7 $mmol.g^{-1}$. Another way of considering the carbonyl content of PFA is the notion of "Degree of Open Structure". In this case, 3.7 $mmol.g^{-1}$ translates into 15 % of open furan ring. In other words, 1/6 of PFA's furan rings may be opened

Chapter 3 was dedicated to the structural investigation of carbonyls within PFA and dealt with the following questions. *Where are the carbonyls located in the macromolecular chains of PFA ? What is their chemical environment ? Why may a crust forms of the surface of PFA resins ?*

To deal with these questions, bidimensional NMR and MALdI-ToF were employed. This chapter highlights that the furans located in the end of the polymer chains are the most reactive ones. Indeed, in the case of PFA prepared in aqueous condition, the methyl furans tend to open into levulinic-like units through a hydrolytic pathway.

In the case of neat PFAs, the methylfurans tend to transform into terminal lactones. In both systems, the monosubstituted terminal furans are sensitive to oxidation by air. As a consequence, they open into conjugated 1,4-ketoaldehydes. Overall, the aldehydes account for 10 to 20 % of the carbonyls present in PFA. Finally, conjugated aldehydes are prone to react with furans through a Diels-Alder cycloaddition. This additional crosslinking leads to a progressive darkening and hardening of the surface of PFA resins.

Two questions were at the center of chapter 4. *What is the structural evolution of PFA after its polymerization and before its carbonization ? What is the impact of the oxidation-induced surface crosslinking on the properties of the materials ?*

Chapter 4 investigated the influence of oxidative and inert atmospheres at 200 °C on the properties of PFAs. It oxidized samples displayed a significant amount of aromatic spectrometric signals on the surface of the polymer while non oxidized samples displayed only furanic signals.

It was suggested that the cycloadduct resulting from the oxidation-induce surface crosslinking is prone to aromatization. The oxidation and crosslinking can be observed in TGA and DMA. The thickness of the oxidized layer was average to about 20 µm. The oxidized layer had little effect on the mechanical properties of the materials, aside from a small decrease of damping capacity. In addition, this oxidized layer allowed a 50 °C increase of oxidation onset temperature in comparison with non-oxidized PFA.

Finally, chapter 5 dealt with the questions related to the functionalization of PFA's self-generated carbonyls. *Are the carbonyls within PFA suitable for amine functionalization ? Can amines mitigate the brittleness of PFA while maintaining the thermal stability of PFA ? What is the extent of tunability offered by the amines ?*

First, a proof of concept was performed using Priamine 1071, a diamine sourced from fatty acids. The chemical reactions between PFA and Priamine yielded both imines and pyrroles. The stoichiometric ratio of NH_2/C=O was varied between 0.1 and 1.0. As a result, the T_g of the PFA/Priamine could range from 60 to 20 °C for the highest proportions of Priamine. As a result, the elongation at break could be multiplied by seven and the Young's modulus divided by a hundred.

Other mechanical properties such as the ultimate strength or hardness followed the same trend. An optimum of tensile toughness was found for a NH_2/C=O stoichiometric ratio of 0.25. In addition, the thermal stability of PFA, one of its key features, was maintained for all the PFA/Priamine materials. Moreover, the stability of PFA/Priamine towards mild hydrolysis was ensured. Finally, the possibility to mechanically recycle non-aged PFA and PFA/Priamine materials was highlighted. This proof of concept was followed by deeper investigations focusing on four factors susceptible of influencing the properties of PFA/Amine materials.

First, the influence of the amine's structure on the properties of the materials was studied. Briefly, flexible amines (Priamine 1071, Jeffamine D2000) allow an increase of the molecular mobility while rigid amines such as isophorone diamine have the opposite effect.

All studies combined, the T_g of PFA/Amine materials could be tuned between -44 and 145 °C, i.e. a range of almost 200 °C, while maintaining the thermal stability of PFA.

Chapter 3 and 4 highlighted air oxidation as a source of a structural evolution of PFA. Hence, a similar study was performed on PFA/amine materials using Jeffamine D2000. Two post-curing environment, oxidative and inert, were compared agains't the proportion of amine in the material. For PFA alone, little effect on the properties were observed, in concordance with chapter 4. Similarly, samples with less than 25 %w showed little sensitivity to the post-curing environment.

However, between 75 and 50 %w, tremendous effects were observed. In these cases, the samples formed a crust, most-likely linked to the oxidation-induced surface crosslinking. The formation of the crust shifted the T_g of these samples by up to 40 °C, i.e. from below to above the room temperature. As a consequence, the mechanical properties (Young's modulus, ultimate strength, …) shifted by orders of magnitude towards a rigid behavior. Hence, if one desires to flexibilize PFA, it is recommended to either use large amounts of amines and/or protect the materials from oxidations. A coating or the inclusion of anti-oxidants might be effective for this purpose.

The conversion degree of PFA prior to its functionalization proved to be a factor of influence. In this study, 1,6-diaminohexane was used. PFAs at conversion degrees between 0.3 and 0.95 can all be employed to produce PFA/Amine materials. However, the basicity of amines may interfere with the acid-catalyzed polymerization of FA. As a consequence, if one wants to manufacture rigid PFA/amine materials, it is advised to employe PFAs at conversion degrees of 0.9 and above although solubility issues might be encountered.

Finally, in the state of the art, it was shown that knowledge on the structure of PFA was not required to employe it in a variety of applications for more than fifty years. Yet, the deeper knowledge of PFA acquired in recent studies and this manuscript might pave the way to a rebirth of PFA towards a set of highly tunable polymers, sourced from agricultural wastes (PFA) or biorefinery wastes (humins).

5.8 Perspectives

The perspective revolving around PFA and its functionalization are numerous. Three studies are still on-going at the time this section is being written. The first one deals with the reduction of PFA's carbonyls to hydroxyl and the properties of the resulting materials. The second one is dedicated to the manufacture and characterization of PFA/Chitosan composites. The third one focuses on toughening PFA by incorporating poly(butadiene) rubber in the material.

The carbonyls of PFA could be exploited in a number of ways. The transformation of carbonyls into primary amines was attempted. Comments on these attempts are available in annexes together with other observations made during this thesis. An exhaustive list of the carbonyls' chemical reaction would not be appropriate here. Yet, relevant examples include the conversion of carbonyls to epoxies or aminophosphates for the manufacture of high-performance thermosetting resins. In addition, the transformation of non-conjugated C=O to C=C by the Wittig reaction could open room for post functionalization or radical polymerization.

The carbonyls could also be exploited to modify the surface properties of PFA coatings. For instance, (super)hydrophobic, anti-oxidant, fire retardant or anti-bacterial moieties could be attached to PFA, providing enhanced properties.

The carbonyls could also be a source of recyclability. Indeed, their reactivity could allow aged PFA – containing carbonyls - to be included in another material or in fresh PFA as a reactive charge. Up to 50 %w of oxidized PFA can be incorporated into fresh PFA and cohesive material can be achieved, as shown in annexes.

Finally, carbonyls are not the only reactive species in PFA. The furan by itself is susceptible to Diels-Alder cycloaddition. Such approach could be used to introduce new properties in PFA materials. This is the subject of a current collaboration with the university of Poitiers.

Annexes

Other work

Going back to PFA systems. The Leuckart reaction was attempted on insoluble humins, soluble PFAs and cured PFAs to transform the carbonyls into primary amines. This reaction is a two step reaction. First the formation of a formamide derivatives (T > 120°C) and then hydrolysis of the formamide to free a primary amine).

The first step was successfully achieved on cured PFA, at 170 °C and under nitrogen. This is shown by the orange FTIR spectrum next page though a shift of the C=O band towards a lower wavenumber typical of amides. Nitrogen is mandatory to avoid aromatization and further formation of carbonyls. The hydrolysis complexified the FTIR spectra. Altough bands can be attributed to amines (3000 – 3550 cm^{-1} and 1580-1650 cm^{-1}) no definitive attribution can be done. In addition, quantification of amines is complex for insoluble materials and amine presence tests can only be performed on soluble amines. Overall, the Leuckart reaction is most-likely feasible on PFA systems. However, such investigation would requires frequent access to equipment capable of handling insoluble materials (MALDI-ToF, ssNMR, elemental analyses, XPS,…).

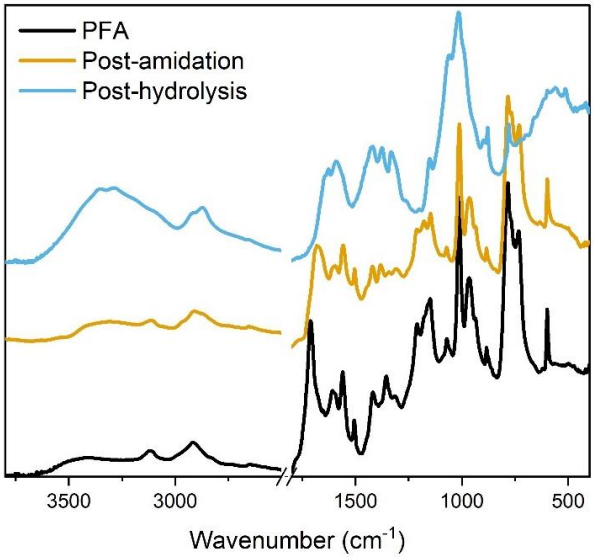

FTIR spectra of PFA, and a PFA subjected to the first (post-amidation) and second (post-hydrolysis) steps of the Leuckart reaction.

Other attempts to transform the C=O of PFA into primary amines were conducted by bubbling NH_3 into a solution of PFA followed by $NaBH_3$ reduction. Theses attempts did not lead to primary amines, possibly due to the instability of imines. It might be possible to perform similar reaction using high pressure systems involving NH_3 and H_2 or using NH_3 dissolved in dry ethanol or methanol

Work indirectly link to the thesis

During my PhD thesis I also participated un FUR4Sutain COST action (Meeting, summer school, HH, STSM program). During my STSM (Short Term Scientific Mission), I spent 3 weeks in the group of Dr. Andreia Sousa at the university of Aveiro. We investigated the recyclability humins and PFA using innovative solvents in addition to acquiring the ssNMR spectra of humins.

In addition, several other parallel studies were conducted. The first one was a collaboration with Politecnico Di Torino. The goal was to use furan allyl derivatives for the production of coatings by photopolymerization. In this work, I performed the UV assisted synthesis of cis-cyclobutane-1,2-dicarboxylic acid from trans-3-(2-furyl) acrylic acid. [334]

The second collaboration was with the university of Thessaloniki in the scope of a STSM grant (FUR4Sustain COST action). Here, I participated to the fabrication of composite made from cellulose nanofibers and PFA. The work conducted during this period lead to a publication currently under submission.

Mechanical reprocessability of PFA

In chapter 5, the reprocessability of non-aged PFA was observed. It was not clear if it was caused by reversible chemical reactions or lack of curing. This led to the following investigation. PFA and Ox-PFA powders from chapter 4 were compression molded at 200 °C for 2 h at 30 bars. Pictures of the samples are displayed bellow. The sample made from Ox-PFA powder was not cohesive. For PFA, a cohesive sample yet extremally brittle sample was achieved.

Fully cured, reprocessed PFA

Fully cured and oxidized, reprocessed Ox-PFA

In addition, it was tested to mix Ox PFA powder with uncured PFA powder (α = 0.95) and mold the powders for 2 h at 150 °C under 30 bars. The picture bellow showcase samples comprising 25 %w and 50 %w of Ox PFA. Both weigth fractions lead to cohesive materials.

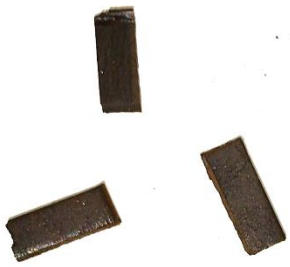

50 %w Ox-PFA

25 %w Ox-PFA

This work could be continued to prove the concept that Ox PFA could be recycled in fresh resins without impact on the properties

PFA and wrinkled surfaces

During my PhD, I tried to soften PFA using Jeffamine m600 (a large monoamine). When the Jeffamine m600 was mixed with PFA, no materials could be achieved at 150 °C, even after 15 h of curing. So, the temperature was increased to 200 °C for 3 hours and then to 250 °C for 3 h. The picture bellow displays the sample that came out of the oven. The sample had a hard crust and a soft heart. Interestingly, the topology of the surface is somewhat similar to the wrinkled PFAs obtained under UV light. In addition, the FTIR spectra bellow correspond to the sides of the sample facing the air and the aluminum mold. The spectra clearly show structural differences between the air-exposed and air-protected sides. In addition, the air-side spectrum show resemblance with a PFA prepared using UV (cf section 2.4.4), i.e. little furan signals, potential aromatic C=C, and qualitatively high amount of potential C=O and COOH. Maybe, the oxidative ring-opening and surface crosslinking take somehow part in the formation of wrinkles in these PFAs.

PFA/Jeffamine m600 sample

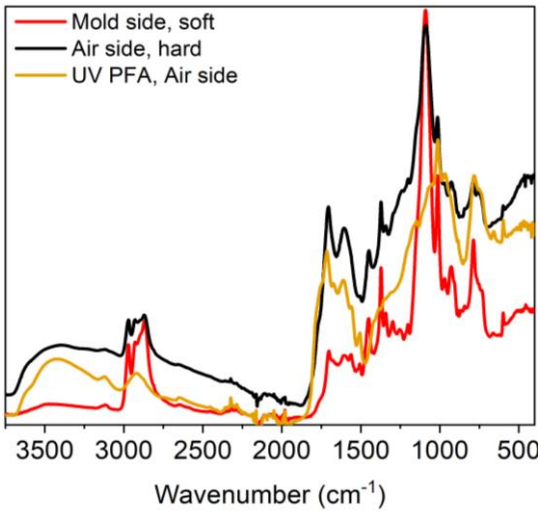

FTIR spectra of the PFA/Jeffamine m600 sample of both sides (air-facing and mold-facing)

Accepted publications:

Macromolecules

pubs.acs.org/Macromolecules Article

Monitoring the Degree of Carbonyl-Based Open Structure in a Furanic Macromolecular System

Pierre Delliere and Nathanael Guigo*

Cite This: https://doi.org/10.1021/acs.macromol.1c02098 Read Online

ACCESS | Metrics & More | Article Recommendations | Supporting Information

ABSTRACT: Hydrolytic furan ring opening is exploited to open biobased furanic molecules into levulinic-like platform molecules. However, the occurrence of ring opening in furanic macromolecules—considered so far as a side reaction—has never been quantitatively assessed. Poly(furfuryl alcohol) (PFA) was chosen to highlight the concept that furan ring opening can be monitored during polymerization. Both oximation and ^{19}F NMR quantification methods were employed to address this issue. This investigation shows that a substantial quantity of carbonyl species is formed during the polymerization, thus introducing the concept of degree of open structure (DOS). Polymerization of furfuryl alcohol (FA) in a 50 wt % aqueous solution approximately doubles the fraction of structures that are opened—leading up to 15% of opened furanic entities (i.e., ~3.5 mmol of carbonyl per gram of PFA)—compared to FA polymerization conducted without additional water. The DOS was observed to increase continuously throughout the polymerization. Finally, steric hindrance has a role in the accessibility of carbonyls in PFA.

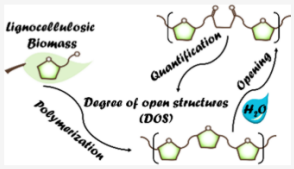

molecules MDPI

Article

Conditions to Control Furan Ring Opening during Furfuryl Alcohol Polymerization

Lucie Quinquet †, Pierre Delliere † and Nathanael Guigo *

Institut de Chimie de Nice, Université Côte d'Azur, CNRS, UMR 7272, 06108 Nice, France;
lucie.quinquet@univ-cotedazur.fr (L.Q.); pierre.delliere@univ-cotedazur.fr (P.D.)
* Correspondence: nathanael.guigo@univ-cotedazur.fr
† These authors contributed equally to this work.

Abstract: The chemistry of biomass-derived furans is particularly sensitive to ring openings. These side reactions occur during furfuryl alcohol polymerization. In this work, the furan ring-opening was controlled by changing polymerization conditions, such as varying the type of acidic initiator or the water content. The degree of open structures (DOS) was determined by quantifying the formed carbonyl species by means of quantitative ^{19}F NMR and potentiometric titration. The progress of polymerization and ring opening were monitored by DSC and FT-IR spectroscopy. The presence of additional water is more determining on ring opening than the nature of the acidic initiator. Qualitative structural assessment by means of ^{13}C NMR and FT-IR shows that, depending on the employed conditions, poly(furfuryl alcohol) samples can be classified in two groups. Indeed, either more ester or more ketone side groups are formed as a result of side ring opening reactions. The absence of additional water during FA polymerization preferentially leads to opened structures in the PFA bearing more ester moieties.

Keywords: biobased poly(furfuryl alcohol); ring-opening; degree of open structures

ACS Macro Letters

pubs.acs.org/macroletters Letter

Exploring New Horizons for Bio-Based Poly(furfuryl alcohol) by Exploiting Functionalities Offered by Side Reactions

Pierre Delliere and Nathanael Guigo*

Cite This: ACS Macro Lett. 2022, 11, 1202−1206 Read Online

ACCESS | Metrics & More | Article Recommendations | Supporting Information

ABSTRACT: Poly(furfuryl alcohol) is a bio-based thermoset resin with a limited application portfolio due to its brittleness. Side ring-opening reactions that occur during polymerization lead to carbonyl moieties. Such unique self-generated functionality was exploited to generate tough and ductile materials via the creation of Schiff-based macromolecular architectures.

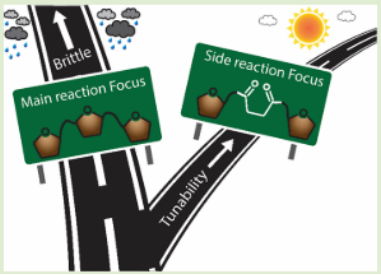

European Polymer Journal 187 (2023) 111869

Contents lists available at ScienceDirect

European Polymer Journal

journal homepage: www.elsevier.com/locate/europolj

Revealed pathways of furan ring opening and surface crosslinking in biobased polyfurfuryl alcohol

Pierre Delliere, Nathanael Guigo *

Institut de Chimie de Nice, Université Côte d'Azur, CNRS, UMR 7272, 06108 Nice, France

ARTICLE INFO

Keywords:
Poly(furfuryl alcohol)
2D-NMR
Biobased thermoset
Surface crosslinking
Ring-opening
Oxidation

ABSTRACT

Poly(furfuryl alcohol) – (PFA) is a biobased thermoset known for its highly crosslinked structure. Bidimensional NMR (2D-NMR) was employed to give new insights on the complex structural organization in PFA with a special emphasis on the side structures resulting from furan ring-opening. Interestingly, the presence of aldehyde functions was for the first time clearly highlighted and quantified in PFA resins. Overall, the aldehydes account for about 20 % of the total carbonyls present in PFA. Results from HSQC and HMBC sequences allowed proposing two pathways for the furan ring opening reactions. The first one is an hydrolytic-ring opening leading to levulinic like species. The second one is rather an oxidative furan-ring opening leading to conjugated aldehydes. These conjugated aldehydes are prone to crosslink via Diel-Alder cycloadditions with furanic entities thus leading to crosslinking. At macroscopic scale, this newly proposed crosslinking pathway would explain the formation of the rigid shell formed at the external surfaces of PFA resins.

polymers

MDPI

Article

Structural Variations in Biobased Polyfurfuryl Alcohol Induced by Polymerization in Water

Pierre Delliere [1], Antonio Pizzi [2] and Nathanael Guigo [1,*]

[1] Institut de Chimie de Nice, Université Côte d'Azur, CNRS, UMR 7272, 06108 Nice, France
[2] LERMAB-ENSTIB, University of Lorraine, 27 rue Philippe Seguin, 88000 Epinal, France
* Correspondence: nathanael.guigo@univ-cotedazur.fr; Tel.: +33-489150126

Abstract: Poly(furfuryl alcohol) is a thermostable biobased thermoset. The polymerization of furfuryl alcohol (FA) is sensitive to a number of side reactions, mainly the opening of the furan ring into carbonyl species. Such carbonyls can be used to introduce new properties into the PFA materials through derivatization. Hence, better understanding of the furan ring opening is required to develop new applications for PFA. This article studies the structural discrepancies between a PFA prepared in neat conditions versus a PFA prepared in aqueous conditions, i.e., with more carbonyls, through NMR and MALDI ToF. Overall, the PFA prepared in water exhibited a structure more heterogeneous than the PFA prepared in neat conditions. The presence of ketonic derivatives such as enols and ketals were highlighted in the case of the aqueous PFA. In this line, the addition of water at the beginning of the polymerization stimulated the production of aldehydes by a factor two. Finally, the PFA prepared in neat conditions showed terminal lactones instead of aldehydes.

Keywords: Poly(furfuryl alcohol); furan resin; ring opening; NMR; carbonyls

Progress in Organic Coatings 173 (2022) 107203

Contents lists available at ScienceDirect

Progress in Organic Coatings

journal homepage: www.elsevier.com/locate/porgcoat

Thiol-ene biobased networks: Furan allyl derivatives for green coating applications

Lorenzo Pezzana [a], Giuseppe Melilli [b], Pierre Delliere [b], Dumitru Moraru [a], Nathanael Guigo [b], Nicolas Sbirrazzuoli [b,*], Marco Sangermano [a,*]

[a] *Dipartimento di Scienza Applicata e Tecnologia, Politecnico di Torino, C.so Duca degli Abruzzi 24, 10129 Torino, Italy*
[b] *Université Côte d'Azur, Institut de Chimie de Nice (ICN), UMR CNRS 7272, 06108 Nice Cedex 02, France*

ARTICLE INFO

Keywords:
Thiol-ene chemistry
UV-curing
Furans
Bio-based monomers
[2+2] cycloaddition

ABSTRACT

Biomass feedstocks are playing a crucial role toward the development of new sustainable materials with the aim to replace the fossil-based ones limiting the emissions and waste. Among the other, cellulose, and hemicellulose are gaining interest as a source of new bio-based building blocks such as furan derivatives. In this study, two furan derivatives were selected as bio-based monomers to design four innovative UV-curable coatings. Specifically, 2,5-Furandimethanol (FDM), and cis-cyclobutane-1,2-dicarboxylic acid (CBDA-2) derived from Furylacrylic acid were modified by allylation of their respective OH groups. The bis allyl derivatives were combined with commercial tris- and tetra-functional thiols compounds and cured by means of UV-light through a thiol-ene reaction. The UV-curing was deeply investigated by means of real-time FT-IR, photo-DSC and photorheology. Successively, the bio-based thermosets were characterized by DMTA and tensile test to examine the thermal-mechanical behavior. The results indicated comparable properties with previous studied bio-based thiol-ene thermoset raising the possibility to use the studied material for coating applications.

Taking advantage of side reactions: the example of furfuryl alcohol polymerization

Pierre Dellière[1], Lucie Quinquet[1], Nathanaël Guigo[1]

1 Université Côte d'Azur, Institut de Chimie de Nice, UMR 7272, 2, France

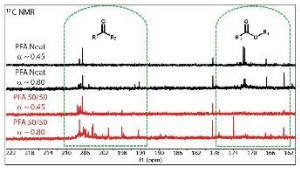

Depending on the polymerization conditions - i.e. neat/water/isopropanol - more or less esters can be formed

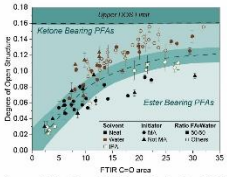

L. Quinquet, P. Dellière, N. Guigo, *Molecules*, 27, 3212 (2022).

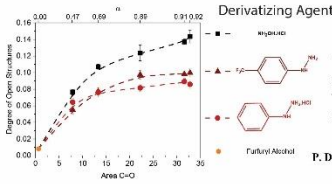

The size/nature of the derivatizing agent influences the DOS value. Thus it gives insights on the chemical availability of the carbonyls within PFA.

P. Delliere, N. Guigo, *Macromolecules*, 55, 1196 (2022).

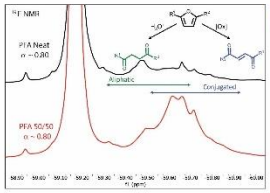

The carbonyls in PFA systems comprise both aliphatic and conjugated moities

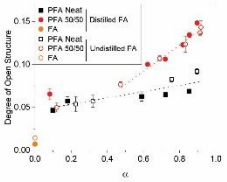

Steady DOS increase throughout the polymerization for both PFA Neat and PFA 50/50

Monitoring

Acknowledgements

The authors would like to acknowledge the French Agence Nationale de la Recherche - ANR - for funding the project FUTURES (ANR-19-CE06-0005)

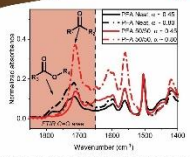

Neat PFA systems exhibit both ketones and ester while in aqueous PFA systems mostly ketones are formed.

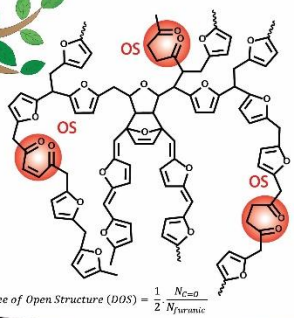

$$Degree\ of\ Open\ Structure\ (DOS) = \frac{1}{2} \cdot \frac{N_{C=O}}{N_{furanic}}$$

Furfuryl Alcohol

Bio refinery

Lignocellulosic biomass

Acid-catalyzed polymerisation

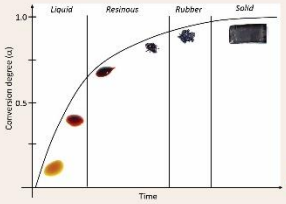

In the polymerization of furfuryl alcohol, the chain growth is concomitant with a progressive darkening, crosslinking and ring opening reactions.

Brittle bio-based thermoset

Metal casting
Wood reinforcement

Water-induced disruption of thermomecanical properties though furan's ring opening

Degree of Open Structure (DOS)

G. Falco, N. Guigo, et al., *ChemSusChem*, 11, 1805 (2018).

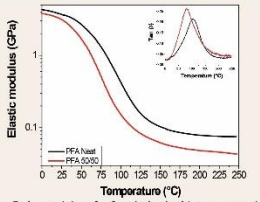

Polymerizing furfuryl alcohol in water rather than neat system decreases the T_g and crosslink density while increasing the damping

Remerciments

Trois ans se sont écoulés depuis mon arrivée à Nice. A 23 ans, trois années cela paraissait long. Elles sont passées en un éclair. Pourquoi sont-elles passées si vite ? Pour tout un tas de raisons. La première et principale c'est Nathanaël Guigo.

On m'avait dit qu'on bon rapport doctorant/directeur de thèse était essentiel pour que celle-ci se déroule bien. Je pense que c'est vrai. Lors de l'entretien, on ne s'est vu qu'à travers un écran et le bon ressenti que j'ai eu n'a fait que se confirmer au fil du temps. Merci, de m'avoir accordé ta confiance ! Merci de m'avoir fait découvrir cette polymérisation bigarrée qu'est celle du FA ! Merci de m'avoir permis de laisser libre cours à ma créativité ! Du quart de siècle que j'ai vécu, tu es une des personnes les plus humaines et empathiques que j'ai pu rencontrer et qui en plus, s'avère être un excellent scientifique ! Merci encore pour tout !

J'aimerais également remercier toutes les personnes qui m'ont permis d'en arriver là ainsi que de celles qui ont touché de près ou de loin à ma thèse.

First, I'd like to thank the rapporteurs of my jury, Pr Minna Hakkarainen and Pr Mohamed Naceur Belgacem.! I would also like to thank Pr Marco Sangermano, and Dr François Jerôme for accepting to be in my jury. It is an honor for me to have four internationally recognized experts such as you to evaluate my thesis. Thank you !

Bien sûr, j'aimerais également remercier l'ANR pour le financement de ma thèse. Également merci Pr Nicolas Sbirrazzuoli pour son accueil au sein de l'équipe MAPEC ainsi que ses conseils. Merci aussi Dr Luc Vincent, tu m'as dépatouillé plus d'une fois ! De plus, j'aimerais remercier les personnes que j'ai pu côtoyer au quotidien au laboratoire pour leurs échanges et bonne ambiance. Merci Guiseppe, Emilie, Mona, Nadir, Lorenzo, Marie, Maria, Sandra et Apostolos.

Un merci tout particulier à toi, Lucie, pour tes travaux pendant ton stage et ta chaleureuse compagnie lors de ta poursuite en thèse ! Merci également à Pierre et Baptiste pour votre aide précieuse lors de ma thèse !

I’d also like to thank the FUR4Sustain COST action for all the training schools, meeting and STSM! In this line, I’d like to thank Dr Andreia Sousa, Beatriz and Simao for welcoming me in Portugal. Also thank you Eleni everything you have done during your STSM.

Merci également à tout le personnel qui a pu m’aider pendant ma Thèse, Merci au pôle gestion, Martine, Patricia, Amina², Stéphanie et plus récemment Emilie, Sébastien, Laëtitia, Eftychia et Elodie ! Merci également à Marc, Lionel, Fabio, François et Sophie pour leur précieuse aide en analyse structural et microscopie ! Merci également à Dominique pour ses coups de main !

J’aimerais remercier Dr Nicolas Desilles et Dr Cyril Ronco pour leurs conseils lors de mes comités de thèse ! Un grand merci à Olivier pour tout depuis mon stage chez Sika. Également merci au Dr Fabrice Decroix pour ses conseils durant le stage qui m’ont beaucoup servi par la suite ! Merci également à Dr Nasreddine Kebir pour avoir renforcé ma passion pour les matériaux polymères ! Merci à Sandrine Gaurrand pour m’avoir accueilli transmis de précieuses connaissance en RMN ! Merci Geoffrey pour tes conseils avant la thèse ! Thank you Dr Sami Hietala and Dr Vladimir Aseyev for everything you have done during my internship with you! Enfin, merci au Dr Olivier Colombani, vous m’avez transmis la passion des polymères ! Merci aussi à toi, Antoine, pour avoir été là durant toutes ces années !

Enfin, merci ma famille pour avoir été là dès le début. Plus particulièrement mes parents et mes frères sans qui je n’en serais pas où j’en suis !

List of Figures, Tables and Schemes

5.9 Table of Figures

5.10 Table of Tables

5.11 Table of schemes

References

1 https://echa.europa.eu/fr/substance-information/-/substanceinfo/100.256.326, last accessed (29/09/2023)

2 https://woo.opec.org/chapter.php?chapterNr=312&tableID=328, last accessed (29/09/2023)

3 Geyer, R.; Jambeck, J. R.; Law, K. L. Production, Use, and Fate of All Plastics Ever Made. *Sci. Adv.* **2017**, *3* (7), 25–29. https://doi.org/10.1126/sciadv.1700782.

4 https://www.eia.gov/todayinenergy/detail.php?id=4710#, last accessed (29/09/2023)

5 https://woo.opec.org/chapter.php?chapterNr=315&chartID=1539, last accessed (29/09/2023)

6 Srivastava, R. K.; Vineed, S.; Akhtar, N.; Kumar, P.; Subudhi, S.; Prasad, K.; Govarthanan, M. Effective Hydrolysis for Waste Plant Biomass Impacts Sustainable Fuel and Reduced Air Pollution Generation : A Comprehensive Review. *Sci. Total Environ.* **2023**, *859*, 160260. https://doi.org/10.1016/j.scitotenv.2022.160260.

7 Mariscal, R.; Maireles-Torres, P.; Ojeda, M.; Sádaba, I.; López Granados, M. Furfural: A Renewable and Versatile Platform Molecule for the Synthesis of Chemicals and Fuels. *Energy Environ. Sci.* **2012**, *9*, 1144–1189. https://doi.org/10.1039/c5ee02666k.

8 Lange, J. P.; Van Der Heide, E.; Van Buijtenen, J.; Price, R. Furfural-A Promising Platform for Lignocellulosic Biofuels. *ChemSusChem* **2012**, *5*, 150–166. https://doi.org/10.1002/cssc.201100648.

9 Rehm, B. H. A. Bacterial Polymers: Biosynthesis, Modifications and Applications. *Nat. Rev. Microbiol.* **2010**, *8* (8), 578–592. https://doi.org/10.1038/nrmicro2354.

10 De Jong, E.; Stichnothe, H.; Bell, G.; Jorgensen, H. Bio-Based Chemicals: A 2020 Update, *IEA Bioenergy Task 42*, **2020**.

11 Wertz, J.-L.; Deleu, M.; Coppée, S.; Richel, A. *Hemicelluloses and Lignin in Biorefineries*; Taylor & Francis Group, 2018. ISBN: 9781138720985

12 Faisal, M.; Shaheen, H.; Wu, A. Cell Wall Hemicellulose for Sustainable Industrial Utilization. *Renew. Sustain. Energy Rev.* **2021**, *144*, 110996. https://doi.org/10.1016/j.rser.2021.110996.

13 Rowell, R. M. *Handbook of Wood Chemistry and Wood Composites 2nd Edition*; Taylor & Francis Group, **2013**, ISBN: 9781032099163

14 Asif, M. *Sustainability of Timber, Wood and Bamboo in Construction*; Woodhead Publishing Limited, **2009**, ISBN: 9781845693497

15 Chio, C.; Sain, M.; Qin, W. Lignin Utilization: A Review of Lignin Depolymerization from Various Aspects. *Renew. Sustain. Energy Rev.* **2019**, *107*, 232–249. https://doi.org/10.1016/j.rser.2019.03.008

16 Akhtar, A.; Krepl, V.; Ivanova, T. A Combined Overview of Combustion, Pyrolysis, and Gasification of Biomass. *Energy and Fuels* **2018**, *32*, 7294–7318. https://doi.org/10.1021/acs.energyfuels.8b01678

17 Nazari, L.; Xu, C. C.; Ray, M. B. *Advanced and Emerging Technologies for Resource Recovery from Wastes*; Springer, **2021**, ISBN: 9789811592669

18 Arantes, V.; Dias, I. K. R.; Berto, G. L.; Pereira, B.; Marotti, B. S.; Nogueira, C. F. O. The Current Status of the Enzyme-Mediated Isolation and Functionalization of Nanocelluloses: Production, Properties, Techno-Economics, and Opportunities. *Cellulose.* **2020**, *27* (18), 10571–10630. https://doi.org/10.1007/s10570-020-03332-1.

19 Saunders, C. W.; Taylor, L. T. A Review of the Synthesis, Chemistry and Analysis of Nitrocellulose. *J. Energ. Mater.* **1990**, *8* (3), 149–203. https://doi.org/10.1080/07370659008012572

20 Vatanpour, V.; Pasaoglu, M. E.; Barzegar, H.; Kaya, R.; Bastug, M.; Khataee, A.; Koyuncu, I. Chemosphere Cellulose Acetate in Fabrication of Polymeric Membranes : A Review. *Chemosphere.* **2022**, *295*, 133914. https://doi.org/10.1016/j.chemosphere.2022.133914.

21 Rahman, S.; Hasan, S.; Nitai, A. S.; Nam, S.; Ahmed, M. B. Recent Developments of Carboxymethyl Cellulose. *Polymers.* **2021**, *13*, 1345. https://doi.org/10.3390/polym13081345.

22 Liu, Y.; Ahmed, S.; Sameen, D. E.; Wang, Y.; Lu, R.; Dai, J.; Li, S.; Qin, W. Trends in Food Science & Technology A Review of Cellulose and Its Derivatives in Biopolymer-Based for Food Packaging Application. *Trends Food Sci. Technol.* **2021**, *112*, 532–546. https://doi.org/10.1016/j.tifs.2021.04.016.

23 Rol, F.; Belgacem, M. N.; Gandini, A.; Bras, J. Recent Advances in Surface-Modified Cellulose Nanofibrils. *Prog. Polym. Sci.* **2019**, *88*, 241–264. https://doi.org/10.1016/j.progpolymsci.2018.09.002.

24 Tanpichai, S.; Boonmahitthisud, A.; Soykeabkaew, N. Review of the Recent Developments in All-Cellulose Nanocomposites : Properties and Applications. *Carbohydr. Polym.* **2022**, *286*, 119192. https://doi.org/10.1016/j.carbpol.2022.119192

25 Sharma, A.; Thakur, M.; Bhattacharya, M.; Mandal, T. Commercial Application of Cellulose Nano-Composites – A Review. *Biotechnol. Reports.* **2019**, e00316. https://doi.org/10.1016/j.btre.2019.e00316.

26 Li., Z.; Wang, J.; Xu, Y.; Shen, M.; Duan, C.; Dai, L.; Ni, Y. Green and Sustainable Cellulose-Derived Humidity Sensors : A Review. *Carbohydr. Polym.* **2021**, *270*, 118385. https://doi.org/10.1016/j.carbpol.2021.118385.

27 Gauss, C.; Pickering, K. L.; Muthe, L. P. The Use of Cellulose in Bio-Derived Formulations for 3D / 4D Printing : A Review. *Compos. Part C Open Access.* **2021**, *4*, 100113. https://doi.org/10.1016/j.jcomc.2021.100113.

28 Robertson, G. P.; Hamilton, S. K.; Barham, B. L.; Dale, B. E.; Izaurralde, R. C.; Jackson, R. D.; Landis, D. A.; Swinton, S. M.; Thelen, K. D.; Tiedje, J. M. Cellulosic Biofuel Contributions to a Sustainable Energy Future: Choices and Outcomes. *Science.* **2017**, *356* (6345), eaal2324. https://doi.org/10.1126/science.aal2324.

29 Corma Canos, A.; Iborra, S.; Velty, A. Chemical Routes for the Transformation of Biomass into Chemicals. *Chem. Rev.* **2007**, *107* (6), 2411–2502. https://doi.org/10.1021/cr050989d.

30 Ralph, J.; Lapierre, C.; Boerjan, W. Lignin Structure and Its Engineering. *Curr. Opin. Biotechnol.* **2019**, *56*, 240–249. https://doi.org/10.1016/j.copbio.2019.02.019.

31 Li, T.; Takkellapati, S. The Current and Emerging Sources of Technical Lignins and Their Applications. *Biofuels, Bioprod. Biorefining* **2018**, *12* (5), 756–787. https://doi.org/10.1002/bbb.1913.

32 Buisman, G. J. H.; Lange, J. H. M. *Industrial Biorenewables*; John Wiley & Sons Ltd, **2016**, ISBN 9781118843796

33 Aro, T.; Fatehi, P. Production and Application of Lignosulfonates and Sulfonated Lignin. *ChemSusChem* **2017**, *10* (9), 1861–1877. https://doi.org/10.1002/cssc.201700082.

34 Wang, H.; Pu, Y.; Ragauskas, A.; Yang, B. From Lignin to Valuable Products–Strategies, Challenges, and Prospects. *Bioresour. Technol.* **2019**, *271*, 449–461. https://doi.org/10.1016/j.biortech.2018.09.072.

35 Mahajan, J. S.; O'Dea, R. M.; Norris, J. B.; Korley, L. S. T. J.; Epps, T. H. Aromatics from Lignocellulosic Biomass: A Platform for High-Performance Thermosets. *ACS Sustain. Chem. Eng.* **2020**, *8* (40), 15072–15096. https://doi.org/10.1021/acssuschemeng.0c04817.

36 Decostanzi, M.; Auvergne, R.; Boutevin, B.; Caillol, S. Biobased Phenol and Furan Derivative Coupling for the Synthesis of Functional Monomers. *Green Chem.* **2019**, *21* (4), 724–747. https://doi.org/10.1039/c8gc03541e.

37 Arzami, A. N.; Ho, T. M.; Mikkonen, K. S. Valorization of Cereal By-Product Hemicelluloses : Fractionation and Purity Considerations. *Food Res. Int.* **2022**, *151*, 110818. https://doi.org/10.1016/j.foodres.2021.110818

38 Zhao, Y.; Sun, H.; Yang, B.; Weng, Y. Hemicellulose-Based Film : Potential Green Films for Food Packaging. *Polymers.* **2020**, *12*, 1775. https://doi.org/10.3390/polym12081775.

39 Figueiredo, R.; Araújo, P.; Pablo, J.; Paulo, P. L. Suberin and Hemicellulose in Sugarcane Cell Wall Architecture and Crop Digestibility : A Biotechnological Perspective. *Food Energy Secur.* **2019**, *8* (3), e00163. https://doi.org/10.1002/fes3.163.

40 5-(hydroxymethyl)-2-furaldehyde, EC N° 200-654-9 https://echa.europa.eu/fr/substance-information/-/substanceinfo/100.000.595 Last accessed (29/09/2023)

41 Van Putten, R.-J.; de Vries, J. G.; van der Waal, J. C.; de Jong, E.; Rasrendra, C. B.; Heeres, H. J. Hydroxymethylfurfural, A Versatile Platform Chemical Made from Renewable Resources. *Chem. Rev.* **2013**, *113* (3), 1499–1597. https://doi.org/10.1021/cr300182k.

42 Liguori, A.; Hakkarainen, M. Designed from Biobased for Recycling: Imine-Based Covalent Adaptable Networks. *Macromol. Rapid Commun.* **2022**, *43* (13), 2100816. https://doi.org/10.1002/marc.202100816.

43 Thoma, C.; Konnerth, J.; Sailer-Kronlachner, W.; Rosenau, T.; Potthast, A.; Solt, P.; van Herwijnen, H. W. G. Hydroxymethylfurfural and Its Derivatives: Potential Key Reactants in Adhesives. *ChemSusChem* **2020**, *13* (20), 5408–5422. https://doi.org/10.1002/cssc.202001539

44 Forestier, E.; Combeaud, C.; Guigo, N.; Sbirrazzuoli, N.; Billon, N. Understanding of Strain Induced Crystallization Developments Scenarios for Polyesters: Comparison of Poly(Ethylene Furanoate), PEF, and Poly(Ethylene Terephthalate), PET. *Polymer.* **2020**, *203*, 122755. https://doi.org/10.1016/j.polymer.2020.122755.

45 Forestier, E.; Combeaud, C.; Guigo, N.; Sbirrazzuoli, N. Mechanical Behaviour and Induced Microstructural Development upon Simultaneous and Balanced Biaxial Stretching of Poly(Ethylene Furandicarboxylate), PEF. *Polymers.* **2023**, *15* (3), 661. https://doi.org/10.3390/polym15030661.

46 Forestier, E.; Combeaud, C.; Guigo, N.; Corvec, G.; Pradille, C.; Sbirrazzuoli, N.; Billon, N. Comparative Analysis of the Mechanical Behaviour of PEF and PET Uniaxial Stretching Based on the Time/Temperature Superposition Principle. *Polymers.* **2021**, *13* (19), 3295. https://doi.org/10.3390/polym13193295.

47 De Jong, E.; Visser, H. R. A.; de Sousa Dias, A. S. V; Harvey, C.; Gruter, G. M. The Road to Bring FDCA and PEF to the Market. *Polymers.* **2022**, *14* (5), 943. https://doi.org/https://doi.org/10.3390/polym14050943.

48 Gruter, G.; Jong, E. De. Furanics : Novel Fuel Opt¡ons from Carbohydrates. *Biofuels Technol.* **2009**, 1, 11–17.

49 Levulinic acid, EC N° 204-649-2 https://echa.europa.eu/fr/substance-information/-/substanceinfo/100.004.228 Last accessed (29/09/2023)

50 Van Der Waal, J. C.; De Jong, E. Avantium Chemicals: The High Potential for the Levulinic Product Tree. *Ind. Biorenewables A Pract. Viewp.* **2016**, 97–120. https://doi.org/10.1002/9781118843796.ch4.

51 Bozell, J. J.; Petersen, G. R. Technology Development for the Production of Biobased Products from Biorefinery Carbohydrates—the US Department of Energy's "Top 10" Revisited. *Green Chem.* **2010**, *12* (4), 539–555. https://doi.org/10.1039/b922014c.

52 Okolie, J. A.; Mukherjee, A.; Nanda, S.; Dalai, A. K.; Kozinski, J. A. Next-Generation Biofuels and Platform Biochemicals from Lignocellulosic Biomass. *Int. J. Energy Res.* **2021**, *45* (10), 14145–14169. https://doi.org/10.1002/er.6697.

53 Badgujar, K. C.; Badgujar, V. C.; Bhanage, B. M. A Review on Catalytic Synthesis of Energy Rich Fuel Additive Levulinate Compounds from Biomass Derived Levulinic Acid. *Fuel Process. Technol.* **2020**, *197*, 106213. https://doi.org/10.1016/j.fuproc.2019.106213.

54 Rackemann, D. W.; Doherty, W. O. S. The Conversion of Lignocellulosics to Levulinic Acid. *Biofuels, Bioprod. Biorefining* **2011**, *5*, 198–214. https://doi.org/10.1002/BBB.267

55 Hoydonckx, H. E.; Rhijn, W. M. Van; De Vos, D. E.; Jacobs, P. A. Furfural and Derivatives H. In *Encyclopedia of industrial chemistry: Third Edition*; 2007; Vol. 16, pp 285–313. https://doi.org/10.1016/B978-0-12-386454-3.00147-0.

56 Kabbour, M.; Luque, R. *Furfural as a Platform Chemical: From Production to Applications*; Elsevier B.V., 2019. https://doi.org/10.1016/B978-0-444-64307-0.00010-X.

57 Zeitsch, K. J. *The Chemistry and Technology of Furfural and Its Many By-Products*; Elsevier Sience B. V., 2000. ISBN: 044450351X

58 Lattuati-Derieux, A.; Bonnassies-Termes, S.; Lavédrine, B. Identification of Volatile Organic Compounds Emitted by a Naturally Aged Book Using Solid-Phase Microextraction/Gas Chromatography/Mass Spectrometry. *J. Chromatogr. A* **2004**, *1026* (1–2), 9–18. https://doi.org/10.1016/j.chroma.2003.11.069.

59 Furfural, EC N° 202-627-7 https://echa.europa.eu/fr/substance-information/-/substanceinfo/100.002.389 Last accessed (29/09/2023),

60 Yong, K. J.; Wu, T. Y.; Lee, C. B. T. L.; Lee, Z. J.; Liu, Q.; Jahim, J. M.; Zhou, Q.; Zhang, L. Furfural Production from Biomass Residues: Current Technologies, Challenges and Future Prospects. *Biomass and Bioenergy* **2022**, *161*, 106458. https://doi.org/10.1016/j.biombioe.2022.106458.

61 Kapanji, K. K.; Haigh, K. F.; Görgens, J. F. Techno-Economics of Lignocellulose Biorefineries at South African Sugar Mills Using the Biofine Process to Co-Produce Levulinic Acid, Furfural and Electricity along with Gamma Valeractone. *Biomass and Bioenergy* **2021**, *146*, 106008. https://doi.org/10.1016/j.biombioe.2021.106008.

62 Pawar, H. S. Sulfonic Acid Anchored Heterogeneous Acid-Catalyst DICAT-3 for Conversion of Xylose into Furfural in Biphasic Solvent System. *ChemistrySelect* **2020**, *5* (2), 916–923. https://doi.org/10.1002/slct.201903894.

63 Zhao, Y.; Xu, H.; Wang, K.; Lu, K.; Qu, Y.; Zhu, L.; Wang, S. Enhanced Furfural Production from Biomass and Its Derived Carbohydrates in the Renewable Butanone-Water Solvent System. *Sustain. Energy Fuels* **2019**, *3* (11), 3208–3218. https://doi.org/10.1039/c9se00459a.

64 Luo, Y.; Li, Z.; Li, X.; Liu, X.; Fan, J.; Clark, J. H.; Hu, C. The Production of Furfural Directly from Hemicellulose in Lignocellulosic Biomass: A Review. *Catal. Today* **2019**, *319*, 14–24. https://doi.org/10.1016/j.cattod.2018.06.042.

65 Zang, G.; Shah, A.; Wan, C. Techno-Economic Analysis of an Integrated Biorefinery Strategy Based on One-Pot Biomass Fractionation and Furfural Production. *J. Clean. Prod.* **2020**, *260*, 120837. https://doi.org/10.1016/j.jclepro.2020.120837.

66 Zhang, T.; Li, W.; Xiao, H.; Jin, Y.; Wu, S. Recent Progress in Direct Production of Furfural from Lignocellulosic Residues and Hemicellulose. *Bioresour. Technol.* **2022**, *354*, 127126. https://doi.org/10.1016/j.biortech.2022.127126.

67 Ghosh, S.; Falyouna, O.; Malloum, A.; Othmani, A.; Bornman, C.; Bedair, H.; Onyeaka, H.; Al-Sharify, Z. T.; Jacob, A. O.; Miri, T.; Osagie, C.; Ahmadi, S. A General Review on the Use of Advance Oxidation and Adsorption Processes for the Removal of Furfural from Industrial Effluents. *Microporous Mesoporous Mater.* **2022**, *331*, *111638*. https://doi.org/10.1016/j.micromeso.2021.111638.

68 Gandini, A.; Belgacem, M. N. Furans in Polymer Chemistry. *Prog. Polym. Sci.* **1997**, *22* (6), 1203–1379. https://doi.org/10.1016/S0079-6700(97)00004-X

69 Kamm, B.; Gruber, P. R.; Kamm, M. *Biorefineries - Industrial Processes and Products*; 2006, ISBN: 9783527310272

70 Furfuryl alcohol, EC N° 202-626-1 https://echa.europa.eu/fr/substance-information/-/substanceinfo/100.002.388 Last accessed (29/09/2023),

71 Long, J.; Zhao, W.; Li, H.; Yang, S. Furfural as a Renewable Chemical Platform for Furfuryl Alcohol Production. In *Biomass, Biofuels, Biochemicals: Recent Advances in Development of Platform Chemicals*; **2019**, 299–322. https://doi.org/10.1016/B978-0-444-64307-0.00011-1.

72 Sixta, H.; Millan, G. G. Towards the Green Synthesis of Furfuryl Alcohol in A One-Pot System from Xylose : A Review. *Catalyst.* **2020**, *10*, 1101. https://doi.org/10.3390/catal10101101.

73 Qin, L.; Di, J.; He, Y. Efficient Synthesis of Furfuryl Alcohol from Corncob in a Deep Eutectic Solvent System. *Processes.* **2022**, *10* (9), 0–10. https://doi.org/10.3390/pr10091873.

74 Schmitt, C. R. Polyfurfuryl Alcohol Resins. *Polym. Plast. Technol. Eng.* **1974**, *3* (2), 121–158. https://doi.org/10.1080/03602557408545025.

75 Chalmpes, N.; Bourlinos, A. B.; Talande, S.; Bakandritsos, A.; Moschovas, D.; Avgeropoulos, A.; Karakassides, M. A.; Gournis, D. Nanocarbon from Rocket Fuel Waste: The Case of Furfuryl Alcohol-Fuming Nitric Acid Hypergolic Pair. *Nanomaterials.* **2021**, *11* (1), 1–13. https://doi.org/10.3390/nano11010001.

76 González Maldonado, G. M.; Assary, R. S.; Dumesic, J.; Curtiss, L. A. Experimental and Theoretical Studies of the Acid-Catalyzed Conversion of Furfuryl Alcohol to Levulinic Acid in Aqueous Solution. *Energy Environ. Sci.* **2012**, *5* (5), 6981–6989. https://doi.org/10.1039/c2ee03465d.

77 Chappaz, A.; Lai, J.; De Oliveira Vigier, K.; Morvan, D.; Wischert, R.; Corbet, M.; Doumert, B.; Trivelli, X.; Liebens, A.; Jérôme, F. Selective Conversion of Concentrated Feeds of Furfuryl Alcohol to Alkyl Levulinates Catalyzed by Metal Triflates. *ACS Sustain. Chem. Eng.* **2018**, *6* (3), 4405–4411. https://doi.org/10.1021/acssuschemeng.8b00100.

78 Hayes, M. H. B.; Mylotte, R.; Swift, R. S. *Humin: Its Composition and Importance in Soil Organic Matter*, 1st ed.; Elsevier Inc., 2017; https://doi.org/10.1016/bs.agron.2017.01.001.

79 Velasco, C.; Arora, J. S.; Mushrif, S. H. Mechanistic Investigation into the Formation of Humins in Acid- Catalyzed Biomass Reactions. *ACS Omega* **2022**, *7*, 44786–44795. https://doi.org/10.1021/acsomega.2c04783.

80 Zandvoort, I. van; Wang, Y.; Rasrendra, C. B.; Eck, E. R. H. van; Bruijnincx, P. C. A.; Heeres, H. J.; Weckhuysen, B. M. Formation, Molecular Structure, and Morphology of Humins in Biomass Conversion : Influence of Feedstock and Processing Conditions. *ChemSusChem* **2013**, *6* (9), 1745–1758. https://doi.org/10.1002/cssc.201300332.

81 Herzfeld, J.; Rand, D.; Matsuki, Y.; Daviso, E.; Mak-Jurkauskas, M.; Mamajanov, I. Molecular Structure of Humin and Melanoidin Via Solid State NMR. *J. Phys. Chem. B* **2011**, *115* (19), 5741–5745. https://doi.org/10.1021/jp1119662.

82 Shen, H.; Shan, H.; Liu, L. Evolution Process and Controlled Synthesis of Humins with 5- Hydroxymethylfurfural (HMF) as Model Molecule. *ChemSusChem* **2019**, *13* (3), 513–519. https://doi.org/10.1002/cssc.201902799.

83 Muralidhara, A.; Bado-Nilles, A.; Marlair, G.; Engelen, V.; Len, C.; Pandard, P. Humins in the Environment: Early Stage Insights on Ecotoxicological Aspects. *Biofuels, Bioprod. Biorefining* **2019**, *13* (3), 464–470. https://doi.org/10.1002/bbb.1964.

84 Wassenberg, A.; Esser, T.; Poller, M. J.; Albert, J. Catalytic Valorization of Humins. *Materials.* **2023**, *16*, 2864. https://doi.org/10.3390/ ma16072864.

85 Wang, Y.; Agarwal, S.; Heeres, H. J. Catalytic Liquefaction of Humin Substances from Sugar Biore Fi Neries with Pt/C in 2 - Propanol. *ACS Sustain. Chem. Eng.* **2017**, *5*, 469–480. https://doi.org/10.1021/acssuschemeng.6b01834.

86 Björnerbäck, F.; Hedin, N. Microporous Humins Prepared from Sugars and Bio-Based Polymers in Concentrated Sulfuric Acid. *ACS Sustain. Chem. Eng.* **2019**, *7* (1), 1018–1027. https://doi.org/10.1021/acssuschemeng.8b04658.

87 Kang, S.; Fu, J.; Deng, Z.; Jiang, S.; Zhong, G.; Xu, Y.; Guo, J.; Zhou, J. Valorization of Biomass Hydrolysis Waste: Activated Carbon from Humins as Exceptional Sorbent for Wastewater Treatment. *Sustainability* **2018**, *10* (6), 1795. https://doi.org/10.3390/su10061795.

88 Tosi, P.; Klink, G. P. M. Van; Celzard, A.; Fierro, V.; Vincent, L. Auto-Crosslinked Rigid Foams Derived from Biorefinery Byproducts. *ChemSusChem* **2018**, *11* (16), 2797–2809. https://doi.org/10.1002/cssc.201800778.

89 Chernysheva, D. V.; Chus, Y. A.; Klushin, V. A.; Lastovina, T. A.; Pudova, L. S.; Smirnova, N. V.; Kravchenko, O. A.; Chernyshev, V. M.; Ananikov, V. P. Sustainable Utilization of Biomass Refinery Wastes for Accessing Activated Carbons and Supercapacitor Electrode Materials. *ChemSusChem* **2018**, *11* (20), 3599–3608. https://doi.org/10.1002/cssc.201801757.

90 Sangregorio, A.; Guigo, N.; van der Waal, J. C.; Sbirrazzuoli, N. Humins from Biorefineries as Thermoreactive Macromolecular Systems. *ChemSusChem* **2018**, *11* (24), 4246–4255. https://doi.org/10.1002/cssc.201802066.

91 Dinu, R.; Mija, A. Cross-Linked Polyfuran Networks with Elastomeric Behaviour Based on Humins Biorefinery by-Products. *Green Chem.* **2019**, *21* (23), 6277–6289. https://doi.org/10.1039/c9gc01813a.

92 Dinu, R.; Montes, S.; Orange, F.; Mija, A. Reprocessable Humins Thermosets and Composites. *Compos. Sci. Technol.* **2021**, *207*, 108655. https://doi.org/10.1016/j.compscitech.2021.108655.

93 Sangregorio, A.; Muralidhara, A.; Guigo, N.; Marlair, G.; Jong, E. De; Sbirrazzuoli, N. Natural Fibre Composites with Furanic Thermoset Resins . Comparison between Polyfurfuryl Alcohol and Humins from Sugar Conversion. *Compos. Part C Open Access* **2021**, *4*, 100109. https://doi.org/10.1016/j.jcomc.2021.100109.

94 Pin, J. M.; Guigo, N.; Mija, A.; Vincent, L.; Sbirrazzuoli, N.; Van Der Waal, J. C.; De Jong, E. Valorization of Biorefinery Side-Stream Products: Combination of Humins with Polyfurfuryl Alcohol for Composite Elaboration. *ACS Sustain. Chem. Eng.* **2014**, *2* (9), 2182–2190. https://doi.org/10.1021/sc5003769.

95 Sangregorio, A.; Muralidhara, A.; Guigo, N.; Thygesen, L. G.; Marlair, G.; Angelici, C.; De Jong, E.; Sbirrazzuoli, N. Humin Based Resin for Wood Modification and Property Improvement. *Green Chem.* **2020**, *22* (9), 2786–2798. https://doi.org/10.1039/c9gc03620b.

96 Sangregorio, A.; Guigo, N.; Vincent, L.; de Jong, E.; Sbirrazzuoli, N. Furanic Humins from Biorefinery as Biobased Binder for Bitumen. *Polymers.* **2022**, *14* (5), 1019. https://doi.org/10.3390/polym14051019

97 Leitheiser, R. H.; Londrigan, M. E.; Rude, C. A. Furan Resinous Cements. *ACS Symp. Ser.* **1979**, No. 113, 7–26. https://doi.org/10.1021/bk-1979-0113.ch002.

98 Holtzer, M.; Dańko, R. Molds and Cores Systems in Foundry. *SpringerBriefs Mater.* **2015**, 27–42. https://doi.org/10.1007/978-3-319-14583-9_2.

99 Pizzi, A.; Mittal, K.; Gandini, A.; Naceur Belgacem, M. Furan-Based Adhesives. *Handb. Adhes. Technol. Revis. Expand.* **2003**, https://doi.org/10.1201/9780203912225.ch30.

100List patents https://worldwide.espacenet.com/patent/search/family/083520703/publication/CN115178703A?f=oprid%3Ain%3D20220101-20221231%7Cpublications.pd%3Ain%3D20220101-20221231&q=nftxt%20%3D%20%22foundry%22%20AND%20nftxt%20%3D%20%22furan%20resin%22&queryLang=en%3Ade%3Afr Last accessed (29/09/2023)

101 Yan Hailun; Resin composition for 3D printing, 3D printing product and preparation method and application thereof. CN114918364A, **2022**

102
Su Fei; Su Shaojing; Chen Siming; He Yuan, Song Bo; Chiller for 3D printing sand mold and using method thereof. CN114769547A, **2022**

103
Han Wen; Yang Yang; Xing Jinlong; Furan resin for hot core box as well as preparation method and use method of furan resin. CN115178703A, **2022**

104 Fan Xiumei; High-viscosity furan resin for casting and preparation method thereof. CN115109216A, **2022**

105 Han Haitao; Han Jilei; Wang Dawei; Li Haipeng; Liu Ning; Shi Chunsheng; Wei Feng; Li Bao'e; Regeneration method of casting clay mixed old sand containing resin organic binder. CN115533022A, **2022**

106 Lyu Wiang; Casting process for sequential solidification of wind power torque arm. CN115383075A, **2022**

107 Song Xiangyang; Yuan Xiuming; Xing Beibei; Zhang Xinxia; Furan resin heating temperature control device. CN217617584U, **2022**

108 Wan, P.; Li, Y. cai; Ling, H. jiang; Wang, W. qing; Zhi, H. yi; Xue, J. Development of a New Instrument for Measurement of High Temperature Mechanical Properties of Resin-Bonded Sand. *China Foundry* **2017**, *14* (4), 286–291. https://doi.org/10.1007/s41230-017-6023-4.

109 Acharya, S. G.; Vadher, J. A.; Sheladiya, M. A Furan No-Bake Binder System Analysis for Improved Casting Quality. *Int. J. Met.* **2016**, *10* (4), 491–499. https://doi.org/10.1007/s40962-016-0059-x.

110 Sundaram, D.; Svidró, J. T.; Svidró, J.; Diószegi, A. On the Relation between the Gas-Permeability and the Pore Characteristics of Furan Sand. *Materials* **2021**, *14*, 3803. https://doi.org/10.3390/ma14143803

111 Mizuki, T.; Kanno, T. Establishment of Casting Manufacturing Technology by Introducing an Artificial Sand Mold with Furan Resin and Realizing a Clean Foundry. *Int. J. Met.* **2018**, *12* (4), 772–778. https://doi.org/10.1007/s40962-018-0209-4.

112 Chate, G. R.; Patel, G. C. M.; Bhushan, S. N. B.; Parappagoudar, M. B.; Deshpande, A. S. Comprehensive Modelling, Analysis and Optimization of Furan Resin-Based Moulding Sand System with Sawdust as an Additive. *J. Brazilian Soc. Mech. Sci. Eng.* **2019**, 41 (4). 143 https://doi.org/10.1007/s40430-019-1684-0.

113 Liu, F.; Yang, L.; Huang, Y.; Jiang, P.; Li, G.; Jiang, W.; Liu, X.; Fan, Z. Performance of Resin Bonded Sand for Magnesium Alloy Casting. *J. Manuf. Process.* **2017**, *30*, 313–319. https://doi.org/10.1016/j.jmapro.2017.10.002.

114 Budavári, I.; Gyarmati, G.; Varga, L. The Influence of Acid Hardener on the Strength and Hot-Distortion Properties of No-Bake Sand Cores. *Int. J. Met.* **2022**, *16* (3), 1415–1431. https://doi.org/10.1007/s40962-021-00700-w.

115 Li, Y. lei; Wu, G. hua; Liu, W. cai; Chen, A. tao; Zhang, L.; Wang, Y. xin. Effect of Reclaimed Sand Additions on Mechanical Properties and Fracture Behavior of Furan No-Bake Resin Sand. *China Foundry* **2017**, 14 (2), 128–137. https://doi.org/10.1007/s41230-017-6024-3.

116 Zymankowska-Kumon, S.; Bobrowski, A.; Grabowska, B. Comparison of the Emission of Aromatic Hydrocarbons from Moulding Sands with Furfural Resin with the Low Content of Furfuryl Alcohol and Different Activators. *Arch. Foundry Eng.* **2016**, *16* (4), 187–190. https://doi.org/10.1515/afe-2016-0107.

117 Wang, Y.; Yu, R.; Yin, S.; Tan, R.; Lou, Y. Effect of Gel Time of 3D Sand Printing Binder System on Quality of Sand Mold / Core. *China Foundry* **2021**, *18* (6), 581–586. https://doi.org/10.1007/s41230-021-1085-8

118 Primkulov, B.; Chalaturnyk, J.; Chalaturnyk, R.; Zambrano Narvaez, G. 3D Printed Sandstone Strength: Curing of Furfuryl Alcohol Resin-Based Sandstones. 3D Print. Addit. Manuf. 2017, 4 (3), 149–155. https://doi.org/10.1089/3dp.2017.0032.

119 Picture furan resin casting mold https://vietnamcastiron.com/furan-resin-sand-casting/ Last accessed (29/09/2023)

120 Picture of furan-based flooring https://www.atlasmin.com/post/atlas-fills-industry-demand-for-furan-mortar Last accessed (29/09/2023)

121 Muthukumar, M.; Mohan, D. Optimization of Mechanical Properties of Polymer Concrete and Mix Design Recommendation Based on Design of Experiments. *J. Appl. Polym. Sci.* **2004**, *94* (3), 1107–1116. https://doi.org/10.1002/app.21008.

122 Muthukumar, M.; Mohan, D. Studies on Polymer Concretes Based on Optimized Aggregate Mix Proportion. *Eur. Polym. J.* 2004, 40 (9), 2167–2177. https://doi.org/10.1016/j.eurpolymj.2004.05.004.

123 Muthukumar, M.; Mohan, D. Studies on Furan Polymer Concrete. *J. Polym. Res.* **2005**, *12* (3), 231–241. https://doi.org/10.1007/s10965-004-3206-7.

124 Alakbari, F. S.; Mohyaldinn, M. E.; Muhsan, A. S.; Hasan, N.; Ganat, T. Chemical Sand Consolidation: From Polymers to Nanoparticles. *Polymers* **2020**, *12* (5). https://doi.org/10.3390/POLYM12051069.

125 Tabbakhzadeh, M. N.; Esmaeilzadeh, F.; Zabihi, R.; Mowla, D. Experimental Study of Chemical Sand Consolidation Using Epoxy and Furan Resins for Oil Wells: Experimental Design Models. *Int. J. Rock Mech. Min. Sci.* **2020**, *135*, 104486. https://doi.org/10.1016/j.ijrmms.2020.104486.

126 Gopal, R. Polymer Concrete Composites for Enhancement of Mobility of Troops in Desert Operations. *Mater. Sci. Eng. B Solid-State Mater. Adv. Technol.* **2006**, *132* (1–2), 129–133. https://doi.org/10.1016/j.mseb.2006.04.001.

127 Kumar, R. A Review on Epoxy and Polyester Based Polymer Concrete and Exploration of Polyfurfuryl Alcohol as Polymer Concrete. *J. Polym.* **2016**, *2016*, 1–13. https://doi.org/10.1155/2016/7249743.

128 Deville Jay; Nguyen Philip; Zha Weibin; Sanders Michael; Sand Consolidation with a Curable Resin and Filtercake Removal Fluid. US11492531, **2021**

129 Sharma, M.; Chopra, E. A. Comparative Analysis of Furan Resin Modified Asphalt Mix and Conventional Asphalt Mix. *Int. J. Civ. Eng. Technol.* **2019**, *10* (3), 1574–1582.

130 Bostancioğlu, M.; Oruç, Ş. Effect of Furfural-Derived Thermoset Furan Resin on the High-Temperature Performance of Bitumen. *Road Mater. Pavement Des.* **2015**, *16* (1), 227–237. https://doi.org/10.1080/14680629.2014.990048.

131 Bostancioğlu, M.; Oruç, Ş. Effect of Activated Carbon and Furan Resin on Asphalt Mixture Performance. *Road Mater. Pavement Des.* **2016**, *17* (2), 512–525. https://doi.org/10.1080/14680629.2015.1092465..

132 Schneider Marc; Furan Polymer Impregnated Wood. EP1368167, **2004**.

133 Zelinka, S. L.; Altgen, M.; Emmerich, L.; Guigo, N.; Keplinger, T.; Kymäläinen, M.; Thybring, E. E.; Thygesen, L. G. Review of Wood Modification and Wood Functionalization Technologies. *Forests* **2022**, *13*, 1004. https://doi.org/10.3390/f13071004.

134 Esteves, B.; Nunes, L.; Pereira, H. Properties of Furfurylated Wood (Pinus Pinaster). *Eur. J. Wood Wood Prod.* **2011**, *69* (4), 521–525. https://doi.org/10.1007/s00107-010-0480-4.

135 Martin, L. S.; Jelavić, S.; Cragg, S. M.; Thygesen, L. G. Furfurylation Protects Timber from Degradation by Marine Wood Boring Crustaceans. *Green Chem.* **2021**, *23* (20), 8003–8015. https://doi.org/10.1039/d1gc01524a

136 Shen, X.; Guo, D.; Jiang, P.; Li, G.; Yang, S.; Chu, F. Reaction Mechanisms of Furfuryl Alcohol Polymer with Wood Cell Wall Components. *Holzforschung* **2021**, *75* (12), 1150–1158. https://doi.org/10.1515/hf-2020-0271.

137 Zhu, X.; Bruijnaers, B.; Lourençon, T. V.; Balakshin, M. Structural Analysis of Lignin-Based Furan Resin. *Materials* **2022**, *15* (1), 350. https://doi.org/10.3390/ma15010350.

138 Thygesen, L. G.; Ehmcke, G.; Barsberg, S.; Pilgård, A. Furfurylation Result of Radiata Pine Depends on the Solvent. *Wood Sci. Technol.* **2020**, *54* (4), 929–942. https://doi.org/10.1007/s00226-020-01194-1.

139 Zhang, L.; Zhang, W.; Peng, Y.; Wang, W.; Cao, J. Thermal Behavior and Flame Retardancy of Poplar Wood Impregnated with Furfuryl Alcohol Catalyzed by Boron/Phosphorus Compound System. *Ind. Crops Prod.* **2022**, *176*, 114361. https://doi.org/10.1016/j.indcrop.2021.114361.

140 Villa made from Kebony wood https://kebony.com/projects/villa-porto-vecchio/ Last accessed (29/09/2023)

141 Picture of Kebony wood https://norddeck.com/en/kebony-tree/ Last accessed (29/09/2023)

142 S. Giannis; Arnold, E.; Hoydonckx, H. E.; Weager, B. .; Martin, R. H. Development of High Performance Bio-Composite Based on Furan Bio Resin for Vehicle Panel. *13th Eur. Conf. Compos. Mater.* **2008**,

143 Colin Peackock. Composite Automatic Gate Paddle. WO2023287761, **2023**.

144 Draper Michael; Ka Lun To Bio-Composite Sustainable Doctor Blade. US20230151546, **2022**.

145 Salomon Pierre; Jaffrenou Boris. Concentrated Solution of Poly(Furfuryl Alcohol) for Sizing Organic or Mineral Fibers. WO 2018167429, **2018**.

146 Salomon, Pierre; Azevedo Joel; Jaffrenou Boris. Method for Manufacturing an Insolution Product Made from Mineral Fiber. WO 2018/234652, **2018**.

147 Obert Edouard; Kiefer Lionel.; Kaplan Benjamin. Binder Composition Based on Non-Reducing Saccharides and Hydrogenated Saccharides, and Its Use for Producing Insulating Products. EP3131857, **2019**.

148 Arnold, E. L.; Weager, B. M.; Way, B.; Hoydonckx, H. E.; Madsen, B. Next generation of sustainable composites: development and processing of fruan-flax biocomposites. *17th International Conference on Composite Materials - Edinburgh, United Kingdom;* **2009**

149 Galego, N.; Vazquez, A. Composites of Furan Resin Cured with Acid Catalyst. *Polym. Plast. Technol. Eng.* **1995**, *34* (1), 65–78. https://doi.org/10.1080/03602559508017213.

150 Ma, C. C. M.; Yn, M. S.; Han, J. L.; Chang, C. J.; Wu, H. D. Pultruded Fibre-Reinforced Furfuryl Alcohol Resin Composites: 1. Process Feasibility Study. *Compos. Manuf.* **1995**, *6* (1), 45–52.

151 Crossley, R.; Schubel, P.; Stevenson, A. Furan Matrix and Flax Fibre as a Sustainable Renewable Composite: Mechanical and Fire-Resistant Properties in Comparison to Phenol, Epoxy and Polyester. *J. Reinf. Plast. Compos.* **2014**, *33* (1), 58–68. https://doi.org/10.1177/0731684413502108.

152 Odiyi, D. C.; Sharif, T.; Choudhry, R. S.; Mallik, S. Cure Mechanism and Kinetic Prediction of Biobased Glass/Polyfurfuryl Alcohol Prepreg by Model-Free Kinetics. *Thermochim. Acta* **2022**, *708*, 179133. https://doi.org/10.1016/j.tca.2021.179133.

153 Porte folio of TransFuran Chemicals https://www.transfurans.be/products Last accessed (29/09/2023)

154 Mak, K.; Fam, A. Fatigue Performance of Furfuryl Alcohol Resin Fiber-Reinforced Polymer for Structural Rehabilitation. *J. Compos. Constr.* **2020**, *24* (3), 04020012. https://doi.org/10.1061/(asce)cc.1943-5614.0001018.

155 Wang, Z.; Cao, N.; He, J.; Du, R.; Liu, Y.; Zhao, G. Mechanical and Anticorrosion Properties of Furan/Epoxy-Based Basalt Fiber-Reinforced Composites. *J. Appl. Polym. Sci.* **2017**, *134* (19), 44799. https://doi.org/10.1002/app.44799.

156 Wang, Z.; Meng, F.; Li, X.; Zhang, X.; Hu, W.; Zhao, G. Cure Behaviors of Furfuryl Alcohol/Epoxy/Methyltetrahydrophthalic Anhydride and Their Enhanced Mechanical and Anti-Acid Properties of Basalt Fiber Reinforced Composites. *Compos. Part B Eng.* **2018**, *154* (April), 263–271. https://doi.org/10.1016/j.compositesb.2018.08.011.

157 López De Vergara, U.; Sarrionandia, M.; Gondra, K.; Aurrekoetxea, J. Impact Behaviour of Basalt Fibre Reinforced Furan Composites Cured under Microwave and Thermal Conditions. *Compos. Part B Eng.* **2014**, *66*, 156–161. https://doi.org/10.1016/j.compositesb.2014.05.009.

158 Elejoste, P. A.; Allue, A.; Ballestero, J.; Neira, S.; Gómez-Alonso, J. L.; Gondra, K. Development and Characterisation of Sustainable Prepregs with Improved Fire Behaviour Based on Furan Resin and Basalt Fibre Reinforcement. *Polymers* **2022**, *14* (9), 1864. https://doi.org/10.3390/polym14091864.

159 Malaba, T.; Wang, J. Unidirectional Cordenka Fibre-Reinforced Furan Resin Full Biocomposite: Properties and Influence of High Fibre Mass Fraction. *J. Compos.* **2015**, *2015*, 1–8. https://doi.org/10.1155/2015/707151.

160 Tumolva, T.; Kubouchi, M.; Aoki, S.; Sakai, T. Evaluating the Carbon Storage Potential of Furan Resin-Based Green Composites. *ICCM Int. Conf. Compos. Mater.* **2011**

161 Deka, H.; Misra, M.; Mohanty, A. Renewable Resource Based "All Green Composites" from Kenaf Biofiber and Poly(Furfuryl Alcohol) Bioresin. *Ind. Crops Prod.* **2013**, *41* (1), 94–101. https://doi.org/10.1016/j.indcrop.2012.03.037.

162 Pohl, T.; Bierer, M.; Natter, E.; Madsen, B.; Hoydonckx, H.; Schledjewski, R. Properties of Compression Moulded New Fully Biobased Thermoset Composites with Aligned Flax Fibre Textiles. *Plast. Rubber Compos.* **2011**, *40* (6–7), 294–299. https://doi.org/10.1179/1743289810Y.0000000017.

163 Crossley, R. J.; Schubel, P. J.; Stevenson, A.; Moreira, M. The Development and Processing of a Sustainable Fully Bio Derived Polyfurfuryl Alcoholmatrix Flax Fibre Prepreg. *ECCM 2012 - Compos. Venice, Proc. 15th Eur. Conf. Compos. Mater.* **2012**

164 Toriz, G.; Arvidsson, R.; Westin, M.; Gatenholm, P. Novel Cellulose Ester-Poly(Furfuryl Alcohol)-Flax Fiber Biocomposites. *J. Appl. Polym. Sci.* **2003**, *88* (2), 337–345. https://doi.org/10.1002/app.11730.

165 Motaung, T. E.; Mngomezulu, M. E.; Hato, M. J. Effects of Alkali Treatment on the Poly(Furfuryl) Alcohol–Flax Fibre Composites. *J. Thermoplast. Compos. Mater.* **2018**, *31* (1), 48–60. https://doi.org/10.1177/0892705716679478.

166 Menager, C.; Guigo, N.; Wu, X.; Vincent, L.; Sbirrazzuoli, N. "Green" Composites Prepared from Polyfurfuryl Alcohol and Cork Residues: Thermal and Mechanical Properties. *Compos. Part A Appl. Sci. Manuf.* **2019**, *124*, 105473. https://doi.org/10.1016/j.compositesa.2019.105473.

167 Guigo, N.; Mija, A.; Vincent, L.; Sbirrazzuoli, N. Eco-Friendly Composite Resins Based on Renewable Biomass Resources: Polyfurfuryl Alcohol/Lignin Thermosets. *Eur. Polym. J.* **2010**, *46* (5), 1016–1023. https://doi.org/10.1016/j.eurpolymj.2010.02.010.

168 Deka, H.; Mohanty, A.; Misra, M. Renewable-Resource-Based Green Blends from Poly(Furfuryl Alcohol) Bioresin and Lignin. *Macromol. Mater. Eng.* **2014**, *299* (5), 552–559. https://doi.org/10.1002/mame.201300221.

169 Zhang, J.; Wang, W.; Zhou, X.; Liang, J.; Du, G.; Wu, Z. Lignin-Based Adhesive Crosslinked by Furfuryl Alcohol-Glyoxal and Epoxy Resins. *Nord. Pulp Pap. Res. J.* **2019**, *34* (2), 228–238. https://doi.org/10.1515/npprj-2018-0042

170 Gosselink, R. J. A.; Van Dam, J. E. G.; De Jong, E.; Gellerstedt, G.; Scott, E. L.; Sanders, J. P. M. Effect of Periodate on Lignin for Wood Adhesive Application. *Holzforschung* **2011**, *65* (2), 155–162. https://doi.org/10.1515/HF.2011.025.

171 Hemmilä, V.; Adamopoulos, S.; Hosseinpourpia, R.; Ahmed, S. A. Ammonium Lignosulfonate Adhesives for Particleboards with PMDI and Furfuryl Alcohol as Crosslinkers. *Polymers.* **2019**, *11* (10), 1633 https://doi.org/10.3390/polym11101633.

172 Luckeneder, P.; Gavino, J.; Kuchernig, R.; Petutschnigg, A.; Tondi, G. Sustainable Phenolic Fractions as Basis for Furfuryl Alcohol-Based Co-Polymers and Their Use as Wood Adhesives. *Polymers* **2016**, *8* (11), 396 https://doi.org/10.3390/polym8110396.

173 Kim, M. G.; Wasson, L.; Burris, M.; Wu, Y.; Watt, C.; Strickland, R. C. Furfuryl Alcohol Emulsion Resins as Co-Binders for Urea-Formaldehyde Resin-Bonded Particleboards. *Wood Fiber Sci.* **1998**, *30* (3), 238–249.

174 Varodi, A. M.; Beldean, E.; Timar, M. C. Furan Resin as Potential Substitute for Phenol-Formaldehyde Resin in Plywood Manufacturing. *BioResources* **2019**, *14* (2), 2727–2739. https://doi.org/10.15376/biores.14.2.2727-2739.

175 Abdullah, U. H. B.; Pizzi, A. Tannin-Furfuryl Alcohol Wood Panel Adhesives without Formaldehyde. *Eur. J. Wood Wood Prod.* **2013**, *71* (1), 131–132. https://doi.org/10.1007/s00107-012-0629-4.

176 Cesprini, E.; Jorda, J.; Valentini, L.; Causin, V. Bio-Based Tannin-Furanic-Silk Adhesives: Applications in Plywood and Chemical Cross-Linking Mechanisms. *ACS Appl. Polym. Mater.* **2023**, No. May. https://doi.org/10.1021/acsapm.3c00539.

177 Xi, X.; Wu, Z.; Pizzi, A.; Gerardin, C.; Lei, H.; Du, G. Furfuryl Alcohol-Aldehyde Plywood Adhesive Resins. *J. Adhes.* **2020**, *96* (9), 814–838. https://doi.org/10.1080/00218464.2018.1519435.

178 Zhang, J.; Liu, B.; Zhou, Y.; Essawy, H.; Chen, Q.; Zhou, X.; Du, G. Preparation of a Starch-Based Adhesive Cross-Linked with Furfural, Furfuryl Alcohol and Epoxy Resin. *Int. J. Adhes. Adhes.* **2021**, *110*, 102958. https://doi.org/10.1016/j.ijadhadh.2021.102958.

179 Kherroub, D. E.; Belbachir, M.; Lamouri, S. Study and Optimization of the Polymerization Parameter of Furfuryl Alcohol by Algerian Modified Clay. *Arab. J. Sci. Eng.* **2015**, *40* (1), 143–150. https://doi.org/10.1007/s13369-014-1512-x

180 Zavaglia, R.; Guigo, N.; Sbirrazzuoli, N.; Mija, A.; Vincent, L. Complex Kinetic Pathway of Furfuryl Alcohol Polymerization Catalyzed by Green Montmorillonite Clays. *J. Phys. Chem. B* **2012**, *116* (28), 8259–8268. https://doi.org/10.1021/jp301439q.

181 Kherroub, D. E.; Belbachir, M.; Lamouri, S. Synthesis of Poly(Furfuryl Alcohol)/Montmorillonite Nanocomposites by Direct in-Situ Polymerization. *Bull. Mater. Sci.* **2015**, *38* (1), 57–63. https://doi.org/10.1007/s12034-014-0818-3.

182 Pranger, L.; Tannenbaum, R. Biobased Nanocomposites Prepared by in Situ Polymerization of Furfuryl Alcohol with Cellulose Whiskers or Montmorillonite Clay. *Macromolecules* **2008**, *41* (22), 8682–8687. https://doi.org/10.1021/ma8020213.

183 Pranger, L. A.; Nunnery, G. A.; Tannenbaum, R. Mechanism of the Nanoparticle-Catalyzed Polymerization of Furfuryl Alcohol and the Thermal and Mechanical Properties of the Resulting Nanocomposites. *Compos. Part B Eng*. **2012**, *43* (3), 1139–1146. https://doi.org/10.1016/j.compositesb.2011.08.010.

184 Guigo, N.; Mija, A.; Zavaglia, R.; Vincent, L.; Sbirrazzuoli, N. New Insights on the Thermal Degradation Pathways of Neat Poly(Furfuryl Alcohol) and Poly(Furfuryl Alcohol)/SiO2 Hybrid Materials. *Polym. Degrad. Stab.* **2009**, *94* (6), 908–913. https://doi.org/10.1016/j.polymdegradstab.2009.03.008.

185 Monti, M.; Hoydonckx, H.; Stappers, F.; Camino, G. Thermal and Combustion Behavior of Furan Resin/Silica Nanocomposites. *Eur. Polym. J.* **2015**, *67*, 561–569. https://doi.org/10.1016/j.eurpolymj.2015.02.005.

186 Bosq, N.; Guigo, N.; Vincent, L.; Sbirrazzuoli, N. Thermomechanical Behavior of a Novel Biobased Poly(Furfurylalcohol)/Silica Nanocomposite Elaborated by Smart Functionalization of Silica Nanoparticles. *Polym. Degrad. Stab.* **2015**, *118*, 137–146. https://doi.org/10.1016/j.polymdegradstab.2015.04.018.

187 Ma, Y.; Du, Y.; Zhao, J.; Yuan, X.; Hou, X. Preparation and Characterization of Furan-Matrix Composites Blended with Modified Hollow Glass Microsphere. *Polymers* **2020**, *12* (7), 1–12. https://doi.org/10.3390/polym12071480.

188 Spange, S.; Heublein, B.; Schramm, A. Composites from Furfuryl Alcohol and Inorganic Solids by Cationic Initiation, 1. *Makrornol. Chern*, **1992**, *13*, 511–515. https://doi.org/10.1002/marc.1992.030131106

189 Spange, S.; Schütz, H.; Martinez, R. Composites from Furfuryl Alcohol and Inorganic Solids by Cationic Initiation, 2. Spectroscopic Studies of Poly(Furfuryl Alcohol)-silica Composites Obtained by Trifluoroacetic Acid Initiation. *Die Makromol. Chemie* **1993**, *194* (6), 1537–1544. https://doi.org/10.1002/macp.1993.021940602.

190 Faculty, M.; Spangel, S. Composites from Furfuryl Alcohol and Inorganic Solids 3. *Die Angew. Makromol. Chemie* **1993**, *208*, 125–131. https://doi.org/10.1002/apmc.1993.052080112

191 Yi, B.; Rajagopalan, R.; Foley, H. C.; Kim, U. J.; Liu, X.; Eklund, P. C. Catalytic Polymerization and Facile Grafting of Poly(Furfuryl Alcohol) to Single-Wall Carbon Nanotube: Preparation of Nanocomposite Carbon. *J. Am. Chem. Soc.* **2006**, *128* (34), 11307–11313. https://doi.org/10.1021/ja063518x.

192 Edwards, E. R.; Oishi, S. S.; Botelho, E. C. Analysis of Chemical Polymerization between Functionalized MWCNT and Poly(Furfuryl Alcohol) Composite. *Polimeros* **2018**, *28* (1), 15–22. https://doi.org/10.1590/0104-1428.07016.

193 Men, X. H.; Zhang, Z. Z.; Yang, J.; Zhu, X. T.; Wang, K.; Jiang, W. Effect of Different Functional Carbon Nanotubes on the Tribological Behaviors of Poly (Furfuryl Alcohol)–Derived Carbon Nanocomposites. *Tribol. Trans.* **2011**, *54* (2), 265–274. https://doi.org/10.1080/10402004.2010.540367.

194 Men, X. H.; Zhang, Z. Z.; Song, H. J.; Wang, K.; Jiang, W. Functionalization of Carbon Nanotubes to Improve the Tribological Properties of Poly(Furfuryl Alcohol) Composite Coatings. *Compos. Sci. Technol.* **2008**, *68* (3–4), 1042–1049. https://doi.org/10.1016/j.compscitech.2007.07.008.

195 Conejo, L. S.; Costa, M. L.; Oishi, S. S.; Botelho, E. C. Degradation Behavior of Carbon Nanotubes/Phenol-Furfuryl Alcohol Multifunctional Composites with Aerospace Application. *Mater. Res. Express* **2017**, *4* (10), 105701. https://doi.org/10.1088/2053-1591/aa8f60.

196 Montagna, L. S.; da Silva, A. P. B.; de Melo Morgado, G. F.; Ribeiro, B.; Passador, F. R.; Rezende, M. C. PFA Nanocomposites: The Influence of Three Carbon Nanofillers on the Mechanical and Electromagnetic Properties. *J. Polym. Res.* **2021**, *28* (7), 253. https://doi.org/10.1007/s10965-021-02613-y.

197 Quynh, T. N. T.; Phuong, C. T.; Khue, V. T.; Hung, N. D.; Ngoc, D. T. B.; Tai, D. C.; Thang, C. X. One-Pot Synthesis of Graphene Oxide/Poly(Furfuryl Alcohol) in Deep Eutectic Solvent: A Metal-Free Electrocatalyst for Non-Enzymatic Glucose Sensor Application. *Vietnam J. Chem.* **2022**, *60* (6), 809–816. https://doi.org/10.1002/vjch.202200077.

198 Li, C.; Li, S.; Yan, S. Facile and Green Preparation of Biobased Graphene Oxide/Furan Resin Nanocomposites with Enhanced Thermal and Mechanical Properties. *RSC Adv.* **2016**, *6* (67), 62572–62578. https://doi.org/10.1039/c6ra11247a.

199 Montagna, L. S.; Oishi, S. S.; Diniz, M. F.; Do Amaral Montanheiro, T. L.; Da Silva, F. S.; Passador, F. R.; Rezende, M. C. Multifunctional Green Nanostructured Composites: Preparation and Characterization. *Mater. Res. Express* **2018**, *5* (5). https://doi.org/10.1088/2053-1591/aabf66.

200 Zhu, Z.; Bai, S.; Wu, J.; Xu, L.; Li, T.; Ren, Y.; Liu, C. Friction and Wear Behavior of Resin/Graphite Composite under Dry Sliding. *J. Mater. Sci. Technol.* **2015**, *31* (3), 325–330. https://doi.org/10.1016/j.jmst.2014.10.004.

201 Shibutani, K.; Nakai, J.; Aphichartsuphapkhajorn, K.; Kayaki, Y.; Kuwata, S.; Arao, Y.; Kubouchi, M. The Activation of Furfuryl Alcohol Polymerization by Oxygen and Its Enhanced Mechanical Properties. *J. Appl. Polym. Sci.* **2020**, *138* (17), 50311. https://doi.org/10.1002/app.50311.

202 Motaung, T. E.; Gqokoma, Z.; Linganiso, L. Z.; Hato, M. J. The Effect of Acid Content on the Poly(Furfuryl) Alcohol/Cellulose Composites T.E. *Polym. Compos.* **2015**, *16* (2), 101–113. https://doi.org/10.1002/pc.23428.

203 Ahmad, E. E. M.; Luyt, A. S.; Djoković, V. Thermal and Dynamic Mechanical Properties of Bio-Based Poly(Furfuryl Alcohol)/Sisal Whiskers Nanocomposites. *Polym. Bull.* **2013**, *70* (4), 1265–1276. https://doi.org/10.1007/s00289-012-0847-2.

204 Lems, E. M.; Winklehner, S.; Hansmann, C.; Gindl-Altmutter, W.; Veigel, S. Reinforcing Effect of Poly(Furfuryl Alcohol) in Cellulose-Based Porous Materials. *Cellulose* **2019**, *6*. 4431–4444 https://doi.org/10.1007/s10570-019-02348-6.

205 Davide Beneventi; Didier Chaussy; Khaoula Bouzidi; Alessandro, Gandini. Thermosetting Composite Material and Associated Printing Process. WO2021151893, **2021**

206 Bouzidi, K.; Chaussy, D.; Gandini, A.; Bongiovanni, R.; Beneventi, D. 3D Printable Fully Biomass-Based Composite Using Poly(Furfuryl Alcohol) as Binder and Cellulose as a Filler. *Carbohydr. Polym.* **2022**, *293*, 119716. https://doi.org/10.1016/j.carbpol.2022.119716.

207 Lépine, O.; Birot, M.; Deleuze, H. Preparation of a Poly(Furfuryl Alcohol)-Coated Highly Porous Polystyrene Matrix. *Macromol. Mater. Eng.* **2009**, *294* (9), 599–604. https://doi.org/10.1002/mame.200900102

208 Szczurek, A.; Fierro, V.; Thébault, M.; Pizzi, A.; Celzard, A. Structure and Properties of Poly(Furfuryl Alcohol)-Tannin PolyHIPEs. *Eur. Polym. J.* **2016**, *78*, 195–212. https://doi.org/10.1016/j.eurpolymj.2016.03.037.

209 Hou, B.; He, H.; Jia, R.; Fu, M.; Cao, Y.; He, S.; Luo, L.; Huang, Y. A Novel Temperature-Tolerant Foamed Resin for Enhanced Oil Recovery. *J. Appl. Polym. Sci.* **2019**, *136* (10), 47161. https://doi.org/10.1002/app.47161.

210 Feng, Y.; Wang, Y.; Wang, Y.; Yao, J. Furfuryl Alcohol Modified Melamine Sponge for Highly Efficient Oil Spill Clean-up and Recovery. *J. Mater. Chem. A* **2017**, *5* (41), 21893–21897. https://doi.org/10.1039/c7ta06966a.

211 Wang, T.; Sun, H.; Long, J.; Wang, Y. Z.; Schiraldi, D. Biobased Poly(Furfuryl Alcohol)/Clay Aerogel Composite Prepared by a Freeze-Drying Process. *ACS Sustain. Chem. Eng.* **2016**, *4* (5), 2601–2605. https://doi.org/10.1021/acssuschemeng.6b00089

212 Pin, J. M.; Misra, M.; Mohanty, A. Green Design of Nanoporous Materials and Carbonaceous Foams from Polyfurfuryl Alcohol and Epoxidized Linseed Oil. *Mater. Lett.* **2017**, *196*, 238–241. https://doi.org/10.1016/j.matlet.2017.03.058

213 Wang, P.; Deng, G.; Zhang, H.; Yin, J.; Xiong, X.; Zhang, X.; Zhu, H. Microstructural Feature and Tribological Behaviors of Pyrolytic Carbon-Coated Copper Foam/Carbon Composite. *J. Mater. Sci.* **2019**, *54* (21), 13557–13568. https://doi.org/10.1007/s10853-019-03857-2

214 Chen, X.; Guigo, N.; Pizzi, A.; Sbirrazzuoli, N.; Li, B.; Fredon, E.; Gerardin, C. Ambient Temperature Self-blowing Tannin–Humins Biofoams. *Polymers* **2020**, *12* (11), 2732. https://doi.org/10.3390/polym12112732.

215 Harmer Mark Andrew; Kapur Vivek; Williams, Sharlene Renee. Closed-Cell Tannin-Based Foam without Formaldehyde. WO2012162645, **2012**.

216 Acosta, A.; Aramburu, A. B.; Beltrame, R.; Gatto, D. A.; Amico, S.; Labidi, J.; Delucis, R. de A. Wood Flour Modified by Poly(Furfuryl Alcohol) as a Filler in Rigid Polyurethane Foams: Effect on Water Uptake. *Polymers.* **2022**, *14* (24), 5510. https://doi.org/10.3390/polym14245510.

217 Zolghadr, M.; Zohuriaan-Mehr, M. J.; Shakeri, A.; Salimi, A. Epoxy Resin Modification by Reactive Bio-Based Furan Derivatives: Curing Kinetics and Mechanical Properties. *Thermochim. Acta* **2019**, *673*, 147–157. https://doi.org/10.1016/j.tca.2019.01.025.

218 Mohajeri, S.; Vafayan, M.; Ghanbaralizadeh, R.; Pazokifard, S.; Zohuriaan Mehr, M. J. Advanced Isoconversional Cure Kinetic Analysis of Epoxy/Poly(Furfuryl Alcohol) Bio-Resin System. *J. Appl. Polym. Sci.* **2017**, *134* (42), 45432. https://doi.org/10.1002/app.45432.

219 Mohajeri, S.; Zohuriaan-Mehr, M. J.; Pazokifard, S. Epoxy Matrix Toughness Improvement via Reactive Bio-Resin Alloying. *High Perform. Polym.* **2017**, *29* (7), 772–784. https://doi.org/10.1177/0954008316656743.

220 Moazzen, K.; Zohuriaan-Mehr, M. J.; Jahanmardi, R.; Kabiri, K. Toward Poly(Furfuryl Alcohol) Applications Diversification: Novel Self-Healing Network and Toughening Epoxy–Novolac Resin. *J. Appl. Polym. Sci.* **2018**, *135* (12), 45921. https://doi.org/10.1002/app.45921.

221 Hanifpour, A.; Miraghaie, S.; Zohuriaan-Mehr, M. J.; Behzadnasab, M.; Bahri-Laleh, N. Poly(Furfuryl Alcohol) Bioresin-Modified LY5210 Epoxy Thermosets. *J. Polym. Res.* **2019**, *26* (8). https://doi.org/10.1007/s10965-019-1876-4.

222 Karami, Z.; Zohuriaan-Mehr, M. J.; Rostami, A. Biobased Diels-Alder Engineered Network from Furfuryl Alcohol and Epoxy Resin: Preparation and Mechano-Physical Characteristics. *ChemistrySelect* **2018**, *3* (1), 40–46. https://doi.org/10.1002/slct.201702387.

223 Mashouf Roudsari, G.; Misra, M.; Mohanty, A. K. A Study of Mechanical Properties of Biobased Epoxy Network: Effect of Addition of Epoxidized Soybean Oil and Poly(Furfuryl Alcohol). *J. Appl. Polym. Sci.* **2017**, *134* (1), 44352. https://doi.org/10.1002/app.44352.

224 Pin, J. M.; Guigo, N.; Vincent, L.; Sbirrazzuoli, N.; Mija, A. Copolymerization as a Strategy to Combine Epoxidized Linseed Oil and Furfuryl Alcohol: The Design of a Fully Bio-Based Thermoset. *ChemSusChem* **2015**, *8* (24), 4149–4161. https://doi.org/10.1002/cssc.201501259.

225 Ribeiro, B. O.; Valério, V. S.; Gandini, A.; Lacerda, T. M. Copolymers of Xylan-Derived Furfuryl Alcohol and Natural Oligomeric Tung Oil Derivatives. *Int. J. Biol. Macromol.* **2020**, *164*, 2497–2511. https://doi.org/10.1016/j.ijbiomac.2020.08.095.

226 Valentino, H. A. S.; de Tarso Laia dos Reis e Silva Pupio, P.; Gandini, A.; Lacerda, T. M. Furfuryl Alcohol/Tung Oil Matrix-Based Composites Reinforced with Bacterial Cellulose Fibres. *Cellulose* **2021**, *28* (11), 7109–7121. https://doi.org/10.1007/s10570-021-03999-0.

227 Liang, J.; Wu, Z.; Lei, H.; Xi, X.; Li, T.; Du, G. The Reaction between Furfuryl Alcohol and Model Compound of Protein. *Polymers.* **2017**, *9* (12), 711. https://doi.org/10.3390/polym9120711.

228 Sun, K.; Zhang, L.; Xu, Q.; Zhang, Z.; Shao, Y.; Dong, D.; Gao, G.; Liu, Q.; Wang, S.; Hu, X. Evidence for Cross-Polymerization between the Biomass-Derived Furans and Phenolics. *Renew. Energy* **2020**, *154*, 517–531. https://doi.org/10.1016/j.renene.2020.03.030.

229 Zhang, J.; Liu, B.; Zhou, Y.; Essawy, H.; Chen, Q.; Zhou, X.; Du, G. Preparation of a Starch-Based Adhesive Cross-Linked with Furfural, Furfuryl Alcohol and Epoxy Resin. *Int. J. Adhes. Adhes.* **2021**, *110*, 102958. https://doi.org/10.1016/j.ijadhadh.2021.102958.

230 Nanni, G.; Heredia-Guerrero, J. A.; Paul, U. C.; Dante, S.; Caputo, G.; Canale, C.; Athanassiou, A.; Fragouli, D.; Bayer, I. S. Poly(Furfuryl Alcohol)-Polycaprolactone Blends. *Polymers* **2019**, *11* (6), 1069. https://doi.org/10.3390/POLYM11061069

231 Sharib, M.; Kumar, R.; Kumar, K. D. Polylactic Acid Incorporated Polyfurfuryl Alcohol Bioplastics: Thermal, Mechanical and Curing Studies. *J. Therm. Anal. Calorim.* **2018**, *132* (3), 1593–1600. https://doi.org/10.1007/s10973-018-7087-0.

232 Kandola, B. K.; Ebdon, J. R.; Chowdhury, K. P. Flame Retardance and Physical Properties of Novel Cured Blends of Unsaturated Polyester and Furan Resins. *Polymers* **2015**, *7* (2), 298–315. https://doi.org/10.3390/polym7020298.

233 Ruelens, W.; Koolen, G.; Gricourt, B.; Willem van Vuure, A.; Smet, M. Co-Polymerisation of Furfuryl Alcohol for Furan Resins with Increased Toughness. *Mater. Lett.* **2022**, *328*, 133025. https://doi.org/10.1016/j.matlet.2022.133025.

234 Shi, Z.; Li, P.; Zhao, G.; Du, R. Curing Characteristics of Bismaleimide/Furan Blends. *J. Phys. Conf. Ser.* **2019**, *1213* (5). https://doi.org/10.1088/1742-6596/1213/5/052050.

235 Mashouf Roudsari, G.; Mohanty, A. K.; Misra, M. A Statistical Approach to Develop Biocomposites from Epoxy Resin, Poly(Furfuryl Alcohol), Poly(Propylene Carbonate), and Biochar. *J. Appl. Polym. Sci.* **2017**, *134* (38), 45307. https://doi.org/10.1002/app.45307.

236 Ebert, T.; Wollbrink, A.; Seifert, A.; John, R.; Spange, S. Multiple Polymerization-Formation of Hybrid Materials Consisting of Two or More Polymers from One Monomer. *Polym. Chem.* **2016**, *7* (44), 6826–6833. https://doi.org/10.1039/c6py01619g.

237 Zhang, L.; Shi, Z.; Hu, W.; Zhang, X.; Zhu, H.; Zhao, G.; Wang, Z. Curing Mechanism, Heat Resistance, and Anticorrosion Properties of a Furan/Methyl Phenyl Silicone Coating. *Polym. Adv. Technol.* **2018**, *29* (7), 1913–1921. https://doi.org/10.1002/pat.4300.

238 Wang, Z.; Zhang, L.; Hu, W.; Zhang, X.; Zhao, G. Ultra-Heat Resistant, Adhesive and Anticorrosive Properties of Poly(Dimethylsiloxane) Resin/Furan Coating. *Prog. Org. Coatings* **2018**, *125*, 500–506. https://doi.org/10.1016/j.porgcoat.2018.10.005.

239 Naderizadeh, S.; Dante, S.; Picone, P.; Di Carlo, M.; Carzino, R.; Athanassiou, A.; Bayer, I. S. Bioresin-Based Superhydrophobic Coatings with Reduced Bacterial Adhesion. J. Colloid Interface Sci. 2020, 574, 20–32. https://doi.org/10.1016/j.jcis.2020.04.031.

240 Men, X. H.; Zhang, Z. Z.; Yang, J.; Wang, K.; Jiang, W. A Facile Method for Preparation of Superhydrophobic Surfaces with Poly(Furfuryl Alcohol)/PTFE Composites. *J. Dispers. Sci. Technol.* **2010**, *31* (6), 780–783. https://doi.org/10.1080/01932690903333291.

241 Chen, S. W.; Guo, B. L.; Wu, W. S. A Novel Fabrication of Superhydrophobic Surfaces for Universal Applicability. *Appl. Phys. A Mater. Sci. Process.* **2011**, *105* (4), 861–866. https://doi.org/10.1007/s00339-011-6587-6.

242 Men, X.; Zhang, Z.; Yang, J.; Zhu, X.; Wang, K.; Jiang, W. Spray-Coated Superhydrophobic Coatings with Regenerability. *New J. Chem.* **2011**, *35* (4), 881–886. https://doi.org/10.1039/c0nj00954g.

243 He, L.; Li, D.; Dong, D.; Yao, J.; Huang, Y.; Wang, H. Effects of Polymerization Conditions on the Properties of Poly(Furfuryl Alcohol) Composite Membranes. *J. Appl. Polym. Sci.* **2012**, *124* (4), 3383–3391. https://doi.org/10.1002/app.35356.

244 He, L.; Li, D.; Wang, K.; Suresh, A. K.; Bellare, J.; Sridhar, T.; Wang, H. Synthesis of Silicalite-Poly(Furfuryl Alcohol) Composite Membranes for Oxygen Enrichment from Air. *Nanoscale Res. Lett.* **2011**, *6*, 637. https://doi.org/10.1186/1556-276X-6-637.

245 Remiš, T.; Dodda, J. M.; Tomáš, M.; Novotný, P.; Bělský, P. Influence of Polyfurfuryl Alcohol (PFA) Loading on the Properties of Nafion Composite Membranes. *J. Macromol. Sci. Part A Pure Appl. Chem.* **2016**, *53* (12), 757–767. https://doi.org/10.1080/10601325.2016.1237814.

246 Acharya, M.; Foley, H. C. Spray-Coating of Nanoporous Carbon Membranes for Air Separation. *J. Memb. Sci.* **1999**, *161* (1–2), 1–5. https://doi.org/10.1016/S0376-7388(99)00173-8.

247 Hou, J.; Zhang, H.; Hu, Y.; Li, X.; Chen, X.; Kim, S.; Wang, Y.; Simon, G. P.; Wang, H. Carbon Nanotube Networks as Nanoscaffolds for Fabricating Ultrathin Carbon Molecular Sieve Membranes. *ACS Appl. Mater. Interfaces* **2018**, *10* (23), 20182–20188. https://doi.org/10.1021/acsami.8b04481.

248 Picture of resin impregnated graphite heat exchanger https://cgthermal.com/blog/graphite-impregnation-the-corrosive-fight-in-heat-transfer-processes/ Last accessed (29/09/2023)

249 Lafyatis, D. S.; Tung, J.; Foley, H. C. Poly(Furfuryl Alcohol)-Derived Carbon Molecular Sieves: Dependence of Adsorptive Properties on Carbonization Temperature, Time, and Poly(Ethylene Glycol) Additives. *Ind. Eng. Chem. Res.* **1991**, *30* (5), 865–873. https://doi.org/10.1021/ie00053a008.

250 Ba, Y.-Q.; Wang, Y.-S.; Li, T.-Y.; Zheng, Z.; Hao, G.-P.; Lu, A.-H. Fine Tuning CO2 Adsorption and Diffusion Behaviors in Ultra-Microporous Carbons for Favorable CO2 Capture at Moderate Temperature. *Sustain. Chem. Clim. Action* **2023**, *2*, 100015. https://doi.org/10.1016/j.scca.2023.100015.

251 Wang, Z.; Yan, X.; Cong, C.; Xing, G.; Wang, Z.; Wang, J. Green Synthesis of Size-Controllable Polyfurfuryl Alcohol Nanospheres as Novel Bio-Adsorbents. *ACS Sustain. Chem. Eng.* **2023**, *11* (15), 6032–6042. https://doi.org/10.1021/acssuschemeng.3c00480.

252 Machowski, K.; Kuštrowski, P.; Dudek, B.; Michalik, M. Elimination of Ketone Vapors by Adsorption on Spherical MCM-41 and MCM-48 Silicas Decorated with Thermally Activated Poly(Furfuryl Alcohol). *Mater. Chem. Phys.* **2015**, *165*, 253–260. https://doi.org/10.1016/j.matchemphys.2015.09.026.

253 Hawes, G. F.; Yilman, D.; Noremberg, B. S.; Pope, M. A. Supercapacitors Fabricated via Laser-Induced Carbonization of Biomass-Derived Poly(Furfuryl Alcohol)/Graphene Oxide Composites. *ACS Appl. Nano Mater.* **2019**, *2* (10), 6312–6324. https://doi.org/10.1021/acsanm.9b01284.

254 Arnaiz, M.; Nair, V.; Mitra, S.; Ajuria, J. Furfuryl Alcohol Derived High-End Carbons for Ultrafast Dual Carbon Lithium Ion Capacitors. *Electrochim. Acta* **2019**, *304*, 437–446. https://doi.org/10.1016/j.electacta.2019.03.029.

255 Dong, D.; Yao, J.; Li, C. Z.; Wang, H. Poly(Furfuryl Alcohol)-Assisted Pyrolysis Synthesis of Ceramic Nanoparticles for Solid Oxide Fuel Cells. *Mater. Res. Bull.* **2012**, *47* (7), 1661–1665. https://doi.org/10.1016/j.materresbull.2012.03.052.

256 Ling, H. Y.; Su, Z.; Chen, H.; Hencz, L.; Zhang, M.; Tang, Y.; Zhang, S. Biomass-Derived Poly(Furfuryl Alcohol)–Protected Aluminum Anode for Lithium-Ion Batteries. *Energy Technol.* **2019**, *7* (8), 1800995. https://doi.org/10.1002/ente.201800995.

257 Yadav, M.; Pophali, A.; Verma, N.; Kim, T. Oxidation of VOCs on a Highly Stabilized Furfuryl Alcohol-Based Activated Carbon Supported Nickel Oxide Catalyst. *J. Ind. Eng. Chem.* **2022**, *105*, 313–323. https://doi.org/10.1016/j.jiec.2021.09.032.

258 Bouzidi, K.; Chaussy, D.; Gandini, A.; Flahaut, E.; Bongiovanni, R.; Beneventi, D. Bio-Based Formulation of an Electrically Conductive Ink with High Potential for Additive Manufacturing by Direct Ink Writing. *Compos. Sci. Technol.* **2022**, *230*, 109765. https://doi.org/10.1016/j.compscitech.2022.109765.

259 Fitzer, E.; Schäfer, W. The Effect of Crosslinking on the Formation of Glasslike Carbons from Thermosetting Resins. *Carbon N. Y.* **1970**, *8* (3), 353–364. https://doi.org/10.1016/0008-6223(70)90075-8.

260 Janus, R.; Natkański, P.; Wądrzyk, M.; Lewandowski, M.; Michalik, M.; Kuśtrowski, P. Deposition of Poly(Furfuryl Alcohol) in Mesoporous Silica Template Controlled by Solvent Polarity: A Cornerstone of Facile and Versatile Synthesis of High-Quality CMK-Type Carbon Replicas. Nanocasting of SBA-15, SBA-16, and KIT-6. *Carbon N. Y.* **2022**, *195*, 292–307. https://doi.org/10.1016/j.carbon.2022.04.025.

261 Torres, J. M.; Stafford, C. M.; Vogt, B. D. Photoinitator Surface Segregation Induced Instabilities from Polymerization of a Liquid Coating on a Rigid Substrate. *Soft Matter* **2012**, *8* (19), 5225–5232. https://doi.org/10.1039/c2sm00037g

262 Gaillard, J. G.; Hendrus, C.; Vogt, B. D. Tunable Wrinkle and Crease Surface Morphologies from Photoinitiated Polymerization of Furfuryl Alcohol. *Langmuir* **2013**, *29* (48), 15083–15089. https://doi.org/10.1021/la4038167.

263 Principe, M.; Martínez, R.; Ortiz, P.; Rieumont, J. The Polymerization of Furfural Alcohol with P-Toluenesulfonic Acid: Photo-Crosslinkeable Feature of the Polymer. *Polim. Cienc. e Tecnol.* **2000**, *10* (1), 8–14. https://doi.org/10.1590/S0104-14282000000100004.

264 Sthel, M.; Rieumont, J.; Martinez, R. Testing a Furfuryl Alcohol Resin as a Negative Photoresist. *Polym. Test.* **1999**, *18* (1), 47–50. https://doi.org/10.1016/S0142-9418(98)00006-3.

265 Sthel, M. S.; Rieumont, J.; Martinez, R. Study on the Spatial Resolution of a Furfuryl Alcohol-Negative Photoresist Using a Holographic System. *J. Appl. Polym. Sci.* **1999**, *71* (11), 1749–1751. https://doi.org/10.1002/(SICI)1097-4628(19990314)71:11<1749::AID-APP4>3.0.CO;2-S.

266 Kim, T.; Assary, R. S.; Pauls, R. E.; Marshall, C. L.; Curtiss, L. A.; Stair, P. C. Thermodynamics and Reaction Pathways of Furfuryl Alcohol Oligomer Formation. *Catal. Commun.* **2014**, *46*, 66–70. https://doi.org/10.1016/j.catcom.2013.11.030.

267 Sun, S.; Yang, R.; Sun, P.; Ma, C.; Chen, J. Kinetics of Furfuryl Alcohol Condensation over Acid Catalyst for Preparing Diesel Precursor. *Energy* **2017**, *135*, 577–584. https://doi.org/10.1016/j.energy.2017.06.052.

268 Chan, X.; Yang, P.; Ooi, C.; Cen, J.; Orlov, A.; Kim, T. Separation and Purification of Furfuryl Alcohol Monomer and Oligomers Using a Two-Phase Extracting Process. *ACS Sustain. Chem. Eng.* **2016**, *4* (8), 4084–4088. https://doi.org/10.1021/acssuschemeng.6b01067

269 Chappaz, Alban; Jerome, Francois; De oliveira Vigier, Karine.; Muller, Eric; Lai, Jonathan. Process for the Preparation of Levulinate Esters. WO2018112779, **2018**.

270 Dunlop, A. P.; Peters, F. N. The Nature of Furfuryl Alcohol. *Ind. Eng. Chem.* **1942**, *34* (7), 814–817. https://doi.org/10.1021/ie50391a010.

271 Gandini, A.; Belgacem, M. N. Furan Resins, In *Handbook of Thermoset Plastics*, **2022**. https://doi.org/10.1016/b978-0-12-821632-3.00006-3

272 Conley, R. T.; Metil, I. An Investigation of the Structure of Furfuryl Alcohol Polycondensates with Infrared Spectroscopy. *J. Appl. Polym. Sci.* **1963**, *7* (1), 37–52. https://doi.org/10.1002/app.1963.070070104.

273 Wewerka, E. M.; Loughran, E. D.; Walters, K. L. A Study of the Low Molecular Weight Components of Furfuryl Alcohol Polymers. *J. Appl. Polym. Sci.* **1971**, *15* (6), 1437–1451. https://doi.org/10.1002/app.1971.070150612.

274 Barr, J. B.; Wallon, S. B. The Chemistry of Furfuryl Alcohol Resins. *J. Appl. Polym. Sci.* **1971**, *15* (5), 1079–1090. https://doi.org/10.1002/app.1971.070150504.

275 Fawcett, A. H.; Dadamba, W. Characterization of Furfuryl Alcohol Oligomers by 1H and 13C NMR Spectroscopy. *Die Makromol. Chemie* **1982**, *183* (11), 2799–2809. https://doi.org/10.1002/macp.1982.021831115.

276 Buchwalter, S. L. Polymerization of Furfuryl Acetate in Acetonitrile. *J. Polym. Sci. A1*. **1985**, *23* (12), 2897–2911. https://doi.org/10.1002/pol.1985.170231202.

277 Gandini, A.; Martinez, R. Cationic Polymerization of 2-Alkenyl Furans. *J. Polym. Sci.* **1976**, *90* (56), 79–90. https://doi.org/10.1002/polc.5070560110.

278 Maciel, G. E.; Chuang, I. S.; Myers, G. E. 13C NMR Study of Cured Furfuryl Alcohol Resins Using Cross Polarization and Magic-Angle Spinning. *Macromolecules* **1982**, *15* (4), 1218–1220. https://doi.org/10.1021/ma00232a058.

279 Chuang, I. S.; Maciel, G. E.; Myers, G. E. 13C NMR Study of Curing in Furfuryl Alcohol Resins. *Macromolecules* **1984**, *17* (5), 1087–1090. https://doi.org/10.1021/ma00135a019.

280 Gonzalez, R.; Martinez, R.; Ortiz, P. Polymerization of Furfuryl Alcohols with Trifluoroacetic Acid : The Influence of Experimental Conditions. *Macromol. Chem. Phys.* **1992**, *193* (1), 1–9. https://doi.org/10.1002/macp.1992.021930101.

281 Choura, M.; Belgacem, N. M.; Gandini, A. Acid-Catalyzed Polycondensation of Furfuryl Alcohol: Mechanisms of Chromophore Formation and Cross-Linking. *Macromolecules* **1996**, *29* (11), 3839–3850. https://doi.org/10.1021/ma951522f.

282 Zhang, X.; Solomon, D. H. The Reaction of Furfuryl Alcohol Resins with Hexamethylenetetramine: A 13C and 15N High-Resolution Solid-State NMR Study. *J. Polym. Sci. Part B Polym. Phys.* **1997**, *35* (14), 2233–2243. https://doi.org/10.1002/(SICI)1099-0488(199710)35:14<2233::AID-POLB4>3.0.CO;2-X.

283 Falco, G.; Guigo, N.; Vincent, L.; Sbirrazzuoli, N. Opening Furan for Tailoring Properties of Bio-Based Poly(Furfuryl Alcohol) Thermoset. *ChemSusChem* **2018**, *11* (11), 1805–1812. https://doi.org/10.1002/cssc.201800620

284 Tondi, G.; Cefarin, N.; Sepperer, T.; D'Amico, F.; Berger, R. J. F.; Musso, M.; Birarda, G.; Reyer, A.; Schnabel, T.; Vaccari, L. Understanding the Polymerization of Polyfurfuryl Alcohol: Ring Opening and Diels-Alder Reactions. *Polymers* **2019**, *11* (12), 2126. https://doi.org/10.3390/polym11122126.

285 Principe, M.; Ortiz, P.; Martínez, R. An NMR Study of Poly(Furfuryl Alcohol) Prepared with p-Toluenesulphonic Acid. *Polym. Int.* **1999**, *48* (8), 637–641. https://doi.org/10.1002/(sici)1097-0126(199908)48:8<637::aid-pi206>3.0.co;2-c.

286 González, R.; Figueroa, J. M.; González, H. Furfuryl Alcohol Polymerisation by Iodine in Methylene Chloride. *Eur. Polym. J.* **2002**, *38* (2), 287–297. https://doi.org/10.1016/S0014-3057(01)00090-8.

287 Montero, A. L.; Montero, L. A.; Martínez, R.; Spange, S. Ab Initio Modelling of Crosslinking in Polymers. A Case of Chains with Furan Rings. *J. Mol. Struct. THEOCHEM* **2006**, *770* (1–3), 99–106. https://doi.org/10.1016/j.theochem.2006.05.027.

288 Bertarione, S.; Bonino, F.; Cesano, F.; Damin, A.; Scarano, D.; Zecchina, A. Furfuryl Alcohol Polymerization in H - Y Confined Spaces : Reaction Mechanism and Structure of Carbocationic Intermediates. *J. Phys. Chem. B* **2008**, *112*, 2580–2589. https://doi.org/10.1021/jp073958q.

289 Kim, T.; Assary, R. S.; Marshall, C. L.; Gosztola, D. J.; Curtiss, L. A.; Stair, P. C. Acid-Catalyzed Furfuryl Alcohol Polymerization: Characterizations of Molecular Structure and Thermodynamic Properties. *ChemCatChem* **2011**, *3* (9), 1451–1458. https://doi.org/10.1002/cctc.201100098.

290 Kim, T.; Assary, R. S.; Kim, H.; Marshall, C. L.; Gosztola, D. J.; Curtiss, L. A.; Stair, P. C. Effects of Solvent on the Furfuryl Alcohol Polymerization Reaction: UV Raman Spectroscopy Study. *Catal. Today* **2013**, *205*, 60–66. https://doi.org/10.1016/j.cattod.2012.09.033.

291 Kim, T.; Jeong, J.; Rahman, M.; Zhu, E.; Mahajan, D. Characterizations of Furfuryl Alcohol Oligomer/Polymerization Catalyzed by Homogeneous and Heterogeneous Acid Catalysts. *Korean J. Chem. Eng.* **2014**, *31* (12), 2124–2129. https://doi.org/10.1007/s11814-014-0322-x.

292 Barsberg, S.; Berg, R. W. Combined Raman Spectroscopic and Theoretical Investigation of Fundamental Vibrational Bands of Furfuryl Alcohol (2-Furanmethanol). *J. Phys. Chem. A* **2006**, *110* (30), 9500–9504. https://doi.org/10.1021/jp061642x.

293 Barsberg, S.; Thygesen, L. G. Poly(Furfuryl Alcohol) Formation in Neat Furfuryl Alcohol and in Cymene Studied by ATR-IR Spectroscopy and Density Functional Theory (B3LYP) Prediction of Vibrational Bands. *Vib. Spectrosc.* **2009**, *49* (1), 52–63. https://doi.org/10.1016/j.vibspec.2008.04.013.

294 Barsberg, S. T.; Thygesen, L. G. A Combined Theoretical and FT-IR Spectroscopy Study of a Hybrid Poly(Furfuryl Alcohol) – Lignin Material: Basic Chemistry of a Sustainable Wood Protection Method. *ChemistrySelect* **2017**, *2* (33), 10818–10827. https://doi.org/10.1002/slct.201702104.

295 Nordstierna, L.; Lande, S.; Westin, M.; Karlsson, O.; Furó, I. Towards Novel Wood-Based Materials: Chemical Bonds between Lignin-like Model Molecules and Poly(Furfuryl Alcohol) Studied by NMR. *Holzforschung* **2008**, *62* (6), 709–713. https://doi.org/10.1515/HF.2008.110.

296 D'Amico, F.; Musso, M. E.; Berger, R. J. F.; Cefarin, N.; Birarda, G.; Tondi, G.; Bertoldo Menezes, D.; Reyer, A.; Scarabattoli, L.; Sepperer, T.; Schnabel, T.; Vaccari, L. Chemical Constitution of Polyfurfuryl Alcohol Investigated by FTIR and Resonant Raman Spectroscopy. *Spectrochim. Acta - Part A Mol. Biomol. Spectrosc.* **2021**, *262*, 120090. https://doi.org/10.1016/j.saa.2021.120090

297 Krishnan, T. A.; Chanda, M. Kinetics of Polymerisation of Furfuryl Alcohol in Aqueous Solution. *Die Angew. Makromol. Chemie* **1975**, *43* (1), 145–156. https://doi.org/10.1002/apmc.1975.050430110.

298 Chanda, M.; Dinesh, S. R. Monitoring the Curing of Furan Resins through the Exothermic Heat of Reaction. *Die Angew. Makromol. Chemie* **1978**, *69* (1), 85–98. https://doi.org/10.1002/apmc.1978.050690107.

299 Domínguez, J. C.; Grivel, J. C.; Madsen, B. Study on the Non-Isothermal Curing Kinetics of a Polyfurfuryl Alcohol Bioresin by DSC Using Different Amounts of Catalyst. *Thermochim. Acta* **2012**, *529*, 29–35. https://doi.org/10.1016/j.tca.2011.11.018.

300 Cao, T. P.; Hang, C. N.; Vu-Quang, H.; Kabtamu, D. M.; Kumar, S.; Nguyen, V. C.; Cao, X. T. Catalyst-Free Synthesis of Poly(Furfuryl Alcohol) Using Deep Eutectic Solvents. *New J. Chem.* **2022**, 3786–3793. https://doi.org/10.1039/d1nj05723e.

301 Falco, G.; Guigo, N.; Vincent, L.; Sbirrazzuoli, N. FA Polymerization Disruption by Protic Polar Solvents. *Polymers* **2018**, *10* (5), 1–14. https://doi.org/10.3390/polym10050529.

302 Marefat Seyedlar, R.; Imani, M.; Mirabedini, S. M. Curing of Poly(Furfuryl Alcohol) Resin Catalyzed by a Homologous Series of Dicarboxylic Acid Catalysts: Kinetics and Pot Life. *J. Appl. Polym. Sci.* **2016**, *133* (43), 1–11. https://doi.org/10.1002/app.44009.

303 Behzadfar, A.; Imani, M.; Farahmandghavi, F. Shelf-Life of Polyfurfuryl Alcohol Resin: An Accelerated Rheokinetics Study. *Polym. Bull.* **2019**, *76* (11), 5903–5918. https://doi.org/10.1007/s00289-019-02692-4.

304 Herold, N.; Dietrich, T.; Grigsby, W. J.; Franich, R. A.; Winkler, A.; Buchelt, B.; Pfriem, A. Effect of Maleic Anhydride Content and Ethanol Dilution on the Polymerization of Furfuryl Alcohol in Wood Veneer Studied by Differential Scanning Calorimetry. *BioResources* **2013**, *8* (1), 1064–1075. https://doi.org/10.15376/biores.8.1.1064-1075.

305 Sadler, J. M.; Yeh, I. C.; Toulan, F. R.; McAninch, I. M.; Rinderspacher, B. C.; La Scala, J. J. Kinetics Studies and Characterization of Poly(Furfuryl Alcohol) for Use as Bio-Based Furan Novolacs. *J. Appl. Polym. Sci.* **2018**, *135* (34), 46608. https://doi.org/10.1002/app.46608.

306 Vargas, M. A.; Scheubner, M.; Guthausen, G. Reaction Kinetics of Polyfurfuryl Alcohol Bioresin and Nanoparticles by 1H-NMR Transverse Relaxation Measurements Maria. *Polym. Compos.* **2017**, *39* (9), 3280–3288. https://doi.org/DOI 10.1002/pc.24342

307 Guigo, N.; Mija, A.; Vincent, L.; Sbirrazzuoli, N. Chemorheological Analysis and Model-Free Kinetics of Acid Catalysed Furfuryl Alcohol Polymerization. *Phys. Chem. Chem. Phys.* **2007**, *9* (39), 5359–5366. https://doi.org/10.1039/b707950h.

308 Domínguez, J. C.; Madsen, B. Chemorheological Study of a Polyfurfuryl Alcohol Resin System-Pre-Gel Curing Stage. *Ind. Crops Prod.* **2014**, *52*, 321–328. https://doi.org/10.1016/j.indcrop.2013.11.006.

309 Lopez De Vergara, U.; Sarrionandia, M.; Gondra, K.; Aurrekoetxea, J. Polymerization and Curing Kinetics of Furan Resins under Conventional and Microwave Heating. *Thermochim. Acta* **2014**, *581*, 92–99. https://doi.org/10.1016/j.tca.2014.02.017.

310 Hoshi, K.; Tanabe, Y.; Yasuda, E. Effects of Sonication on Curing Process in Furan Resin. *Tanso* **1998**, *184*, 199–201. https://doi.org/10.7209/tanso.1998.199.

311 Hoshi, K.; Akatsu, T.; Tanabe, Y.; Yasuda, E. Curing Properties of Furfuryl Alcohol Condensate with Carbonaceous Fine Particles under Ultrasonication. *Ultrason. Sonochem.* **2001**, *8* (2), 89–92. https://doi.org/10.1016/S1350-4177(00)00028-6

312 Hoshi, K.; Iiyama, T.; Akatsu, T.; Tanabe, Y.; Yasuda, E. Characterization of Cured Furan Resin Prepared by High Power Ultrasonic Irradiation. *Tanso* **1999**, *190*, 289–292. https://doi.org/10.7209/tanso.1999.289

313 De Souza, M. F. Furfuryl Alcohol Polymerisation inside Capilaries. *Synth. Met.* **1999**, *101*, 635–636. https://doi.org/10.1016/S0379-6779(98)00822-4.

314 Swasti, Y. R.; Murkovic, M. Characterization of the Polymerization of Furfuryl Alcohol during Roasting of Coffee. *Food Funct.* **2012**, *3* (9), 965–969. https://doi.org/10.1039/c2fo30020f.

315 Pezzana, L.; Melilli, G.; Guigo, N.; Sbirrazzuoli, N.; Sangermano, M. Photopolymerization of Furan-Based Monomers: Exploiting UV-Light for a New Age of Green Polymers. *React. Funct. Polym.* **2023**, *185*, 105540. https://doi.org/10.1016/j.reactfunctpolym.2023.105540.

316 Merino, P. Oxidative Cleavage of Furans. In *Organic Reactions*; **2015** https://doi.org/10.1002/0471264180.or087.01.

317 Bryant, W. M. D.; Smith, D. M. Improved Hydroxylamine Method for the Determination of Aldehydes and Ketones. Displacement of Oxime Equilibria by Means of Pyridine. *J. Am. Chem. Soc.* **1935**, *57* (1), 57–61. https://doi.org/10.1021/ja01304a017.

318 Black, S.; Ferrell, J. R. Determination of Carbonyl Groups in Pyrolysis Bio-Oils Using Potentiometric Titration: Review and Comparison of Methods. *Energy and Fuels* **2016**, *30* (2), 1071–1077. https://doi.org/10.1021/acs.energyfuels.5b02511.

319 Faix, O.; Andersons, B.; Zakis, G. Determination of Carbonyl Groups of Six Round Robin Lignins by Modified Oximation and FTIR Spectroscopyy. *Holzforschung* **1998**, *52* (3), 268–274. https://doi.org/10.1515/hfsg.1998.52.3.268.

320 Li, J.; Hu, H. C.; Chai, X. S. Rapid Method for Determination of Carbonyl Groups in Lignin Compounds by Headspace Gas Chromatography. *J. Chromatogr. A* **2015**, *1404*, 39–43. https://doi.org/10.1016/j.chroma.2015.05.055.

321 Milne, T. A.; Chum, H. L.; Agblevor, F.; Johnson, D. K. Standardized Analytical Methods. *Biomass and Bioenergy* **1992**, *2* (1–6), 341–366. https://doi.org/10.1016/0961-9534(92)90109-4.

322 Balakshin, M. Y.; Capanema, E. A.; Santos, R. B.; Chang, H. M.; Jameel, H. Structural Analysis of Hardwood Native Lignins by Quantitative 13C NMR Spectroscopy. *Holzforschung* **2016**, *70* (2), 95–108. https://doi.org/10.1515/hf-2014-0328.

323 Sevillano, R. M.; Mortha, G.; Barrelle, M.; Lachenal, D. 19F NMR Spectroscopy for the Quantitative Analysis of Carbonyl Groups in Lignins. *Holzforschung* **2001**, *55* (3), 286–295. https://doi.org/10.1515/HF.2001.048.

324Ahvazi, B. C.; Argyropoulos, D. S. 19F Nuclear Magnetic Resonance Spectroscopy for the Elucidation of Carbonyl Groups in Lignins. 1. Model Compounds. *J. Agric. Food Chem.* **1996**, *44* (8), 2167–2175. https://doi.org/10.1021/jf960154r.

325 Huang, F.; Pan, S.; Pu, Y.; Ben, H.; Ragauskas, A. J. 19F NMR Spectroscopy for the Quantitative Analysis of Carbonyl Groups in Bio-Oils. *RSC Adv.* **2014**, *4* (34), 17743–17747. https://doi.org/10.1039/c4ra01293c.

326 Constant, S.; Lancefield, C. S.; Weckhuysen, B. M.; Bruijnincx, P. C. A. Quantification and Classification of Carbonyls in Industrial Humins and Lignins by 19F NMR. *ACS Sustain. Chem. Eng.* **2017**, *5* (1), 965–972. https://doi.org/10.1021/acssuschemeng.6b02292.

327 Schaefer, J.; Stejskal, E. O. Carbon-13 Nuclear Magnetic Resonance of Polymers Spinning at the Magic Angle. *J. Am. Chem. Soc.* **1976**, *98* (4), 1031–1032. https://doi.org/10.1021/ja00420a036.

328 Socrates, G. *Infrared and Raman Characteristic Group Frequencies. Tables and Charts*; John Wiley & Sons, Ltd **2001.** ISBN: 0470093072

329 Van Zandvoort, I.; Van Eck, E. R. H.; De Peinder, P.; Heeres, H. J.; Bruijnincx, P. C. A.; Weckhuysen, B. M. Full, Reactive Solubilization of Humin Byproducts by Alkaline Treatment and Characterization of the Alkali-Treated Humins Formed. *ACS Sustain. Chem. Eng.* **2015**, *3* (3), 533–543. https://doi.org/10.1021/sc500772w.

330 Silverstein, R. M.; Webster, F. X.; Kiemle, D. J.; Bryce, D. L. Spectrometric Identification of Organic Compounds. John Wiley & Sons, Ltd **2016**. ISBN: 9780470616376

331 Alvi, S.; Ali, R. An Expeditious and Highly Efficient Synthesis of Substituted Pyrroles Using a Low Melting Deep Eutectic Mixture. *Org. Biomol. Chem.* **2021**, *19* (44), 9732–9745. https://doi.org/10.1039/d1ob01618k.

332 Shi, N.; Liu, Q.; Cen, H.; Ju, R.; He, X.; Ma, L. Formation of Humins during Degradation of Carbohydrates and Furfural Derivatives in Various Solvents. *Biomass Convers. Biorefinery* **2020**, *10* (2), 277–287. https://doi.org/10.1007/s13399-019-00414-4.

333 Li, W.; Wang, H.; Ren, D.; Yu, Y. S.; Yu, Y. Wood Modification with Furfuryl Alcohol Catalysed by a New Composite Acidic Catalyst. *Wood Sci. Technol.* **2015**, *49* (4), 845–856. https://doi.org/10.1007/s00226-015-0721-0.

334 Pezzana, L.; Melilli, G.; Delliere, P.; Moraru, D.; Guigo, N.; Sbirrazzuoli, N.; Sangermano, M. Thiol-Ene Biobased Networks: Furan Allyl Derivatives for Green Coating Applications. *Prog. Org. Coatings* **2022**, *173*, 107203. https://doi.org/10.1016/j.porgcoat.2022.107203.

335 Piancatelli, G.; D'Auria, M.; D'Onofrio, F. Synthesis of 1,4-Dicarbonyl Compounds an Cyclopentanones from Furans. *Synthesis.* **1994**, *9*, 867–889. https://doi.org/10.1055/s-1994-25591.

336 Zelina, E. Y.; Nevolina, T. A.; Sorotskaja, L. N.; Skvortsov, D. A.; Trushkov, I. V.; Uchuskin, M. G. Route to Pyrrolo[1,2-a]Quinoxalines via a Furan Ring Opening-Pyrrole Ring Closure Sequence. *Tetrahedron Lett.* **2020**, *61* (9), 151532. https://doi.org/10.1016/j.tetlet.2019.151532.

337 Soininen, P. Quantitative 1H NMR Spectroscopy - Chemical and Biological Applications, *Doctoral dissertation*, **2008**, Uuniversity of Kuopio

338 Mansfield, S. D.; Kim, H.; Lu, F.; Ralph, J. Whole Plant Cell Wall Characterization Using Solution-State 2D NMR. *Nat. Protoc.* **2012**, *7* (9), 1579–1589. https://doi.org/10.1038/nprot.2012.064.

339 Balakshin, M. Y.; Capanema, E. A.; Chen, C. L.; Gracz, H. S. Elucidation of the Structures of Residual and Dissolved Pine Kraft Lignins Using an HMQC NMR Technique. *J. Agric. Food Chem.* **2003**, *51* (21), 6116–6127. https://doi.org/10.1021/jf034372d.

340 Fernández-Costas, C.; Gouveia, S.; Sanromán, M. A.; Moldes, D. Structural Characterization of Kraft Lignins from Different Spent Cooking Liquors by 1D and 2D Nuclear Magnetic Resonance Spectroscopy. *Biomass and Bioenergy* **2014**, *63*, 156–166. https://doi.org/10.1016/j.biombioe.2014.02.020.

341 Tobimatsu, Y.; Chen, F.; Nakashima, J.; Escamilla-Treviño, L. L.; Jackson, L.; Dixon, R. A.; Ralph, J. Coexistence but Independent Biosynthesis of Catechyl and Guaiacyl/Syringyl Lignin Polymers in Seed Coats. *Plant Cell* **2013**, *25* (7), 2587–2600. https://doi.org/10.1105/tpc.113.113142.

342 Ghosh, A. K.; Brindisi, M. Achmatowicz Reaction and Its Application in the Syntheses of Bioactive Molecules. *RSC Adv.* **2016**, *6* (112), 111564–111598. https://doi.org/10.1039/C6RA22611F.

343 Clayden, J.; Greeves, N.; Warren, S. *Organic Chemistry*, Oxford Uni.; **2012**. https://doi.org/10.1016/b978-0-12-676950-0.50001-8.

344 Hu, X.; Jiang, S.; Kadarwati, S.; Dong, D.; Li, C. Z. Effects of Water and Alcohols on the Polymerization of Furan during Its Acid-Catalyzed Conversion into Benzofuran. *RSC Adv.* **2016**, *6* (46), 40489–40501. https://doi.org/10.1039/c6ra04745a.

345 Palframan, M. J.; Pattenden, G. The Versatility of Furfuryl Alcohols and Furanoxonium Ions in Synthesis. *Chem. Commun.* **2014**, *50* (55), 7223–7242. https://doi.org/10.1039/c4cc01196a.

346 Kaïm, L. El; Grimaud, L.; Wagschal, S. Palladium Catalyzed Ring Opening of Furans as a Route to α,β-Unsaturated Aldehydes. *Chem. Commun.* **2011**, *47* (6), 1887–1889. https://doi.org/10.1039/c0cc04164e.

347 Blank, S. J.; Stephens, C. E. Oxidative Ring Opening of 2,5-Diarylfurans by Selectfluor®. *Tetrahedron Lett.* **2006**, *47* (38), 6849–6850. https://doi.org/10.1016/j.tetlet.2006.07.071.

348 Gelmini, A.; Albonetti, S.; Cavani, F.; Cesari, C.; Lolli, A.; Zanotti, V.; Mazzoni, R. Oxidant Free One-Pot Transformation of Bio-Based 2,5-Bis-Hydroxymethylfuran into α-6-Hydroxy-6-Methyl-4-Enyl-2H-Pyran-3-One in Water. *Appl. Catal. B Environ.* **2016**, *180*, 38–43. https://doi.org/10.1016/j.apcatb.2015.06.003.

349 Simeonov, S. P.; Ravutsov, M. A.; Mihovilovic, M. D. Biorefinery via Achmatowicz Rearrangement: Synthesis of Pentane-1,2,5-Triol from Furfuryl Alcohol. *ChemSusChem* **2019**, *12* (12), 2748–2754. https://doi.org/10.1002/cssc.201900601.

350 Liu, X.; Li, B.; Han, G.; Liu, X.; Cao, Z.; Jiang, D. en; Sun, Y. Electrocatalytic Synthesis of Heterocycles from Biomass-Derived Furfuryl Alcohols. *Nat. Commun.* **2021**, *12* (1), 1868 . https://doi.org/10.1038/s41467-021-22157-5.

351 Noutsias, D.; Alexopoulou, I.; Montagnon, T.; Vassilikogiannakis, G. Using Water, Light, Air and Spirulina to Access a Wide Variety of Polyoxygenated Compounds. *Green Chem.* **2012**, *14* (3), 601–604. https://doi.org/10.1039/c2gc16397g.

352 Plutschack, M. B.; Seeberger, P. H.; Gilmore, K. Visible-Light-Mediated Achmatowicz Rearrangement. *Org. Lett.* **2017**, *19* (1), 30–33. https://doi.org/10.1021/acs.orglett.6b03237.

353 Wang, T.; Zhang, M.; Zheng, Y.; Seong, J.; Lah, M. S.; Koo, S. Furan Oxidation by Mn(Iii)/Co(Ii) Catalysts-Application to Benzofuran Synthesis. *RSC Adv.* **2021**, *11* (50), 31395–31399. https://doi.org/10.1039/d1ra05305a.

354 Kikaš, I.; Horváth, O.; Škoric, I. Photocatalytic and Thermal Oxygenation of a Furan Derivative. *Tetrahedron Lett.* **2011**, *52*, 6255–6259. https://doi.org/10.1016/j.tetlet.2011.09.076.

355 Banfi, D.; Patiny, L. Www.Nmrdb.Org: Resurrecting and Processing NMR Spectra on-Line. *Chimia.* **2008**, *62* (4), 280–281. https://doi.org/10.2533/chimia.2008.280.

356 Malherbe, J. S.; Meyer, C. J. A Mini-Qualitative Carbohydrate Analysis Session. *J. Chem. Educ.* **1997**, *74* (11), 1304–1305. https://doi.org/https://doi.org/10.1021/ed074p1304.

357 Weiser, J. R.; Ricapito, N. G.; Yueh, A.; Weiser, E. L.; Putnam, D. A Mechanistic Analysis of the Quantitation of α-Hydroxy Ketones by the Bicinchoninic Acid Assay. *Anal. Biochem.* **2012**, *430* (2), 116–122. https://doi.org/10.1016/j.ab.2012.08.009.

358 Volponi, J. E.; Innocentini Mei, L. H.; dos Santos Rosa, D. Use of Oxidation Onset Temperature Measurements for Evaluating the Oxidative Degradation of Isotatic Polypropylene. *J. Polym. Environ.* **2004**, *12* (1), 11–16. https://doi.org/10.1023/B:JOOE.0000003123.68569.0e.

359 Shindo, A.; Izumino, K. Structural Variation during Pyrolysis of Furfuryl Alcohol and Furfural-Furfuryl Alcohol Resins. *Carbon N. Y.* **1994**, *32* (7), 1233–1243. https://doi.org/10.1016/0008-6223(94)90107-4.

360 Bertarione, S.; Bonino, F.; Cesano, F.; Jain, S.; Zanetti, M.; Scarano, D.; Zecchina, A. Micro-FTIR and Micro-Raman Studies of a Carbon Film Prepared from Furfuryl Alcohol Polymerization. *J. Phys. Chem. B* **2009**, *113* (31), 10571–10574. https://doi.org/10.1021/jp9050534.

361 Burket, C. L.; Rajagopalan, R.; Marencic, A. P.; Dronvajjala, K.; Foley, H. C. Genesis of Porosity in Polyfurfuryl Alcohol Derived Nanoporous Carbon. *Carbon N. Y.* **2006**, *44* (14), 2957–2963. https://doi.org/10.1016/j.carbon.2006.05.029.

362 Tondi, G.; Pizzi, A.; Pasch, H.; Celzard, A. Structure Degradation, Conservation and Rearrangement in the Carbonisation of Polyflavonoid Tannin/Furanic Rigid Foams - A MALDI-TOF Investigation. *Polym. Degrad. Stab.* **2008**, *93* (5), 968–975. https://doi.org/10.1016/j.polymdegradstab.2008.01.024
.
363 Tondi, G.; Pizzi, A.; Pasch, H.; Celzard, A.; Rode, K. MALDI-ToF Investigation of Furanic Polymer Foams before and after Carbonization: Aromatic Rearrangement and Surviving Furanic Structures. *Eur. Polym. J.* **2008**, *44* (9), 2938–2943. https://doi.org/10.1016/j.eurpolymj.2008.06.029.

364 Janus, R.; Wach, A.; Kuśtrowski, P.; Dudek, B.; Drozdek, M.; Silvestre-Albero, A. M.; Rodríguez-Reinoso, F.; Cool, P. Investigation on the Low-Temperature Transformations of Poly(Furfuryl Alcohol) Deposited on MCM-41. *Langmuir* **2013**, *29* (9), 3045–3053. https://doi.org/10.1021/la3041852.

365 Ilnicka, A.; Lukaszewicz, J. P. Alternative Synthesis Method for Carbon Nanotubes. *Small* **2019**, *15* (51), 1904132. https://doi.org/10.1002/smll.201904132.

366 Conley, R. T.; Metil, I. A Study of the Oxidative Degradation of Furfuryl Alcohol Polycondensates by Infrared Spectroscopy. *J. Appl. Polym. Sci.* **1963**, *7* (3), 1083–1091. https://doi.org/10.1002/app.1963.070070323.

367 Vassallo, A. M.; Hanna, J. V. 13C Nmr and Ftir Study of Thermal Annealing Amorphous Hydrogenated. *Carbon N. Y.* **1993**, *31* (4), 569–575. https://doi.org/https://doi.org/10.1016/0008-6223(93)90111-M.

368 Vyazovkin, S.; Chrissafis, K.; Di Lorenzo, M. L.; Koga, N.; Pijolat, M.; Roduit, B.; Sbirrazzuoli, N.; Suñol, J. J. ICTAC Kinetics Committee Recommendations for Collecting Experimental Thermal Analysis Data for Kinetic Computations. *Thermochim. Acta* **2014**, *590*, 1–23. https://doi.org/10.1016/j.tca.2014.05.036.

369 Sbirrazzuoli, N. Determination of Pre-Exponential Factor and Reaction Mechanism in a Model-Free Way. *Thermochim. Acta* **2020**, *691*, 178707. https://doi.org/10.1016/j.tca.2020.178707.

370 Vyazovkin, S.; Burnham, A. K.; Favergeon, L.; Koga, N.; Moukhina, E.; Pérez-Maqueda, L. A.; Sbirrazzuoli, N. ICTAC Kinetics Committee Recommendations for Analysis of Multi-Step Kinetics. *Thermochim. Acta* **2020**, *689*, 178597. https://doi.org/10.1016/j.tca.2020.178597.

371 Peterson, J. D.; Vyazovkin, S.; Wight, C. A. Kinetics of the Thermal and Thermo-Oxidative Degradation of Polystyrene, Polyethylene and Poly(Propylene). *Macromol. Chem. Phys.* **2001**, *202* (6), 775–784. https://doi.org/10.1002/1521-3935(20010301)202:6<775::AID-MACP775>3.0.CO;2-G.

372 Budrugeac, P.; Segal, E. Application of Isoconversional and Multivariate Non-Linear Regression Methods for Evaluation of the Degradation Mechanism and Kinetic Parameters of an Epoxy Resin. *Polym. Degrad. Stab.* **2008**, *93* (6), 1073–1080. https://doi.org/10.1016/j.polymdegradstab.2008.03.017.

373 Dwyer, D. B.; Gallego, N. C.; Niedziela, J. L.; Kapsimalis, R. J.; Duckworth, D. C. Product Specific Thermal Degradation Kinetics of Bisphenol F Epoxy in Inert and Oxidative Atmospheres Using Evolved Gas Analysis–Mass Spectrometry. *J. Anal. Appl. Pyrolysis* **2022**, *165*, 105563. https://doi.org/10.1016/j.jaap.2022.105563.

374 Flory J., P. *Principles of Polymer Chemistry*; Cornell University Press: New York, **1953**. ISBN: 0801401348

375 Ecochard, Y.; Auvergne, R.; Boutevin, B.; Caillol, S. Linseed Oil-Based Thermosets by Aza-Michael Polymerization. *Eur. J. Lipid Sci. Technol.* **2020**, *122* (1), 1900145. https://doi.org/10.1002/ejlt.201900145.

376 Liu, J.; Zhang, L.; Liu, C.; Zheng, X.; Tang, K. Tuning Structure and Properties of Gelatin Edible Films through Pullulan Dialdehyde Crosslinking. *Lwt* **2021**, *138*, 110607. https://doi.org/10.1016/j.lwt.2020.110607.

377 Codou, A.; Guigo, N.; Heux, L.; Sbirrazzuoli, N. Partial Periodate Oxidation and Thermal Cross-Linking for the Processing Ofthermosetall-Cellulose Composites. *Compos. Sci. Technol.* **2015**, *117*, 54–61. https://doi.org/10.1016/j.compscitech.2015.05.022.

378 Priamine 1071 EC N° 100.066.601 https://echa.europa.eu/fr/substance-information/-/substanceinfo/100.066.601 Last accessed (29/09/2023)

379 Froidevaux, V.; Negrell, C.; Caillol, S.; Pascault, J. P.; Boutevin, B. Biobased Amines: From Synthesis to Polymers; Present and Future. *Chem. Rev.* **2016**, *116* (22), 14181–14224. https://doi.org/10.1021/acs.chemrev.6b00486.

380 Ranganathan, P.; Chen, C. W.; Rwei, S. P. Highly Stretchable Fully Biomass Autonomic Self-Healing Polyamide Elastomers and Their Foam for Selective Oil Absorption. *Polymers.* **2021**, *13* (18), 3089 https://doi.org/10.3390/polym13183089.

381 Włoch, M.; Datta, J.; Błażek, K. The Effect of High Molecular Weight Bio-Based Diamine Derivative of Dimerized Fatty Acids Obtained from Vegetable Oils on the Structure, Morphology and Selected Properties of Poly(Ether-Urethane-Urea)S. *J. Polym. Environ.* **2018**, *26* (4), 1592–1604. https://doi.org/10.1007/s10924-017-1059-5.

382 Carré, C.; Bonnet, L.; Avérous, L. Solvent- and Catalyst-Free Synthesis of Fully Biobased Nonisocyanate Polyurethanes with Different Macromolecular Architectures. *RSC Adv.* **2015**, *5* (121), 100390–100400. https://doi.org/10.1039/c5ra17638g.

383 Hajiali, F.; Tajbakhsh, S.; Marić, M. Thermally Reprocessable Bio-Based Polymethacrylate Vitrimers and Nanocomposites. *Polymer.* **2021**, *212*, 123126 https://doi.org/10.1016/j.polymer.2020.123126.

384 Zhou, Z.; Su, X.; Liu, J.; Liu, R. Synthesis of Vanillin-Based Polyimine Vitrimers with Excellent Reprocessability, Fast Chemical Degradability, and Adhesion. *ACS Appl. Polym. Mater.* **2020**, *2* (12), 5716–5725. https://doi.org/10.1021/acsapm.0c01008.

385 Zhao, S.; Abu-Omar, M. M. Recyclable and Malleable Epoxy Thermoset Bearing Aromatic Imine Bonds. *Macromolecules* **2018**, *51* (23), 9816–9824. https://doi.org/10.1021/acs.macromol.8b01976.

386 Memon, H.; Liu, H.; Rashid, M. A.; Chen, L.; Jiang, Q.; Zhang, L.; Wei, Y.; Liu, W.; Qiu, Y. Vanillin-Based Epoxy Vitrimer with High Performance and Closed-Loop Recyclability. *Macromolecules* **2020**, *53* (2), 621–630. https://doi.org/10.1021/acs.macromol.9b02006.

387 Subramaniyan, S.; Najjarzadeh, N.; Vanga, S. R.; Liguori, A.; Syrén, P. O.; Hakkarainen, M. Designed for Circularity: Chemically Recyclable and Enzymatically Degradable Biorenewable Schiff Base Polyester-Imines. *ACS Sustain. Chem. Eng.* **2023**, *11* (8), 3451–3465. https://doi.org/10.1021/acssuschemeng.2c06935.

388 Subramaniyan, S.; Bergoglio, M.; Sangermano, M.; Hakkarainen, M. Vanillin-Derived Thermally Reprocessable and Chemically Recyclable Schiff-Base Epoxy Thermosets. *Glob. Challenges* **2023**, *7* (4), 2200234. https://doi.org/10.1002/gch2.202200234.

389 Hakkarainen, M.; Xu, Y.; Odelius, K. Photocurable, Thermally Reprocessable, and Chemically Recyclable Vanillin-Based Imine Thermosets. *ACS Sustain. Chem. Eng.* **2020**, *8* (46), 17272–17279. https://doi.org/10.1021/acssuschemeng.0c06248.

390 Liguori, A.; Subramaniyan, S.; Yao, J. G.; Hakkarainen, M. Photocurable Extended Vanillin-Based Resin for Mechanically and Chemically Recyclable, Self-Healable and Digital Light Processing 3D Printable Thermosets. *Eur. Polym. J.* **2022**, *178*, 111489. https://doi.org/10.1016/j.eurpolymj.2022.111489.

391 Dhers, S.; Vantomme, G.; Avérous, L. A Fully Bio-Based Polyimine Vitrimer Derived from Fructose. *Green Chem.* **2019**, *21* (7), 1596–1601. https://doi.org/10.1039/c9gc00540d.

392 Tachibana, Y.; Hayashi, S.; Kasuya, K. I. Biobased Poly(Schiff-Base) Composed of Bifurfural. *ACS Omega* **2018**, *3* (5), 5336–5345. https://doi.org/10.1021/acsomega.8b00466.

393 Jiang, L.; Tian, Y.; Cheng, J.; Zhang, J. A Biomass-Based Schiff Base Vitrimer with Both Excellent Performance and Multiple Degradability. *Polym. Chem.* **2021**, *12* (45), 6527–6537. https://doi.org/10.1039/d1py01003d.

394 Dunky, M. Wood Adhesives Based on Natural Resources: A Critical Review. *Rev. Adhes. Adhes.* **2021**, *9* (2), 189–268. https://doi.org/10.7569/RAA.2021.097307.